

# **Automated Manufacturing of Smart Tunnel Segments**

Tresor K. Tshimbombo

A thesis submitted for the degree of Doctor of Philosophy to the Department of Civil and  
Environmental Engineering

University of Strathclyde

December 2023

This thesis is the result of the author's original research. It has been composed by the author and has not been previously submitted for examination which has led to the award of a degree.

The copyright of this thesis belongs to the author under the terms of the United Kingdom Copyright Acts as qualified by University of Strathclyde Regulation

3.50. Due acknowledgement must always be made of the use of any material contained in, or derived from, this thesis.

Signed:

Date:

## **Abstract**

Tunnels, essential infrastructures, require regular inspections and maintenance to ensure their prolonged service life. While conventional methods heavily rely on expert human manpower, modern tunnel structural monitoring techniques, such as sensor-based Structural Health Monitoring (SHM), are increasingly utilized in both existing and newly constructed tunnels. Despite providing valuable insights into post-construction structural behaviour, these methods often overlook the behaviour of individual precast elements, such as tunnel segments, before their installation.

This thesis explores the concept of smart tunnel segments instrumented by robotic means to address this gap. In this project lab-scale tunnel segments were instrumented using a 6-axis robotic arm making them smart enabling their properties to be tracked from manufacturing through the operational phase of the tunnel. The research involves a comprehensive review of current tunnel instrumentation practices, identifying structural strains as the most monitored parameters. Vibrating Wire Strain Gauges (VWSGs) were identified as the most suitable sensors for this application due to their compatibility with a modular system and superior long-term properties, especially when embedded in concrete.

Furthermore, the study identifies untapped potential in fully automated precast factories and proposes repurposing certain features of industrial robots to deploy VWSGs nodes via robotic pick-and-place. Through a novel evaluation framework, the research demonstrates the effectiveness of automated sensor deployment by robots. This includes the robotic installation of a pair of embedded VWSGs in lab-scale tunnel segments, thereby rendering them "smart," and subjecting them to repetitive flexural loadings to evaluate their performance and accuracy. The calculated strain transfer exhibits consistent and repeatable behaviour across segments.

Finally, the thesis outlines the economic justification for smart segments, which outperform traditional on-site wired and wireless alternatives, thereby contributing to a more comprehensive and cost-effective tunnel maintenance strategy.

# Acknowledgements

Big thanks to my academic supervisors, Marcus Perry and Enrico Tubaldi, and industrial supervisors, Chris Hoy, Efi Tzoura, and Chrysoula Litina. Your support was invaluable, without exaggerating.

Massive shout-out to the *civ auto* crew for pulling off some great work throughout these years. Marcus, again, you've been a great boss to work for and in many ways a great mentor. Jack, you're the unsung hero – thanks for helping me unravel those electronic and coding messes. And big ups to Sanj and Hamish for getting down and dirty with different sides of my research. Your support, whether hands-on or just being curious about what the hell I was doing, meant a lot.

Gavin, Dereck, and Jim, you're real pros. Thanks a ton for being so involved in to making those segments. I'll miss those collaborative moments, especially during covid when we had the all lab for ourselves.

To my parents, Andre Kadita and Denise Mpoyi. I hope you're proud of me having spent four more years at school. Your prayers and love reached me across the thousands of miles and years. And to my siblings, thanks for keeping me grounded with those marathon WhatsApp sessions, reliving the good old times.

And a big thanks to all my friends, old and new, for having my back and making this journey a lot less bumpy.

# Contents

Acknowledgements.....	i
List of Figures.....	vi
List of Tables .....	ix
List of Appendices .....	x
Glossary of Abbreviations .....	xi
Chapter 1. Introduction.....	1
1.1 Research Justification .....	2
1.2 Principal contributions .....	3
1.3 Thesis overview .....	4
1.4 Publications.....	5
1.4.1 Journal Articles .....	5
1.4.2 Conference Papers .....	5
Chapter 2. Tunnels And Their Instrumentation .....	7
2.1 Tunnel Generalities .....	7
2.1.1 Some notions on tunnels.....	7
2.1.2 Concrete tunnel segments .....	7
2.2 Tunnel Instrumentation .....	15
2.2.1 Traditional tunnel structural inspection .....	15
2.2.2 Structural health monitoring.....	17
2.2.3 Wired SHM.....	18
2.2.4 Wireless SHM.....	24
2.2.5 Other examples of monitoring systems in civil engineering .....	29
2.3 Tunnel instrumentation in the real world .....	31
2.3.1 Real world tunnel projects with Instrumentation.....	31
2.3.2 Gaps in existing instrumented tunnels.....	33

2.4	Summary .....	38
Chapter 3. Sensors Selection and Design .....		39
3.1	Background .....	39
3.2	Choice of sensors .....	40
3.2.1	Embedded sensors .....	40
3.2.2	Electronic sensors .....	40
3.2.3	Vibrating wire strain gauge.....	42
3.2.4	Comparison and final choice .....	43
3.2.5	Sensor choice .....	45
3.3	Electronics and programming .....	46
3.3.1	Communication mode.....	46
3.3.2	Wireless Communication:.....	47
3.3.3	VWSG node.....	47
3.3.4	Sensors interrogation process .....	48
3.4	Initial calibration results on the VWSG and results.....	49
3.5	Summary .....	52
Chapter 4. Robotic deployment of sensors .....		54
4.1	Background .....	54
4.1.1	Automation during the operation/maintenance phase .....	54
4.1.2	Automation during construction phase .....	56
4.1.3	Automated deployment of sensors using UAVs and mobile robots .....	58
4.2	Robotic process to deploy VWSGs on smart segment .....	59
4.2.1	Robotic tools.....	59
4.2.2	Robotic process.....	63
4.2.3	Sensor packaging .....	65
4.3	Pick-and-place implementation .....	65
4.3.1	Steps to evaluate PnP performance of the magnetic box.....	67

4.3.2	Results .....	69
4.4	Summary .....	71
Chapter 5.	Automated Manufacturing of Smart tunnel Segment .....	74
5.1	Background .....	74
5.2	Design and fabrication of lab-scale segment .....	76
5.2.1	Discussion on the scale .....	76
5.2.2	Characterisation of concrete .....	78
5.3	Smart segment characterisation and performance assessment.....	81
5.3.1	Mechanical tests on segments.....	81
5.3.2	Instrumented segments on straight beams .....	86
5.4	Smart segment performance evaluation.....	91
5.4.1	Steps.....	91
5.4.2	Sensors.....	92
5.4.3	Number of segments .....	93
5.4.4	Tests .....	93
5.4.5	Models (numerical and analytical) .....	93
5.4.6	Performance evaluation. ....	94
5.5	Results and discussion .....	96
5.5.1	Results .....	96
5.5.2	Discussion.....	98
5.6	Summary .....	100
Chapter 6.	Economic justification for smart segments.....	101
6.1	Justification of the study .....	101
6.1.1	Stakeholders needs' identification .....	101
6.1.2	Benefits and advantages of smart segments .....	103
6.2	Cost-benefit analysis .....	105
6.2.1	General considerations/assumptions.....	106

6.2.2	Cost benefit study .....	109
6.3	Results and discussions .....	111
6.3.1	NPV .....	111
6.3.2	Additional discussions .....	116
6.4	Summary .....	120
Chapter 7. Conclusions and Futures Works .....		122
7.1	Conclusions .....	122
7.2	Future work .....	123
7.2.1	Automated deployment on real segments .....	123
7.2.2	X-ray computerised tomography .....	123
7.2.3	Characterisation of sensors behaviour for instrumented ring .....	124
7.2.4	Deployment of additional sensors .....	124
7.2.5	Cost Benefit Analysis using a probabilistic approach. ....	125
A.	Appendix .....	126
Bibliography .....		181



# List of Figures

Figure 2-1. Representation of a segmental tunnel ring with the key in blue, the trapezoidal at each side of the key and the rectangular in red.....	9
Figure 2-2. Examples of (a) bending and (b) compression tests performed on full scale segments from the Monte Liro Water Tunnel <sup>12</sup> .....	11
Figure 2-3. Production of tunnel precast segments. (a) Demoulding; (b), (c), (d) cleaning and preparation of mould, (e) & (f) concreting and smoothing of segments extrados (g) removing residual concrete (h)segment entering curing chamber. All photos courtesy of the International Tunnelling and Underground Space Association (ITA- AITES).....	14
Figure 2-4. Resistive strain gauge organised in a quarter-bridge Wheatstone configuration .....	20
Figure 2-5. Vibrating wire operation principle .....	21
Figure 2-6. Representation of an FBG operational principle .....	22
Figure 2-10. FOS classification .....	23
Figure 2-7. Standalone Wireless system (a) schematic representation (b) example of lab-made wireless node to interrogate a vibrating wire strain gauge.....	25
Figure 2-8. Wireless network topology .....	26
Figure 2-9. Wireless Technology <sup>53,54</sup> .....	27
Figure 2-11. Loadings on tunnel segment pre-construction. The top line shows image of segment during various manipulation pre-construction and the second line show the corresponding structural diagram showing the types of loadings on the segment. The image have been obtained courtesy of ITATech <sup>10</sup> .....	37
Figure 3-1. Example of an EGP embedment strain sensor. Image courtesy Micro Measurement.....	41
Figure 3-2. Examples of KM strain transducers. Image courtesy Tokyo Measurement Instruments Laboratory Co., Ltd. The image presents three specimens of strain transducers which uses vary depending on their application. The smallest option would be more adapted to be used in laboratory concrete elements. ....	42
Figure 3-3. Examples of Geokon concrete embedment VWSG. Image courtesy Geokon	43
Figure 3-4. Ad-hoc Interrogation device .....	48
Figure 3-5. VWSG interrogation flowchart.....	49
Figure 3-6. Tensile tester during VWSG calibration test.....	51

Figure 3-7. An example of VWSGs calibration results on one VWSG. The correlation is significantly high and the gauge factor close to the one specified by the manufacturer which is 0.395.....	51
Figure 4-1. Robotic system used in concrete prefab factories. (a), (b) Robotic arm used for shuttering and deshuttering in (b) notice the combine function of a ‘plotter’ to help in the positioning of shutters. (c) A dedicated plotter that transfers CAD data to nozzle to plot on shuttering profile (d) robotic arm used for placing and removing profiles. Images courtesy of Progress (a and b) and Weckenmann. (c and d) .....	58
Figure 4-2. Different deployments of wireless environmental sensors using UAVs <sup>163</sup> ....	61
Figure 4-3. Universal Robot 10. UR 10 is a 6-axis robotic arm with a payload capacity of 10 kilogrammes and a reach of 1300 mm.....	62
Figure 4-4. (a) 3D illustration of the ad-hoc gripper finger (b) the robotiq Hand E gripper equipped with 3D-printed fingers .....	64
Figure 4-5. VWSG box.....	66
Figure 4-6. Modified box to improve the gripping.....	66
Figure 4-7. Set up for PnP .....	67
Figure 4-8. On the left. A photo of the box after the pose. On the right, a representative drawing with geometric deviations.....	69
Figure 4-9. VWSG Strain transformation (a) ideal state (b) rotated state .....	69
Figure 4-10. Statistical distributions of geometric errors $\Delta X$ , $\Delta Y$ , and $\Delta\theta$ for the manual and robotic scenarios. The density is expressed in proportion. ....	72
Figure 4-11. Average Strain Error with Standard Deviation.....	73
Figure 5-1. Manual deployment of an embedded sensor for a precast grandstand element <sup>168</sup> .....	75
Figure 5-2. Lower Thames Crossing tunnel ring geometry.....	76
Figure 5-3. Geometry of small-scale segment (dimensions in mm).....	79
Figure 5-4. Three-point-bending test experimental layout .....	82
Figure 5-5. Compression test experimental layout .....	82
Figure 5-6. On the left the segment formwork is shown. The right shows the segment being casted. ....	84
Figure 5-7. Left: segment on the Dartec rig. Right: segment in hydraulic testing rig.....	84
Figure 5-8. Displacement versus Load of segments with and without dummy box.....	85
Figure 5-9. Cracking patterns of instrumented (above) and plain beam (below).....	85

Figure 5-10 Segment formwork with a new partition divides the formwork into two regions for pouring the same SFRC. This configuration enables simultaneous casting of an instrumented segment and a plain segment, the latter used in the failure test.....	86
Figure 5-11. Experimental setup of 3-point bending test on 100x100x500 mm beam. ....	88
Figure 5-12. Timeseries for measured Load, Displacement, and the Strains. The left column shows the raw measurements and the right column present the same measurements readjusted to eliminate the drift .....	89
Figure 5-13. FE model for the prismatic SFRC beam. ....	90
Figure 5-14. Robotic deployment of the VWSGs on smart tunnel segment formwork. ...	91
Figure 5-15. VWSGs deployed on the smart segment formwork .....	92
Figure 5-16. Smart segment in the flexural rig during the cyclic test .....	93
Figure 5-17. Illustration of straight beam approximation of a curved beam .....	94
Figure 5-18. Curved beam FE model .....	95
Figure 5-19. Time series showing measured strains during the cyclic three-point bending test.....	96
Figure 5-20. Curved beam FE model .....	97
Figure 5-21. Example of peak strains scatter plot illustrating the definition of the strain transfer .....	97
Figure 6-1. Tunnel ring equipped with smart segments. ....	102
Figure 6-2. Typical instrumented tunnel section. In this case the instrumented section has three instrumented rings. ....	108
Figure 6-3. NPV results in different scenarios showing the constant negative NPV for the baseline solution .....	113
Figure 6-4. Lowest (top) and highest (bottom) positive NPV for smart segment solution. ....	114
Figure 6-5. Lowest (top) and highest (bottom) positive NPV for on-site wireless solution. ....	115
Figure 6-6. Lowest (top) and highest (bottom) positive NPV for on-site wired solution. ....	116

# List of Tables

Table 2-1. Summary of typical internal diameters in function of ring configurations <sup>10</sup> ...	10
Table 2-2. Examples of parameters monitored in tunnel project and corresponding instrumentation .....	18
Table 2-3. Wireless technologies used for SHM <sup>53,54</sup> .....	27
Table 2-4. Summary of instrumented projects consulted .....	36
Table 3-1 Comparison of Technical Specifications between Electronic Sensors (EGP and KM) and VWSG Geokon Model 4202 .....	45
Table 4-1. Robotic solutions for manufacturing of tunnel segments. Images courtesy of Herrenknecht Formwork.....	60
Table 4-2. Two-finger grippers selections. Images courtesy of Robotiq. ....	64
Table 4-3. Geometric and strain errors of robotic PnP vs Manual PnP.....	70
Table 5-1. List of segment model scales.....	77
Table 5-2. Scale down aggregate max size and fibres length .....	78
Table 5-3. Steel fibres properties .....	80
Table 5-4. Range of proportions for SFRC components <sup>179</sup> .....	80
Table 5-5. Steel reinforced concrete mix design .....	80
Table 5-6. SFRC mechanical properties. Where $f_L$ , $f_{Ri}$ are respectively the elastic limit and the residual strength with crack opening at 0.5, 1.5, 2.5, and 3.5 mm as defined in <sup>183</sup> ....	81
Table 5-7. Lab-scale smart segment strain transfer .....	98
Table 6-1. Smart segments Stakeholders' needs .....	103
Table 6-2. Types of inspection conducted on tunnels <sup>191,192</sup> .....	106
Table 6-3. Simulation on the amount of general and principal inspections.....	107
Table 6-4. Cashflow for different simulations .....	110
Table 6-5. Investment cost for the 4 instrumentation solutions.....	110
Table 6-6. NPV code-coloured matrix for the three instrumented solutions. ....	118
Table 6-7. Safety code-coloured matrix for the three instrumented solutions.....	119
Table 6-8. Data quality code-coloured matrix for the three instrumented solutions .....	120

# List of Appendices

A. 1 Sensors datasheet .....	127
A. 2 Arduino Code .....	132
A. 3 VWSG initial calibration results .....	137
A. 4 Smart segment Peak strains – Finite Element Model .....	142
A. 5 Smart segment Peak strains – Straight beam approximation .....	152
A. 6 Tunnel Monitored Reviewed From COWI .....	162
A. 7 Instrumentation Cost .....	170
A. 8 NPV Detailed Results .....	174

# Glossary of Abbreviations

<b>CBA</b>	Cost-Benefit Analysis
<b>DFOS:</b>	Distributed Fibre Optic Sensor
<b>FBG:</b>	Fibre Bragg Gratings
<b>FO:</b>	Fibre Optic
<b>FOS:</b>	Fibre Optic Sensor
<b>FRC:</b>	Fibre reinforced concrete
<b>GF:</b>	Gauge Factor
<b>ICC:</b>	Interclass Correlation Coefficient
<b>LTC:</b>	London Thames Crossing
<b>LVDT:</b>	Linear Variable Differential Transformers
<b>MEMS:</b>	Micro electromechanical systems
<b>NDT:</b>	Non-Destructive Technique
<b>NPV:</b>	Net-Present Value
<b>PnP:</b>	Pick-and-Place
<b>SFRC:</b>	Steel Fibre Reinforced Concrete
<b>SHM:</b>	Structural Health Monitoring
<b>STCR:</b>	Single Task Construction Robots
<b>TBM:</b>	Tunnel Boring Machine
<b>UAV:</b>	Unmanned Aerial Vehicle
<b>UK</b>	United Kingdom
<b>UR10:</b>	Universal Robot with 10kg payload
<b>VWGS:</b>	Vibrating Wire Strain Gauge

**VW:** Vibrating Wire  
**WSN:** Wireless Sensor Network

# Chapter 1. Introduction

Tunnels, as critical and costly infrastructure assets, require great care not only in their design and construction but also during their operation. The latter is assured by putting in place a monitoring framework to regularly inspect and maintain tunnels ensuring therefore their safety, structural integrity, and optimal functionality. The United Kingdom alone, has an extensive network of about 33 km<sup>1</sup> of road tunnels that necessitate annual inspections and periodic maintenance. The imperative to enhance the resilience of these structures and extend their lifespan has led to a growing emphasis on integrating technology and meticulous maintenance planning throughout the tunnel's operational lifetime<sup>2</sup>.

Traditionally, tunnel inspections have relied on human intervention and periodic assessments, presenting challenges such as time-consuming processes, high costs, and limited real-time data provision. The gradual integration of new methods alongside conventional techniques supports inspection operations preceding maintenance or repairs. This evolving landscape has ultimately seen a surge of interest in instrumenting tunnels with permanent sensors to allow later Structural Health Monitoring (SHM).

However, conventional sensor instrumentation faces certain limitations, including wired connections that hinder modularity and the lack of oversight of structural behaviour before sensor fit-out post-construction. While wired SHM systems represent a mature technology, recent advances in wireless sensing offer a more flexible alternative, particularly suited for modular constructions like segmental tunnels. Furthermore, the miniaturization of sensor nodes enables seamless integration into precast concrete elements without significant size effects on elements.

The growing demand for comprehensive insights at every stage of the construction life cycle<sup>3,4</sup> propels the integration of monitoring systems to capture the structural behaviour of precast elements before installation. Modular wireless SHM systems not only capture early-stage structural behaviour but later can seamlessly form ad-hoc wireless networks once deployed within the infrastructure.

On the other hand, the precast manufacturing of elements, though one of the most automated areas of the construction fields, are increasingly leveraging the use of articulated robotic solutions to enhance their processes<sup>5</sup>. These robotic solutions in form of industrial robotic arms contribute to various tasks such as preparing formwork, cleaning, lubricating,



tightening bolts, and post-concreting smoothing of precast elements surfaces. While not yet pervasive in the industry, these robotic solutions can enhance safety and operational efficiency. Moreover, these existing robotics solutions hold the potential to be repurposed for deploying sensors.

Against this background, this project aims to present a proof of concept for the automated deployment of sensors in lab-scaled smart tunnel segment. Smart segment being concrete precast elements equipped with sensors able to track its properties during the segment lifetime. In this innovative approach, strain sensors will be deployed using a manufacturing robotic arm, showcasing the potential synergy between robotics and the accurate deployment of sensors to support tunnels inspections. Characterisation tests were later conducted on robotically instrumented lab-scale smart segments.

## **1.1 Research Justification**

The integration of a SHM system to civil infrastructures can reduce the operation and maintenance costs by producing better quality information<sup>6,7</sup> to support on-site statutory inspection visits. Smart segments enhance this advantage by allowing the structural monitoring of individual instrumented segments before they are installed. Sensors embedded in precast segment can track physical as well as mechanical properties from early stages while potentially used to support quality control operations during the manufacturing.

On-site Wired and wireless monitoring systems are usually deployed during the fitout period following the completion of the construction. They are labour intensive and if done while the construction is still ongoing will necessitate to halt the other works and can potentially lead to delays. The potential gains in using smart segments to reduce or completely eliminate human intervention on-site are immense as the deployment is done by an automated process in a more controlled environment than a construction worksite.

In terms of automation, the precast manufacturing of elements is the more advanced field in the construction industry. In addition to well established automated process to manufacture structural precast elements, modern precast factories are starting to integrate articulated robots equipped with dedicated end-tools to perform some operations currently done by humans. While this is an encouraging trend, there is still untapped potential worth exploring. In this work, a demonstration on the repurposing of the robotic built-in capability in the precast industry to extend the reach of operations that can be done is demonstrated.

At lab-scale a collaborative robotic arm equipped with an ad-hoc end-tool was used to perform the task of deploying sensors.

In the instrumentation of concrete elements, a reliable capturing of the structural behaviour of elements requires an accurate placement of the sensors. For embedded sensors, this can be achieved by tying them to the reinforcement to prevent them from moving during the casting process. In the case of fibre reinforced concrete (FRC), though, this can represent a challenge. Through a combination of design of a packaging of adequate shape and size and the use of magnets to improve the adhesion of the sensor packaging on the steel formwork accurate robotic placement of sensors was achieved.

## **1.2 Principal contributions**

The principal contributions to the field of smart infrastructures and automation in construction are as follows:

### **1. Exploration of the notion of tunnel smart segment:**

This research project explored the notion of smart tunnel segments as components of tunnel Structural Health Monitoring (SHM), with the main aim of capturing pre-construction structural behaviour, which can be more critical for steel-reinforced concrete segments than construction and service loadings.

This approach has clear potential, when fully deployed on an actual tunnel project, to improve the understanding of the structural behaviour of individual segments in a phase that is usually not considered, as the current practice is to instrument the tunnel post-construction. The information gathered before and after construction would help validate structural design assumptions, providing a more comprehensive outlook than on-site wired and wireless approaches.

### **2. Smart segment Modularity:**

The Smart segment is designed to incorporate wireless sensors. Similar to their parent segments, these sensors embedded within the segments will be modular, offering the potential to establish ad-hoc wireless networks when fully developed. This will enable self-identification, location reporting, and continuous monitoring of structural information throughout the entire asset lifecycle.

While this project did not fully delve into the development of wireless solutions, it demonstrated the automated deployment of such wireless nodes on 3D-printed prototypes and establish a framework to evaluate the repeatability of the process. Delivering a truly integrated monitoring without additional human effort increasing simultaneously the sensor reliability and performance.

### **3. Economic Justification of Smart Segments:**

The potential for scaling the smart segment technology was demonstrated through an economic justification. This involved both quantitative analysis, employing the NPV, and qualitative analysis, integrating factors such as enhanced safety and improved information quality. The study highlighted the demonstrated superiority of smart segments over on-site wireless and wired solutions. Additionally, it provides a valuable decision-making tool for selecting appropriate instrumentation solutions and a framework for producing cost-benefit analysis of tunnels SHM system.

## **1.3 Thesis overview**

This thesis starts by presenting generalities on segmental tunnels, their design principles and their manufacturing process. Later, the tunnels instrumentation methods are presented and some case studies of most recent tunnels in Europe have been reviewed to highlight the types of parameters and methods currently used to monitor their structural behaviours.

In the next chapter, the strain sensors selection process is presented. Electronics and vibrating wire technologies were favoured for their potential to be integrated into a modular system. A series of criteria such as the strain transfer capability, the ease of interrogation and communication, the sensor degradation, the sensor outer body material and the cost were presented and thoroughly discussed to justify the choice of vibrating wire strain gauges (VWSGs) as the best alternative. Later both the interrogation process of the VWSGs and their calibration is presented.

Chapter 4 focuses at discussing the robotics deployment of sensors. It starts by reviewing existing automation solutions during the operation and maintenance phases of infrastructures followed by existing solutions during the construction, before presenting some cases of automated sensors deployment. The chapter then present the robotic tool used in this study and the end-tool to pick-and-place (PnP) the sensors. The chapter finally outlines the

methodology to evaluate the PnP process, the implementation on lab designed setup and results obtained after implementation on a flat surface.

In chapter 5, the design, fabrication, and testing of lab-scale smart tunnel segment is presented. After discussing considerations that led to the choice of the downsizing scale of the lab segment based on early design of the London Thames Crossing (LTC), the discussion moves on presenting the steps involved in the manufacturing, testing and evaluating the smart segments. The evaluation of segments containing two VWSGs robotically deployed sensors involved defining two theoretical models to compare measured strains in order to calculate strains transfers. The strain transfers obtained on 10 smart segments were assessed for repeatability.

Chapter 6 showcases the collaboration with the industry undertaken during the course of this project by presenting an economic justification for using smart segments. After identifying main stakeholders needs, the discussion moved to presenting the different benefits of using smart segment when comparing it to a baseline solution (zero instrumentation), on-site wired and wireless solutions. The NPV was used to evaluate the economic viability of smart segment when compared to other solutions. Finally, and in order to bolster the choice of smart segment a qualitative approach was suggested based on criteria such as safety and data quality.

Chapter 7 concludes this work and suggest future works.

## **1.4 Publications**

### **1.4.1 Journal Articles**

#### **Manuscript submitted to the IEEE Journal of Sensors**

1. **T. Tshimbombo**, M Perry, H Dow, J McAlorum, C Hoy, and C Litina, “Robotic Deployment of Embedded Strain Sensors in Precast Tunnel Segments”, IEEE Sensors Journal, vol xx, pp xx-xxx, 202x

### **1.4.2 Conference Papers**

1. **Tresor Tshimbombo**, Marcus Perry, Hamish Dow, Jack McAlorum, Chris Hoy, and Chrysoula Litina "Automated manufacturing of smart tunnel segment", Proc.

SPIE 12486, Sensors and Smart Structures Technologies for Civil, Mechanical, and Aerospace Systems 2023, 124861C (18 April 2023); <https://doi.org/10.1117/12.2657113>

2. **T. Tshimbombo**, M. Perry, C. Hoy, E. Tzoura, C. Vlachakis and J. McAlorum, "Robotic Installation of Wireless Strain Gauges into Precast Concrete Elements," 2021 IEEE International Instrumentation and Measurement Technology Conference (I2MTC), Glasgow, United Kingdom, 2021, pp. 1-6, doi: 10.1109/I2MTC50364.2021.9459824.

# Chapter 2. Tunnels And Their Instrumentation

This chapter takes a closer look at tunnels and their instrumentation, offering an overview of generalities related to the design and construction of tunnels, with a specific emphasis on segmental tunnels. Following this, it discusses different tunnel instrumentation techniques, both traditional and recent, with a focus on sensor-based solutions. Concluding the chapter, there's a review of real-world tunnels, discussing their limitations that led to make a compelling case for the adoption of smart segments.

## 2.1 Tunnel Generalities

### 2.1.1 Some notions on tunnels

Tunnels are significant underground structures constructed for various purposes, including transportation (such as roads and railways), mining, hydroelectric power generation, rain-water or wastewater management, and utility conduit installation (for electrical cabling)<sup>8</sup>. Tunnels can be categorized based on their construction method (e.g., cut and open, bored) or the services they provide (e.g., road, railway, wastewater handling), the nature of the surrounding soil (soft ground or hard ground), or the materials used in their construction. Concerning the latter classification, masonry, cast iron, and concrete are frequently employed. Masonry tunnels are often associated with historical structures, while large-scale use of concrete sprayed linings is uncommon, segmental linings are prevalent in contemporary major projects. Therefore, this thesis focused on segmental linings.

### 2.1.2 Concrete tunnel segments

Concrete segmental linings offer versatility in tunnel construction, making them suitable for various types of relatively uniform ground. The successful execution of a tunnel project depends on a meticulous design process that considers all phases involved.

The construction process begins at the precast manufacturing plant, where segments are fabricated to precise design specifications, considering material properties (mechanical, physical, and chemical) and geometric tolerances. Once these segments are cured, they are transported to the construction site for installation. Tunnel boring machines (TBMs) are

used, along with manual labour, to complete the assembly, which includes tasks like tightening bolts and fitting gaskets and other finishing components.

In this section, a concise presentation of the steps involved in the design, manufacturing, and installation of tunnel segments is presented. Furthermore, a brief description of the common types of failures usually encountered in tunnel segments is given.

### 2.1.2.1 Design considerations.

Beyond the design considerations common to all types of tunnels presented in specialised literature<sup>9</sup>, the aim here is to discuss two important aspects of segments design:

- The geometric design
- The structural design

#### 2.1.2.1.1 Geometric design

The following 4 elements are important parameters to determine during the geometric design of a tunnel (Figure 2-1 shows a typical tunnel ring):

- **Thickness:** The initial thickness of the segment is determined by considering historical data, regulatory guidelines, and structural requirements. The tunnel must be robust enough to withstand the stresses of installation, transient loads during construction, and the service loads it will encounter once in operation.
- **Internal Diameter:** The diameter of the segment is a critical design element, and it varies depending on the type of tunnel. For road tunnels, it must meet specific horizontal and vertical clearances, as well as accommodate necessary equipment. Utility tunnels consider the size requirements of utilities and the space needed for maintenance. Water tunnels' diameter is determined by factors such as the volume of water to be conveyed or design storm criteria set by local authorities.
- **Length of the Ring:** Achieving the right balance in the length of tunnel rings is essential. Longer segments can reduce the number of joints, leading to cost savings in production and maintenance. On the other hand, shorter segments make handling and erection more manageable.
- **Ring Configurations:** The number of segments in each ring is a critical factor optimised for the specific tunnel project. More rings can facilitate transportation, handling, and segment erection. Conversely, fewer segments (larger

segments) can reduce production costs, resulting in stiffer rings, and expedited construction process.

- **Individual Segment Geometry:** There are four primary types of segment geometries to choose from: hexagonal, rectangular (shown in Figure 2-1), trapezoidal, and rhomboidal. The selection depends on project-specific requirements, prevailing ground conditions, and the availability of construction tools. Each geometry type has its unique advantages and disadvantages.

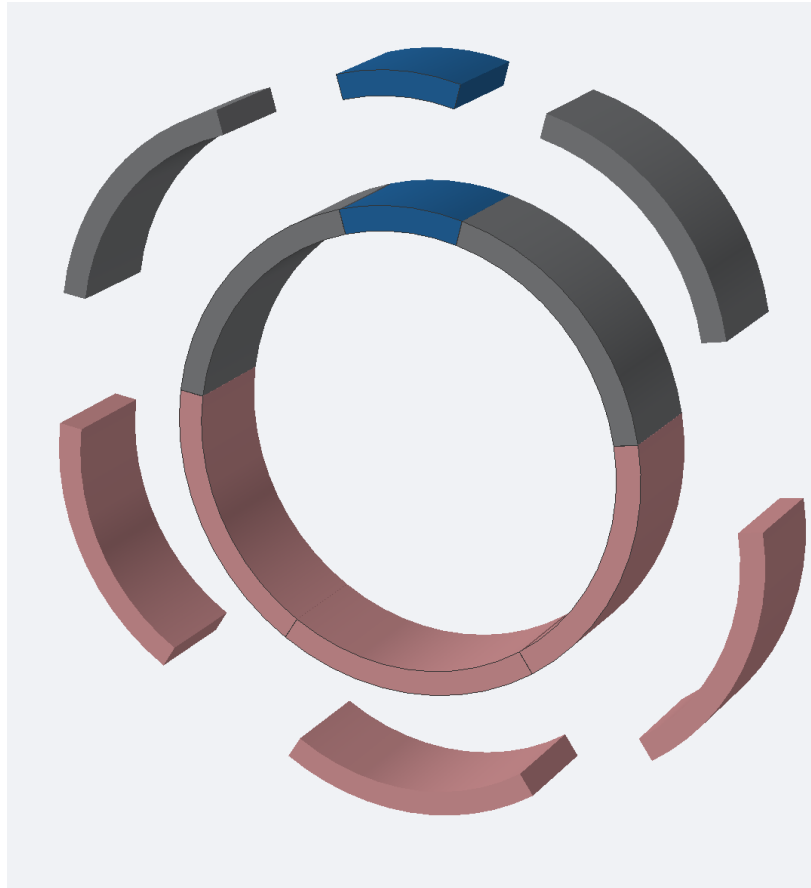


Figure 2-1. Representation of a segmental tunnel ring with the key in blue, the trapezoidal at each side of the key and the rectangular in red.

Based on the review of tunnels projects over the years, Table 2-1 summarised the typical values for the internal diameter in function of the ring configuration. Such information is usually employed by tunnel engineers in early design stages.

#### 2.1.2.1.2 Structural design

There are three methods commonly used to structurally design tunnel segments:

- Analytical method



- Numerical method
- Design aided by full scale testing.

Depending on the materials (bar reinforced or fibre reinforced concrete), there would be some specification of the design method. In this study, the main focus was on briefly presenting the design methods specific to FRC.

Table 2-1. Summary of typical internal diameters in function of ring configurations <sup>10</sup>

<b>Internal Diameter (m)</b>	<b>Configuration</b>
4-6	5+1 (ordinary + key)
6-8	6+1
8-11	7+1
11-14	8 ordinary segments.
14+	9+1

### ***Analytical method***

The design of FRC sections detailed in dedicated guidelines<sup>11</sup> defines key parameters, and the analysis is based on the post-cracked behaviour of residual strength provided by fibres. In Service Limit States (SLS), fibres can improve FRC durability behaviour by reducing crack openings and spacing. In Ultimate Service State (ULS), the ductility provided by the fibres can generally be considered when checking the stability of the elements.

### ***Numerical method***

Numerical method based on Finite Element Analysis can allow a more refined elastic or plastic analysis FRC behaviour. While it is a powerful tool, it is generally recommended to use proven hand calculations method to check the reliability of the modelling. Numerical modelling is also more adequate, although complex and mostly limited in the research field, to simulate FRC time dependant behaviour such as creep of both concrete and fibres.

For the two methods, though, the following structural design checks are performed:

- Individual segments loads are checked against flexion loads during the manutention and transport of segments from the manufacturing plant to the construction site. They are also checked against compression loads from the TBM thrust during the installation in rings.
- Once installed, a series of critical rings are checked against the permanent ground loading and other unusual loadings like earthquake, flooding, collision, or fire.

- The general bending of the tunnel along the axis is also checked.

***Design aided by full scale testing.***

In certain cases, and given the novel nature of the FRC, the segment design is aided by laboratory testing results on real-world segments. The tests commonly involved are:

- The 3-point or 4-point bending test (Figure 2-2 (a)) aiming at evaluating the flexion bearing capacity of segment under temporary cases (demoulding, storage, and transport) and under asymmetrical soil pressure.
- The compression test (Figure 2-2 (b)) aimed at evaluating the effects of the TBM thrust on segments during their installation.

The results of the tests permit to identify critical load at which cracks starts appearing and the propagation of the latter as much as loads at which the segment bursts under compression. The identification of such elements can play an important role at iteratively modifying the dimension and the composition of the FRC segment, to accordingly calibrate the TBM rams loading capacity to match more accurately the real-world conditions.



(a)



(b)

Figure 2-2. Examples of (a) bending and (b) compression tests performed on full scale segments from the Monte Liro Water Tunnel<sup>12</sup>

### **2.1.2.2 Segment Manufacturing**

Tunnel segments are produced in specialized precast facilities, employing dedicated equipment and stringent quality control measures to achieve desired physical, mechanical, and geometric performances. Due to the controlled environment they operate in, precast factories are among the construction sectors with the highest level of automation integration.

#### 2.1.2.2.1 Types of Production

Two methods are commonly employed to manufacture segments. They differentiate by the location of the moulds.

- *Static Moulds*: in this method, moulds remain stationary while the concrete delivery system is mobile. Multiple static moulds are typically used, which may lead to a significant factory footprint. This approach is suitable for factories with moderate production volumes.
- *Carousel System*: The carousel system involves mobile moulds and a fixed concrete delivery system. It is particularly well-suited for high-volume production plants. This system usually occupies less space compared to static moulds and allows for efficient production. The carousel system is also highly conducive to further automation integration.

#### 2.1.2.2.2 Steps for Segment Production

The production process for precast segments, shown in Figure 2-3, regardless of the chosen method, follows a consistent sequence of steps:

- *Mould Preparation*: Before casting, the moulds undergo meticulous preparation, including thorough cleaning to ensure a clean and smooth surface, the application of release agents or oil to facilitate easy segment removal, and the installation of joints and other necessary segment components.
- *Concreting*: Following mould preparation, concrete is poured into the moulds. Depending on the factory's setup, this can be accomplished using either a fixed (in a carousel system) or mobile concreting system (in a static system). Great care is taken to ensure that the concrete is correctly placed, compacted, and finished to meet the specified design requirements.
- *Curing*: The freshly cast segments are placed in curing chambers. Curing is a critical step for achieving the desired strength and durability of the segments. It is typically conducted using steam or dry heat. This controlled curing process allows for demoulding in as little as 6-7 hours, which expedites the production process.
- *Demoulding and Storage*: Once the segments have completed the curing process, they are demoulded, undergo meticulous quality inspection, and are then transported to a designated storage area within the manufacturing facility. These cured segments are organised and prepared for transportation to the construction site.

In 4.1.2.2 opportunities to embed embedded sensors in some or all of these phases using industrial robotic arm in a modern precast manufacturing plant are discussed.

### **2.1.2.3 Segmental tunnel lining**

Once manufactured segments are on-site, they are erected using a tunnel boring machine (TBM). The TBM choice is the subject of a thorough selection process as it must take into account factors such as: the ground conditions, the segments material properties, the project schedule, access and logistic, maintenance and serviceability, experience and expertise, etc.

In TBM excavation, the machine itself plays a dual role. It not only excavates the tunnel face using a cutting head but also simultaneously installs the segmental lining. As the TBM progresses, it positions the precast concrete segments one by one to create the tunnel's lining, lowering them into place through the back of the TBM. Often, gaskets are used between segments to provide a watertight seal and ensure structural stability.

The segments are installed sequentially to form circular rings, and some rings include "key" segments previously encountered. Once the segments are in place, grout is injected into the joints to fill gaps and improve structural integrity. Waterproofing measures may also be applied to prevent water ingress and ensure the tunnel remains dry.

During its operational lifetime, segments can be subjected to environmental and loading conditions that can with time generate deterioration including cracking, spalling, corrosion of reinforcement, excessive deformations.

Understanding and addressing these types of deterioration is essential for ensuring the long-term structural integrity and functionality of segmental tunnels. Regular inspection, maintenance, and appropriate protective measures are crucial to mitigate these issues. To support these post-construction operations, the use of instrumentation is increasingly integrated, either in the form of tools to carry out punctual measurement or structural-based instruments for continuous collection of structural information, supporting a more proactive maintenance and inspection strategy.



(a)



(b)



(c)



(d)



(e)



(f)



(g)



(h)

Figure 2-3. Production of tunnel precast segments. (a) Demoulding; (b), (c), (d) cleaning and preparation of mould, (e) & (f) concreting and smoothing of segments extrados (g) removing residual concrete (h) segment entering curing chamber. All photos courtesy of the International Tunnelling and Underground Space Association (ITA- AITES)

## **2.2 Tunnel Instrumentation**

Tunnels are complex, and expensive structures and are built to last 60-150 years<sup>6,8</sup>. Achieving such long-lasting performance relies on robust design, meticulous construction, and consistent maintenance. During both the construction and maintenance phases, it is crucial to establish a monitoring system, whether occasional or continuous, to assess the structure's physical and mechanical aspects and keep an eye on the surrounding environmental conditions. This monitoring can be conducted through scheduled or unplanned inspection visits, or in more recent times, by employing sensor-based Structural Health Monitoring (SHM) systems.

This section is an overview of the current techniques available for inspecting and evaluating tunnel structures. It begins with a discussion of conventional methods, including basic on-site visual inspections and their potential complementation with non-destructive testing (NDT). Following that, SHM techniques for tunnels were discussed, encompassing wired and wireless approaches and other modern techniques.

### **2.2.1 Traditional tunnel structural inspection**

#### **2.2.1.1 On-site visual inspections**

Tunnel inspections typically rely on experienced inspectors who conduct visual assessments. These inspections are planned beforehand and carried out on-site. The information gathered is used to create reports that inform future inspections. There are two main types of inspections: scheduled and unscheduled. Scheduled inspections can be either superficial or detailed. Superficial inspections are done more often and focus on visible defects, while detailed inspections are more thorough but less frequent. Unscheduled inspections usually occur in response to natural or human-made disasters, where an assessment of their impact is needed. In all types of inspections, modern practices involve using equipment to take on-site measurements, providing quantitative data to complement expert qualitative observations.

When it comes to tunnels, unscheduled inspections are similar across different types of tunnels. However, scheduled inspections can vary in terms of frequency and scope. For instance, a sewage tunnel might be inspected less frequently than a road tunnel due to

factors such as unpleasant odours, potential disruption of tunnel activities, and the presence of adjacent installations.

Tunnel inspectors employ a range of tools to identify potential defects within tunnels. Among these essential instruments are flashlights and headlamps for adequate illumination, mirrors for inspecting hard-to-reach areas, digital cameras for documentation, tape measures for dimensional assessments, binoculars or monocular for distant observations, magnifying glasses or loupes for detailed inspections, and borescopes to examine enclosed or inaccessible spaces. Additionally, inspectors have recently integrated remotely controlled inspection robots and drones into their inspection processes. In addition to tools to enhance the visual inspections, in some cases it is customary to pair them with NDTs.

### **2.2.1.2 On-site NDTs inspections**

To gain insights on the structural behaviour of the tunnel as a whole or of some part of interest, it is customary to run non-destructive test during the inspections or to collect samples from the structure for further analysis. NDTs offer quantitative results, and are notably rapid to implement, offering significantly greater coverage compared to traditional visual inspections. For tunnel inspection, the most commonly used NDTs are: Ground-penetrating radar (GPR)<sup>13</sup>, infrared thermography method<sup>14</sup>, and impact echo technology<sup>15</sup>. These techniques can be used separately or in conjunction. In road tunnels, for example, the inspectors can run the test along the tunnel lining on one lane while keeping the other lane open for usage. More advanced NDTs techniques such as 3D-scanner or ultrasound equipment mounted on robots or drones<sup>16-20</sup> have also been successfully demonstrated.

Traditional visual inspections, often supplemented by NDTs, and recently supported by cutting-edge technology remain widely utilised for tunnel linings and have a proven track record of delivering reliable results. However, these traditional inspection methods come with inherent limitations that can make them challenging and costly to implement:

- *Punctual Information:* Data collected through traditional inspections are typically point-in-time snapshots, with inspections conducted at intervals of several years. This means that the maintenance actions informed by intermittent inspections tends to be reactive rather than predictive. Optimising interventions through predictive maintenance is cheaper and improves a structure's resilience<sup>21</sup>.

- *Human Expertise Dependence*: These inspections heavily rely on human expertise throughout the process, from preparation to execution and post-inspection analysis, which can increase overall operational costs.
- *Accessibility Challenges*: There is a risk of missing structural defects located in areas not directly accessible to human inspectors, potentially leading to overlooked issues.
- *Health and Safety*: Inspections can be dangerous as they are often conducted at height or in hazardous environments.

To address these limitations associated with on-site inspections, a growing trend involves equipping structures with a permanent set of monitoring equipment to continuously track its structural behaviour. This practice has given rise to the field of Structural Health Monitoring (SHM).

## **2.2.2 Structural health monitoring**

SHM aims to detect, localise, and quantify the impact of damages that occur to a structure. SHM systems, comprised of monitoring systems, human expertise and algorithms, are deployed on structures to provide continuous insights into their structural behaviour. At the heart of any SHM system lie sensors, responsible for gathering data that is subsequently transmitted, processed, and analysed to generate actionable reports.

The parameters to be monitored can vary significantly depending on various factors, including the tunnel's life cycle phase, age, occurrence of exceptional events (natural or human-made), and the objectives of the monitoring. Therefore, establishing clear monitoring objectives is a crucial step before discussing which parameters to track. Some authors <sup>22</sup> identified several objectives that help define the general requirements of an SHM system:

- Monitoring and controlling the construction process.
- Validating structural designs and characterizing structural performance.
- Detecting anomalous infrastructure behaviour.
- Identifying the causes of known problems.
- Designing appropriate retrofit measures.
- Protecting existing assets and their operation.
- Assisting with infrastructure maintenance.



- Triggering pre-planned contingency actions related to emergency response efforts, including building evacuations and traffic control.
- Supporting research and development.

Once project stakeholders agree on the monitoring objectives, they can determine which parameters to monitor. These monitoring parameters can be broadly categorized into two major groups:

- *Structural parameters.* These encompass any features that enable the assessment of the structure's integrity or its structural behaviour during and after construction.
- *Environmental parameters.* This category includes any physical features of interest for understanding the surrounding environmental conditions that may affect the structural behaviour.

Table 2-2, adapted from specialised tunnel design publications<sup>23</sup>, provides a list of commonly monitored parameters for tunnels along with their corresponding instrumentation.

Table 2-2. Examples of parameters monitored in tunnel project and corresponding instrumentation.

Parameters	Instrumentation example	Category
Lateral displacement	Extensometer	Structural
Change in inclination	Electro level, tilt meters	
Changes in earth pressure	Pressure cells	
Crack or joint movement	Vibrating wire Joint-meters	
Strain in structural member	VW strain gauges	
Tunnel lining diametrical distortion	Tape extensometers Strain gauged boreholes extensometers	
Lining stresses	Pressure or load cells	Environmental
Lining leakage	Flow metre	
Changes in water pressure	Piezometers	
Vibration	seismograph	
Temperature	Thermocouples	

### 2.2.3 Wired SHM

Wired SHM methods can be characterized by the following features:

- *Wired Data Transmission:* These methods rely on wired connections to transmit data collected by sensors. Data is typically transmitted through physical cables or wires.

- *Discrete or Point Sensors*: In conventional SHM, sensors are discrete or point sensors. They are individual sensors strategically placed at specific locations to monitor specific parameters of interest within the structure.
- *Mature technology*: these methods rely on mature and well-established technology.

### 2.2.3.1 Wired SHM using point sensors

#### 2.2.3.1.1 Electronic

Electronic sensors function by measuring a structural or environmental parameter and transmitting this information in the form of an electrical signal, typically as Voltage or Current. These sensors leverage the correlation between electrical characteristics such as resistance, capacitance, or inductance, and structural parameters like strain. This correlation opens up opportunities for various measurement technologies, with resistive strain gauges being one of the most widely used.

The fundamental principle behind a strain gauge lies in the linear relationship between strain and the variation in electrical resistance, expressed in Equation ( 2-1), where R represents resistance,  $\Delta R$  the change in resistance,  $\epsilon$  the strain, and K is the gauge factor.

$$\Delta R/R = K\epsilon \quad ( 2-1)$$

A typical strain gauge consists of a zig-zag patterned metal or semiconductor wire mounted onto a plastic backing sheet. As strain is applied, both the shape of the wire and its resistance change accordingly.

However, the resistance variation in a strain gauge under typical loads is minuscule, making precise measurements challenging. To overcome this limitation, it is common practice to employ a Wheatstone Bridge configuration (see Figure 2-4), whether in a quarter, half, or full bridge setup.

Basic strain gauges can also be integrated into commercial transducers such as strain transducers, load cells, and piezometers, expanding their utility and application in various industries.

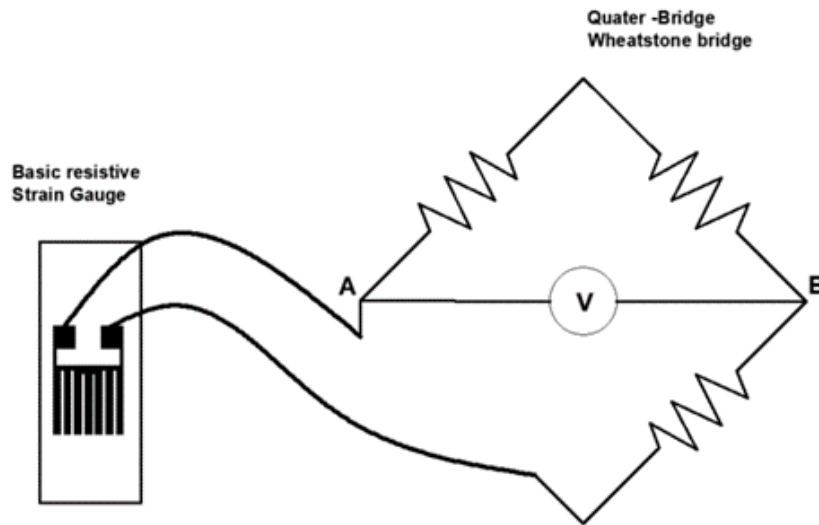


Figure 2-4. Resistive strain gauge organised in a quarter-bridge Wheatstone configuration.

Although a basic strain gauge in form of a thin metal foil can be directly embedded in concrete, after attaching it to the reinforcement<sup>24</sup>, it is usual to incorporate them inside strain transducers<sup>25</sup> with an appropriate protective coating. There are commercially available solutions that are discussed in 3.2.2.

#### 2.2.3.1.2 Vibrating wire strain gauges (VWSG)

Vibrating wires (VW) shown in Figure 2-5, were among the first types of strain sensors utilized in civil engineering applications<sup>26</sup>. The fundamental physical principle underlying these sensors involves a tensioned wire whose tension (strain) is intricately linked to its resonant frequency. Any alteration in the tension of the wire, fixed at its two extremities, leads to a corresponding change in its resonant frequency<sup>27</sup>.

The fundamental principle behind a vibrating wire strain gauge lies in the linear relationship between strain and the variation in electrical resistance, expressed in Equation ( 2-2), where  $L$ ,  $\sigma$ , and  $\rho$  represent the length of the vibrating wire, stress, and density, respectively. This provides a general equation that can correlate the resonant frequency  $f_0$  with various structural parameters. In the second part of the Equation ( 2-2),  $E$ ,  $\epsilon_0$ , and  $g$ , corresponds to the modulus of elasticity, strain, and gravitational acceleration respectively.

$$f_0 = \frac{1}{2L} \sqrt{\frac{\sigma}{\rho}} = \frac{1}{2L} \sqrt{\frac{E \varepsilon_0 g}{\rho}} \quad (2-2)$$

Similar to resistive strain gauges, the Vibrating Wire principle can be replicated and integrated into commercial transducers to measure parameters such as tilt, temperature, pore pressure, and loads.

Over the years, VW sensors have emerged as the favoured choice for embedding sensors in long-term strain monitoring of concrete-based civil structures. They offer several advantages, including greater accuracy compared to electrical strain gauges<sup>28</sup>, robustness<sup>29,30</sup>, and the ability to generate stable measurements<sup>31</sup>. Moreover, VW sensors exhibit minimal long-term drift, practically approaching zero-drift levels with almost zero-drift<sup>32</sup>. A further evaluation of VWSG is discussed in 3.2.3.

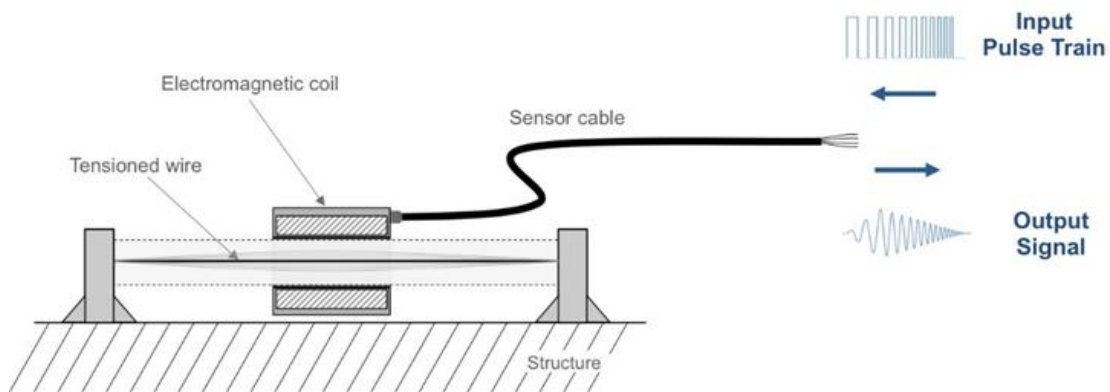


Figure 2-5. Vibrating wire operation principle

#### 2.2.3.1.3 Fibre-Bragg Gratings

Fibre Bragg Gratings (FBG), as shown in Figure 2-6, are discrete optical fibre sensors. They are created by exposing the core of a single-mode fibre to a periodic pattern of intense laser light generated by the interrogation unit. This exposure causes a permanent change in the refractive index of the fibre's core, forming a fixed index pattern known as a grating. When the fibre undergoes deformation, the wavelength of reflected light changes, enabling calibration for measuring physical parameters like temperature or structural characteristics.

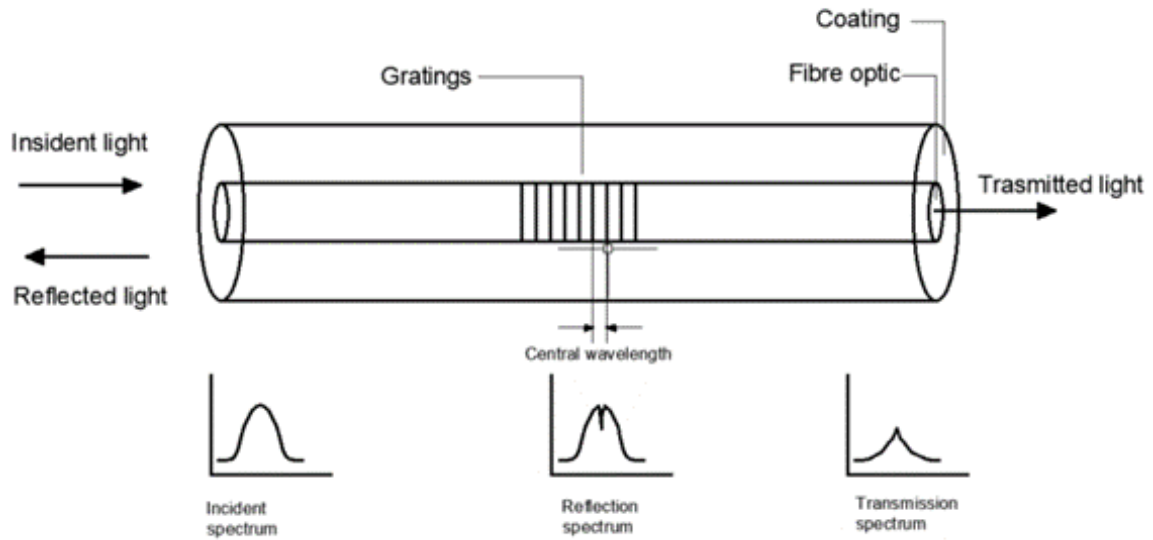


Figure 2-6. Representation of an FBG operational principle

Much like resistive and VW strain gauges, FBG technology have been adapted and incorporated into commercial transducers. This versatility allows for the measurement of various parameters, including tilts, temperature, pore pressure, and loads.

### 2.2.3.2 Wired SHM with fibre optics

#### 2.2.3.2.1 Fibre optical sensors

Fibre optics used in structural health monitoring closely resemble those used for data transmission. They consist of a thin glass wire, typically with a core diameter of 5-10  $\mu\text{m}$  and up to 125  $\mu\text{m}$  when including the cladding layer, in which light propagates and reflects along the fibre. Fibre optic sensors (FOS) used in SHM can be used either as a wire to transmit the signal or a sensing element or a combination of both. Following the mode of signal transmission, FOS can be grouped into three categories:

- **Point Sensors** (Figure 2-7.a.): These sensors provide measurement data at a specific point along the optical fibre, making them suitable for highly accurate and precise, but very localized monitoring. One such type of point fibre sensor is the Fabry-Perot interferometer. 2.2.3.1.3
- **Quasi-Distributed (Multiplexed) Sensors** (Figure 2-7.b): Quasi-distributed sensors enable multiple measurements along the fibre by multiplexing or combining data from different points. This approach offers a level of spatial coverage beyond

point sensors. An example of a sensor suitable for quasi-distributed measurements is the fibre Bragg grating (FBG).

- **Distributed Sensors** (Figure 2-7.c): Distributed sensors offer continuous measurement capabilities throughout the entire length of the optical fibre. This distributed nature makes them particularly valuable for capturing variations and changes in the monitored parameter along the fibre's span. They are appropriate for global SHM and can track effectively cracks and settlement, covering from 20cm to over 75km of distance <sup>33</sup>.

#### 2.2.3.2.2 Distributed FOS

Distributed Fibre Optics Sensors (DFOS) are the most commonly used in tunnel applications. Their ability to cover larger regions make them particularly suitable to monitor the tunnel global structural behaviour or some sections of interest. DFOS can be surface mounted on existing tunnels <sup>34-40</sup> or embedded into newly built tunnels <sup>41-46</sup>.

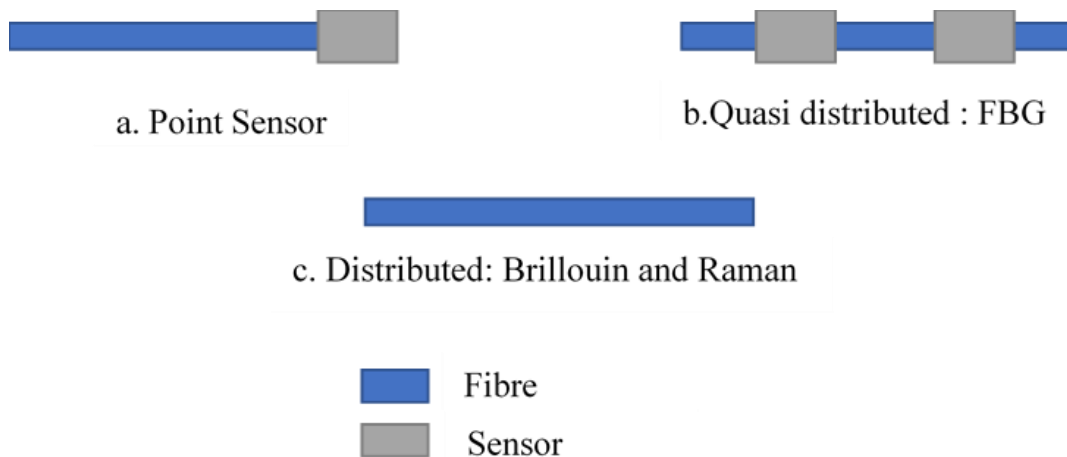


Figure 2-7. FOS classification

Although in the latter case a better adhesion to the material and protection of the fibre are more guaranteed, a larger number of existing systems are generally surface-mounted. This could be due to the fact that the parameters to monitor are not always clear when building and their identification depends on factors not always possible to predict before the construction. For example, while it is possible to anticipate the need for embedded sensors to measure water pore pressure in a section of the tunnel traversing a groundwater zone during the construction, it is not clear that during the same stage of the project the need for embedded strain and deformation sensors will manifest itself with the same criticality as when

a new construction (an underground or over ground structure) is built in the direct vicinity many years after the tunnel is completed.

Several instances of real-world deployments of DFOS in both newly-constructed and existing tunnels have been identified<sup>34–36,40,43–50</sup>. One major drawback of DFOS are the trade-offs between spatial resolutions, measurand resolutions and measurement times. Achieving highly localised measurements of strain in a structure is often difficult in practice, and this can make it challenging to interpret the data and so the impacts on structural health. An effective distributed system should therefore be complemented by point sensing in locations of interest to reduce uncertainty.

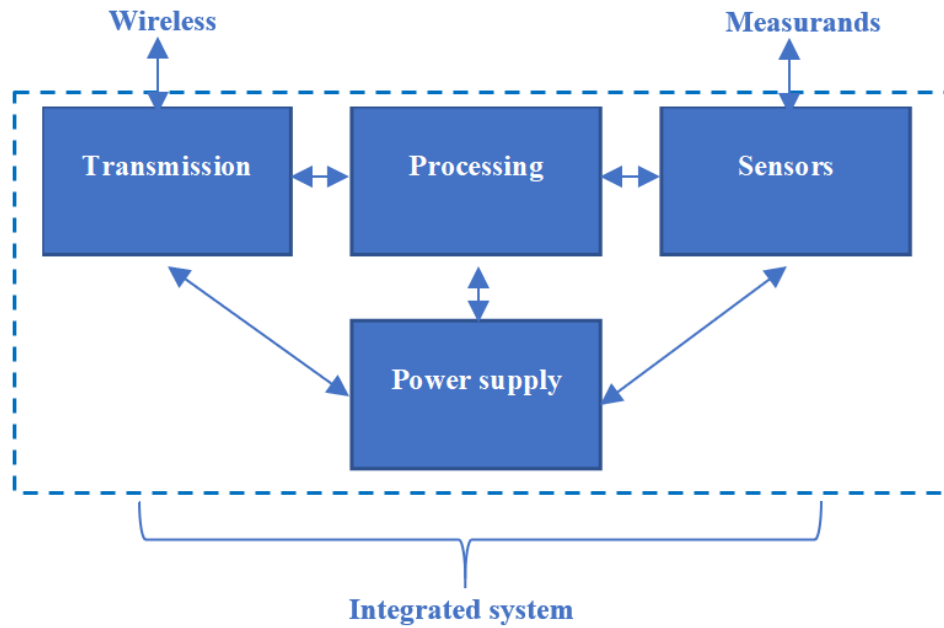
Overall, regardless of whether they are point, quasi- or fully- distributed FOS networks lack the modularity and adaptability of wireless sensor networks. Adding new sensors to the network or coupling pre-installed sensors from individual segmental elements is neither straightforward nor convenient, and the loss of a fibre line means a loss of all sensing along that line.

## **2.2.4 Wireless SHM**

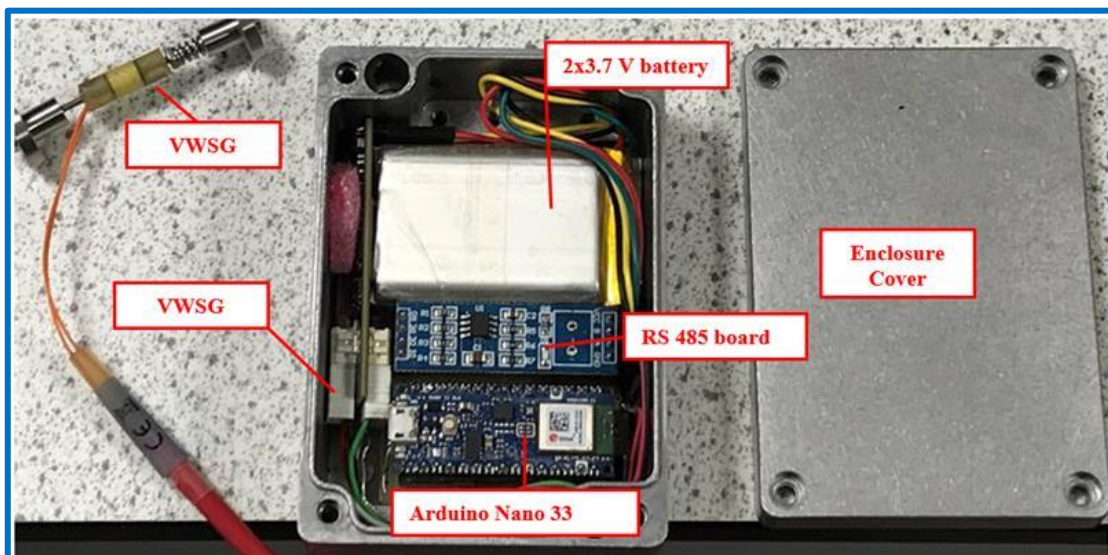
While the experimental phase of this project did not entail the creation of a fully developed wireless node, it was deemed essential to address some common features of wireless technology applicable to the smart segment once fully developed. The features of wireless technology and the issues outlined in this section were crucial aspects of the discussion that informed the selection of sensor technology, as well as the size and shape of the box to house the node electronics.

### **2.2.4.1 General features of wireless sensors**

A wireless sensor system includes the sensor, the unit for data acquisition, transmission, aggregation, processing and storage and the power unit. When assembled, the set is referred as wireless sensor or wireless node which is part of a wireless sensor network (WSN). Figure 2-8 (a) is a schematic representation of a standalone wireless node, where all the components are presented and Figure 2-8(b) is an example of a wireless node prototype assembled in the lab.



(a)



(b)

Figure 2-8. Standalone Wireless system (a) schematic representation (b) example of lab-made wireless node to interrogate a vibrating wire strain gauge

Sustained developments in the field of wireless communication and increased miniaturisation of electronics have made possible an increased integration of WSN technology replacement of wired system of conventional SHM.

Every WSN is generally composed of wireless nodes and a gateway. A node is the basic component that generally sense, process and transmit data to the gateway. The gateway can also assume the former role in addition to its primary function of acting as a gate between



data from fields' nodes and the wider network or internet. One important aspect of WSN is their topology, which is the configuration of different nodes in the network. For SHM purpose there are generally three topologies represented in Figure 2-9: star, cluster tree, and mesh networks. Star and cluster tree topologies are the most used in civil SHM applications while the mesh configuration tends to be less used because of its higher power consumption<sup>51</sup>.

The most commonly used wireless technologies for civil infrastructures SHM presented in Table 2-3, feature their typical characteristics that allow to compare them between themselves (see Figure 2-10). In addition to the four technologies listed in Table 2-3. There are other technologies relying on internet mobile technologies such as the 4G, the LTE, or the 5G, that we do not discuss here except to say that they present a higher power consumption and depend on good network signals<sup>52</sup> (difficult to achieve for tunnelling projects), which can be an important disadvantage for a continuous monitoring.

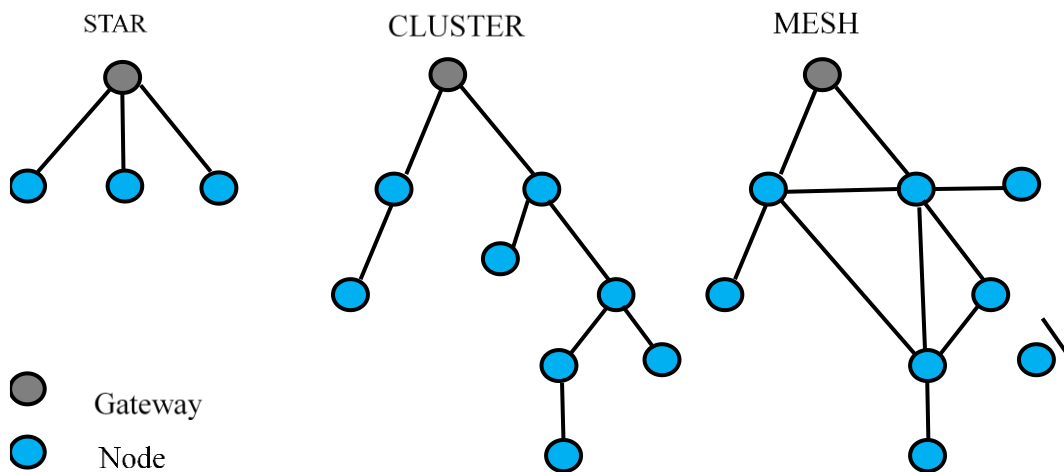


Figure 2-9. Wireless network topology

The wireless nodes used for civil SHM include both commercial and research options. While they may not always be as robust as commercial options, wireless sensing nodes used in research are customised to fit the design requirements of their deployment<sup>51</sup> Today, there are also several commercial solutions for wireless nodes with one popular choice being the *Waspote* by *Libellium*.

Table 2-3. Wireless technologies used for SHM <sup>53,54</sup>

Attribute	Wi-Fi	Bluetooth	Zigbee	LoRa
Range	15m – 100 m	10m – 1.5km	30m – 100 m	2 km – 20 km
Throughput	54 Mbps – 1.3 Gbps	125 kbps – 2 Mbps	20 kbps – 250 kbps	10 kbps – 50 kbps
Power consumption	High	Medium	Low	Low
Battery life	Minutes-hours	Hours-days	Days-years	Years
Module cost	High	Low	Low	Low

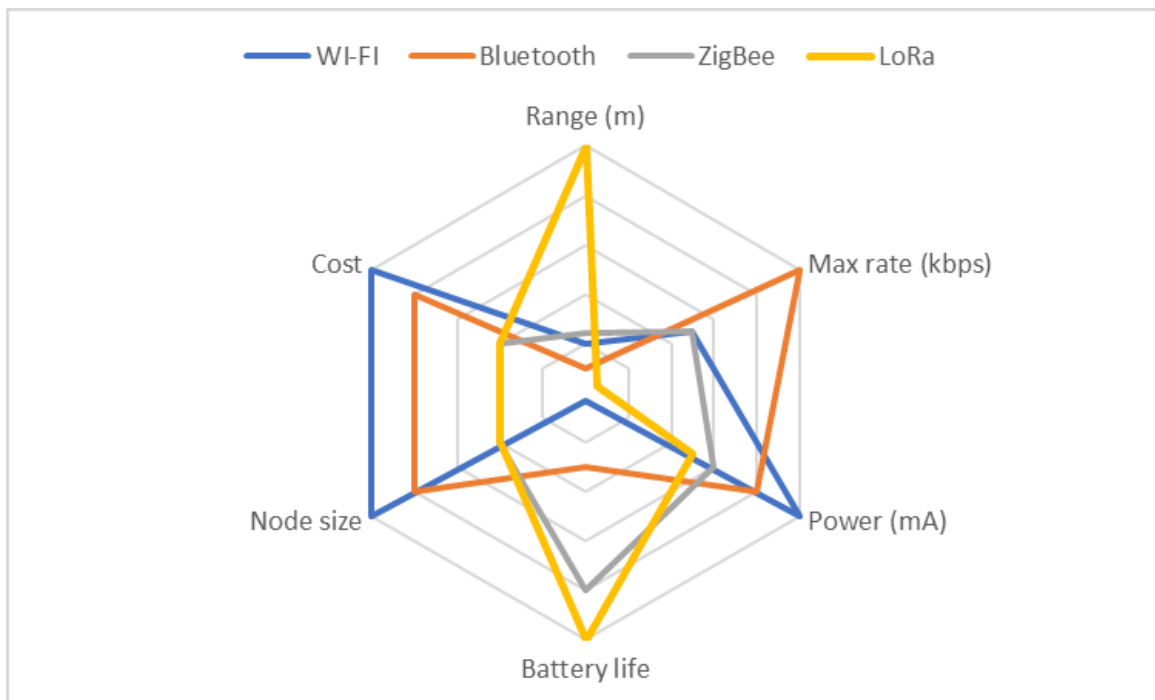


Figure 2-10. Wireless Technology <sup>53,54</sup>

### WSN Operating Systems

For a WSN to operate smoothly and efficiently, it must fulfil several critical requirements:

- *Low Power Consumption:* The network should be energy-efficient to prolong the life of battery-powered nodes.
- *Efficient Resource Management:* Effective utilization of constrained resources, including bandwidth, processing time, storage, and memory, is crucial.
- *Concurrent Task Management:* The network should efficiently manage multiple tasks happening simultaneously.
- *Sensor Compatibility:* Flexibility to accommodate different types of sensors such as strain gauges, accelerometers, and load cells is essential.

To meet these requirements on a fixed hardware platform, the role of the Operating System (OS) is pivotal. Several OSs have been developed to address these concerns, with ready-to-use solutions available for implementation in newly deployed monitoring systems. Notably, Contiki, TinyOS, and Wasmote are the three most popular open-source OSs widely used in the field of civil Structural Health Monitoring (SHM)<sup>51</sup>.

#### **2.2.4.2 Issues with wireless sensors**

While Wireless Sensor Networks (WSNs) offer numerous advantages, it is important to acknowledge the challenges they still face. Several of these challenges have been extensively explored in specialised literature<sup>51</sup>.

One of these challenges is the power consumption. Wireless sensors are uniquely affected by power supply challenges, unlike wired systems that can use cables for both sensor power and communication. This becomes particularly relevant for long-term applications. One possible solution is to replace drained batteries during scheduled maintenance, but this is feasible only for easily accessible sensors, such as surface-mounted ones. The challenge for SHM engineers is twofold: designing low-power units that are easy to recharge or replace batteries. Achieving this goal involves optimizing the power consumption of the sensing node as a whole and exploring alternatives to wired power sources.

Optimization strategies may vary depending on the sensing mode. For active sensing (where energy is imparted to the structure by the sensing node), parameters like sampling intervals, excitation power, and data transmission rates directly impact power consumption. In passive sensing, the focus shifts to memory capacity since power is supplied externally.

Energy harvesting have been studied for more than two decades by researchers and have already some real-world applications to replace conventional powering methods of autonomous sensors<sup>55-57</sup>. They are an interesting option for sensors difficult to access and help in increasing the service-life of wireless nodes<sup>55</sup>. Energy can be harvested from environmental sources such as solar, wind, mechanical, thermal, magnetic, and biochemical<sup>58</sup>. While solar, wind, and thermal energies are well known technologies and are commercially available, they are not suitable for tunnels. While approaches such as piezoelectric energy harvester can offer a viable solution in established fields<sup>59-65</sup>, or as experimental approach<sup>66-69</sup>, they are still limited and alternative approaches such as energy management strategies are preferred.

Energy management strategies could include the following:

- In road tunnels, the surrounding installations (such as HVAC and electrical systems) provide a readily available power source that can be redirected to power the wireless node.
- Due to their relatively static nature, the structural behaviour of tunnels experiences little dynamic loading and can be considered more regular compared to structures like bridges. Adjusting the sampling rate of tunnels to lower frequencies during service life can prolong battery life.
- The extension of battery life can also be achieved through the use of appropriate computation algorithms (specific examples should be provided) and selecting the most suitable wireless communication protocol.

### **2.2.5 Other examples of monitoring systems in civil engineering**

This section briefly presents other monitoring methods used in the tunnels. Some are well established techniques and others are still experimental. These techniques can be used separately or in conjunction conventional and/or sensor-based methods.

#### **2.2.5.1.1 Total station**

Total stations are widely employed in the civil engineering and construction sectors, primarily for precise infrastructure positioning on site, surveying, and mapping tasks. These instruments measure the distance from the total station to reflectors, along with vertical and horizontal angles. In recent times, advanced robotic total stations have emerged, capable of autonomously locating reflectors, thereby reducing the need for multiple on-site operators. With an angular accuracy of 0.5" and a distance accuracy of 0.6 mm+1 ppm<sup>70</sup>, modern total stations can be instrumental in monitoring structural deformations at the millimetre level, including settlement, joint movements, and critical tunnel cross-sections.

Using a highly accurate automated total station with a 2 mm precision in conjunction with distributed FOS, the Cambridge Centre for Smart Infrastructure and Construction (CSIS) successfully conducted a series of structural monitoring assessments on existing tunnel cross-sections, focusing on relative deformations<sup>34,36,71</sup>. It is worth noting that, although the total station measurements are slightly less precise compared to FO sensors (0.5 mm), they offer a distinct advantage in measuring the "absolute deformation" of the specific

tunnel ring under examination. In contrast, a distributed sensor system can only detect relative deformation within the same section.

#### 2.2.5.1.2 Photogrammetry

Photogrammetry used in SHM consists of imagery to obtain physical or geometric information of structure. In civil engineering, there are two prevalent techniques: particle image velocity (PIV) and digital image correlation (DIC).

Both techniques share a similar underlying operating principle. They are 2D methods adapted from fluid mechanics, wherein a single camera captures a sequence of images to measure the displacement field. Key features, previously identified and selected, are tracked from one point to another, enabling the correlation of displacements across the entire surface<sup>72,73</sup>.

PIV finds extensive use in controlled laboratory environments where lighting, physical conditions, and environmental factors are managed. However, in underground infrastructures, where these variables can significantly vary, PIV faces notable challenges.

DIC on the contrary have already a considerable number of applications in the real world. On such application is from the CSIC. They developed a system called CSattAR or Sattar Image Tracking (SIT) that have been successfully deployed on several underground infrastructures such as London Underground tunnels, the Bond Street upgrade project, the Royal Mail tunnel, the Moorgate escalator 3 (all in London), the CERN tunnel and a couple of more tunnels affected by the excavation of the Crossrail project<sup>74</sup>. The SIT is specifically developed to monitor the movement and deformations of tunnel linings<sup>75</sup>. The system consists of using affordable off-the-shelf digital cameras to take images of preinstalled targets and deduce deformations such as imposed ovalisation<sup>75</sup>, the settlement and the convergence<sup>72</sup> of sections of the tunnel. The precision obtained with SIT can be as low as 0.008mm<sup>72</sup> in some cases, making it equal or even better than conventional systems.

#### 2.2.5.1.3 Micro electromechanical systems

Micro electromechanical systems (MEMS) sensors widely available in smartphones and other modern electronic devices<sup>73</sup> can easily be integrated to WSN. The main advantages they present are the small sensor sizes (from micrometres to millimetres), the fact they can combine the sensing, the computation, and the communication functions of the sensors, the extended lifetime, and their lower cost.

MEMS can be employed for measuring various parameters, including strain, acceleration, tilt, and more. Real-world examples of these sensors, capable of measuring one or more of these features, already exist. One notable illustration is the Utterberry sensor developed by <sup>76</sup> at the CSIC and now available commercially <sup>77</sup>, this sensor has been successfully deployed in numerous tunnels for SHM purposes <sup>78-80</sup>.

## 2.3 Tunnel instrumentation in the real world

### 2.3.1 Real world tunnel projects with Instrumentation

Over the past few decades, sensor-based Structural Health Monitoring (SHM) has seen increasing use in significant tunnel projects. This section discusses key aspects of several successful projects, including instrumentation types, objectives, and monitoring network density. Through case studies, the instrumentation utilized in various tunnels, their age, monitored parameters, applied technologies, and network density are presented. While numerous tunnel projects exist worldwide, the primary sources of information for this section are the projects listed below.

- London based tunnel projects (UK)<sup>34,40,46,72,75,81</sup>
- Semmering Base Tunnel (Austria)<sup>44,45,48,49,82,83</sup>
- Grand Paris Express (France)<sup>84</sup>
- Barcelona High-Speed Rail Tunnel (Spain)<sup>85,86</sup>

While Table 2-4 summarised key information garnered from reviewing some of the pre-mentioned tunnels, a series of noteworthy observations are given below:

1. **Integration of Multiple Monitoring Techniques:** the review revealed a prevalent trend of integrating multiple instrumentation methods.
2. **Parameters Monitored:** Typically, the parameters monitored include abnormal horizontal and vertical tunnel deformations, convergence (relative displacement of two diametrically-opposed points), cracks, joint movements, water leaks, and, in severe cases, potential collapse<sup>87</sup>. Depending on local conditions, measurements of water pore pressure and structural acceleration may also be necessary. In tunnel structural health monitoring using DFOS, the most commonly monitored structural parameter is strain, often coupled with temperature sensors for compensation.

Strain measurements enable the determination of mechanical stress, crack openings, and cross-section ovalisation.

3. **Monitoring in Existing Tunnels:** In existing tunnels, the focus is typically on tracking the evolution of strains, cracks, and various deformations under normal loads (permanent and service) or exceptional loadings, such as the influence of new constructions in the immediate vicinity<sup>38,40,88</sup>, water accumulation, earth slides, or seismic events. Monitoring systems in existing tunnels are generally limited to critical sections where anomalies have occurred or are likely to spread. DFOS is attached at several points, pre-tensioned, and can measure compression. These parameters can be used to deduce others of interest, such as the tunnel's curvature or ovalisation. DFOS is usually coupled with a temperature probe for compensation, except in deep tunnels (>50m) where temperature variations are minimal<sup>36</sup>.
4. **Monitoring in Newly Constructed Tunnels:** In newly constructed tunnels, monitoring serves two main purposes. First, it helps understand the interaction with neighbouring constructions, such as twin tunnelling<sup>40</sup> or the effects of new urban buildings<sup>38</sup>. Data gathered from this monitoring aids in assessing deformations and providing early warnings or enhancing the understanding of structural behaviour, which can validate or improve designs in similar environments. Second, it provides insights into tunnel lining behaviour under short-term loading<sup>89</sup>, which is particularly relevant for segmental tunnels or sprayed concrete lining tunnels<sup>43-45</sup>. Instrumentation in newly constructed tunnels is often concentrated in critical sections, and sensing elements can be surface-mounted or embedded in the tunnel lining, whether in the worksite or precast elements.
5. **Instrumentation Density:** In most case studies, instrumentation is concentrated in sections identified as critical, and the density of instrumentation within the tunnel varies depending on the specific project. For instance, the Semmering Base Tunnel project in Austria includes the systematic installation of DFOS during tunnel excavation and lining, alongside long-term SHM. Additionally, DFOS are typically complemented by other monitoring systems, such as automated total stations, photogrammetry, high-resolution CCTV, and MEMS sensors to measure deformation.
6. **Sensors technology:** The most used strain sensor technology is the VWSG and the long-gauge fibre optics.
7. **Types of tunnel:** Instrumented transport tunnels are the most common of all.

To sum up, monitoring tunnel conditions requires a tailored approach, considering factors beyond local ground conditions and service loads. The tunnel's intended use can significantly influence the parameters that need monitoring. For example, road tunnels in dry ground prioritise structural parameters like strain and displacements, while tunnels near groundwater or sewers may prioritize monitoring environmental parameters such as pore water pressure or pH levels. This project focused on structural parameters. Strains and displacements, especially longitudinal and transversal movements, are crucial structural parameters to monitor in several civil infrastructures. While both parameters are important to measure in a conventional post-construction deployed SHM system, smart segments, that will be discussed in the following lines, have prioritised strain measurements for real-time structural insights as the measurement are intended to go beyond the usual post-construction service life stage of the tunnels.

## **2.3.2 Gaps in existing instrumented tunnels**

### **2.3.2.1 Smart segment**

With a growing emphasis on digitising various aspects of the construction industry to streamline processes throughout the construction lifecycle and contribute to achieving net-zero goals, one promising strategy involves leveraging smart structures. These structures can seamlessly collect and analyse data from various assets to inform their operation and maintenance<sup>2</sup>.

This approach forms the core of our research, as a versatile tool known as the "smart tunnel segment" is proposed. Smart segment fabricated here consisted of lab-scale segment instrumented with commercially available sensors. When fully developed, this tool could better meet the diverse needs of asset owners while also benefiting key short-term stakeholders in projects, such as segment manufacturers and engineering design team.

Based on the early stages of the LTC road tunnel project, a proof-of-concept for a lab-scale smart tunnel segment equipped with customized embedded strain sensors is presented.

#### **2.3.2.1.1 Characterisation of smart segment**

While Section 2.3.1 included concrete-based tunnels in general, here only instrumented segmental linings are discussed.



Several studies<sup>90-94</sup> have been conducted to gain insights into the mechanical behaviour of tunnel segments under both typical and exceptional loading conditions.

The experimental components of these studies typically encompassed the following elements:

- **Instrumentation of Segments:** Segments were instrumented with embedded or surface-mounted sensors and other measurement devices.
- **Application of Real-World Loading Conditions:** The segments were subjected to loading conditions that closely simulated those encountered in real-world tunnel scenarios.
- **Comparison with Models:** The measurements recorded by the sensors were compared with the predictions of numerical or analytical models developed to replicate the testing conditions. This process often involved sensor calibration to ensure accuracy.

This process, found in several studies<sup>95,96</sup>, consisted of tunnel segments being equipped with embedded and surfaces mounted sensors and tested under flexural and compressive loading until failure. Measurements garnered could serve to enhance the design process of the segment. Flexural loadings were similar to the ones applied to segments during their handling in the factory and/or the transportation to the site. Compressive loading simulated the thrust on the segments during their installation by a TBM. A similar approach was used in this project to characterise the lab-scale smart segment.

### 2.3.2.2 Gaps

Smart segments would undergo a series of loadings before their installation on-site, and monitoring the effects of these loadings is critical, especially in the case of more commonly used SFRC segments. Once in a tunnel ring, the segments are usually under compressive loads, and the reinforcement bars in the segments typically serve to resist preconstruction loading generated by diverse manipulations during the pre-construction phase as shown in

Figure 2-11. There is an interest in monitoring the structural state of the segments during this phase, as they may easily be subjected to loads exceeding their design limits in terms of loads, strains, or displacements. In addition to providing critical structural information, strain sensors respond to unique challenges by being able to be extrapolated to calculate maximum displacements and loads, and the technology of available commercial options is

mature enough including in form of concrete-embedded strain sensors as discussed in Chapter 3.





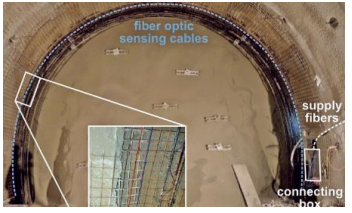
While previous tunnel projects have demonstrated commendable efforts to incorporate monitoring systems, the identified limitations in their implementation underscore the need for further research in this field. One significant drawback lies in the lack of modularity and robustness in FOS, highlighting the necessity for a more adaptable and resilient monitoring system. Additionally, the time and effort involved in deploying sensors, even when wireless technology is employed, presents practical challenges that warrant exploration for more efficient and streamlined processes.

Furthermore, the current approach to monitoring, which primarily focuses on post-construction stages, neglects valuable insights that can be gained from observing key behaviours during the tunnel's segment manufacturing and construction phases. Understanding the structural behaviours at play during these earlier stages is crucial for enhancing overall tunnel monitoring.

Another noteworthy limitation is the manual deployment of sensors by individuals, leading to potential errors in their placement, strain transmission (further discussed in 3.2.4.1) and failure. Addressing these issues is imperative to ensure the accuracy and reliability of collected data, emphasizing the importance of investigating automated or more precise deployment methods.

In conclusion, the identified gaps in existing monitoring systems, such as the lack of modularity, deployment efficiency, and the temporal focus on post-construction phases, substantiate the rationale for the current research. By addressing these limitations, this study aims to contribute to the development of more advanced and comprehensive tunnel monitoring systems that can be integrated into a newly built tunnel, such as the LTC road tunnel.

Table 2-4. Summary of instrumented projects consulted

	Existing tunnel			Newly built tunnel	
	Case Study 1 <sup>34,71</sup>	Case Study 2 <sup>35,71</sup>	Case Study 3 <sup>38</sup>	Case Study 4 <sup>71</sup>	Case Study 5 <sup>43,44,48,50</sup>
Name	Thames link tunnel 	Royal mail tunnel 	TMB L9 	National Grid power tunnel 	Semmering base Tunnel 
Description	Old masonry tunnel (153 years old) 3.6m above the northbound Thameslink 2000 tunnel built in 2005. The DFOS installed is the first of this type and had both a practical and academic interest.	Old cast iron tunnel built in 1917 less than 2 meters above a newly built Crossrail platform tunnel. The DFOS is installed to track effects of the boring of the new tunnel on the existing one.	Recently built bolted segmental tunnel. The DFOS installed in a small section to measure the effects of the construction of a new building 14.40 meters above the tunnel.	Segmental tunnel to carry high voltage power cables. The monitoring system (first of its type) consisted in embedding FOS into precast SFRC segments to measure short-term mechanical effects due to the installation by the TBM.	Shotcrete tunnel part of the TEN-T Network corridor connecting the Baltic and the Adriatic sea. The DFOS are embedded in two layers between the rock and the extrados and between in the lining thickness.
Location	London, UK	London, UK	Barcelona, Spain	London, UK	Austria
Year installation	2005	2013	2018	2014	2017
Parameters monitored	Circumferential and longitudinal strain and cracks	Circumferential and longitudinal strains.	Circumferential and longitudinal	Strain and temperature.	Strain and temperature
DFOS technology	- single-mode fibre optic in a 900 µm - Yokogawa AQ8603 BOTDR to readout the measurements.	- single-mode fibre optic in a 900 µm - Yokogawa AQ8603 BOTDR to readout the measurements.	- Interrogator: ODiSI-A by LUNA Technologies using swept-wavelength coherent interferometry	- Yokogawa AQ8603 BOTDR to readout the measurements.	- A 7.2mm sensing cable containing the FO and five protective layers - fibrisTerre BOFDA analyser -
Other technology	Automatic total station. Manual surveying, CCTV.	Wireless displacement and tilt transducers and photogrammetry	No additional sensors used.		Automated total station, photogrammetry
System density	83m of 100m of the critical section instrumented	40m of over 100m of the critical section were instrumented	Around 8.71m of the 20 m critical section is instrumented.		6.5km of fibre installed for 2x27.3km tunnel (under construction)

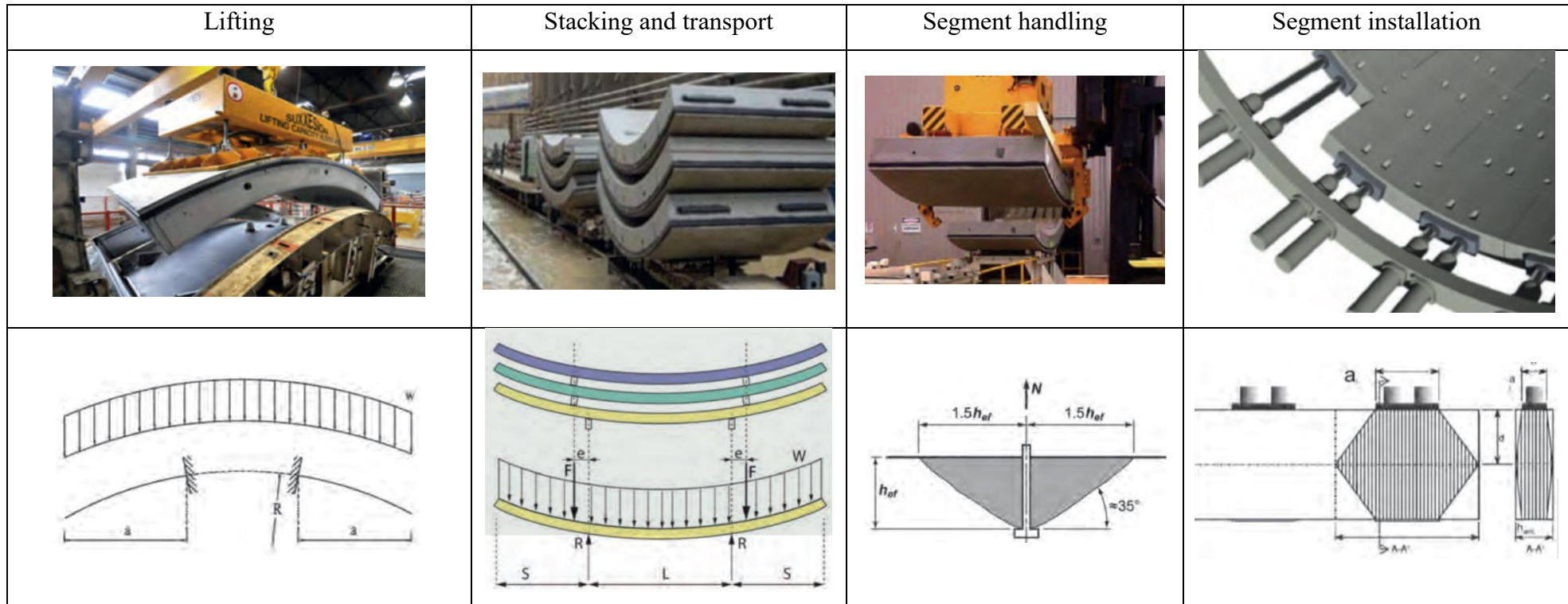


Figure 2-11. Loadings on tunnel segment pre-construction. The top line shows image of segment during various manipulation pre-construction and the second line show the corresponding structural diagram showing the types of loadings on the segment. The image have been obtained courtesy of ITATech<sup>10</sup>

## 2.4 Summary

This chapter focused on the review of tunnel instrumentation with an emphasis on concrete segmental tunnels. The chapter started with the presentation and discussion of some general design features of segmental tunnels. The discussion extended to the diverse methods employed for structurally designing tunnel segments, encompassing analytical and numerical approaches, along with design aided by full-scale testing. Furthermore, the production process of precast tunnel segments was presented discussing the difference between the carousel and static method.

Regarding tunnel instrumentation, the review delved into conventional methods of tunnel structural inspection, including on-site visual inspections and NDTs techniques. The concept of SHM for tunnels is also discussed, involving the use of sensors for continuous monitoring of structural and environmental parameters. The array of sensors used in SHM, such as VWSG, FBG, wireless sensors, and MEMS are also discussed. Finally, a brief description of other techniques employed in conjunction with sensor-based instrumentation or conventional inspection techniques is given.

To illustrate tunnel instrumentation, practical case studies of real-world instrumented tunnel projects were presented. These projects, encompassing both existing and newly constructed tunnels, showcased the diverse parameters monitored, the technologies employed and the limitations of existing monitoring approaches.

This chapter identified several research gaps and limitations in current tunnel instrumentation practices. These included issues related to modularity, deployment efficiency, and an overemphasis on post-construction stages. These identified gaps will inform the design and development of sensors in the subsequent chapter, with the overarching objective of demonstrating the development of smart tunnel segments using robotics to deploy strain sensors.

# Chapter 3. Sensors Selection and Design

The chapter explores the selection process for embedded strain sensors, delving into market solutions for both resistive and VW strain sensors. A thorough analysis of their respective advantages and disadvantages is provided, particularly in the context of their application as embedded sensors. The rationale behind opting for VWSG as the strain sensor for this study is then elucidated. The chapter further covers the programming and initial calibration of VWSGs, along with the design considerations for packaging, ensuring suitability for robotic deployment.

## 3.1 Background

Over the past decades, there has been a growing interest in incorporating SHM systems into civil infrastructures to enhance their operational and maintenance efficiency throughout their service life. This transformation has been made possible due to advancements in sensor technology and the augmented processing power that can be accommodated within increasingly compact components<sup>97,98</sup>. The abundance of data collected and subsequently analysed not only serves the immediate purpose of asset management but also holds the potential to enhance structural design, making it more cost-effective while ensuring durability and safety. In the realm of SHM, sensors are pivotal, as their selection, proper installation, and resilience significantly determine the quality of the entire system.

The sensor based SHM has two main components: the sensor retrofit and post-deployment analysis to generate intelligence to support subsequent inspections and maintenance operations. In this study, the sensor retrofit phase is of utmost interest. To capture the many advantages of the smart segment, it is vital to briefly discuss the features of on-site systems. They include on-site wired and wireless systems. Both systems have in common the following:

- They are deployed post-construction during the fit-out period.
- They are specialized tasks and require expert human workers.
- They do not capture pre-construction behaviour of individual segments.
- Sensors are often surface-mounted.

Smart segments on the contrary, in addition to providing features of post-construction on-site SHM systems, they have other features that make them stand out. They can capture

structural behaviour through strain measurement of instrumented segments pre-construction. Additionally, smart segments are well-suited to a modular structure such as a segmental system and can, once deployed, form ad-hoc modular networks, with each smart segment communicating with others.

As highlighted in an earlier discussion in Section 2.3.1, strain stands out as the most frequently monitored structural parameter in real-world projects. The choice between point, semi-distributed, or distributed strain sensors depends on the specific project objectives. However, when aiming for a modular wireless segment capable of forming ad hoc communication networks on-site, the compatible solutions narrow down to resistive and VW strain sensors. Additionally, point sensors are well-suited for segments of relatively small size, particularly when compared to the entire tunnel. The subsequent section delves into market solutions for resistive and VW strain sensors, providing an overview of the selection process of the definitive solution used in this project.

## **3.2 Choice of sensors**

This section examines features of commercially available strain sensors categorized into two classes: electronic sensors and VW sensors. It outlines the criteria used to determine the most suitable solution for this study and provides justification for the final selection.

### **3.2.1 Embedded sensors**

This short section explains the preference for embedded strain sensors over surface-mounted ones. Embedded sensors are favoured due to several reasons. Firstly, they offer enhanced protection against environmental factors and vandalism or tampering. Secondly, they provide more accurate measurements by directly being in contact with the concrete matrix, eliminating interference from surface effects or potential slippage. Additionally, embedded sensors enable comprehensive continuous monitoring, capturing information from fabrication to later stages.

### **3.2.2 Electronic sensors**

Resistive strain gauges are often preferred for short-term applications due to their vulnerability to environmental factors, which can impact long-term stability. Nevertheless, there are available commercial solutions that can be embedded in concrete. These gauges are

easy to use and present a straightforward interrogation mode that transmits signals as easily convertible voltages, facilitating strain measurements. They are usually a cost-effective choice and offer sufficient accuracy for short-term tasks<sup>31</sup>.

However, once incorporated into concrete, they tend to demonstrate diminished long-term performance, including noticeable drift over time. This issue compromises their suitability for extended use<sup>28</sup>. During the evaluation, two commercially available resistive strain transducers were assessed.

### 3.2.2.1 Prismatic embeddable resistive strain sensor

This type of resistive strain sensor is characterised by its prismatic shape and its rugged body to allow a better adhesion to concrete once embedded. One representative of this sensor is the EGP electrical embedment sensor shown in Figure 3-1 whose datasheet can be found in Appendix A. 1. An EGP sensor contains a single strain gauge inside an almost prismatic polymer body. The strain gauge nominal resistance is either 120 Ohms or 350 Ohms<sup>99</sup> arranged in a  $\frac{1}{4}$  Wheatstone bridge configuration.



Figure 3-1. Example of an EGP embedment strain sensor. Image courtesy Micro Measurement

### 3.2.2.2 Cylindrical resistive strain gauges

This type of sensor has a cylindrical shape, with two discs at the extremity, made of an outer body impervious to water with an elastic module that can be as low as 0.04 GPa and as high as 1 GPa and arranged in a half or full Wheatstone bridge configuration. A best



representation of such sensors are KM strain transducers<sup>100,101</sup> shown in Figure 3-2. Unlike EGP sensors, these KM strain sensors offer a diverse selection of Wheatstone bridge configurations, including both half-bridge and full-bridge options, as well as a range of sizes spanning from 30mm to 200mm in length. Detailed technical information can be found in the datasheet in Appendix A. 1.



Figure 3-2. Examples of KM strain transducers. Image courtesy Tokyo Measurement Instruments Laboratory Co., Ltd. The image presents three specimens of strain transducers which uses vary depending on their application. The smallest option would be more adapted to be used in laboratory concrete elements.

### 3.2.3 Vibrating wire strain gauge

Despite the fact that the Vibrating Wire (VW) sensor technology was discovered after resistive gauges, it quickly found applications in industrial settings due to its straightforward operational principle<sup>26</sup>. Over time, VW sensors have become the preferred choice for embedding in civil structures made of concrete, particularly for long-term strain monitoring. These sensors are renowned for their superior accuracy compared to electrical strain gauges<sup>28</sup>, their robustness<sup>29,102</sup>, and their ability to provide long-term stable measurements<sup>31</sup> with minimal drift<sup>32</sup>. In this study, we specifically considered VWSG from Geokon, shown in Figure 3-3 a company offering a diverse range of sensors suitable for both laboratory and industrial applications. Detailed technical information, are provided in the manufacturer datasheet in Appendix A. 1.



Figure 3-3. Examples of Geokon concrete embedment VWSG. Image courtesy Geokon

### 3.2.4 Comparison and final choice

In this section, the three commercial solutions outlined in 3.2.2 and 3.2.3 are evaluated based on the following criteria:

- strain transmission capability;
- ease of interrogation and communication;
- sensor degradation;
- sensor outer body material;

#### 3.2.4.1 Strain transmission.

Embedded strain transducers must possess specific features to ensure optimal strain transmission. This is typically achieved through the material of the transducer's outer body (polymer or stainless steel) in contact with the concrete, or the shape of the transducer itself (prismatic or cylindrical). In the conventional embedded strain sensors previously described, both these features have been addressed.

For prismatic embedded electrical strain gauges, the outer body consists of a polymer with an irregular contact surface, creating a gripping plane with concrete. Additionally, one end of the transducers terminates with a dovetail that provides an additional anchorage to the concrete.

In contrast, VWSG and resistive strain sensors type-KM rely mainly on anchorage plates at each end of the main cylindrical body to transmit strains from concrete to the sensors. The accurate transmission of strain relies on the quality of the bonding between the extremities and the concrete<sup>103</sup>. To capture the variation of strains in a heterogeneous material such as the concrete, it is recommended that the embedded strain gauge length be at least three times the maximum size of the aggregate<sup>100</sup>.

#### **3.2.4.2 Ease of interrogation**

While resistive strain sensors can be easily interrogated by standard data acquisition systems that measure voltages and subsequently convert them into strain readings, Vibrating VWSGs function differently. VWSGs produce frequencies as output, which require an additional interface to convert them into data compatible with conventional voltage-based interrogation devices.

#### **3.2.4.3 Sensor degradation**

Concrete structures are engineered to last up to 100-120 years, which therefore require long-lasting embedded components. Unlike structural elements like reinforcement bars, which can last as long as the concrete, embedded sensors can and do fail.

Sensor failures can be attributed to various causes, with the most common factors being mechanical and electrical interference, with sensor cables and inadequate handling during installation and the concrete pouring phase<sup>104</sup>.

Failure rates differ between sensor types. In a study on embedded strain sensors in<sup>105</sup>, it was shown that after 7 years of installing embedded strain sensors in a small concrete bridge, electronic strain sensors (type-EGP) had a 70% failure rate, while VWSGs exhibited a lower 22% failure rate. Similarly, in a study focused solely on VWSGs within nuclear facilities, a 33-55% failure rate was observed after 25 years of installation<sup>106</sup>.

Sensor degradation poses a genuine concern and, at times, proves inevitable. Employing strategies like sensor redundancy<sup>24,107</sup>, accurate handling, and selecting sensors based on their suitability for short or long-term use are critical measures for mitigating sensor failures.

#### **3.2.4.4 Sensor packaging material**

When it comes to the material for sensors' outer bodies, the main goal is to minimize disruption to e.g. stress fields in the host material while assuring an optimal adhesion to the host material. This is usually achieved by adjusting the geometry, physical, and mechanical properties to ensure a good fit.

Embedded sensors need to be crush-resistant during installation and their service life. Commercial strain sensors reviewed here use robust materials, such as steel or polymer, for the outer body. The choice of the sensors outer body material can significantly affect the parameters they measure. For instance, differences in packaging materials like hard (stainless steel) and soft (polymer) mainly impact strain measurements in the early stages of concrete, with relatively consistent effects over the long term<sup>108</sup>. Sensors with a low Young's modulus are suitable for measuring strains during the curing process<sup>100,101</sup>, while sensors with a thermal coefficient similar to that of concrete enable a smooth integration under thermal loads<sup>109</sup>. Such variety of properties are only achieved by VWSGs and KM sensors.

### 3.2.5 Sensor choice

Building on the earlier comparative presentation of strain sensor features, the choice of VWSGs was driven by their overall superior performance as previously discussed at length. In this section, technical considerations such as the strain range, resolution, accuracy, and temperature range for both the electronic sensors and VWSGs are summarised in Table 3-1.

Table 3-1 Comparison of Technical Specifications between Electronic Sensors (EGP and KM) and VWSG Geokon Model 4202

	Electronic sensors		VWSGs
	EGP	KM	VWSGs
Range	$\pm 5000 \mu\epsilon$	$\pm 5000 \mu\epsilon$	$\pm 3000 \mu\epsilon$
Resolution	Up to $1 \mu\epsilon$	Up to $0.1 \mu\epsilon$	Up to $0.4 \mu\epsilon$
Accuracy	0.8 % FS	1 % FS	0.5 % FS
Temperature range	$-5^{\circ}\text{C}$ to $50^{\circ}\text{C}$	$-20^{\circ}\text{C}$ to $80^{\circ}\text{C}$	$-20^{\circ}\text{C}$ to $80^{\circ}\text{C}$

VWSGs offer several compelling advantages over Electronic sensors (EGP and KM). Firstly, VWSGs exhibit a narrower range of  $\pm 3000 \mu\epsilon$  compared to the  $\pm 5000 \mu\epsilon$  range of the electronic sensors, making them more suitable for applications requiring precise strain measurements within a limited range.

Secondly, VWSGs boast superior resolution capabilities, with values of up to  $0.1 \mu\epsilon$ , significantly outperforming the resolutions of electronic sensors (ranging from  $0.4 \mu\epsilon$  to  $1 \mu\epsilon$ ). This finer resolution allows for the detection of smaller strain changes, essential in applications where high sensitivity is paramount.

Furthermore, VWSGs demonstrate enhanced accuracy with a specification of 0.5 % Full Scale (FS), surpassing the accuracies of electronic sensors (ranging from 0.8% FS to 1% FS). This higher level of accuracy ensures more reliable and precise strain measurements, crucial for critical structural monitoring and engineering applications.

Moreover, while the temperature range of VWSGs aligns with that of electronic sensors ( $-20^{\circ}\text{C}$  to  $80^{\circ}\text{C}$ ), VWSGs can withstand lower temperatures down to  $-20^{\circ}\text{C}$ , offering versatility in environments with colder climates or extreme temperature fluctuations.

Finally, VWSGs are more suitable for long-term Structural Health Monitoring (SHM) applications when embedded into concrete. VWSG technology has superb long-term stability, less susceptible to interference due to the length of the wiring or the cable splicing. VWSGs are also robust and more appropriate for use in adverse environments <sup>110</sup>.

More precisely, the model 4202 Geokon VWSGs, more adapted to laboratory applications and micro-concrete, will be used in this study.

### **3.3 Electronics and programming**

#### **3.3.1 Communication mode**

Embedded transducers can utilise two modes of communication: the traditional approach through cabling and the newer method employing wireless technology. Instead of delving into detailed descriptions of each method, the focus here is on the problems each technique is adept at addressing and the challenges they each bring.

##### **3.3.1.1 Wired Communication:**

Cabled communication includes both electrical and fibre optic wires. Both cable types share a common structure consisting of a signal transmission element (metallic wire or optical fibre) enclosed in a protective coating. Electrical wiring is the most prevalent medium for communication, whereas fibre optics are employed in specific situations where mitigating risks like lightning or electromagnetic interference is necessary. However,

cables embedded in concrete can introduce water ingress, potentially causing corrosion or sensor damage. They are also likely to be damaged or crushed under high pressure, making the addition of protective plastic tubing advisable. This tubing serves a double role of withstanding mechanical loads and limiting water ingress. Finally, the deployment of cables is demanding in manpower compared to new solutions such as wireless.

### **3.3.2 Wireless Communication:**

Wireless sensors are typically linked to a wireless node, referred to as a "wireless sensing element," which is embedded in concrete<sup>53,111</sup>. The wireless sensors offer some advantages such as greater deployment flexibility, ultimately reducing overall installation costs compared to wired systems<sup>53,112,113</sup>. However, wireless nodes placed within dense or humid materials like concrete face challenges, including issues related to the propagation and propagation loss of radio and electromagnetic waves, along with the disruptive influence of metallic elements such as reinforcement bars and metallic fibres<sup>114</sup>. Despite the wireless sensors challenges, they remain a more attractive option for a modular system of smart segments and have a real potential of cutting the manpower requires during the fitout period of sensors.

In this study, although the wireless node wasn't fully developed—considering this effort as a completed task—the demonstration aimed to showcase the diverse electronic components of the sensor node that could easily be miniaturised in the future.

### **3.3.3 VWSG node**

Due to the reasons outlined in Sections 3.2.5 and 3.3.1.1, the node was specifically developed with wireless communication in mind for this project. The ad-hoc device to interrogate the VWSG developed as part of this PhD project is presented in Figure 3-4 The main hardware components include:

- A microcontroller type Arduino 33 BLE with built-in wireless communication capability
- An RS-485 board
- A VW addressable board interfacing the VWSG and the RS-485 board.

The node components were assembled on a breadboard with jumper cables and drew power from the computer.

The interrogation of the sensor has been automated using code developed within this PhD project, integrally presented in Appendix A. 2. The sensor outputs are the resonant frequency and the temperature. The frequency is correlated to the strain using Equation ( 2-1). The calibration coefficient permitting the conversion of frequency to strain is obtained through a series of repetitive tests on sensors installed into the tensile tester. The detailed process and results of the initial calibration of VWSGs presented in 3.4.

### 3.3.4 Sensors interrogation process

The interrogation of the VWSG illustrated in the flowchart in (Figure 3-5) and is summarised as follows:

1. *Initialisation*: The process starts by initializing the Modbus communication library, setting up necessary pins, specifying the sensor's Modbus address, and configuring the delay for reading strain data.
2. *Setup Function*: within this function, the code configures the communication port, initialises Modbus for communication, sets up call-back functions for data transmission, and prints a setup confirmation message.

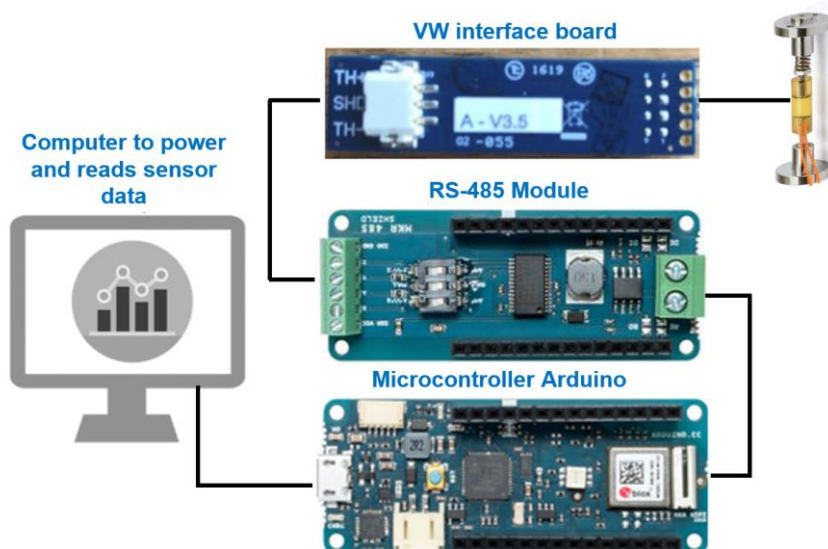


Figure 3-4. Ad-hoc Interrogation device

3. *Loop Function*: This is the core of the code. It continuously reads the frequency and temperature from the VWSG. It then converts the frequency to strain using a practical equation, and finally, prints the frequency, strain, and temperature data.

The Geokon VWSGs have a minimum sampling rate of 370 milliseconds.

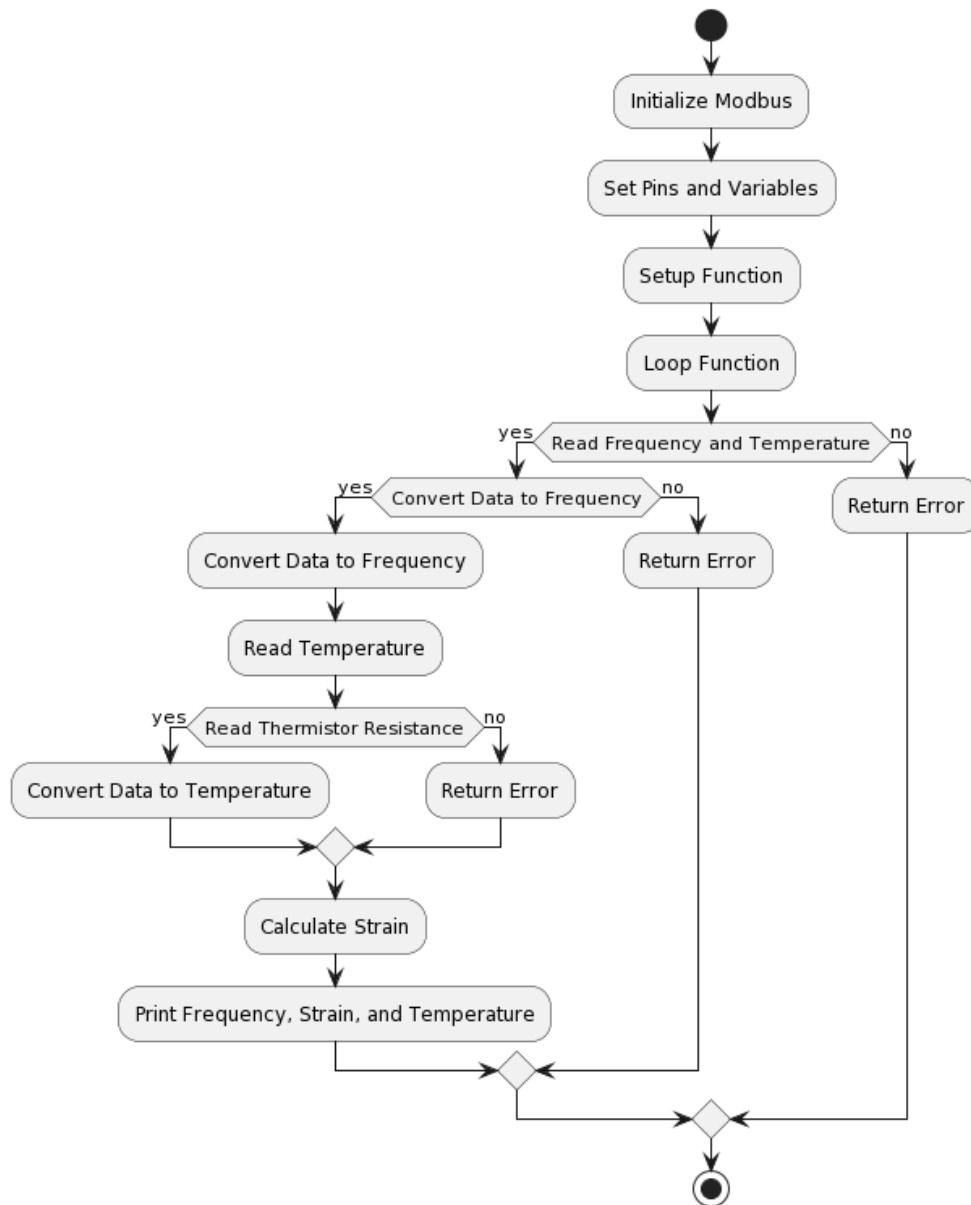


Figure 3-5. VWSG interrogation flowchart

### 3.4 Initial calibration results on the VWSG and results

Manufacturers usually state strain calibration values on data sheets, but these are not always accurate. Calibrating a VWSG using a tensile tester is therefore a critical process in



ensuring accurate strain measurements. The calibration method used in this work involves subjecting the VWSG strain sensor to controlled strains while simultaneously measuring its resonant frequency response. The objective is to establish a linear correlation between the strain applied and the resulting change in resonant frequency, ultimately determining the gauge factor of the strain gauge. This is done using Equation ( 3-1), where  $\epsilon$  is the strain in  $\mu\epsilon$ , GF the gauge factor, F and  $F_0$  are respectively the resonant frequency at instant t and instant t =0.

$$\epsilon = GF \frac{(F^2 - F_0^2)}{1000} \quad (3-1)$$

A description of the calibration process is as follows:

- **Preparation:** Before the calibration begins, the strain gauge is properly installed in the tensile tester (See Figure 3-6).
- **Initial Frequency Measurement:** the initial resonant frequency  $F_0$  of the strain gauge in its unloaded state is recorded. This served as a reference point for future strain calculations.
- **Tensile Testing:** compressive/tensile displacements/strains are applied to the sensors within the strain gauge's range (3000  $\mu\epsilon$ ).
- **Data Collection:** Time-synchronized data points were gathered at regular intervals throughout the calibration test. These data points include the applied displacement/strain, later converted into strains, and the corresponding resonant frequency of the strain sensor. At each measurement point, the hold time was set at 10 seconds, and the frequency values were the averages of 10 consecutive measurements for the applied displacement or strain. The applied strain for each calibrated sensor was sequential and consistent, with displacement measurement point being 0.00, 0.01, 0.05, 0.10, and 0.15 mm in both compression and tension.
- **Linear Correlation:** A data analysis of the collected data follows. First, a graph of the applied strain versus  $(F^2 - F_0^2)/1000$  is plotted as shown in Figure 3-7. The relationship between these variables should be linear within the strain sensor gauge's range. The slope of the linear regression line, represents the gauge factor GF.

Note: Throughout the calibration process, the room temperature remained constant, and the entire test duration was between 110 and 120 seconds per sensor. Due to the combination of these two factors, there was no need to correct the strains to account for temperature effects.

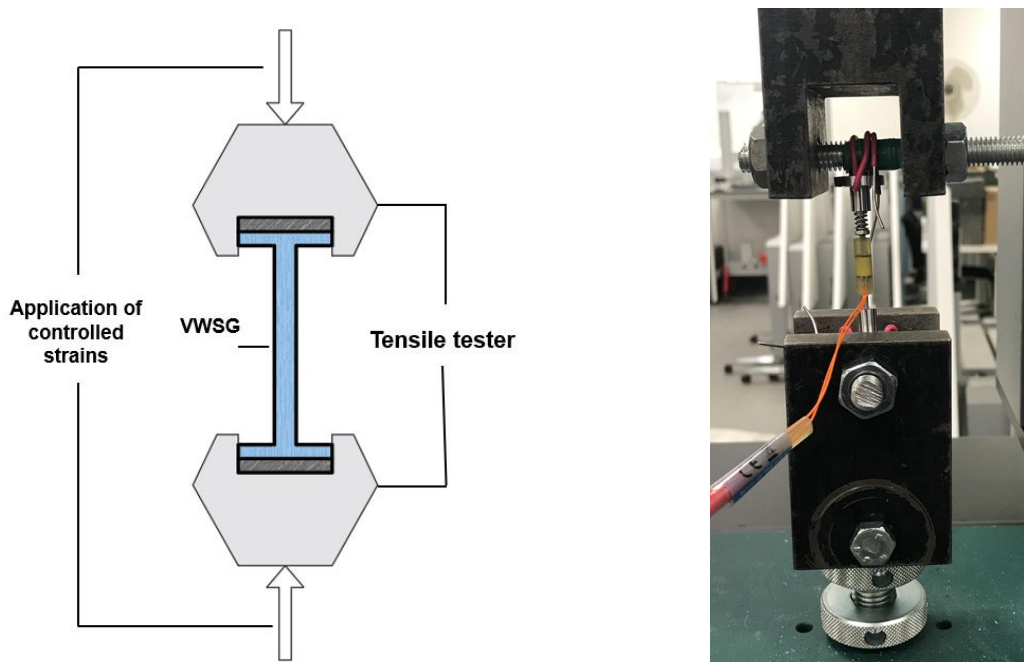


Figure 3-6. Tensile tester during VWSG calibration test

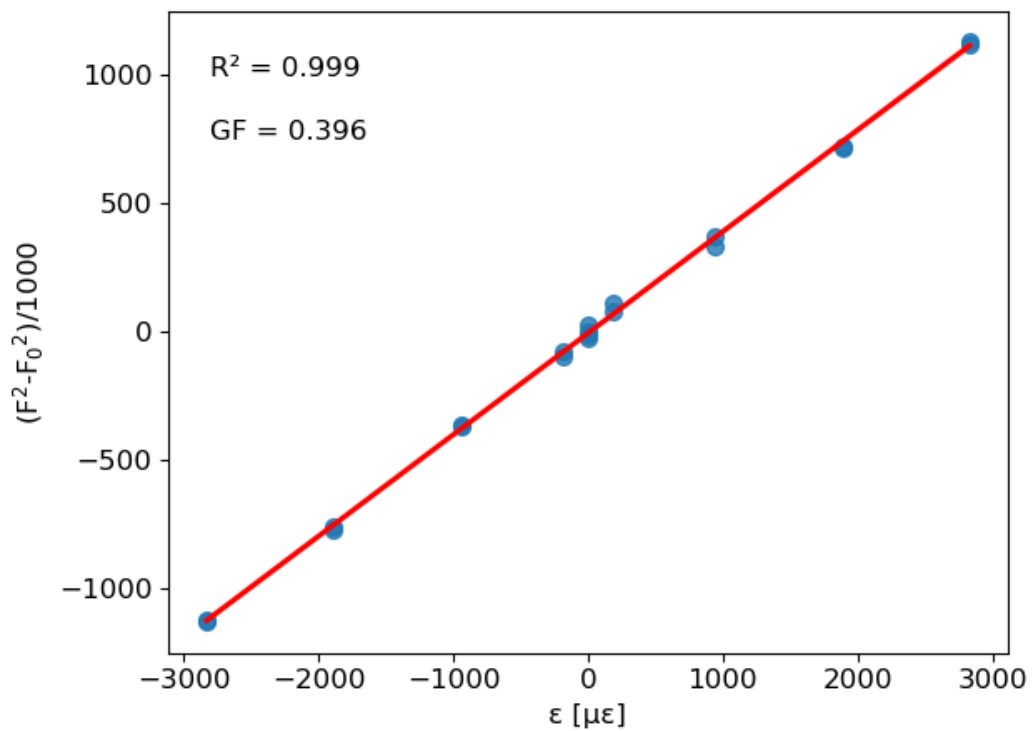


Figure 3-7. An example of VWSGs calibration results on one VWSG. The correlation is significantly high and the gauge factor close to the one specified by the manufacturer which is 0.395.

The calibration test for VWSGs was performed on ten different Geokon VWSGs of model 4202. The calibration results for each sensor are presented in Appendix A. 3. The general observations are as follow:

- The gauge factors across the sample set were consistent, at  $0.394 \pm 0.004$ . This value closely matches the manufacturer's value of 0.395 obtained on a larger sample of sensors.
- In addition to the gauge factor, an additional parameter called the batch factor is applied to the conversion Equation ( 3-1) to calculate strains from the measured frequencies. The batch factor is a calibration factor or correction factor applied to account for variations in the manufacturing process that may result in slight differences in the performance of individual strain gauges within a batch. This value is provided by the sensor manufacturer in the documentation accompanying the sensors and its values vary between 0.9 – 1. In the case of this initial calibration, the sensors tested were all from the same batch, therefore they had the same batch factor of 0.93.
- The initial frequency  $F_0$  varies with the sensor's position and the adjustment of the nut, which can be used to expand or shrink the measurement range. The particular model of VWSG used in this study is highly sensitive to these adjustments.

### 3.5 Summary

In this chapter, the selection of strain sensors to embed in the lab scale tunnel segment is discussed. A comparison between resistive electric sensors and VWSGs is made based on different criteria. Commercially available options are evaluated, and VWSGs are chosen for the specific application due to their superior accuracy, robustness, and stable measurements over extended periods. VWSGs are also more affordable than electrical sensors with similar features, even after adding the extra cost of the addressable board necessary to pair them to a conventional voltage-based microcontroller.

The electronic and programming aspects of the sensor node are also addressed, including the design of an interrogation device and the calibration process for VWSGs. A step-by-step description of the initial calibration process is provided, involving subjecting the strain sensor to controlled strains and measuring its resonant frequency response.

Future work could explore a further miniaturisation and the integration of a battery into the sensor nodes to make them effectively wireless. It is noteworthy that this PhD project serves as a proof of concept, and the decision not to make the nodes wireless is due to the

project's focus on demonstrating the concept rather than solving the wireless connectivity challenge, which is essentially a solved problem.

In the upcoming chapter, the automated deployment of the sensor node will be presented. The discussion will cover the challenges and potential solutions before introducing the robotic deployment developed in the study.

# Chapter 4. Robotic deployment of sensors

While robotics has found broad use in many other industries, its application in construction and civil engineering remains somewhat limited<sup>115</sup>. Nonetheless, there have been ongoing efforts to introduce automation into various aspects of civil engineering projects. These efforts include the increasingly common use of computer-assisted design (CAD) tools for project design and management<sup>116,117</sup>, as well as the deployment of robots or automation during construction to reduce the reliance on human labour. Additionally, robotics is employed during the operational phase of structures to assist with inspection tasks. In this chapter, the automation solutions in the construction industry are reviewed and the repurposing of robotic applications in the precast industry discussed as well as the methodology to robotically deploy VWSGs nodes.

## 4.1 Background

### 4.1.1 Automation during the operation/maintenance phase

Important civil infrastructures, like tunnels, are designed to have a lifespan of up to 120 years and require regular maintenance operations, supported by well-structured inspections throughout their operational life. While traditional techniques are still prevalent for on-site inspections, there is a growing interest in integrating automated devices to augment human inspection capabilities. Automation solutions of particular interest are:

- unmanned aerial vehicles (UAVs)
- mobile robots.

#### 4.1.1.1 UAV inspections

UAVs are increasingly finding valuable applications in tunnel inspections<sup>118,119</sup>. Typically, they are equipped with one or a combination of the following tools: high-resolution cameras, thermal imaging technology, and geomatics sensors. UAVs prove to be ideal for navigating confined spaces, such as sewer or small utilities tunnels, which are often challenging to access, and they provide additional detailed information to complement manual inspections. UAVs in confined spaces have demonstrated their success in various tasks, including mapping infrastructures<sup>120-125</sup>, identifying surface defects like cracks<sup>126-128</sup>, locating sources of fire and smoke<sup>129</sup>, or tracking gas leakages<sup>130,131</sup>.

Although many of these applications remain primarily academic in nature, a few off-the-shelf solutions are available in the market. However, it is important to note that these solutions remain to be relatively expensive and typically require the expertise of trained professionals for operation. Further details regarding some of these solutions have been previously outlined <sup>20</sup>.

UAVs still have room for improvement due to several challenges they face, including limited GPS signals in confined areas, poor performance in poorly lit environments (which is often the case of sewer tunnels), vulnerability to damage from dust and debris, and constraints on payload capacity, limiting the equipment they can carry. Despite these limitations, UAVs adoption is increasing and find wider applications in field like the deployment of sensors as discussed in 4.1.3.

#### **4.1.1.2 Mobile robots' inspections**

Similar to UAVs, mobile robots are equipped with an array of measuring devices, including laser scanners, geo-radars, thermal and high-definition cameras, and they are typically mounted on wheeled vehicles. This solution offers the advantage of carrying a more extensive set of tools compared to drones. These vehicles also possess greater power autonomy, allowing them to perform measurements for extended periods.

The use of mobile robots equipped with LiDAR systems is now firmly established, with numerous real-world applications. These applications span a wide range, from visual inspection robots mounted on a pick-up truck<sup>132</sup> to autonomous battery-powered small vehicles<sup>133–136</sup>. Some of the common operations carried out include the reconstruction of a 3D map of the tunnel to create digital twins, measuring tunnel displacements, and performing crack and void detection on the tunnel linings.

Among all the applications, the most prevalent ones involve the 3D mapping of tunnels using LiDAR and photogrammetry techniques<sup>19</sup>, utilising both temporary and or semi-permanent measuring devices. These techniques find extensive use in real-world applications, and their effectiveness has been amplified by the increased computing power and the utilisation of advanced AI algorithms, allowing for complex operations on a substantial number of images. Another application is the inspection of structural elements of infrastructures such as bridge bearings<sup>137,138</sup>.

Nevertheless, the primary challenge that mobile robot inspections encounter is the limited nature of prelabelled datasets used to train AI models for damage or defect detection. This limitation also hinders their widespread adoption in the industry<sup>19</sup>.

Inspections conducted by robots are distinct operations from using robots to install sensors (See section 4.1.3). While inspections provide one-time measurements, sensors offer the possibility of continuous monitoring. In most cases, monitoring systems are installed after construction is completed. However, this presents several disadvantages: the structural behaviour before the installation of the monitoring system is entirely missed, and the environment for sensor installation becomes challenging, especially for a robot that may lack the same flexibility to combine multiple operations like a human operator within the restricted working conditions.

## **4.1.2 Automation during construction phase**

This section presents automation solutions during both the on-site and off-site construction phase of concrete elements. First, an overview of on-site construction robots will be discussed before expanding on robotic solutions in the precast industry which is the focus of this research.

### **4.1.2.1 Automation on construction sites**

The incorporation of automation into construction operations since the 1970s led to noticeable marginal improvement<sup>139</sup>. One of the first successful solutions of automation solutions was the Single Task Construction Robot (STCR) developed in Japan<sup>139</sup>. STCRs are excellent at executing repetitive tasks consistently and with reduced error compared to human workers. However, they do have a major limitation when compared to human workers: they lack flexibility and are typically programmed for single tasks<sup>140</sup> or tasks with minimal changes in the work environment<sup>141</sup>. These characteristics are essential for unstructured environments such as construction sites. This limitation led to the concept of Automated Sites, which involve incorporating factory-like environments into construction sites. An Automated Site consists of a well-integrated set of STCRs designed to improve site organization and the efficient flow of materials. Such an environment can help optimize the layout of the worksite and reduce the need for human workers.

Although automation solutions on construction sites are still an evolving field, there is valuable reference literature available for more information on both construction robots<sup>142</sup> and automated sites<sup>143</sup>. Additionally, there are more resources detailing current and potential applications of robotic solutions for construction as well as practical challenges still needed addressing<sup>144–148</sup>.

#### **4.1.2.2 Precast manufacturing robots**

Concrete precast elements are produced within more controlled environments, where factors such as temperature, spatial arrangement, and operational sequences are meticulously managed, in contrast to on-site operations. The extensive deployment of machinery for critical tasks, like lifting, transporting, and concrete mixing, not only enhances safety but also optimises production efficiencies. When making a large quantity of the same type of elements, such as tunnel segments, these substantial features allow for the production of 'replicas' with remarkable accuracy. This pre-established setting simplifies the incorporation of robotics into the process.

In the production of flat and prismatic precast elements, robotic solutions, as depicted in Figure 4-1 from<sup>149,150</sup>, are employed for the installation and removal of formwork, as well as for marking lines that define the formwork positions. These specific tasks can be carried out separately or in a coordinated manner.

As for tunnel segment solutions and as previously mentioned in 2.1.2.2, two typical production methods are generally used in the creation of precast elements: the *static* method and the *carousel* method. In addition, in either approach, three major steps, as depicted in Table 4-1, are part of the process for producing tunnel segments: mould preparation, concreting, and demoulding, followed by storage.

In the existing solutions for tunnel segments, robots are deployed during the preparation, concreting and curing phase shown in Table 4-1. They can either partially or completely replace human operators. These robots consist of a series of stationary units, each equipped with different end-tools designed for specific tasks. They are especially well-suited for a carousel system and can be employed for various functions within the same sequence of the production process.



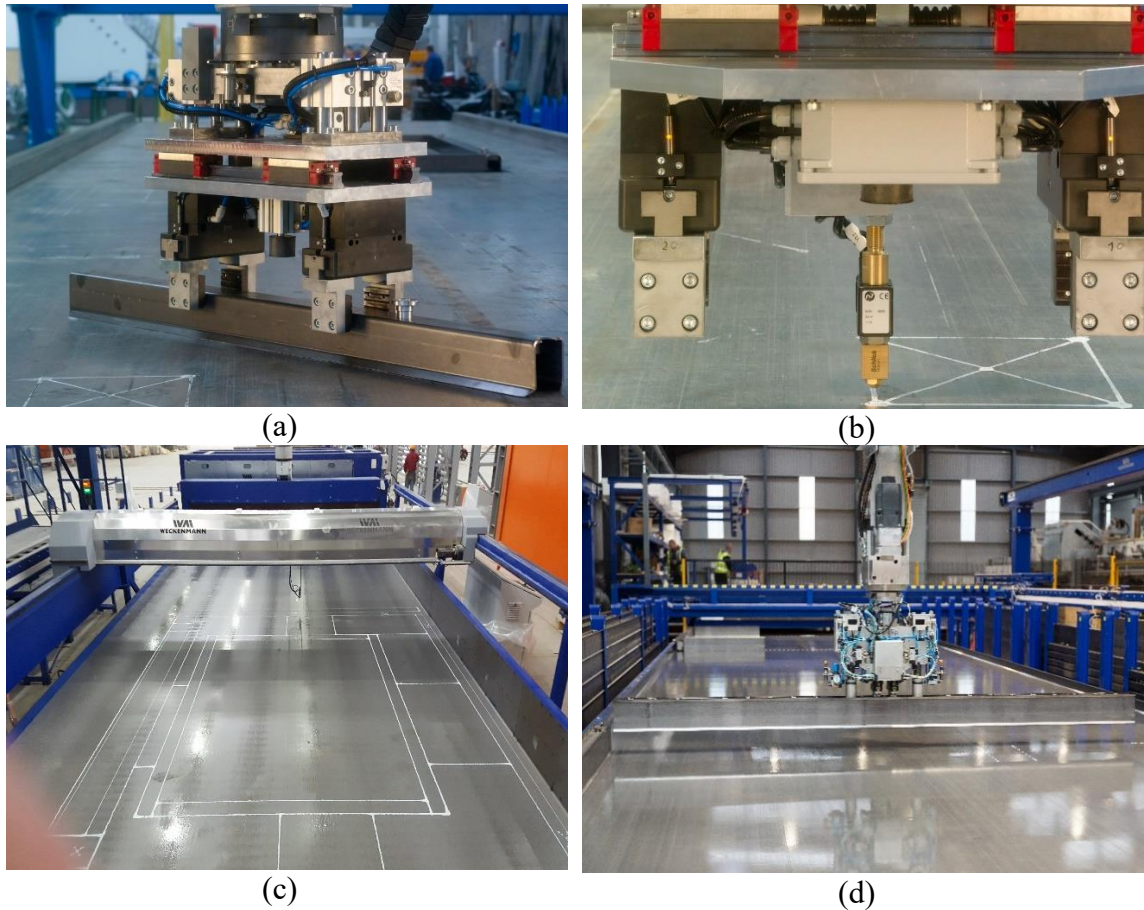


Figure 4-1. Robotic system used in concrete prefab factories. (a), (b) Robotic arm used for shuttering and deshuttering in (b) notice the combine function of a ‘plotter’ to help in the positioning of shutters. (c) A dedicated plotter that transfers CAD data to nozzle to plot on shuttering profile (d) robotic arm used for placing and removing profiles. Images courtesy of Progress (a and b) and Weckenmann. (c and d)

### 4.1.3 Automated deployment of sensors using UAVs and mobile robots

There are a host of studies showing successful deployment of sensors using UAVs<sup>151–156</sup> and robotic devices<sup>157–162</sup>. Sensors deployed using this method are usually small, wireless, and low-cost. The sensors, in the cases of UAVs, can be deployed through dropping, direct placement, or shooting as shown in Figure 4-2. As for the deployment using mobile robots, the sensors are usually parts of the robots and the measurement is temporary and not continuous.

The deployment method using UAVs, suitable for outdoor environments with limited space constraints, may present challenges when trying to replicate it on a construction worksite. The deployment method of mobile robots, as indicated by the robotics community, does not strictly constitute the installation of a permanent SHM system, as traditionally carried

out manually to ensure continuous monitoring of the structural behaviour of the infrastructure.

The current sensors deployment methods using both UAVs and mobile robots are still subjected of intense and promising research, and as of now, they do not provide directly applicable solutions to deploying strain sensors into precast elements manufactured in automated factories.

## **4.2 Robotic process to deploy VWSGs on smart segment.**

The advanced automation technology in the precast manufacturing industry can be repurposed for the successful deployment of VWSGs. An essential initial step was to determine the most suitable robotic process and the ideal end-tool for sensor installation.

In this study, the pick-and-place (PnP) technique was identified as the most appropriate method for deploying VWSGs, which are attached to a box (further details on this will be provided later in the study).

In this section, the selected robotic solution, the procedure for deploying VWSGs, end-tool selection, and the design of VWSG packaging are presented.

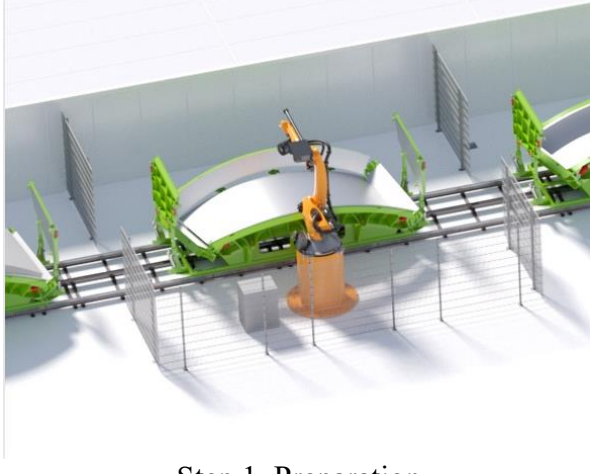








### **4.2.1 Robotic tools**

#### **4.2.1.1 Collaborative robots**

Collaborative robots, often referred to as "cobots," are a type of industrial robot designed to work alongside human operators in a shared workspace. Unlike traditional industrial robots, which are typically caged off and operate independently, cobots are designed with safety features and sensors that allow them to collaborate with humans without posing significant risks.

In this study, a cobot type a 6-axis Universal Robot 10 (UR 10), shown in Figure 4-3, was used to deploy VWSGs sensors. In a precast factory, larger non-collaborative robots can be employed to carry out comparable tasks. While these larger, non-collaborative robots may pose more hazards compared to cobots, their integration into a highly automated precast plant is justified due to the additional reach and robustness they provide. UR10 has many useful features that include:

Table 4-1. Robotic solutions for manufacturing of tunnel segments. Images courtesy of Herrenknecht Formwork.

Manufacturing phase and robotic solution	End-tool
 <p data-bbox="427 813 679 846">Step 1. Preparation</p>	 <p data-bbox="1193 353 1321 421">Cleaning roller</p>  <p data-bbox="1193 589 1369 701">Blow-out and lubrication tool</p>
 <p data-bbox="427 1283 679 1317">Step 2. Concreting</p>	 <p data-bbox="1193 891 1353 958">Smoothing roller</p>  <p data-bbox="1193 1137 1369 1171">Sanding pad</p>
 <p data-bbox="427 1675 679 1709">Step 3. Demoulding</p>	 <p data-bbox="1193 1361 1369 1429">Inserts grippers</p>  <p data-bbox="1193 1574 1385 1608">Torque driver</p>

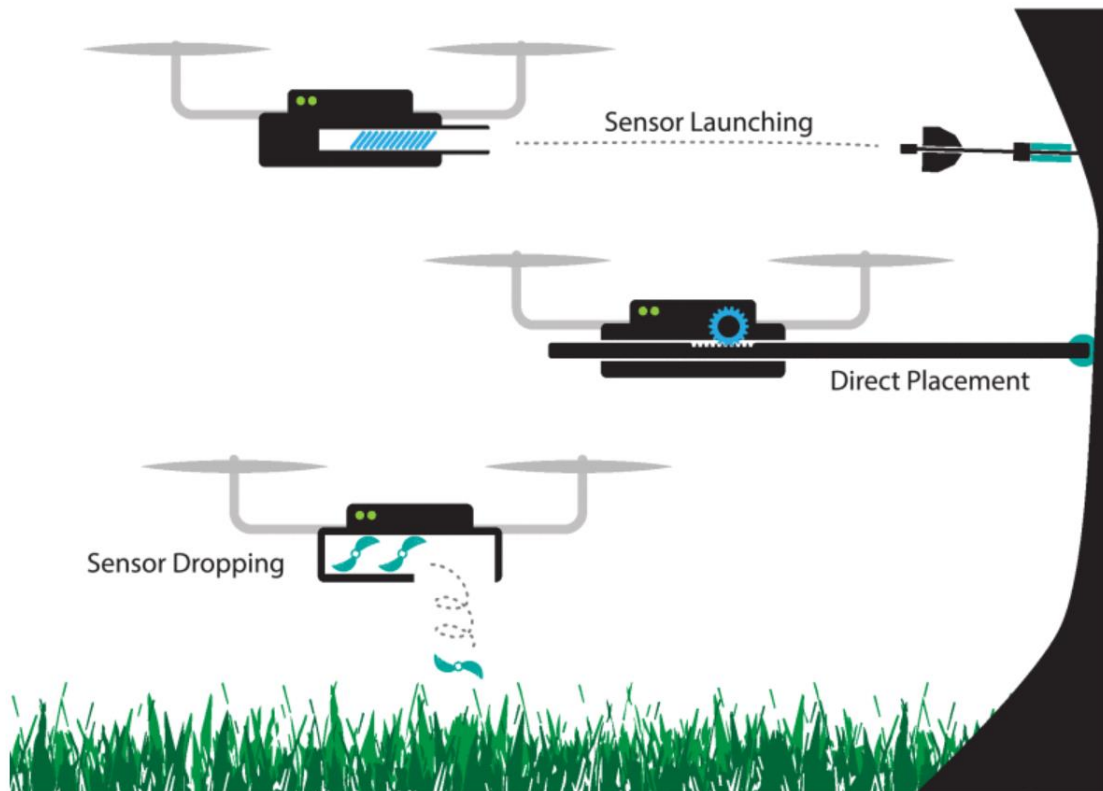


Figure 4-2. Different deployments of wireless environmental sensors using UAVs <sup>163</sup>.

1. Advanced safety features making UR 10 highly responsive to human presence, reducing its speed and impact force, preventing as such dangerous collisions.
2. Easiness to programme thanks to a user-friendly interface.
3. Cost-effective acquisition, deployment, and operation,
4. Enhanced productivity provided a higher payload.
5. Highly suitable for human-machine collaboration environment.

#### 4.2.1.2 Robotic gripper

UR10 being one of the most common types of cobots, it is designed to be compatible to many types of end-tools. In this study, the sensor deployment consisting at a pick-and-place can be achieved with a gripper. Three technology are available for gripping solid elements:

- Suction gripping
- Magnetic gripping
- Finger gripping

The selected gripper technology was the two-finger gripper. This finger-like gripping technology provides the highest versatility and adaptability, making it ideal for a wide range of materials and shapes.

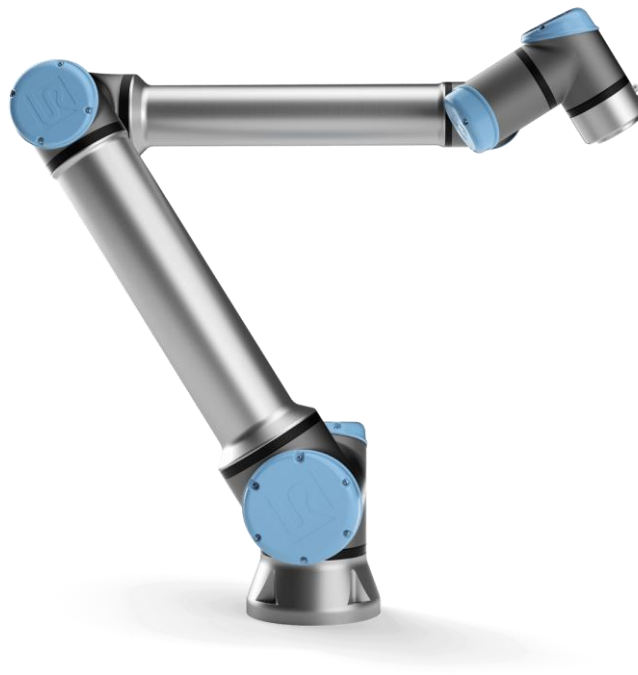


Figure 4-3. Universal Robot 10. UR 10 is a 6-axis robotic arm with a payload capacity of 10 kilogrammes and a reach of 1300 mm.

To make the ultimate selection, a comprehensive assessment of three two finger-gripper options offered by Robotiq, a well-known manufacturer recognized for its user-friendly grippers designed to seamlessly integrate with the UR10 robotic arm was performed in regard of these criteria:

- **Precision:** The chosen gripper must deliver precision equal to or better than the specifications for segment fabrication, as outlined in the BTS Specification for tunnelling, 3rd edition, §3.5.3, which stipulates a range of  $\pm 1$  to  $\pm 1.5$ mm.
- **Environmental Resilience:** The gripper should exhibit a high level of resistance to dust and humidity, ensuring it can be safely employed in both dry and humid concrete environments without suffering damage.
- **Payload Capacity:** The gripper's payload capacity should be equal to or less than the UR10's capacity, which is 10 kg.
- **Gripping Force:** It is imperative that the gripper offers an adequate gripping force suitable for both smooth and rugged surfaces.

In Table 4-2, which outlines the grippers evaluated for selection and their respective characteristics based on the criteria mentioned earlier, it is evident that the Robotiq Hand E gripper stands out as the most favourable choice. Notably, it also comes at a slightly more cost-effective price compared to the alternatives.

Figure 4-4 illustrates the 3D-printed fingers, which have been created as replacements for the original metallic fingers that come with the grippers. The 3D-printed fingers provide the advantage of being longer than the manufacturer-provided metallic fingers. Additionally, they can be easily produced and used in wet and harsh environments, such as concrete.

## 4.2.2 Robotic process




### 4.2.2.1 Robotic PnP

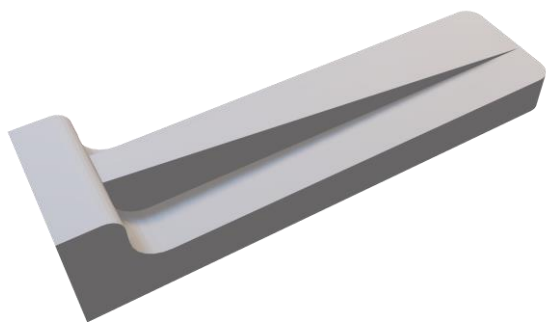
Although the PnP method is commonly used in robotic manipulations, limited options for a specific evaluation framework tailored to solid elements, which could be adapted to this study were encountered. The closest match found was a benchmarking framework designed for the systematic assessment of robotic PnP in the food industry, as discussed in <sup>164,165</sup>. This framework utilizes four evaluation metrics as defined below:

1. **Success Rate (R)**: This is the ratio of successful PnP actions to the total number of PnP attempts.
2. **Mean Picks Per Hour (MPPH)**: It measures the average number of successful pick-and-place actions completed in an hour.
3. **Successful Task Executions Over Total Attempts (SETA)**: This metric estimates the probability that an individual task execution attempt will be successful.
4. **Average Duration (AVGT) and Standard Deviation of Duration (STDCT)**: These metrics capture the average time taken for a successful PnP cycle and the associated variability.

While the previously mentioned metrics are well-suited for assessing the overall performance of a PnP (Pick and Place) system in handling fruits in bins, they may not be ideal for a comprehensive evaluation of the accuracy of individual element poses. A more appropriate approach would involve evaluating geometric errors resulting from robotic positioning and comparing them to similar errors in manual positioning.

Table 4-2. Two-finger grippers selections. Images courtesy of Robotiq.

Manufacturer Model	Image	Resolution (mm)	Protection v. Dust	Protection v. water	Payload (kg)	Grip force (N)
ROBOTIQ Hand-E		0.2	IP67	IP67	3-5kg	20-130
DH ROBOTICS AG-95		0.03	IP54	IP54	3-5kg	15-95
ROBOTIQ 2F-85		0.4	IP40	IP40	5kg	20-235



(a)



(b)

Figure 4-4. (a) 3D illustration of the ad-hoc gripper finger (b) the robotiq Hand E gripper equipped with 3D-printed fingers

#### **4.2.2.2 PnP performance assessment**

The main objective in this context is to attain precise sensor positioning while minimizing geometric variations. Of particular importance is the relationship between geometric inaccuracies and strain errors, underscoring the critical nature of evaluating the performance of the pick-and-place (PnP) process for VWSG sensors.

To be more specific, the performance assessment process will encompass two key aspects:

- Evaluation of Geometric Deviations: This involves analysing translation and rotation errors for both manual and robotic VWSG deployment.
- Evaluation of Strain Sensor Errors: This step focuses on assessing strain sensor errors resulting from geometric deviations for both manual and robotic VWSG deployment.

To achieve this goal effectively, it is necessary to configure the robots appropriately for the pick-and-place operations and to adapt the sensor packaging to enable optimal gripping and positioning.

#### **4.2.3 Sensor packaging**

The box shown in Figure 4-5 serves a dual role: it provides support for the VWSG using two hooks and also could house the necessary electronics for sensor interrogation, effectively converting the whole setup into a wireless node when fully developed.

The design of this box underwent multiple iterations to determine the most suitable shape and dimensions. Additionally, Neodymium magnets were incorporated into the box cover to improve adhesion to the formwork surface and enhance positioning accuracy.

To ensure an accurate gripping of the box during the PnP process, certain adjustment to the box have been made as shown in Figure 4-6.

### **4.3 Pick-and-place implementation**

The primary scenario of interest is a robotic PnP of a magnetic box onto a metallic surface using a robotic arm. However, this scenario alone may not provide enough insights to definitively establish its superiority over manual PnP. Therefore, the following scenarios will be investigated:



- Robotic PnP with a Magnetic Box
- Robotic PnP with a Non-Magnetic Box
- Manual PnP with a Magnetic Box
- Manual PnP with a Non-Magnetic Box.

For each of these scenarios, 100 data points have been collected, ensuring a robust dataset for a statistically significant analysis.

To collect the necessary data, a Nikon D3200 camera mounted on a slider, supported by two tripods will be employed in addition to the robotic set up layed out in Figure 4-7.

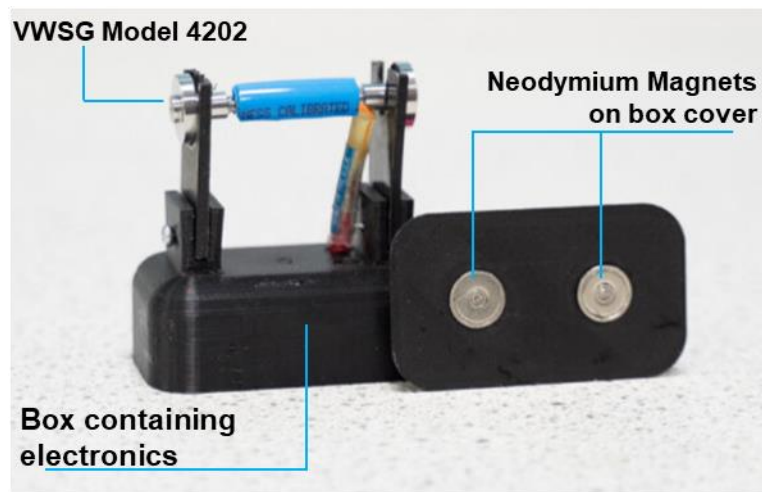


Figure 4-5. VWSG box.

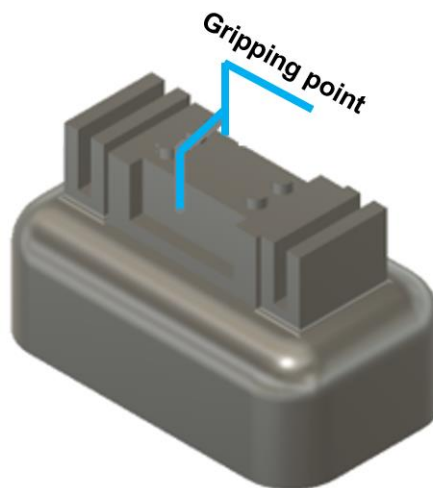


Figure 4-6. Modified box to improve the gripping

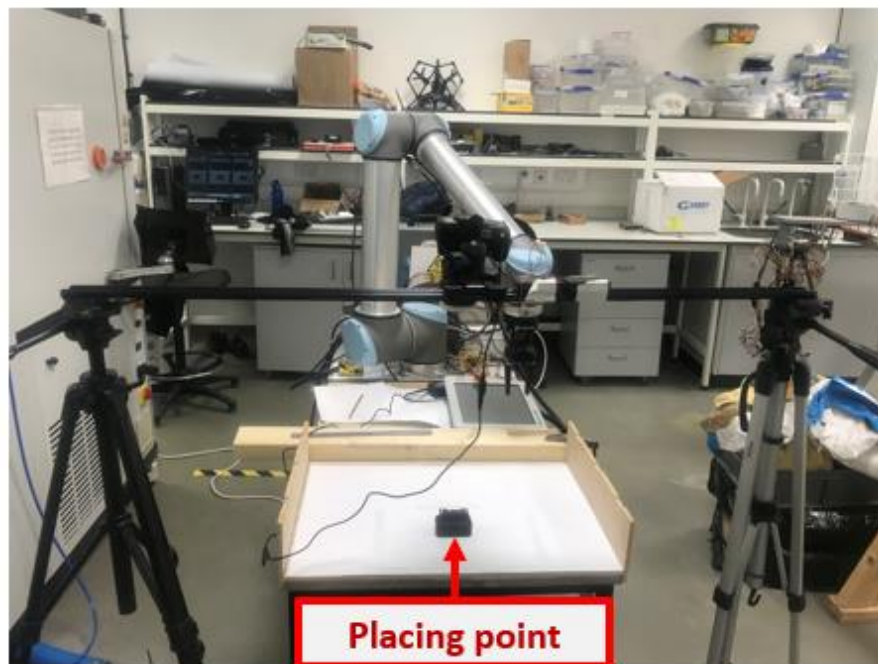
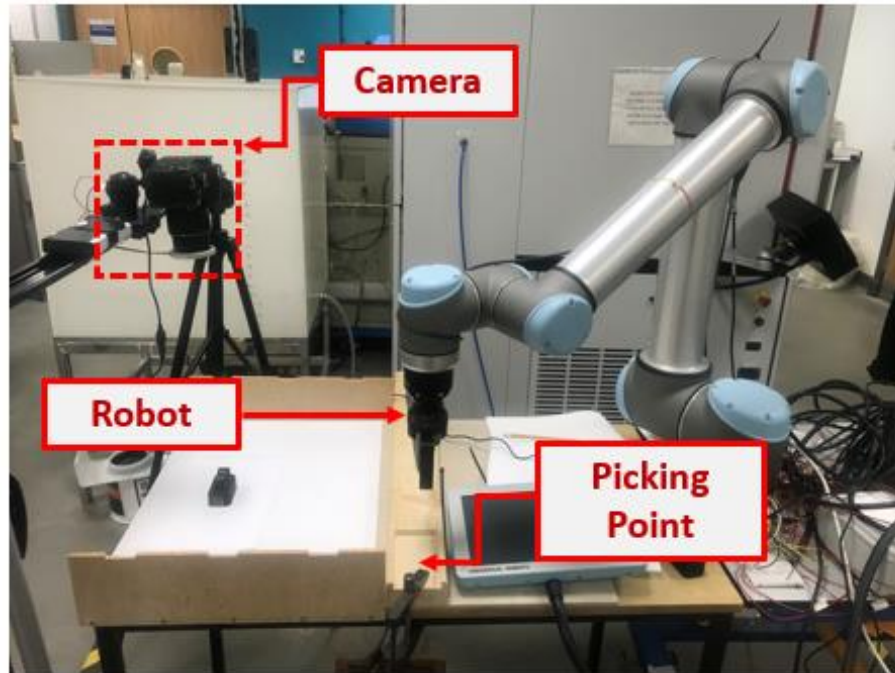


Figure 4-7. Set up for PnP

### 4.3.1 Steps to evaluate PnP performance of the magnetic box

#### 4.3.1.1 Geometric errors evaluations

For each scenario, the following steps are carried out:

1. After positioning the box at its designated spot, whether manually or with the assistance of robots, a photo showing both the box and the target was taken. These photos provide essential geometric data, including  $\Delta X$ ,  $\Delta Y$ , and  $\Delta\Theta$ , as shown in Figure 4-8. The box was gently lowered with the robot up to 25 mm above the target and dropped.
2. The captured images were later converted to grayscale with pixel intensities ranging from 0 (white) to 255 (black). The Otsu thresholding method was then applied to create a binary image of the box. Once the contour of the binary shape found, and the bounding box aligned with the contour's extremities, the centre of the bounding box was then determined at the intersection of the horizontal and vertical axes. The coordinates of the centre were then subtracted from the coordinates of the template's centre, resulting in  $\Delta X$  and  $\Delta Y$ . The angle of rotation was calculated using trigonometry.
3. The geometric deviations  $\Delta\Theta$ ,  $\Delta X$ , and  $\Delta Y$ , obtained in the previous steps, are recorded in tables for further analysis.

#### 4.3.1.2 Strain errors

#### 4.3.1.3 Geometry's impact on strain error

A fundamental connection exists between geometric and strain errors in the context of this discussion. The effect of translational errors on the anticipated strain will be contingent upon the segment's geometry and its ultimate loading. However, when compared to the segment's size, these effects will be relatively minor, and as such, they assume a secondary role in comparison to errors in placement angle. Nonetheless, an angular deviation can directly influence the resulting strain, and it would be valuable to quantify this impact.

For a unitary strain, as shown in Figure 4-9, the change in the angular deviation ( $\Delta\Theta$ ) leads to a change in the value of strain as expressed in Equation ( 4-1). The strain relative change expressed in percentage is shown in Equation ( 4-2).

$$\varepsilon' = \frac{\varepsilon}{2} (1 + \cos 2\Delta\theta) \quad (4-1)$$

$$\frac{\Delta\varepsilon}{\varepsilon} (\%) = \frac{\varepsilon' - \varepsilon}{\varepsilon} * 100 \quad (4-2)$$

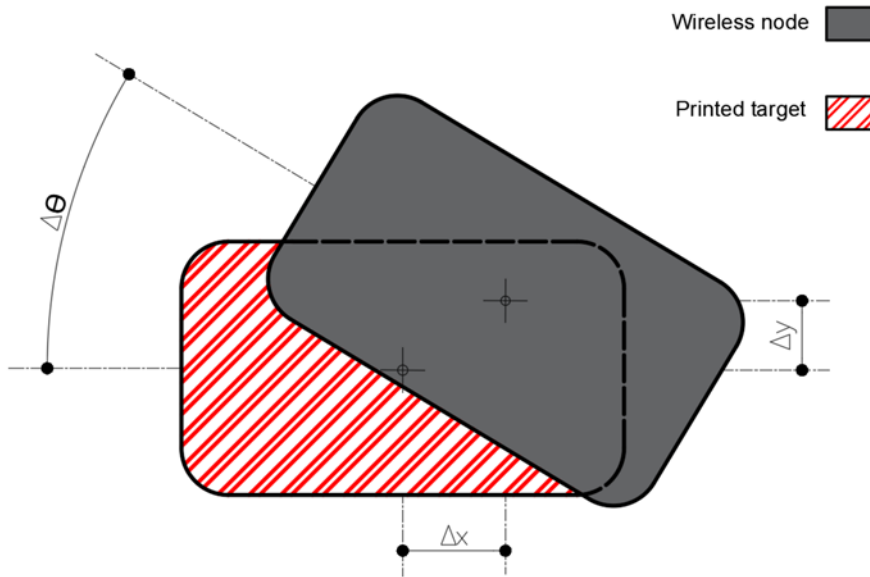


Figure 4-8. On the left. A photo of the box after the pose. On the right, a representative drawing with geometric deviations

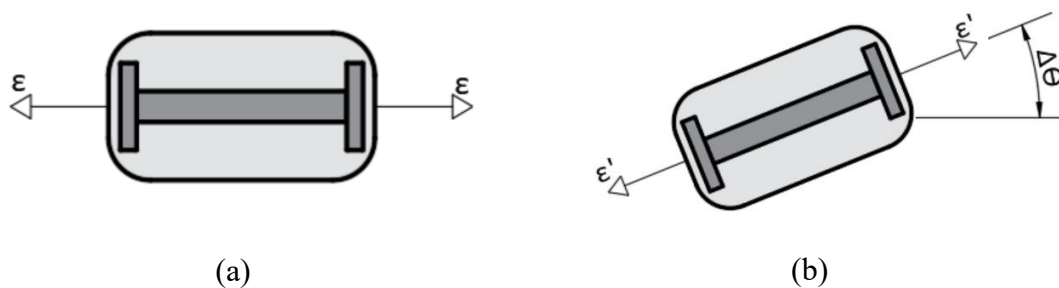


Figure 4-9. VWSG Strain transformation (a) ideal state (b) rotated state

## 4.3.2 Results

### 4.3.2.1 Geometrics errors

Table 4-3 presents the results of the geometric and strain errors of robotic and manual PnP. Similarly, Figure 4-10 shows the distributions of geometric errors across manually and robotically deployed sensor nodes, with and without the use of magnetic attachment. From the results, the following observations were made:

- *Manual vs. Robotic Deployment:* A clear distinction is observed between manual and robotic deployment methods. When sensors are manually placed without the use of magnets, translation errors ( $\Delta X$  and  $\Delta Y$ ) and rotational error ( $\Delta\Theta$ ) exhibit

relatively larger variations. In contrast, robotic deployment yields more consistent and precise results for all three geometric parameters.

- *Magnetic Attachment's Impact:* The inclusion of magnets significantly influences the results. In the manual deployment scenario, using magnets leads to a reduction in translation errors ( $\Delta X$  and  $\Delta Y$ ) and rotational error ( $\Delta\Theta$ ), resulting in a tighter and more accurate sensor placement.
- *Directional Discrepancies:* When looking at the robotic deployment with magnets, there's a peculiar negative value for  $\Delta Y$ , which indicates a slight shift in the opposite direction. This might be due to the interaction between the robotic system and magnetic elements.

Table 4-3. Geometric and strain errors of robotic PnP vs Manual PnP.

Method	Translation error ( $\Delta X$ ) [mm]	Translation error ( $\Delta Y$ ) [mm]	Rotational error $\Delta\Theta$ [deg]	Strain error [%]
Manual (without magnet)	$0.68 \pm 2.76$	$0.44 \pm 4.34$	$1.44 \pm 7.45$	$1.72 \pm 2.53$
Manual (with magnet)	$0.94 \pm 1.91$	$0.29 \pm 2.41$	$1.08 \pm 4.41$	$0.62 \pm 0.99$
Robotic (without magnet)	$4.50 \pm 0.44$	$0.286 \pm 0.86$	$-0.302 \pm 1.01$	$0.23 \pm 0.70$
Robotic (with magnet)	$2.39 \pm 2.89$	$-0.027 \pm 0.63$	$0.098 \pm 0.99$	$0.14 \pm 0.41$

The influence of the magnetic box on the results is relatively undisputed. However, it's important to recognize the study's limitations in comparing manual and robotic deployment methods. In this case, the manual placement was conducted by the authors, which could introduce bias in favour of demonstrating the superiority of robotic deployment. It is noteworthy that the distributions for manual placements conform to Gaussian probability density functions, suggesting that they may not be subject to substantial biases.

#### 4.3.2.2 Relative strain loss

The examination of theoretical strain losses (last column Table 4-3) across the four scenarios presented in Figure 4-11 reveals a consistent trend: robotic magnetic deployment has the potential to reduce errors and the variability in those errors when compared to manual and non-magnetic placement.

It is worth noting that these results do not consider additional factors, such as the influence of vibrations when sensors are embedded within concrete. As a result, it is reasonable to anticipate that practical errors, especially for non-magnetic boxes, could be more pronounced. However, these findings collectively highlight the potential of robotics to contribute to the reliability and consistency of sensor deployments.

## **4.4 Summary**

This chapter began by providing an overview of contemporary robotic solutions in civil infrastructure, addressing both operational and maintenance phases. For operational and maintenance activities, the discussion revolved around UAVs and mobile robots, while the construction phase introduced STCRs and Automated Sites.

The subsequent section explored existing robotic applications in the precast manufacturing industry, emphasizing their common use in tasks like formwork installation, removal, and marking positions. This paved the way for considering the adaptation of these existing solutions for sensor deployment.

Furthermore, the chapter delved into the robotic process for robotically deploying VWSGs on smart tunnel segments. The choice of the PnP technique was discussed, utilizing a cobot UR10 equipped with a two-finger gripper set, equipped with a set of 3D-printed fingers. It also outlined the steps for assessing PnP performance and presented the outcomes regarding geometric and strain errors in both manual and robotic deployments.

The findings in this chapter underlined the higher precision and accuracy of robotic sensor placement compared to manual approaches. It is essential to note that while the experiments were conducted on flat surfaces, their potential applicability to the curved surfaces of smart segment formwork of smart segment, characterized by large curvature, is obvious. In the upcoming chapter the laboratory work of fabricating and testing lab-scale smart tunnel segments following the robotic deployment of VWSGs process will be presented in depth and discussed as well as the evaluation of the fabricated segments performance

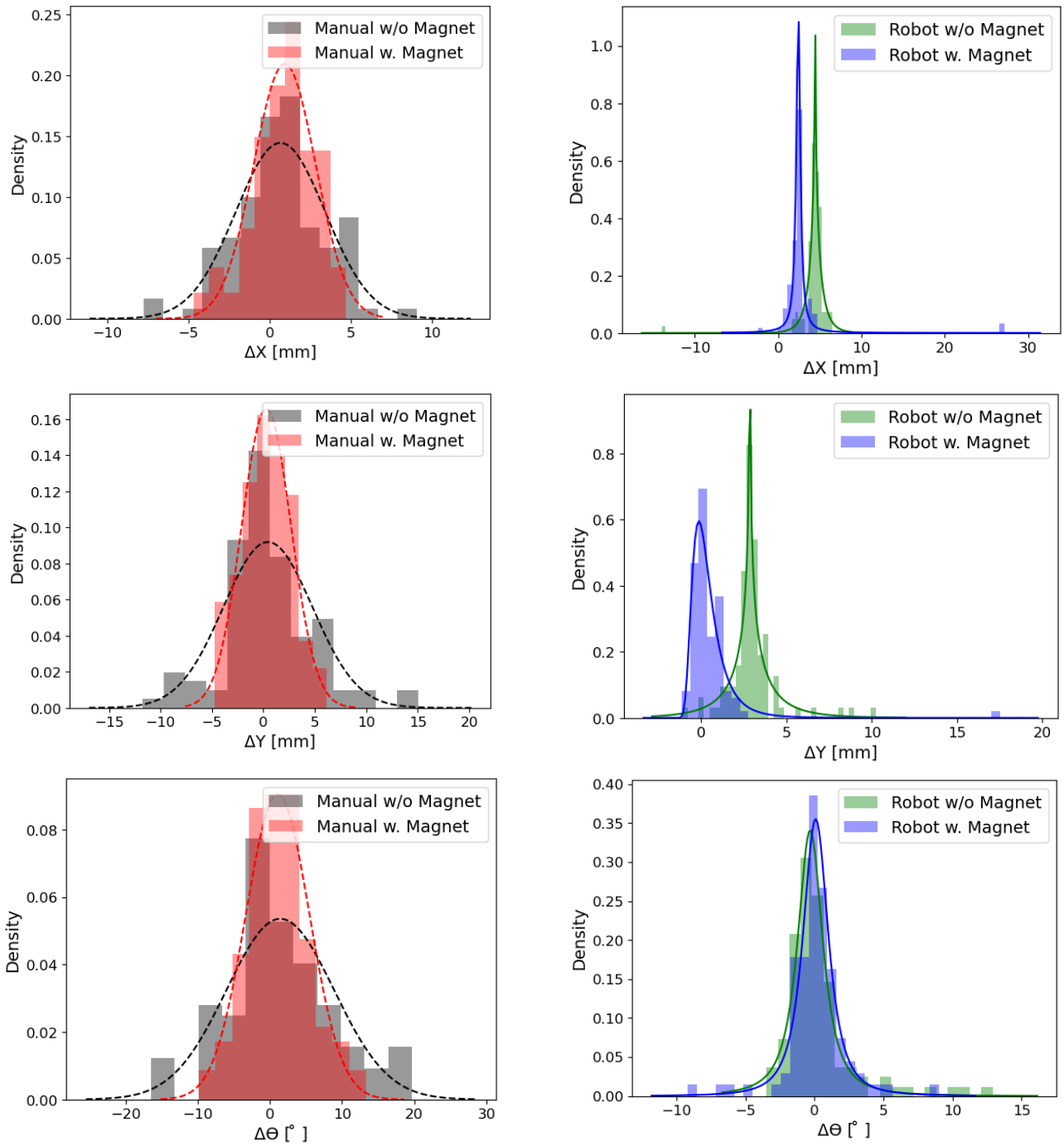


Figure 4-10. Statistical distributions of geometric errors  $\Delta X$ ,  $\Delta Y$ , and  $\Delta \Theta$  for the manual and robotic scenarios. The density is expressed in proportion.

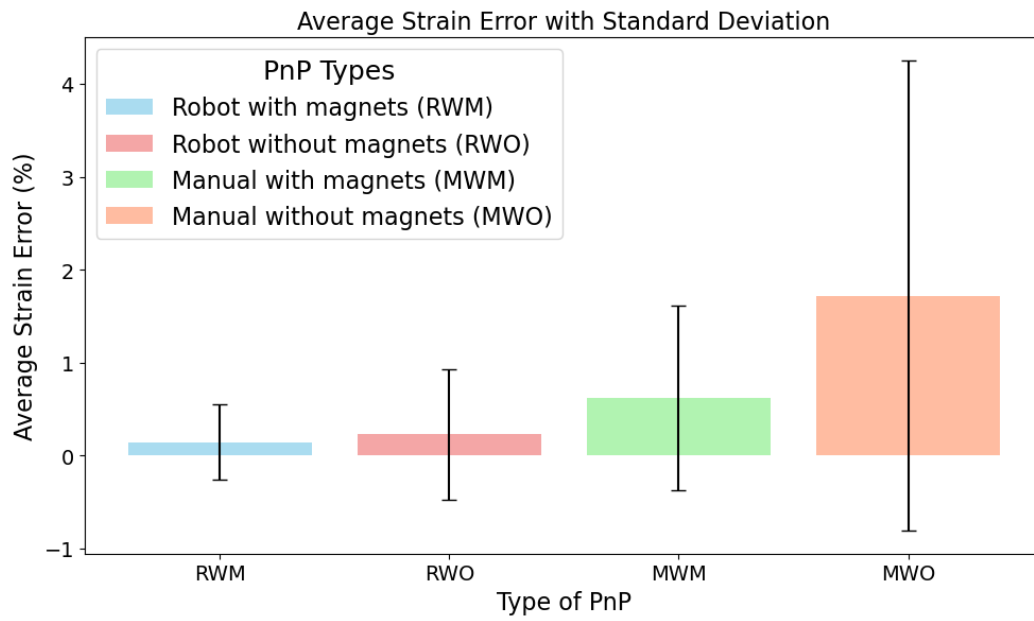


Figure 4-11. Average Strain Error with Standard Deviation



# Chapter 5. Automated Manufacturing of Smart tunnel Segment

In conjunction with Chapter 4, this section forms the heart of this thesis. It presents the practical aspects of the work carried out in the lab, involving the design, fabrication, and assessment of tunnel smart segments. Notably, the deployment of VWSGs through robotic means. This chapter represents the culmination of efforts laid out in preceding sections.

## 5.1 Background

In Chapter 1, the research mentioned the London Thames Crossing (LTC) road tunnel as the focus of this thesis. This tunnel, spanning over 2.6 miles and with the potential of becoming the longest in the UK, represents a substantial endeavour <sup>166</sup>. It will require a collective effort to incorporate state-of-the-art technology for enhanced efficiency in future inspections and maintenance. Construction for the tunnel has not yet begun. Nevertheless, access to preliminary design data has been secured. This data includes information about the tunnel's shape, the number of segments, and the materials to be used. The sources of this information are the tunnel's designer, COWI, and the asset owners, National Highways, who are also generous contributors to the research. Furthermore, interactions with Stanton Bonna, a tunnel segment manufacturer, have proven invaluable in comprehending the practical aspects of segment production and sensor integration.

Utilizing robots for the permanent deployment of sensors on concrete elements is uncommon. However, there is an example in the literature where a collaborative robot (cobot) was equipped with a spray-coating nozzle as an end-tool to deploy self-sensing metakaolin geopolymers for surface crack detection <sup>167</sup>.

A standard procedure for manually embedding sensors into concrete involves attaching them to the reinforcement during the preparation phase, just before the concrete is poured (refer to Figure 5-1). This ensures that the sensor will maintain its position even when subjected to intense vibrations during the subsequent stages of construction. However, modern tunnel segments, such as those used at the LTC, use fibre reinforcement rather than rebars, and so this method is not feasible.



Figure 5-1. Manual deployment of an embedded sensor for a precast grandstand element <sup>168</sup>.

This chapter begins with an introduction to the industrial insights that have informed this work. The subsequent focus is on the practical experiments concerning the smart segment materials and their properties. Following that, a presentation of the experimental setup for fabricating the smart segment and preparing the VWSGs for sensor deployment. Finally, the concluding part is dedicated to the presentation of the performance assessment of smart segments and the discussion of the results obtained.

## 5.2 Design and fabrication of lab-scale segment

### 5.2.1 Discussion on the scale

The segment's design is based on the design drawings for the LTC project, as provided by COWI. In Figure 5-2, a typical section of the LTC road tunnel consists of a total of 9+1 segments, which are divided into three groups: One principal or "key" segment, two trapezoidal segments, and seven standard segments (refer to 2.1.2.1.1. for definitions of each segment and role).

The lab experiments were conducted on down-sized standard segments, which have the dimensions of 5210x2000x500mm (Length x Width x Thickness).

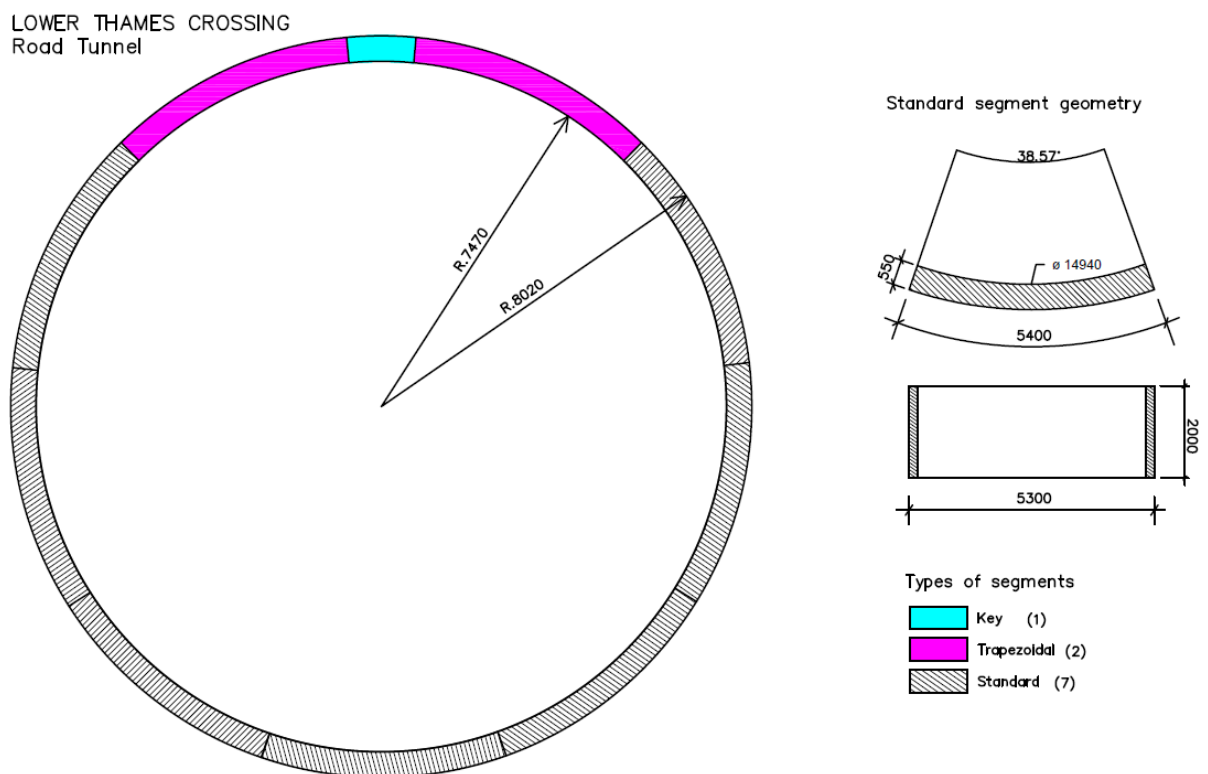


Figure 5-2. Lower Thames Crossing tunnel ring geometry

Scales for reducing the size of concrete element models typically range from 1/12 to 1/2, with 1/5 being the most commonly employed scale<sup>169,170</sup>. The widely accepted guideline for selecting a scale is to aim for the closest possible approximation to a 1:1 scale, but practical considerations often make this ideal difficult to achieve. A balance must be struck between the cost of manufacturing and testing and the potential adverse effects, such as size-related impacts on the mechanical properties of the model, when determining the scale.

Table 5-1 offers a selection of scale options, in recommended ranges, for reducing the size of the standard LTC segment. While the weights of these scaled segments are valuable for adhering to lab handling requirements, the ultimate decision on scale choice must strike a balance. This balance should aim for a scale that both accurately represents the segment's properties and mitigates the impact of size-related effects. Achieving this equilibrium is crucial in ensuring that the experiment provides meaningful and reliable results.

Table 5-1. List of segment model scales

Scale	Extrados Arc length [mm]	Centre arc length [mm]	Horizontal length [mm]	Width [mm]	Thickness [mm]	Weight [kg]
1: 1	5400	5210	5300	2000	550	13,468
1: 2	2700	2605	2650	1000	275	1,683
1: 3	1800	1737	1767	667	183	499
1: 4	1350	1303	1325	500	138	210
1: 5	1080	1042	1060	400	110	108

The selection of laboratory model scales hinges on a set of criteria influenced by laboratory limitations, all of which must be concurrently satisfied for the chosen scale:

- *Weight Limit:* The segment's weight should not surpass 1,000 kg to align with the lab's pallet truck and overhead crane capabilities. For ease of manual handling during placement in testing equipment, keeping the segment weight below 100 kg is recommended, ensuring safe and efficient handling during testing.
- *Sensor Height:* The standalone sensor box, with a maximum height of 80 mm, must not be smaller than the segment's thickness, maintaining a minimum 20 mm cover between the sensor and the nearest segment face.
- *Geometric and Mechanical Similarity:* The selected scale should provide acceptable geometric and mechanical resemblance to the prototype.
- *Minimum Length:* The segment model must be at least 1000 mm in length to fit the testing equipment used for flexion tests.
- *Aggregate and Fibre Scale:* The chosen scale factor should result in small-size aggregates and fibres readily available in the market.

With the criteria established, the focus now shifts to addressing the downsizing of components involved in the FRC composition of the segment. It is generally recommended to

downsize concrete model components using the same scale factor as the model <sup>171</sup>. These elements include:

- *Aggregate Size and Gradation* that directly impact mix workability and can be downscaled using the same factor as the model.
- *Steel fibre Length*: Commonly available steel fibres include lengths of 25/30/35/45/50/60 mm <sup>172</sup>. These cannot be directly scaled, but they must be longer than the aggregate diameter and meet the condition that the double of the aggregate size should be greater than one-third and smaller than two-thirds of the fibre length <sup>173</sup>.

Table 5-2 provides the scaled-down aggregate sizes using the same scale factor as Table 5-1, along with a recommended range of fibre lengths.

Table 5-2. Scale down aggregate max size and fibres length

Scale	Max. aggregate size (mm)	Compatible fibres length (mm)
1/1	20.00	50-60mm
1/3	6.67	35-40mm
1/4	5.00	25-30mm
1/5	4.00	20-25mm

After evaluation of the equipment available in the lab for handling segments and testing them combined with the various length of the fibres available in the market, the scale factor of 1/5 was retained for the length and the thickness of the segment while the scale of 1/4 for the width. Figure 5-3 shows the down-sized smart segment that will be cast and tested in this thesis.

## 5.2.2 Characterisation of concrete

In this section presents the mix composition and the mechanical properties of the SFRC used to fabricate lab-scale segment.

### 5.2.2.1 SFRC mix composition

#### 5.2.2.1.1 Components

##### *Cement*

A CEMII 32.5 cement was consistently used in the concrete mix.

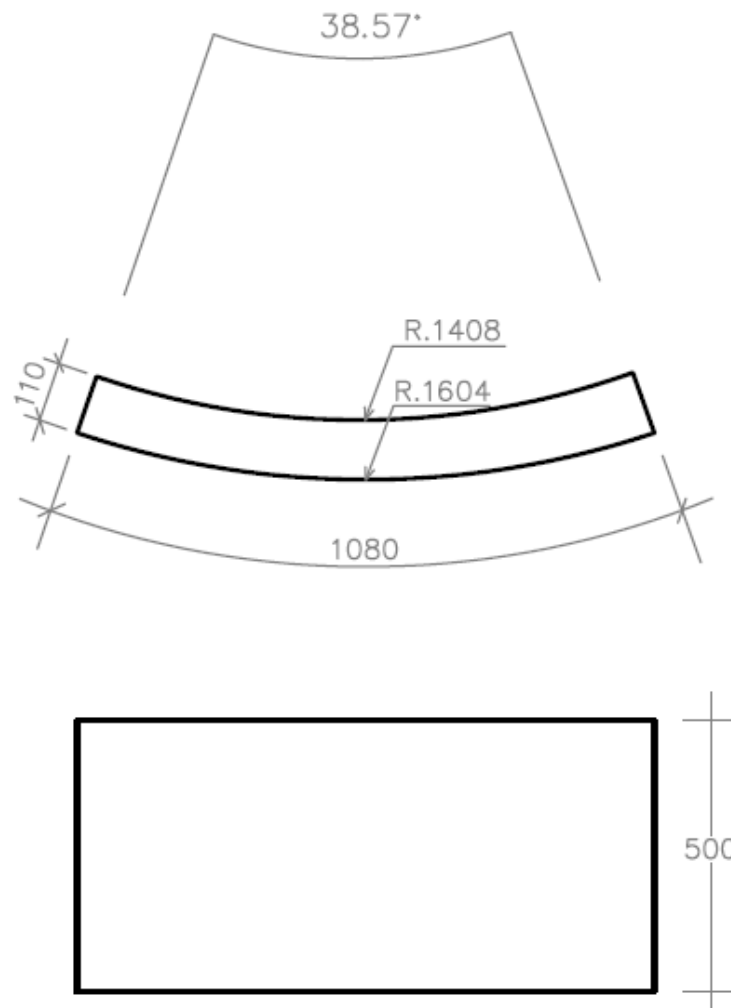


Figure 5-3. Geometry of small-scale segment (dimensions in mm)

### *Aggregates*

The coarse aggregate use was a 6 mm size.

### *Steel fibres*

Three types of steel fibres, in Table 5-3, have been considered in this study. While they were all used for initial concrete mixes, Kramperharex fibres have been retained as they are more in accordance with criteria enounced in section 5.2.1.

### *Admixtures*

DVA XR 3009<sup>174</sup> high-performance superplasticiser was used as admixture.

Table 5-3. Steel fibres properties

Manufacturer	Length L (mm)	Eq. diam. D (mm)	Aspect ratio (L/D)	Tens. Str.
Adfil SF 86 <sup>175</sup>	60mm	0.75mm	80	1225 MPa
Bekaert <sup>176</sup>	35mm	0.55mm	65	1345 MPa
Kramperharex <sup>177</sup>	25mm	0.40mm	63	1200 MPa

#### 5.2.2.1.2 Mix composition

The SFRC composition was formulated by taking guidance from both <sup>178</sup> and <sup>179</sup>. Within the specified range of expected values for workability, compressive strength, and cement class, recommended compositions for the mix elements have been provided, as displayed in Table 5-4.

While the resulting mix, in Table 5-5, may exhibit slight variations from the guidelines previously mentioned, it remains suitable for use in fabricating and testing reduced-scale components, such as the lab-scale tunnel segment targeted for later experiments.

Table 5-4. Range of proportions for SFRC components<sup>179</sup>

Size aggregate	Up to 10mm	Up to 7.5
Cement	270-450 kg/m <sup>3</sup>	227 – 408
w/c	0.35-0.45	0.35-0.5
Sand/Aggregate	45-60%	45-55%
Fibre content	30-80	25-60

Table 5-5. Steel reinforced concrete mix design

Components	Reference concrete	Fibre concrete
Cement (CEM II 32.5R)	350 kg	350 kg
Water	158 l	158 l
Coarse aggregate	1200 kg	1200 kg
Sand	600 kg	600 kg
Fibres	-	40 kg
Superplasticiser		1.4l

#### 5.2.2.2 SFRC characterisation

##### *Fresh concrete*

The Vebe test, as described in <sup>180</sup>, was employed to evaluate the concrete workability. The Vebe value measured before and after the addition of a superplasticizer was 25 seconds and 18 seconds, respectively. Despite the superplasticizer causing a reduction in the Vebe value, the concrete retained its stiffness, a typical characteristic observed in the real-world precast concrete elements <sup>181</sup>.

## Hardened concrete

The SFRC compression obtained by testing a total of six 28 days cured 100 mm cubes <sup>182</sup> and the flexion obtained testing 12 500x100x100 mm beams <sup>183</sup>, are shown in Table 5-6.

Table 5-6. SFRC mechanical properties. Where  $f_L$ ,  $f_{Ri}$  are respectively the elastic limit and the residual strength with crack opening at 0.5, 1.5, 2.5, and 3.5 mm as defined in <sup>183</sup>.

	Compression	Flexion			
	$f_C$ [N/mm <sup>2</sup> ]	$f_L$ [N/mm <sup>2</sup> ]	$f_{R1}$ [N/mm <sup>2</sup> ]	$f_{R2}$ [N/mm <sup>2</sup> ]	$f_{R3}$ [N/mm <sup>2</sup> ]
Strength	40.3±0.53	4.39±0.75	3.98±0.41	4.63±0.85	5.24±1.12

## 5.3 Smart segment characterisation and performance assessment

### 5.3.1 Mechanical tests on segments

Mechanical tests were conducted on reduced-scale segments to assess the behaviour and durability of sensors under controlled laboratory loads. The primary objective was to evaluate the sensors' performance in tracking the structure under 'normal' loading conditions, with the assumption that, should the monitored structure fail, the sensors might also fail. The determination of appropriate load levels for these tests involved collaboration with the structural engineering team from COWI, who were actively engaged in the structural design of the LTC road tunnel.

#### 5.3.1.1 Tests layouts

To characterize instrumented lab-scale standard segments, a compression test and a 3-point bending test were conducted. Further details of these tests are provided later in this document. Previous studies <sup>184,185</sup> on instrumented tunnel segments yielded valuable insights into the placement of embedded sensors, and the use of additional measuring equipment, such as displacement sensors, was crucial in this regard.

##### 5.3.1.1.1 Three-point bending test

The three-point-bending test, shown in Figure 5-4, was conducted to evaluate the response of VWSGs to flexural strains resulting from temporary loadings applied to segments, including those associated with demoulding, stacking, transport, and positioning, as well as the sustained loading from soil pressure. It is imperative to emphasise that the primary



objective of this assessment was not to examine the mechanical properties of the segments. Rather, the study aimed to investigate the behaviour of robotically deployed VWSGs under normal loading conditions, well within the elastic behaviour range of the SFRC. To achieve this goal, the loading was systematically applied in a sequential and repetitive manner until a predetermined fraction of the elastic limit (maximum load before the appearance of cracks) load was attained.

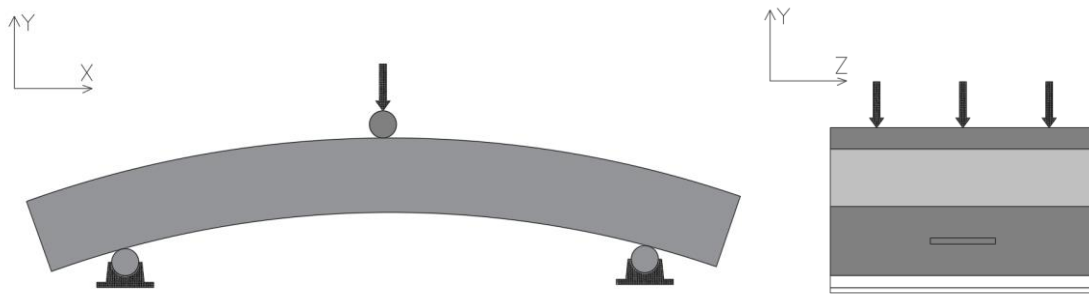


Figure 5-4. Three-point-bending test experimental layout

#### 5.3.1.1.2 Compression

The compression test, shown in Figure 5-5, on lab-scale tunnel segment served to assess the sensors' response to compression forces akin to those induced by the TBM thrust during the installation of the segment. Similarly, the segments were loaded sequentially up to a fraction of the elastic limit.

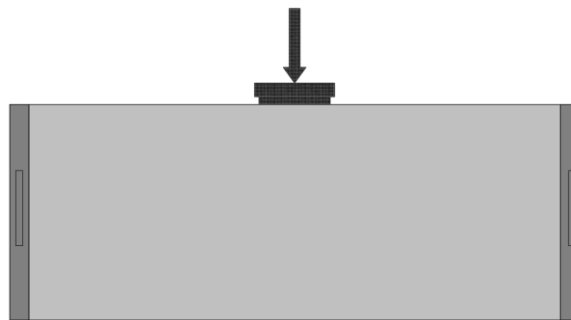


Figure 5-5. Compression test experimental layout

#### 5.3.1.2 Preliminary tests on the lab-scale segments

The purpose of this section is to present the preliminary tests conducted on lab-scale segments, report the observations made during these tests, and propose improvements for subsequent stages.

In the initial phase of this study, non-instrumented segments were subjected to both the three-point bending test and compression tests. The fabrication of laboratory-scale segments served several purposes:

1. **Assessing Handling Conditions:** A primary focus was to evaluate the practical aspects of segment handling within the laboratory environment. This assessment placed particular emphasis on instances where manual handling may be required, notably during the fitting of segments into the flexural testing machine and the universal compression machine.
2. **Comparing Maximum Loads and Crack Patterns:** Additionally, the study sought to draw comparisons between plain segments and segments equipped with a dummy box in terms of the maximum loads they could withstand and the patterns of cracking observed.

To facilitate these investigations, a formwork was fabricated for creating laboratory-scale segments, as shown in Figure 5-6. Subsequently, two pairs of segments were manufactured, with each pair comprising one plain segment and one segment equipped with a dummy box. The first pair underwent evaluation through the three-point bending test, while the second pair was subjected to compression testing. These two initial tests were conducted on the Dartec flexion testing rig and a hydraulic universal compression machine with analogical measurement readings. Both testing layouts are shown in Figure 5-7.

#### 5.3.1.2.1 Segments handling

In the laboratory, handling the 125 kg lab-scale segments proved to be a challenge. A hand truck equipped with an elevator was used to move the segments. Two specific issues arose during this process:

1. The support rollers on the flexion testing rig had to be replaced to be replaced with longer ones, surpassing the usual length of the supports (25cm).
2. The universal compression machine's stroke range (50.5 - 52.5 cm) allowed minimal clearance for inserting the beam.

These two challenges highlighted the need for a precise handling leading to potential equipment adjustments for future testings.



Figure 5-6. On the left the segment formwork is shown. The right shows the segment being casted.



Figure 5-7. Left: segment on the Dartec rig. Right: segment in hydraulic testing rig.

#### 5.3.1.2.2 Maximum loads and crack pattern

The results of the three-point bending test on the two previously examined segments reveal comparable maximum values, approximately 17 kN, for both the segment with a box and the plain segment. Notably, the displacement versus load plots, in Figure 5-8, illustrate close alignment in their peak values. However, the peak load occurred at smaller displacements for plain segment while the segment with a box reached its peak for larger displacements. While the directions of the cracking in the two segments, as illustrated Figure 5-9, are similar, it is worth noting that the initiation of the cracking is slightly different. These findings suggest that the introduction of a box did not substantially alter the overall structural response but may have influenced the crack initiation characteristics. While the latter may have guaranteed further investigation for the understanding of a deep understanding of the structural behaviour of SFRC segment, it did not constitute an impediment for the goal here: determine whether the insertion of a box in the segment changed substantially the maximum value of the load on segment.

Similarly, the compression test corresponding set of the segment containing the box and the plain segment showed that the maximum value of the load was 800 kN.

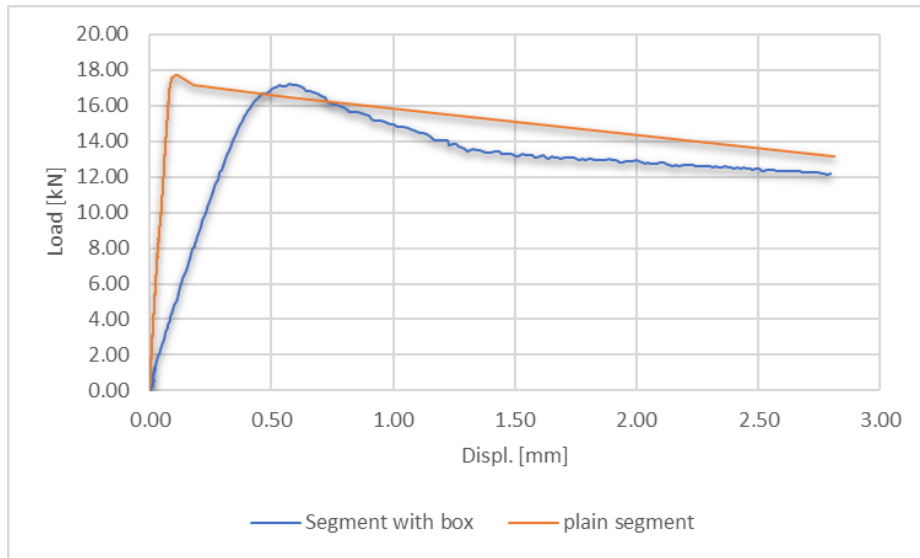


Figure 5-8. Displacement versus Load of segments with and without dummy box

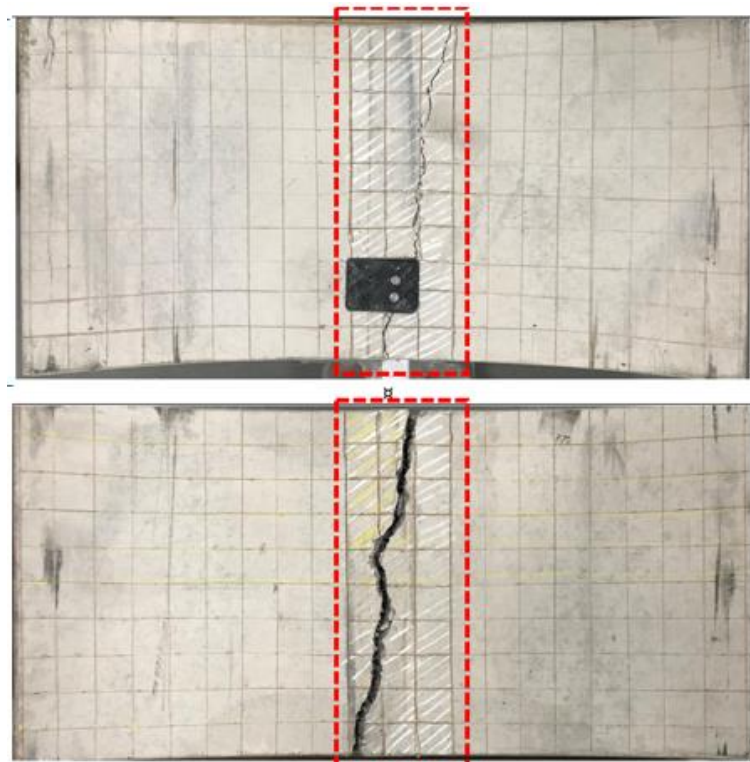


Figure 5-9. Cracking patterns of instrumented (above) and plain beam (below)

### 5.3.1.3 Conclusions of the preliminary test results

The results of the compression and 3-point bending tests indicated a size effect on the initiation of cracking resulting from the insertion of the box. Both the plain segment and the

segment with the box demonstrated remarkably close maximum load values, suggesting minimal influence on overall structural response.

While the handling of the 125 kg segment did not result in any accidents or hazards, it became evident that manual handling was not advisable due to its weight. Despite successful fitting into the universal machine, the reduced spacing in the fitting process added tediousness and a slightly increased risk in manual handling.

In response to the initial testing challenges, the laboratory procured more accurate and suitable equipment with higher testing ranges for both the 3-point bending and compression tests. However, this transition introduced additional lab constraints notably: shorter support and load rollers for the 3-point bending test rig (now at 30 cm); and a reduced maximum space available in the compression machine (30-35 cm).

Consequently, the segment's width was halved, as depicted in Figure 5-10, to align with the new equipment specifications and enhance the overall efficiency and safety of subsequent testing procedures.



Figure 5-10 Segment formwork with a new partition divides the formwork into two regions for pouring the same SFRC. This configuration enables simultaneous casting of an instrumented segment and a plain segment, the latter used in the failure test.

### **5.3.2 Instrumented segments on straight beams**

Prior to embarking on tests involving instrumented curved beams, it was deemed imperative to establish a foundation using straight beams with uncomplicated geometry. This

preliminary phase exclusively includes 2 three-point bending tests, as it will allow a thorough understanding and resolution of potential issues before transitioning to curved beams. Additionally, this initial testing phase lays the groundwork for the subsequent performance evaluation of the smart segment, which will be elaborated upon in later stages.

### 5.3.2.1 Experimental Setup

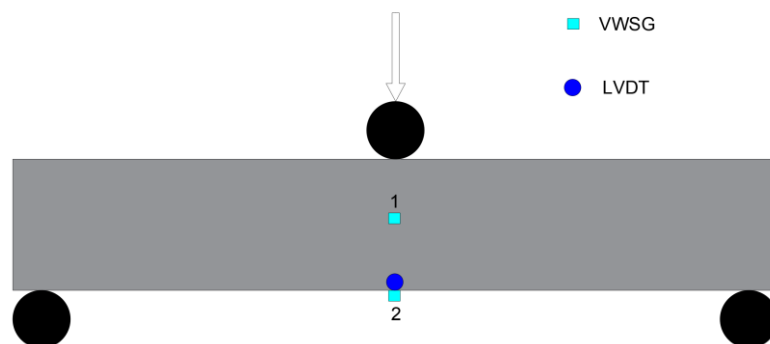
This section presents the results of 3-point bending tests on a pair of 100x100x500 mm concrete beams—one instrumented and one plain.

The experimental layout, shown in Figure 5-11, includes the following components:

- The instrumented beam, featuring two VWSGs. The first VWSG attached to the ad-hoc packaging presented 4.2.3 is embedded within the beam, while the second sensor is surface-mounted at the bottom of the beam.
- An ad hoc data acquisition system, as described in 3.3, is utilized to interrogate the sensors during the bending test and transmit data to an independent computer.
- A universal test machine is employed to execute a customized flexion test. Additionally, two Linear Variable Differential Transformers (LVDTs) are positioned at the midspan to measure the displacement.

The testing procedure commenced with the loading of the plain beam until failure, with the failure load recorded at 7.00 kN. Subsequently, 50% of this value was established as the upper limit for cyclic tests conducted on the instrumented beam.

The test on the instrumented beam involved the gradual application of a concentrated load at the midspan, initially ranging from 0.5-2.5kN, followed by 0.5-3.5kN. This sequence is repeated ten times.



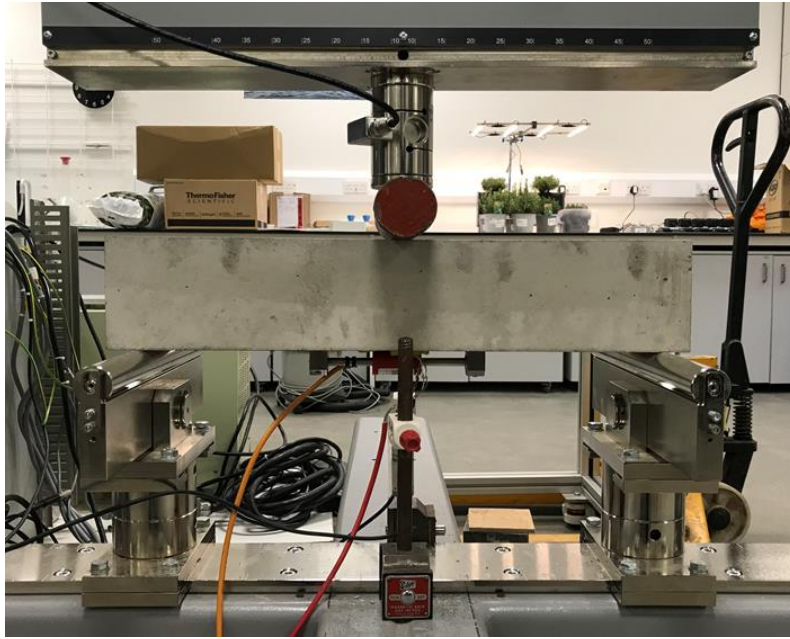


Figure 5-11. Experimental setup of 3-point bending test on 100x100x500 mm beam.

### 5.3.2.2 Results and commentary

#### 5.3.2.2.1 Drift in the results

A drift was observed in both the displacement, as well as in the strain for both the embedded VWSG and the surface-mounted one as shown in Figure 5-12. While the drift can be a matter of concern generally, it is worth noting that they were more visible in this case because of the low range of loadings used in the flexural rig with a resolution of just 0.5 kN. Secondly, given that the cyclic test on instrumented beam was conducted in the elastic zone of the SFRC beam, a drift correction and zeroing of values of the like the one in the right column of Figure 5-12 are guaranteed.

#### 5.3.2.2.2 Material properties

This test further facilitated the estimation of the modulus of elasticity and the Poisson's ratio of the SFRC beam via an iterative finite element modelling (FEM) approach. The FEM of the beam, constructed in Abaqus and depicted in Figure 5-13, replicated the loading and setup conditions of the 3-point bending test performed on actual beams.

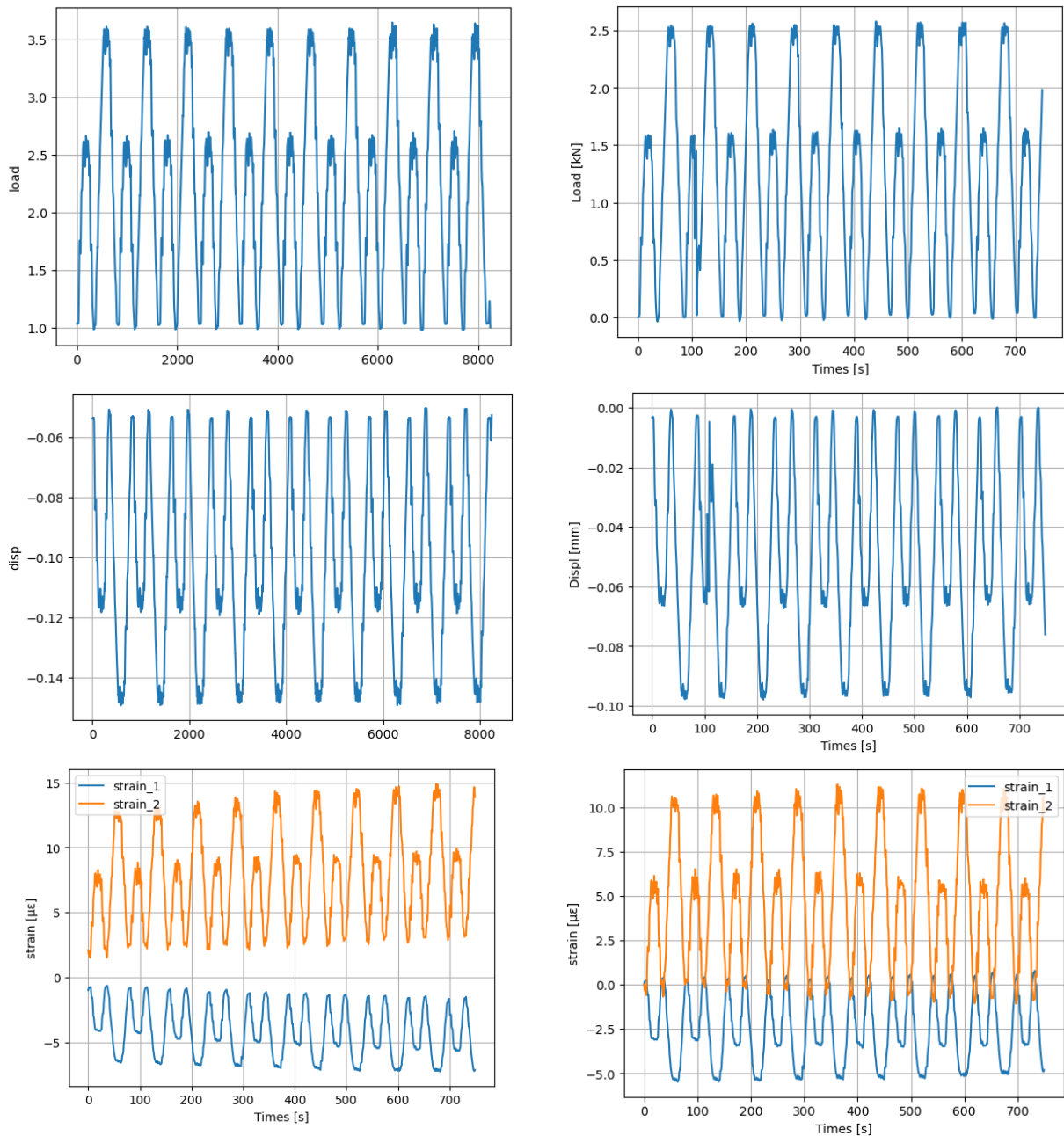


Figure 5-12. Timeseries for measured Load, Displacement, and the Strains. The left column shows the raw measurements and the right column present the same measurements readjusted to eliminate the drift

Through an iterative adjustment of the modulus of elasticity ( $E$ ) and the Poisson's coefficient ( $\nu$ ) in the model, a value of  $E=30$  GPa and  $\nu=0.2$  was determined. These values were found to provide the closest match between the measured and calculated displacements, signifying a successful calibration of the finite element model to the experimental data.



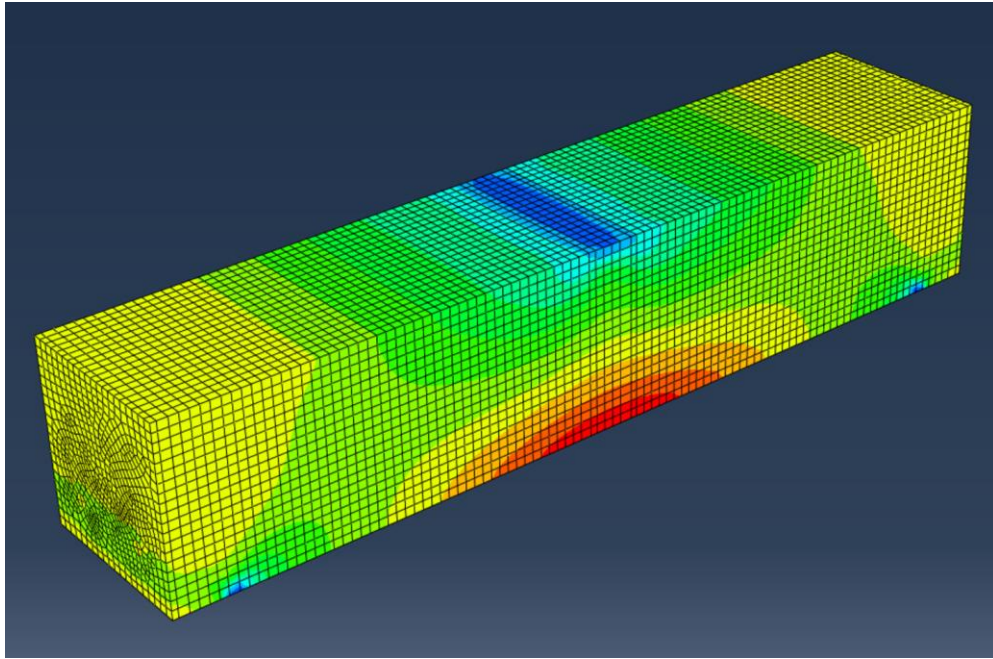


Figure 5-13. FE model for the prismatic SFRC beam.

#### 5.3.2.2.3 Strain transfer

Further insights were obtained by comparing the measured strains with those derived from the finite element (FE) model. This comparison typically involves the concept of strain transfer, which is the ratio of the theoretical strain to the measured strain at the measurement position. For the embedded and surface-mounted Vibrating Wire Strain Gauge (VWSG) sensors, the strain transfer values were found to be 0.53 and 0.71, respectively.

Strain transfer values are typically between 0 and 1, with 1 signifying a perfect correlation between measured and calculated values. In this study, the strain transfer values obtained indicate a superior performance for the surface-mounted VWSGs compared to the embedded VWSGs. However, these values, although within acceptable ranges, are relatively low. This could be attributed to the measurements being conducted across two beams. Moreover, it's noteworthy that the strain values measured by the surface-mounted VWSGs may not accurately capture the strain at the inferior fiber, instead registering strains slightly above it.

#### 5.3.2.3 Summary

This section aim was to run a three-point bending test on an instrumented simple supported beam in order to gain insights to apply to later tests on curved beams. The conclusions at this stage were as follow:

- The measured values of the strains and the deflection had to be readjusted to eliminate the testing machine induced drift.
- The module of elasticity and the coefficient of Poisson obtained through iterative FE modelling were respectively 30 GPa and 0.2.

## 5.4 Smart segment performance evaluation

This section outlines the steps taken to evaluate the performance of a lab-scale smart segment. It also discusses the methodology and provides justification for the different elements involved in the assessment.

### 5.4.1 Steps

The evaluation of the smart segment involves the following steps:

**Step 1:** Simultaneously cast two segments—one instrumented with VWSGs using a robotic deployment, and the other left plain, as shown in Figure 5-14. The desired location for placing the sensor box was marked on the formwork, ensuring precise and consistent positioning across the smart segments.

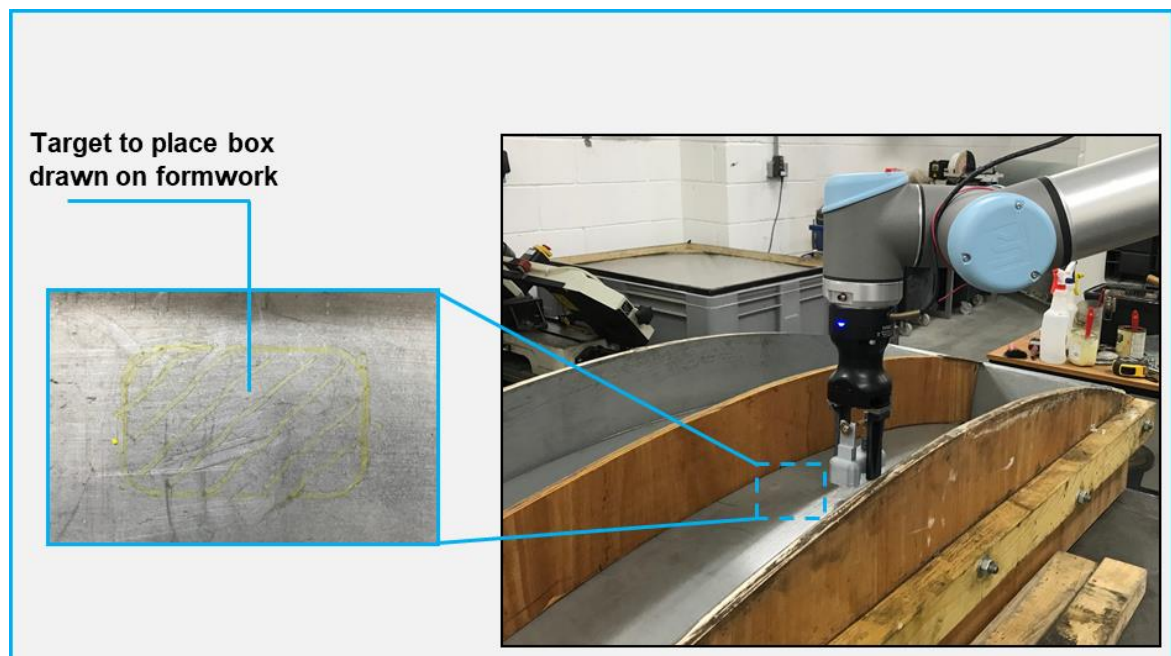


Figure 5-14. Robotic deployment of the VWSGs on smart tunnel segment formwork.

**Step 2:** Once both segments have reached maturity, conduct a test up to failure on the plain segment and record the obtained value.

**Step 3:** Perform a cyclical test on the instrumented segment, limiting the maximum loading to 50% of the average failure loads from the previous step. Throughout the test, the values of loads, displacements, and strain were recorded for further analysis.

**Step 4:** Develop a theoretical model (both numerical and analytical) corresponding to the test conducted on the instrumented segment.

**Step 5:** Evaluate the strain transfer for each segment using the numerical and analytical models.

**Step 6:** Assess the repeatability of the strain transfer across all the tested beams.

### 5.4.2 Sensors

Two VWSGs were embedded in each smart segment, as shown in Figure 5-15. The decision to incorporate two VWSGs in the smart segments, with one serving as an axial sensor and the other as a lateral sensor, is underpinned by the need to capture the segment's behaviour under loading in two principal directions.

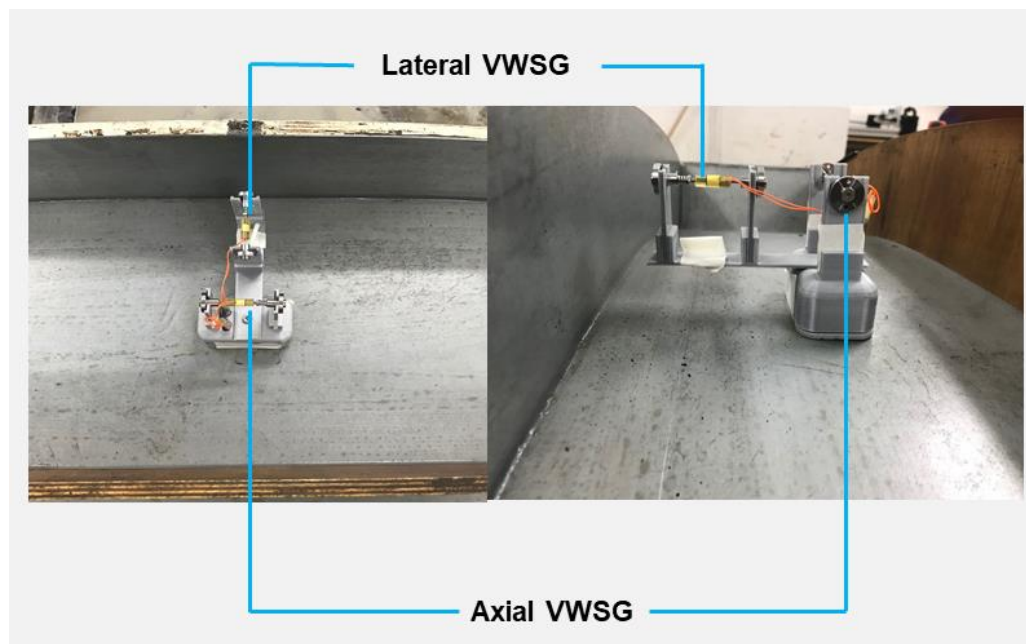


Figure 5-15. VWSGs deployed on the smart segment formwork

### 5.4.3 Number of segments

In the evaluation process of the smart segments, 10 specimens were successfully tested. This number remains sufficiently representative to capture significant variations across the segments offering at the same time valuable insights into their performance.

### 5.4.4 Tests

Prior to testing the instrumented segments, a series of displacement control three-point bending test on plain segments were conducted. The average failure load across 10 segments, was 10.10 kN. Subsequently, for the smart segments, a series of cyclical three-point bending tests, as pictured in Figure 5-16, were undertaken, within a 0.5 - 5.5 kN range. The lower value in the range corresponding to the minimum preload of the machine while the upper limit represents 50% of the average failure load.



Figure 5-16. Smart segment in the flexural rig during the cyclic test

### 5.4.5 Models (numerical and analytical)

The analysis of the 3-point bending test results on the smart segment involved comparing them to two theoretical models implemented with similar loading conditions and material properties as those of the actual beams.

### 5.4.5.1 Model 1: Straight Beam Approximation

In the analysis of the 3-point bending test results on the smart segment, the first theoretical model employed consisted at approximating the segment (curved beam) to a straight beam, as illustrated in Figure 5-17. This simplification was possible due to the segment's large Radius/Thickness ratio, exceeding  $5^{186}$ .

Applying the elastic equations for a straight beam, strains were calculated as functions of the load using Equation ( 5-1) and Equation ( 5-2). In these equations,  $\varepsilon_L$  and  $\varepsilon_T$  represent axial and lateral strain in  $\mu\varepsilon$ , respectively. The parameters include L for the beam span, y for the distance of the sensor location to the neutral axis (both in mm), E for the module of elasticity in N/mm<sup>2</sup>, P for the load in N, and I for the moment of inertia in mm<sup>4</sup>.

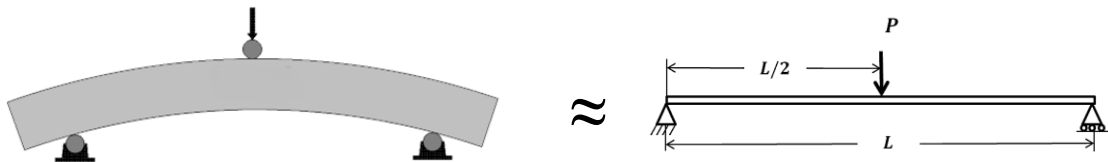


Figure 5-17. Illustration of straight beam approximation of a curved beam

$$\varepsilon_L(P) = -\frac{Ly}{4EI} P \quad (5-1)$$

$$\varepsilon_T(P) = \nu \frac{Ly}{4EI} P \quad (5-2)$$

### 5.4.5.2 Model 2: Finite Element Model (FEM) Simulation

Complementing the straight beam approximation, a second model involved the creation of a FEM using Abaqus, illustrated in Figure 5-18. This detailed simulation replicated real test conditions, incorporating loads identical to those applied during the physical experiment. Measured strains from the experimental setup were then extracted for comparison with the strains predicted by the FEM.

### 5.4.6 Performance evaluation.

The performance evaluation of smart segments will consist of:

1. Estimating the strain transfer of robotically deployed VWSGs using as theoretical models the straight beam approximation and the finite element model.

For each segment, the scatter plot depicting peaks of measured strains versus calculated strains is generated. The ratio between these two values, defines the strain transfer.

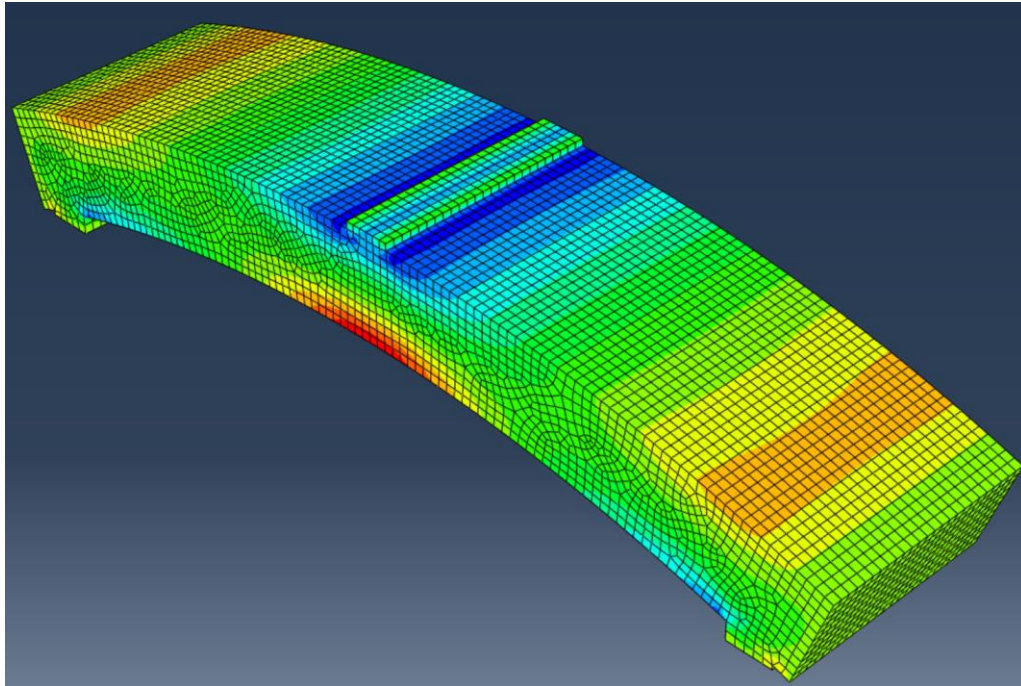


Figure 5-18. Curved beam FE model

2. Assessing the repeatability of the strain transfers across the 10 segments.

For the assessment of repeatability in peak values of strain measurements, the chosen statistical metrics were the estimation of the coefficient of variation and the Intraclass Correlation Coefficient (ICC) of the strain transfer of robotically deployed VWSGs across the 10 smart segments tested. Utilized in reliability studies, ICC offers a robust means to evaluate the consistency and agreement among repeated measurements. This statistical method quantifies the extent to which peak strain values exhibit consistency across multiple tests, providing an objective indicator of the repeatability of strain measurements.

## 5.5 Results and discussion

### 5.5.1 Results

This phase of the study focuses on examining the consistency of strain measurements in smart segments subjected to diverse loading conditions. This analysis holds a crucial importance in evaluating the reliability of strain measurement employed in lab-scale tunnel smart segments. Illustrated in Figure 5-19 are the strain time series from a representative smart segment. Notably, the repetitive pattern observed during load-controlled 3-point bending tests is distinctly reflected in the recorded strain measurements.

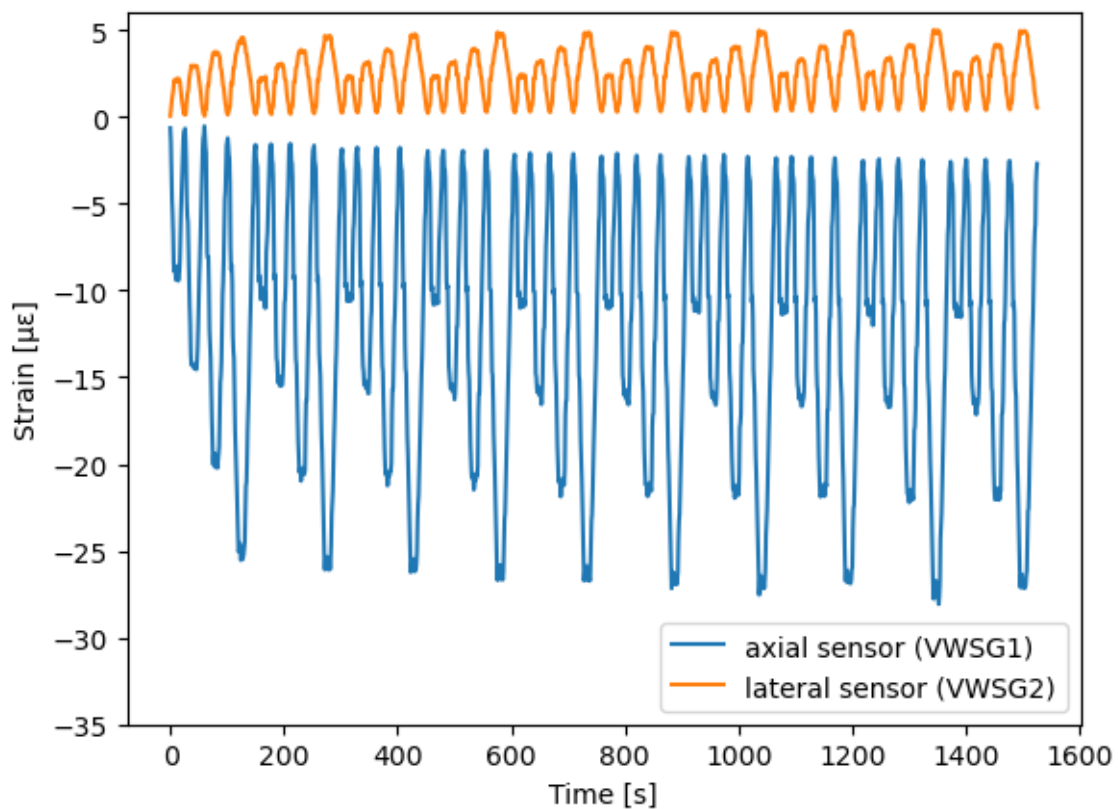


Figure 5-19. Time series showing measured strains during the cyclic three-point bending test

In addition to strains, load data for each segment have been collected and used to calculate corresponding axial and lateral strains using the FE model of the lab-scale segment shown in Figure 5-20 and the straight beam approximation using elastic equations in 5.4.5.

The scatterplot of the measured strain versus calculated strains, illustrated in Figure 5-21 for a sensor in a typical segment using one of the two strain calculation models, the FE mode and the straight beam approximation, permit to obtain the strain transfer. A value of

1.0 would indicate an exact match between measured and predicted strains, therefore the closer to 1 the better. Peak strain for the 10 segments can be found in the Appendices A. 4 and A. 5.

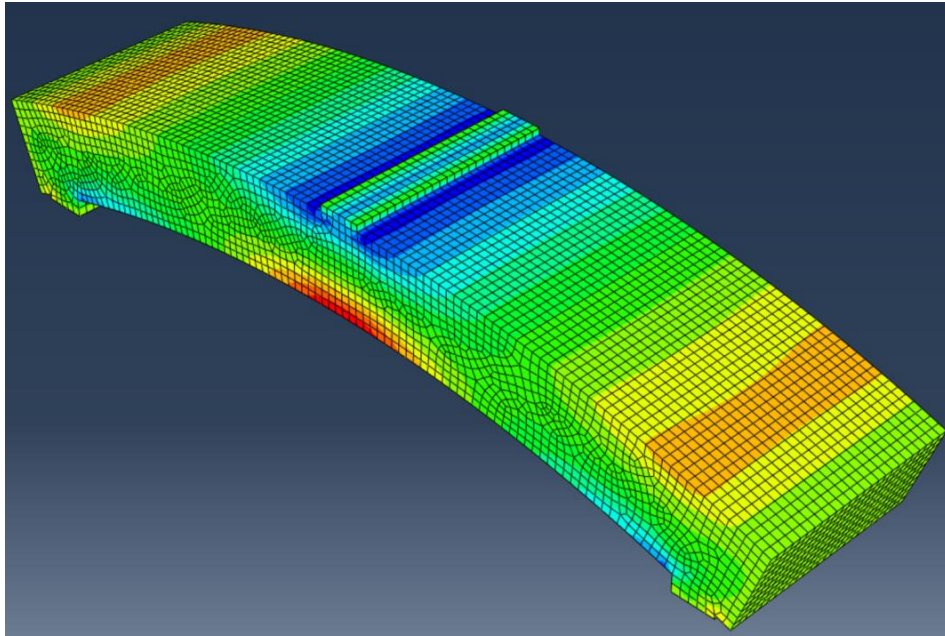


Figure 5-20. Curved beam FE model

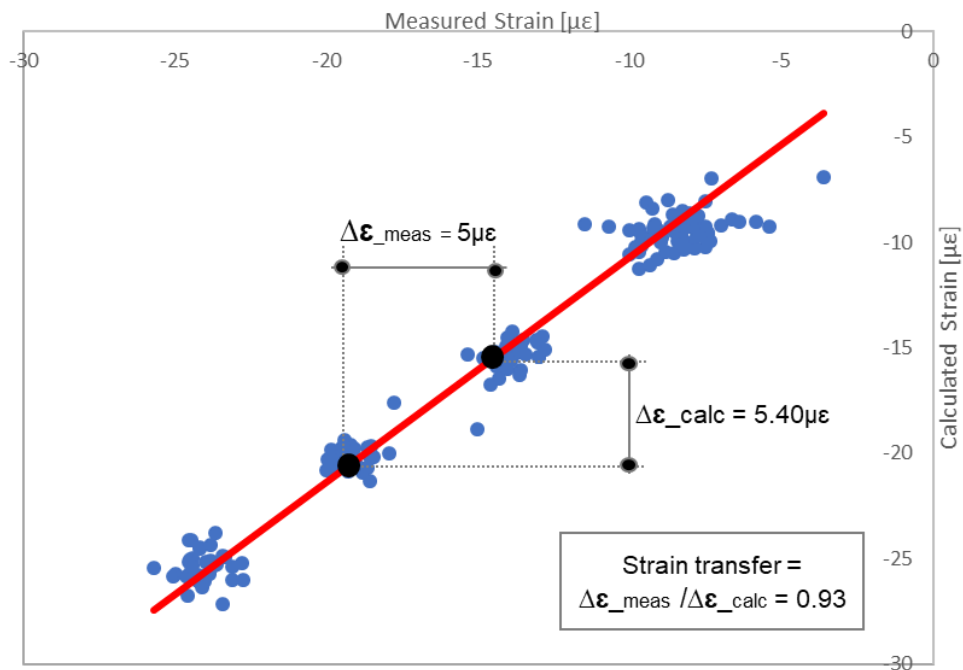


Figure 5-21. Example of peak strains scatter plot illustrating the definition of the strain transfer



Table 5-7 outlines the strain transfer values for both axial and lateral VWSGs across the 10 smart segments. The data is organized based on the respective calculation models employed for estimation, providing a clear overview of the strain transfer characteristics for axial and lateral orientations in the smart segments.

Table 5-7. Lab-scale smart segment strain transfer

FE model		Straight beam approximation	
Axial	Lateral	Axial	Lateral
0.930±0.012	0.567±0.011	0.853±0.042	0.869±0.036

## 5.5.2 Discussion

### 5.5.2.1 Drift correction.

Similar to straight beams in the preliminary tests in 5.3.2.2, the measured strains necessitated a correction of the drift coming from the testing equipment.

### 5.5.2.2 Strain transfer.

#### 5.5.2.2.1 Theoretical model

In one hand the strain transfer of the axial VWSGs are relatively high in both calculation model, notably 0.930±0.012 for the FE model and 0.853±0.042 for the straight beam approximation.

On the other hand, the strain transfer of the lateral VWSGs are different according to the calculation model, notably 0.567±0.011 for the FE model and 0.869±0.036 for the straight beam approximation. The potential reasons for the discrepancy between the two calculation models can be:

- **Complexity of Curvature:** despite having a R/h (where R is the radius of the segment and h the width) ratio of 14.58 which is superior to 5, the straight beam approximation that assumes a simplified linear variation of strain across the cross-section may not accurately capture the non-linear effects introduced by the curvature.
- **Influence of Poisson's Ratio:** the Poisson effect can impact lateral strains. In a curved beam, the lateral contraction may be affected by the interplay of axial and transverse strains, contributing to variations from the straight beam approximation.

Contrary to the linear approximation, the FEM considers the actual geometry and material properties at each point along the beam. They certainly capture the non-linear effects and curvature-related phenomena that are not accounted for in the simplified straight beam approximation.

#### 5.5.2.2.2 Repeatability of measurement

##### *Coefficient of variation*

The coefficient of variation unveils consistently stable strain transfer, with values are 1% for the axial VWSG and 1.9% for the transversal VWSG. The observed strain transfer ratios in both VWSGs indicate a consistent and reliable relationship between calculated and measured strains. This suggests that the calculated strains based on load measurements provide an accurate estimate of the actual strains experienced by the smart segments.

##### *ICC*

The average ICC values across the 10 smart segments is 0.795 for VWSG 1 and 0.396 for VWSG 2. This confirms the previous observation found using the coefficient of variation as a repeatability metric.

#### **5.5.2.3 Robotic process**

While the robotic placement of sensors may introduce strain errors, though not significant as demonstrated in 4.3.2.2, the variability in strain transfer values in both VWSGs can be attributed to the position variations in the casting of the segments in the lab. This discrepancy indirectly captured by the strain transfer, that indicate how close the measurement is close to an ideal model, is more pronounced in the case of the lateral sensors than the axial sensor. It is possible that during the casting of the smart segment the positions of the lateral VWSG have shifted. Additional work including x-ray imaging or destructive testing can shed more lights on this.

## 5.6 Summary

This chapter focused on the design, fabrication, and evaluation of lab-scale smart tunnel segments based on early design stage of the LTC road tunnel project.

The lab experiments on the segment design and materials are then discussed, including the selection of scales for reducing the size of the segments. The downsizing of components involved in the SFRC composition of the segment is also addressed.

The chapter then moves on to the characterization of the concrete mix used for the lab-scale segments, including the mix composition and mechanical properties of the SFRC. The fresh and hardened concrete properties are described, including the workability and mechanical strength of the SFRC.

Next, the chapter discusses the performance evaluation of the smart segments. It outlines the steps involved in the evaluation, including the casting of instrumented and plain segments, failure testing of plain segments, cyclical testing of instrumented segments, and the theoretical models used for strain calculation.

Strain transfer values for the instrumented segments were calculated using both the straight beam approximation and the FEM. The results demonstrated a high reliability of strain measurements, indicating consistent strain transfer values and low coefficients of variation. However, some discrepancy existed between the two theoretical models for lateral strain measurements, possibly attributed to the complexity of curvature and the influence of Poisson's ratio.

These findings on a lab scale and environment underscored the effectiveness of utilising robotic technology for sensor deployment, offering potential advancements in productivity and reliability in the manufacturing of smart tunnel segments. While the results found were satisfactory, future work will involve implementing a study on a full-scale smart segment will assess the repeatability of the robotic process in strain transfers across a larger sample of segments, further advancing our understanding in this area.

The following chapter presents an economic justification study of smart segments, making the case for their suitability in comparison to on-site wired and wireless solutions.

# Chapter 6. **Economic justification for smart segments**

This chapter presents economic justifications for smart tunnel segments equipped with embedded and surface-mounted sensors, as these could offer distinct advantages when compared to traditional methods. Throughout the chapter, the short-term and long-term benefits of smart segments are first presented. Later, a cost-benefit analysis (CBA) was conducted to weigh the financial feasibility of smart tunnel segments. Also, a practical decision-making tool was introduced, serving as a valuable addition to the process of comparatively evaluating various instrumentation options.

## **6.1 Justification of the study**

To justify the large-scale production of smart segments for monitoring segmental tunnels, it is essential to demonstrate their advantages over non-instrumented tunnels and existing approaches such as traditional wired point sensors or on-site wireless. This is usually achieved through a CBA. Varied needs of main stakeholders, namely the assets owner, the design team, and the segment manufacturer, deserve a particular consideration. While the assets owner needs are long-terms and encompass the whole of the project, the segment manufacturer and the structural design team have short-term implication in the life of the asset and their role consists at supporting the asset owner during the corresponding phase of the project.

In this section, the presentation explores how smart tunnel segments meet stakeholders' needs by addressing their requirements. Additionally, it delves into the main benefits of smart segments over non-instrumented and on-site instrumentation solutions.

### **6.1.1 Stakeholders needs' identification**

The smart segment proposed in our study is a standard segmental element of a tunnel ring like the one shown in Figure 6-1. In the context of this economic justification study, the smart segment is robotically instrumented with embedded VWSGs attached to a fully wireless node to monitor both internal temperatures and strains. Other sensors can be added in the precast factory post casting. Being wireless, ideally, the data collection and analysis from the segment can begin during the manufacturing phase and run through to tunnel

construction, operation, and end-of-life. The information generated in some or all stages can be used by all the stakeholders involved in a tunnel project.

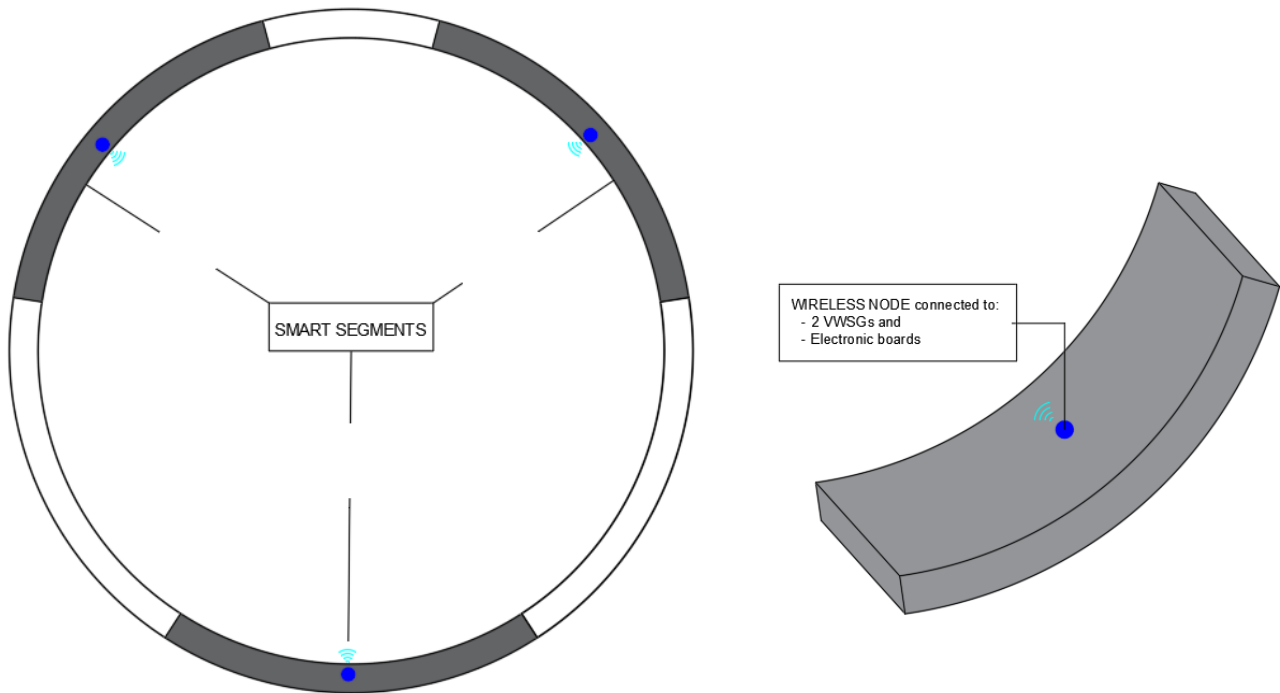


Figure 6-1. Tunnel ring equipped with smart segments.

Table 6-1 provides a concise overview of the identified needs for each stakeholder involved in implementing and operating smart segments in the tunnel lifetime.

- *For asset owners/managers*, the focus is on maintenance and repairs and operational efficiency to minimize costs and disruptions. Integrating smart segments has the potential to reduce inspection visits and facilitate timely maintenance, improving asset management.
- *Segment manufacturers* seek to address challenges such as inefficient production processes, quality control, cost reduction, waste management, and environmental concerns. Smart segments offer potential solutions by incorporating automated manufacturing processes, real-time quality monitoring, optimized concrete mix, and reduced waste generation.
- *The structural design team's* needs revolve around structural design, construction management, safety, risk management, maintenance, and repairs. Smart segments provide real-time feedback to enhance design accuracy, improve construction management, enable proactive risk mitigation, and offer valuable historical data for effective maintenance and repairs.

The adoption of smart segments primarily serves the needs of tunnel owners, optimizing their operational efficiency, reducing costs, and enhancing environmental sustainability in tunnel infrastructure management. The structural design team and segment manufacturers play vital supporting roles in achieving these objectives.

Table 6-1. Smart segments Stakeholders' needs

Stakeholder	Needs	Description
Assets owners/managers	- A1: Maintenance and Repairs	Although statutory inspections (general and principal) are still currently required even on instrumented tunnels, the assumption is that in the future the requirements could be relaxed and the number of inspections reduced.
	- A2: Operational Efficiency	Minimization of closure costs for routine maintenance
	A3: Safety and Risk Management	Proactive monitoring for potential structural problems
	- A4: Maintenance and Repairs	Clear historical data for effective maintenance and repairs
Segments manufacturers	- M1: Efficient production process	Reduction of inefficiencies, delays, and costs in manufacturing
	- M2: Quality control	Real-time monitoring of concrete quality during casting
	- M3: Cost Control	Reduction of manual labour and associated costs
	- M4: Waste reduction	Optimization of concrete mix and reduction of waste
	- M5: Environmental concerns	Reduction of embodied CO2 through improved quality control
Structural design team	- E1: Structural Design	Real-time feedback for accurate and efficient design
	- E2: Construction management	Enhanced construction management and early issue detection

## 6.1.2 Benefits and advantages of smart segments

The following lines outline the short-term and long-term benefits and advantages of smart segments. While the long-term benefits align with established SHM systems, the distinctive strength of smart segments lies in their short-term benefits.

### 6.1.2.1 Short-term benefits

The short-term phase comprises three crucial steps that showcase the advantages of smart segments:

- Sensors' deployment at the precast factory.

- Segments storage, stacking, and transportation to the worksite.
- Configuration of the sensors during the fitout period.

**Stage 1:** Sensor deployment in the prefab manufacturing plant

During this phase, sensors are placed within the smart segment formwork by. Once installed, these sensors allow for the tracking of certain physical and mechanical properties. This feature has several benefits:

- *Reducing the reliance on human intervention* for sensor placement, as robots excel in accurately positioning them on repetitive elements.
- *Enhancing the quality control of concrete curing* through embedded temperature sensors. Additionally, this could improve the scheduling for formwork removal and the entire segment production process.

**Stage 2:** Smart segment storage, stacking, and transportation to the worksite.

This phase includes the storage, stacking, and transport to the worksite. Varied manipulations of the smart segment in the manufacturing plant and the shipping to the worksite. Compared to non-instrumented segments during this phase, smart segment presents the following advantages:

- improved supply chain information storage such as the precast segments manufacturing data (factory, date of manufacturing, concrete mix properties, etc.) loaded in the wireless node during the storage. This feature is like those found on surface-mounted RFID tags used in <sup>187</sup>. Similarly, ad hoc GPS tracker can be fitted in the wireless node to provide a real-time monitoring location of the segments.
- continuous tracking of mechanical properties of smart segments during the storage, stacking, transportation, and the installation on site.

**Stage 3:** Smart segments on-site configuration

A smart segment can continue to collect measurements from the moment it comes out of the factory the end-life of the system. However, in practice it may be necessary to intervene after the tunnel is completed to tune the monitoring system for later use. The configuration would therefore consist of one or all of the following: (i) setting up an adequate sampling frequency; (ii) configuring the wireless networks; or (iii) replacing defective nodes.

Therefore, the main advantage of smart segments over traditional options would be *the reduced configuration intervention time* after the tunnel completion.

#### **6.1.2.2 Long-term benefits**

The long-term benefits of smart segment are the same as the ones described in <sup>188</sup> for any continuous sensor based SHM system and succinctly listed below.

- Significantly reduced needs for operative access;
- monitoring of intrinsic state;
- numbers of readings;
- real-time information;
- much higher volume of information, and higher information delivery speed;
- foundation for intelligence.

While an SHM system provides valuable insights into a structure that would otherwise be difficult to access through periodic inspections, there is currently no clear guidance on the amount of statutory inspections can be reduced to take advantage of the potential cost savings offered by an SHM system.

The CBA study presented in the following section consisted at generating various scenarios for different monitoring solutions to potentially reduce the number of statutory inspections. Various working assumptions were made on both the smart segments as well as the statutory inspections.

## **6.2 Cost-benefit analysis**

A thorough cost-benefit analysis has been conducted to evaluate the effectiveness of smart segments, regarding long-term implications on general and principal inspections. This analysis consisted in assessing the NPV of four solutions:

- i. Solution 1: Baseline scenario - No monitoring systems installed
- ii. Solution 2: the smart segment solution;
- iii. Solution 3: the on-site wireless solution;
- iv. Solution 4: the traditional wired SHM system.



## 6.2.1 General considerations/assumptions

### 6.2.1.1 Tunnel inspection

Guidelines for tunnel inspections vary based on the types of tunnels and are typically country-specific<sup>189–191</sup>. Nevertheless, these guidelines typically encompass information such as the nature and description of inspection operations, their frequency, team composition, tools used, and post-inspection analysis requirements.

In the UK, there are four types of road tunnel inspections recommended during the asset operational life as shown in Table 6-2 and defined in, [5], [6], [7]. While the first three inspections are classified as periodic inspections, it's worth highlighting that only the general and principal inspections include some level of structural assessments. Therefore, these inspections were considered while assessing the potential cost savings with the installation of an SHM system.

During the general and principal inspections, experienced inspectors conduct visual structural assessments. In the case of the principal inspection, it is sometimes necessary to complement the visual inspection with laboratory tests on extracted concrete cores, or with on-site NDTs. For both the general and principal inspection, however, it is reasonable to posit that their total number could be reduced when a SHM system is installed.

Table 6-2. Types of inspection conducted on tunnels<sup>191,192</sup>

Type of Inspection	Team Size (inspectors)	Frequency of Inspection	Duration of Intervention
Superficial inspection	1-2	Weekly or monthly, depending on size and usage of the tunnel	A few hours
General inspection	2-3 <sup>1</sup>	Annually	2-3 nights**
Principal inspection	2-3 <sup>2</sup>	5-6 years	7-10 nights
Special inspection	Varies	As needed, such as after an accident or other significant event that may have affected the tunnel's integrity	Varies depending on the nature and scope of the inspection

<sup>1</sup> 4 additional staff can be required for traffic management

<sup>2</sup> 4 additional staff for traffic control, mobile elevating platforms, and 2 labourers to remove panels

#### 6.2.1.1.1 Tunnel length and type

The tunnel considered in this study is a 1 km, 2-lane road tunnel.

#### 6.2.1.1.2 Instrumentation lifetime

Anticipating the potential for component obsolescence, a 30-year lifespan (equivalent to 1/4th of the tunnel's total lifespan) was assumed for all instrumentation solutions.

#### 6.2.1.1.3 Number of inspections

To assess the potential cost savings resulting from a reduced number of statutory inspections (particularly general and principal inspections) with the installation of an SHM system, the NPV analysis was generated for the three simulations in Table 6-3. For a fixed number of retained general inspections (30, 20, or 10), simulation calculates NPV for principal inspections ranging from one to six.

Table 6-3. Simulation on the amount of general and principal inspections

<b>Simulations</b>	<b>Principal inspection</b>	<b>General inspection</b>
1	1 to 6	30
2	1 to 6	20
3	1 to 6	10

#### 6.2.1.1.4 Cost of inspections

The costs of statutory inspections, in line with the prevailing market rates<sup>193</sup> and standards, for 1 km of a 2-lane road tunnel are:

- £3,000 for each general inspection
- £35,500 for each principal inspection

### 6.2.1.2 Tunnel monitoring system

Over the length of the tunnel, some sections are instrumented as shown in Figure 6-2. The density of instrumentation along the tunnel and in each instrumented section are discussed.

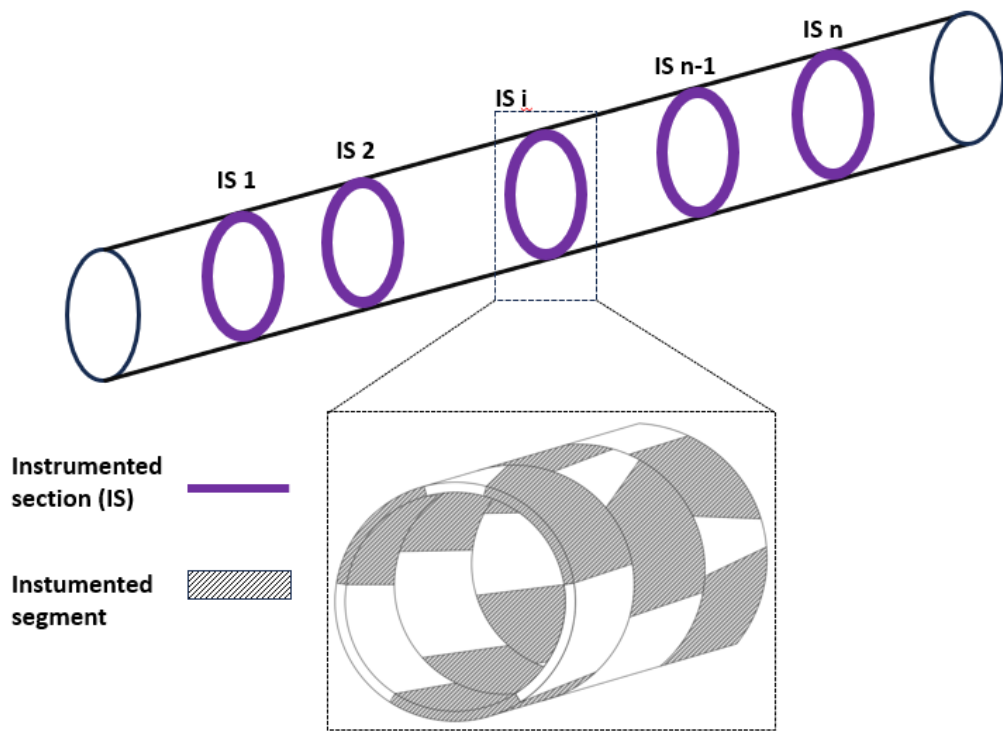


Figure 6-2. Typical instrumented tunnel section. In this case the instrumented section has three instrumented rings.

#### 6.2.1.2.1 Number of instrumented sections

Based on the review of some real-world instrumented tunnels, presented in Appendix A. 6, and common practice in the structural design of tunnels a total of 10 instrumented sections was considered. The specified number, which represents the maximum considered for the structural detailing of the tunnel project, offers a good balance that takes into account a variety of geological and hydrogeological conditions, as well as varying tunnel cover depths. Each section would contain 1-3 three rings

#### 6.2.1.2.2 Number of instrumented rings

In a 5+1 tunnel ring configuration, each ring had three instrumented segments. This quantity ensured an adequate level of redundancy in the measurement system while keeping the costs within acceptable limits.

#### 6.2.1.2.3 Sensors

While this thesis primarily focused on instrumentation with embedded VWSGs, at this stage of the study, it was considered practical to integrate additional sensors to improve the

CB, making it more realistic. Consequently, the segments would be equipped with embedded and surface-mounted VWSGs to measure strains, along with tiltmeters to monitor ring convergence. Depending on the chosen instrumentation system, the tunnel monitoring system could also include data acquisition units, wireless nodes, and a wireless gateway.

#### 6.2.1.2.4 Cost of monitored sections.

The costs of instrumentation, detailed in Appendix A. 7, including the hardware costs and the installation costs are based on the following considerations:

- For on-site wired and wireless instrumentation solutions, the installation cost was estimated at 30% of the total hardware cost. This cost covers the installation of sensors but does not include system configuration.
- For the smart segment, the installation cost is set at zero since all sensors are assumed to be installed at the manufacturing plant. Any subsequent adjustments after segment installation will be made during the configuration phase.

## 6.2.2 Cost benefit study

### 6.2.2.1 Net present value (NPV)

The NPV is an effective metric to assess the financial viability of a long-term investment as an SHM system. As stated before, 30-year life of the SHM system was assumed. The NPV, presented in Equation (6-1), is the difference between the discounted cashflow generated by the investment during its lifetime and the cost of the investment.

$$NPV (\text{£}) = \sum_{i=1}^N \frac{CF_i}{(1+r)^i} - C_{SHM} \quad (6-1)$$

$CF_i$ : annualised cashflow, including costs (negative) and savings (positive)

$N$ : project lifetime

$r$ : discount rate in %/

$C_{SHM}$ : investment in SHM for the baseline, the smart segment, the wireless, and the wired solutions respectively.

For each instrumentation solution, the NPV analysis was calculated for three scenarios (1, 2, and 3 instrumented rings per section) containing three simulations as described in 6.2.1.1..

### 6.2.2.1.1 Cashflow estimation

The cashflow consisted of the annualised cost of the general and the principal inspection and the savings to be made thanks to the instrumentation. For each scenario and simulation, the results are presented in Table 6-4.

Table 6-4. Cashflow for different simulations

		<b>Scenarios 1-3 (Number of instrumented rings)</b>						
		Total number of principal inspections						
		6	5	4	3	2	1	
<b>Simulations</b> (Total number of general inspections)	30	-0.101	-0.089	-0.077	-0.066	-0.054	-0.042	<b>COST</b> (£100,000)
	20	-0.091	-0.079	-0.067	-0.056	-0.044	-0.032	
	10	-0.081	-0.069	-0.057	-0.046	-0.034	-0.022	
	30	+0.000	+0.012	+0.024	+0.036	+0.047	+0.059	<b>SAVINGS</b> (£100,000)
	20	+0.010	+0.022	+0.034	+0.046	+0.057	+0.069	
	10	+0.020	+0.032	+0.044	+0.056	+0.067	+0.079	

### 6.2.2.1.2 Discount rate discussion

A 4% discount rate was used in this study, which aligns with recent infrastructure projects in the UK (London Crossrail), France (Grand Paris Express), and Australia (Inland Rail) 194.

### 6.2.2.1.3 Cost of instrumentation

For each instrumentation solution and varied scenarios, the cost of investment is presented in Table 6-5.

Table 6-5. Investment cost for the 4 instrumentation solutions

<b>SHM Solutions</b>		<b>Scenarios (Number of instrumented rings)</b>		
		1	2	3
Baseline	SHM COST (£100,000)	0.000	0.000	0.000
Smart segment		0.197	0.353	0.509
Wireless		0.256	0.459	0.662
Wired		0.388	0.734	1.08

## **6.3 Results and discussions**

### **6.3.1 NPV**

Detailed results of the NPV combining multiple scenarios of instrumentation density and SHM solutions can be found in Appendix A. 8. General observations on the results are presented in the lines below.

#### **6.3.1.1 Baseline**

The *baseline* solution, which consist of having no instrumentation installed on the tunnel, shows a constant negative return in the form of a negative NPV of -£167,900 as illustrated in Figure 6-3.

#### **6.3.1.2 Smart segment:**

The investment in the smart segment generates a minimum positive NPV of £6,041 (top chart in Figure 6-4) when equipping the instrumented sections of the 1km tunnel with just one smart ring. This scenario assumes only one principal inspection over the 30-year SHM system lifetime and retains the recommended 30 general inspections.

Similarly, the investment achieves its maximum positive NPV of £725,000 (bottom Figure 6-4) under different conditions. In this case, the tunnel is fitted with one instrumented ring per monitored section, with the number of principal inspections still at one, but general inspections reduced to only 10 during the system's lifetime."

#### **6.3.1.3 Wireless**

The investment in an on-site wireless system results in a minimum positive NPV of £3,051 (see top of Figure 6-5) when the instrumented sections of the 1km tunnel are equipped with 3 instrumented rings. In this scenario, one principal inspection is conducted over the 30-year SHM system lifetime, and 20 general inspections are retained.

On the other hand, the investment achieves a maximum positive NPV of £65,700 (see bottom of Figure 6-5) under different conditions. Here, the tunnel is equipped with one instrumented ring per monitored section, with the number of principal inspections still at one, while general inspections are reduced to only 10 throughout the system's lifetime.

#### **6.3.1.4 Wired**

The investment in a wired system results in a minimum positive NPV of £24,800 (See top of Figure 6-6) when equipping each monitored section with 1 instrumented ring. In this scenario, one principal inspection is conducted over the 30-year SHM system lifetime, and 20 general inspections are retained.

Likewise, the investment achieves its maximum positive NPV of £58,000 (See bottom of Figure 6-6) under different conditions. In this case, the tunnel is equipped with one instrumented ring per monitored section, with the number of principal inspections still at one, while general inspections are reduced to only 10 throughout the system's lifetime.

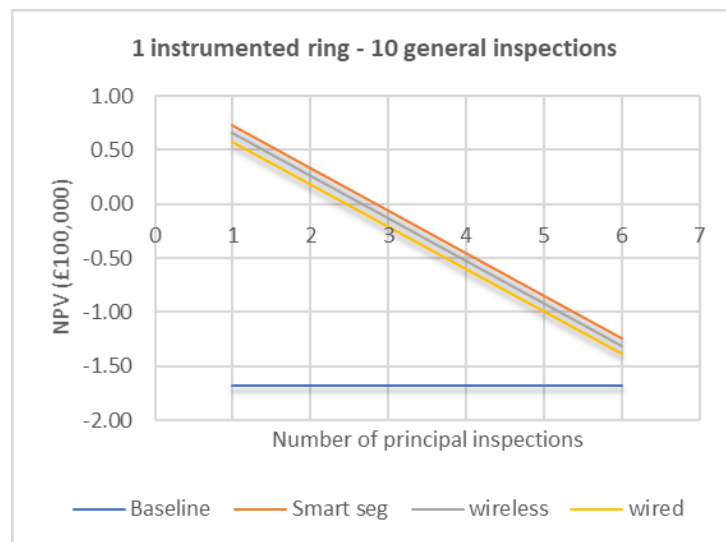
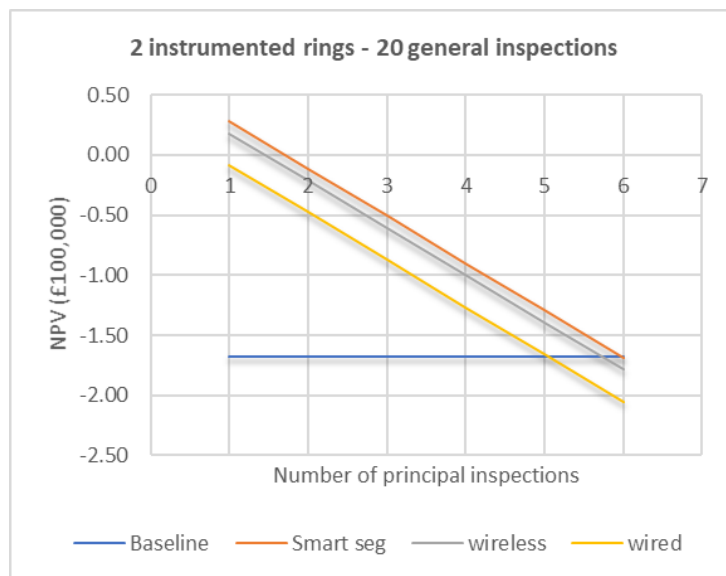
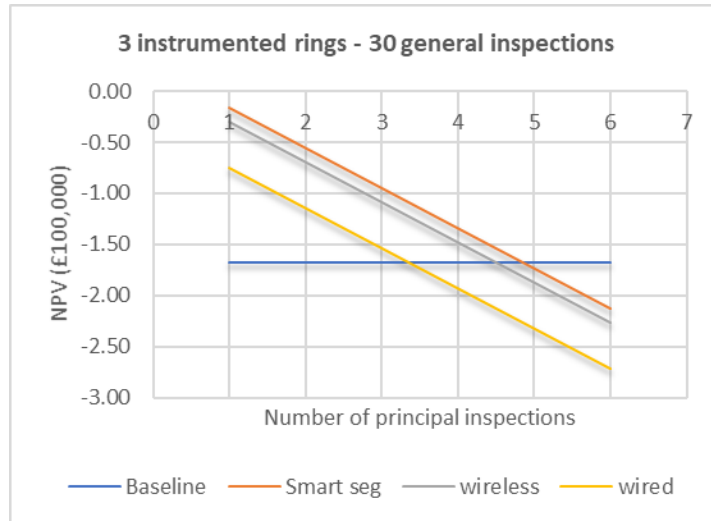


Figure 6-3. NPV results in different scenarios showing the constant negative NPV for the baseline solution



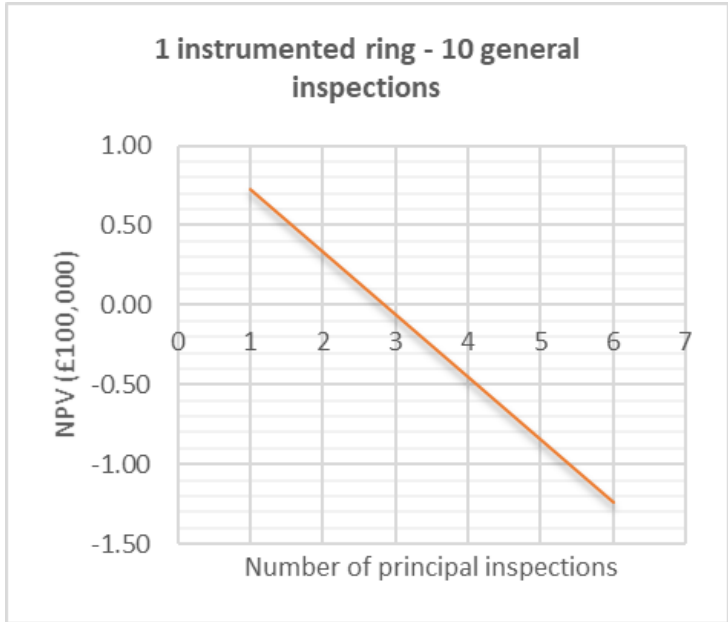
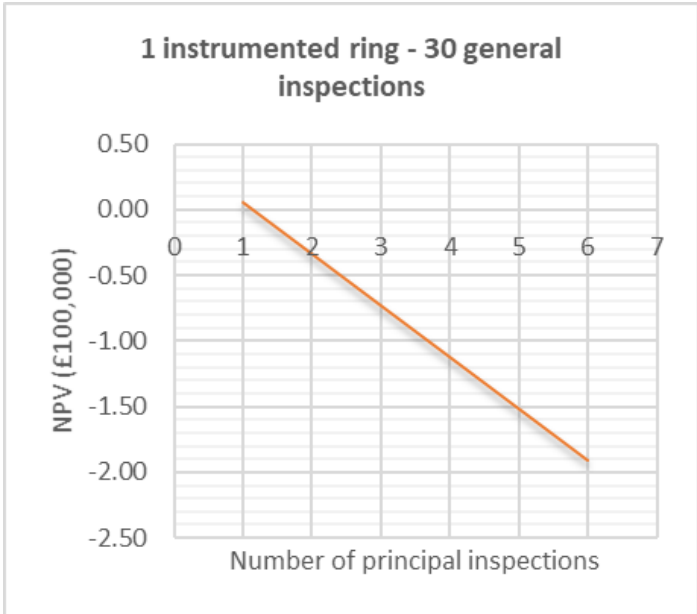


Figure 6-4. Lowest (top) and highest (bottom) positive NPV for smart segment solution.

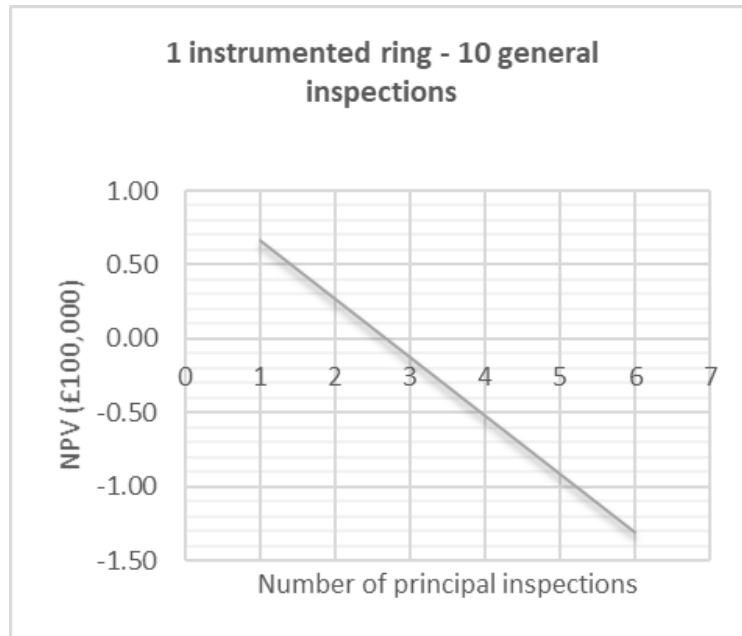
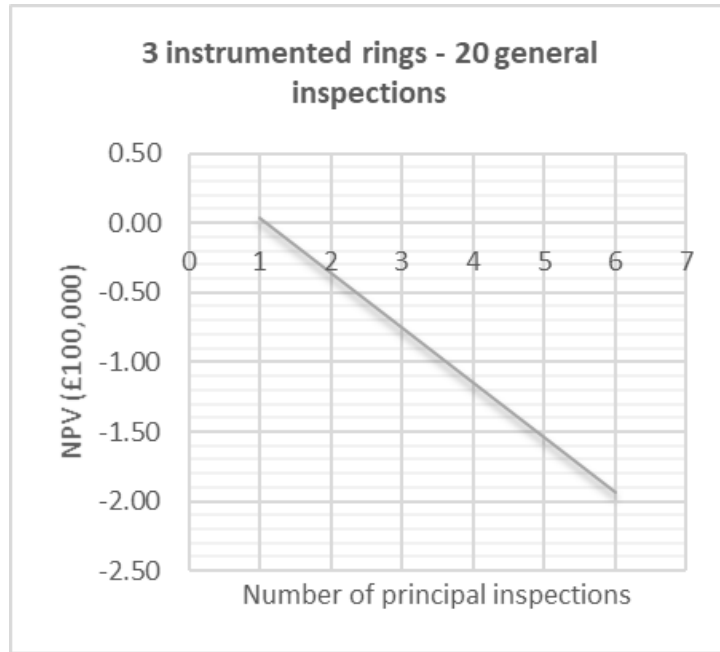


Figure 6-5. Lowest (top) and highest (bottom) positive NPV for on-site wireless solution.

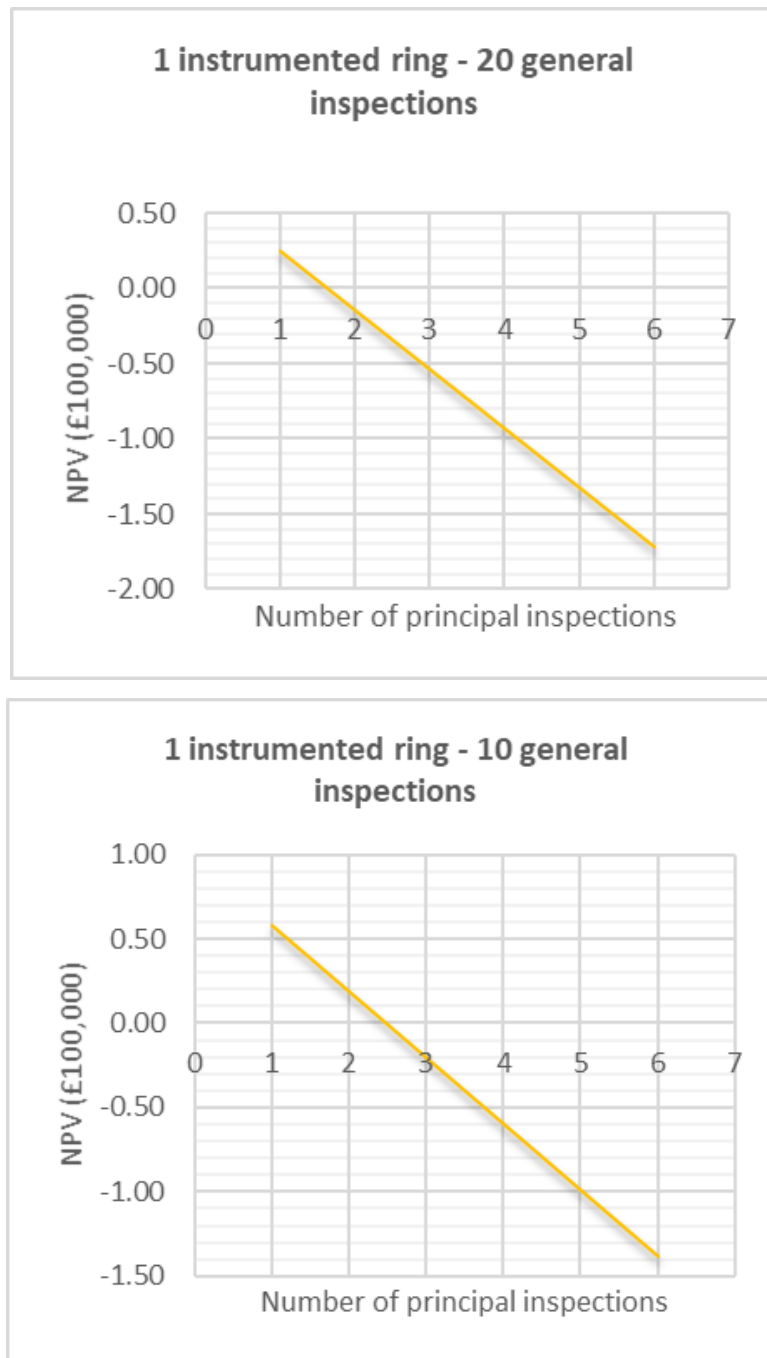


Figure 6-6. Lowest (top) and highest (bottom) positive NPV for on-site wired solution.

### 6.3.2 Additional discussions

While NPV analysis previously presented showed that smart segment fare better when compared to on-site wire and wireless solutions, relying exclusively on NPV results for deciding on tunnel instrumentation may prove insufficient. It is crucial to take into account additional factors, such as the improved safety and the potential enhancement in data quality collected by the SHM system in comparison to traditional inspections solely realised

through on-site visits. To address this challenge, a decision-making tool was developed, involving the comparison of three matrices. These matrices aided in the evaluation of various configurations, including the number of instrumented rings and the total number of inspections (general and principal), considering three key factors: cost (NPV), safety risks, and data quality.

Each matrix will employ a colour-coded system, using red to indicate unsuitable options, orange for acceptable options, and green for recommended choices. The colour ranges in each matrix are explained below, along with brief descriptions to facilitate understanding of their application.

### **6.3.2.1 Matrix NPV**

The three ranges to classify NPV values in a coloured matrix are as follow:

- RED:  $NPV < -£15,000$ . – Investment unsound
- They represent situations where the investment measurable benefits (potential savings in number of inspections), are clearly outweighed by the cost of implementing the SHM system.
- ORANGE:  $-£15,000 < NPV < £15,000$ . – Investment at cost
- This range represents a transition zone around which the investment in a SHM is barely breaking even. With £15,000 approximately representing 5% of the total amount spent in inspections (general and principal) for a non-instrumented tunnel.
- GREEN.  $NPV > £15,000$  – Investment financially sound
- This represents scenarios where the investment produces a clear positive long-term return.
- The NPV matrix presented in Table 6-6 shows very similar colour patterns for each solution. For all configuration and solutions, the investment is not profitable if the number of principal inspections is superior to 3. In the zone where the project is either at cost or making a positive return, the smart segment solution shows a better return pattern than the on-site wireless and wired solutions.

Table 6-6. NPV code-coloured matrix for the three instrumented solutions.

Smart segment										
No rings		3			2			1		
No Gen Insp		30	20	10	30	20	10	30	20	10
No Prinp insp	6	Red	Red	Red	Red	Red	Red	Red	Red	Red
	5	Red	Red	Red	Red	Red	Red	Red	Red	Red
	4	Red	Red	Red	Red	Red	Red	Red	Red	Red
	3	Red	Red	Red	Red	Red	Red	Red	Red	Yellow
	2	Red	Red	Yellow	Red	Yellow	Green	Red	Yellow	Green
	1	Red	Green	Green	Yellow	Green	Green	Yellow	Green	Green
Wireless										
No rings		3			2			1		
No Gen Insp		30	20	10	30	20	10	30	20	10
No Prinp insp	6	Red	Red	Red	Red	Red	Red	Red	Red	Red
	5	Red	Red	Red	Red	Red	Red	Red	Red	Red
	4	Red	Red	Red	Red	Red	Red	Red	Red	Red
	3	Red	Red	Red	Red	Red	Red	Red	Red	Yellow
	2	Red	Red	Yellow	Red	Red	Yellow	Red	Yellow	Green
	1	Red	Yellow	Green	Red	Green	Green	Yellow	Green	Green
Wired										
No rings		3			2			1		
No Gen Insp		30	20	10	30	20	10	30	20	10
No Prinp insp	6	Red	Red	Red	Red	Red	Red	Red	Red	Red
	5	Red	Red	Red	Red	Red	Red	Red	Red	Red
	4	Red	Red	Red	Red	Red	Red	Red	Red	Red
	3	Red	Red	Red	Red	Red	Red	Red	Red	Red
	2	Red	Red	Red	Red	Red	Yellow	Red	Yellow	Green
	1	Red	Red	Yellow	Red	Yellow	Green	Yellow	Green	Green

### 6.3.2.2 Matrix Safety

Knowing that for a 30-year timeframe, the frequencies of statutory inspections are:

- Principal inspections (PI): 5-6 inspections. Which means one inspection every 5-6 years for 30 years.
- General inspections (GI): 15-30 inspections. Which means one inspection every 1-2 years for 30 years.

The ranges to build the safety code-coloured matrix based on the number of general and principal inspections are:

- RED:  $GI < 10$  and  $PI < 3$  – risks too high
- ORANGE:  $10 \leq GI < 15$  and  $3 \leq PI < 5$  – risks acceptable
- GREEN:  $15 \leq GI \leq 30$  and  $5 \leq PI \leq 5$  – risks very low

The resulting matrix presented in shows an exact pattern for each scenario (1-3 rings) with better outcomes provided by number of principal inspections superior or equal to 3 for 20 or 30 general inspections. Configurations with only 10 general inspections show an acceptable to poor outcome depending on the final number of principal inspections.

The matrix depicted in Table 6-7 reveals a consistent pattern across all scenarios (1-3 rings), where better outcomes are observed when the number of principal inspections is equal to or exceeds 3, accompanied by either 20 or 30 general inspections. Configurations with only 10 general inspections display outcomes ranging from acceptable to poor, depending on the final number of principal inspections.

Table 6-7. Safety code-coloured matrix for the three instrumented solutions

		No rings			3			2			1		
		No Gen Insp			30	20	10	30	20	10	30	20	10
No Prinp insp	6	Green	Green	Yellow	Green	Green	Yellow	Green	Green	Yellow	Green	Green	Yellow
	5	Green	Green	Yellow	Green	Green	Yellow	Green	Green	Yellow	Green	Green	Yellow
	4	Green	Green	Yellow	Green	Green	Yellow	Green	Green	Yellow	Green	Green	Yellow
	3	Green	Yellow	Yellow	Green	Yellow	Yellow	Green	Yellow	Yellow	Green	Yellow	Yellow
	2	Yellow	Yellow	Red	Yellow	Yellow	Red	Yellow	Yellow	Red	Yellow	Yellow	Red
	1	Yellow	Red	Red	Yellow	Red	Red	Yellow	Red	Red	Yellow	Red	Red

### 6.3.2.3 Data quality matrix

The data quality matrix (in Table 6-8) assumes that increasing the monitoring density (increasing the number of instrumented rings) increases the redundancy of the system and therefore the reliability of the data collected.

The data quality code-coloured matrix is defined as:

- RED: 1 ring/ monitored section
- ORANGE: 2 rings/monitored section

- GREEN: 3 rings/monitored section

Table 6-8. Data quality code-coloured matrix for the three instrumented solutions

No rings		3			2			1		
No Gen. Insp.		30	20	10	30	20	10	30	20	10
No Prinp insp	6	Green	Green	Green	Yellow	Yellow	Yellow	Red	Red	Red
	5	Green	Green	Green	Yellow	Yellow	Yellow	Red	Red	Red
	4	Green	Green	Green	Yellow	Yellow	Yellow	Red	Red	Red
	3	Green	Green	Green	Yellow	Yellow	Yellow	Red	Red	Red
	2	Green	Green	Green	Yellow	Yellow	Yellow	Red	Red	Red
	1	Green	Green	Green	Yellow	Yellow	Yellow	Red	Red	Red

## 6.4 Summary

This study discussed the economic justification through a CBA study of implementing smart segment. After discussing the short-term and long-term benefits of smart segments, a comparative analysis of smart segment NPV was presented. Working hypothesis on the statutory inspections, the tunnel configuration and the instrumentation density and composition were made.

The CAB analysis consistently showed positive NPV for smart segments solution, in all the scenarios (1, 2 and 3 instrumented rings per section). On-site wireless and wired solutions also yielded positive NPV, but mostly for the 1 instrumented ring scenario.

Finally, in addition to the NPV analysis, the study discussed other factors such as safety risks and data quality that could be factored in the decision making of the most suitable instrumentation solution.

While the study gave satisfactory results, it is worth stating its limitations:

- This study does not account for the financial implications of the time required for a principal or general manual inspection on the local economy, especially in cases where partial or complete closure of the tunnel is necessary. While this perspective may be acceptable from the standpoint of an asset manager, it fails to acknowledge the hidden costs that are ultimately subsidized by society. As a result, manual inspections may appear less expensive than they indeed are.

- Similarly, this study is not considering the full cost of installing the monitoring system for wired or wireless solutions. While the given figures primarily accounts for labour expenses related to installation, it overlooks the substantial impact on the construction project timeline. For example, a week-long involvement of personnel in cable-related tasks at the construction site necessitates additional expenses to retain other contractors or may introduce delays to concurrent project activities. Thus, a more comprehensive evaluation of the true cost should consider the associated labour costs, potential expenses for retaining contractors, and potential project slowdowns.
- No failure rates of the sensors have been included in this analysis. The assumption is that once installed they will be able to serve during the system tunnel lifetime. This is equivalent to saying that the failure rates of sensors will be comparable across all cases, and this may not be the case.
- While the main savings considered in the study consisted of potential reductions of statutory inspections due to instrumentation, there are other significant financial and societal benefits that have not been accounted for such as the ability to proactively plan maintenance to reduce maintenance costs and support resilience, or the ability to use sensor data from live projects to inform design changes that reduce embedded carbon.

While acknowledging certain limitations, it is crucial to emphasize the cost savings and maintenance advantages that contribute to the attractiveness of smart tunnel segments for tunnel infrastructure management.



# Chapter 7. Conclusions and Futures Works

## 7.1 Conclusions

This project successfully demonstrated the robotic deployment of VWSGs into a lab-scale smart tunnel segment. The integration of strain sensors with a modified packaging allowed for efficient deployment and interrogation with minimal disruption to the segment. The robotic approach significantly improved accuracy, evident in the reduction of geometric errors and strain variations.

VWSGs were found to be the most adapted strain sensors for embedding into FRC. An ad-hoc packaging, consisting of a 3D-printed box, including Neodymium magnets, to facilitate its robotic deployment was designed. Similarly, an interrogation set of electronics were put together to interrogate VWSGs laying the ground for a full transitioning into a wireless node which when not done in this project can be considered as something done. The characterisation of the VWSGs conducted in a temperature constant environment gave a GF of  $0.394 \pm 0.004$ , close to manufacturer recommended values.

The use of robotic in the construction industry, though still limited has some applications. The precast industry was found to be the one with the highest level of integration of automated processes and even included the use of industrial robots to perform a series of tasks partially or fully replacing human operators. While some cases of robotic sensors deployment were found in the literature, the pick-and-place method used in this project was considered possible through a repurposing of existing robotic capabilities in the precast manufacturing industry adding a robotic gripper with ad-hoc fingers for VWSGs deployment as demonstrated in the project. The relative strain change  $\Delta\epsilon/\epsilon$ , expressed in %, varied from  $1.72 \pm 2.53$  for a manual PnP of the VWSG box to  $0.14 \pm 0.41$  for a robotically deployed box.

10 specimens of lab-scale smart tunnel segments based on early design of LTC road tunnel geometric features were mechanically successfully evaluated under a three-point bending test. When compared to calculated strains using a FEM, strains from two embedded VWSGs, in each segment to capture axial and lateral behaviours, showed a consistent behaviour across the 10 beams. The repeatability of strain transfers captured by the CV and

the ICC were respectively found to be 1% and 0.795 for the axial sensors and 1.9% and 0.396 for the lateral sensors.

Working with industrial partners, this project demonstrated the economic feasibility of smart segment when implemented on a tunnel project, taking necessary assumptions. The economic analysis of smart segments solutions, run under the assumption of a 30-year life expectancy of the monitoring system, generated scenarios that could reduce the number of general and principal inspections. The smart segment solution has positive NPV varying from £6,041 to £725,000. In addition to the NPV, a qualitative analysis of the perceived safety and quality of collected information was successfully used to widen the range of tools to help the decision-making process in selecting the appropriate technological solution.

## **7.2 Future work**

### **7.2.1 Automated deployment on real segments**

While the characterisation of the robotic deployment of VWSGs on lab-scale segment provided good results, the sample size and the lab-controlled environment are not sufficient to draw broader observations to a real-world setting. A robotic deployment in the real world could shed more lights and assess more effectively the accuracy of the robotic process.

One interesting thing to explore would be the impact of incorporating sensor deployment in the process of fabricating tunnel segment with a fully automated precast factory with industrial robots performing formwork preparation and post casting concrete surface polishing. In addition to analysing geometric errors, this study could study the impact on the time to complete the whole process of both installing sensors and fabricating segments. Herrenknecht Formwork, who is the biggest supplier of tunnelling solutions, have successfully installed fully automated factories and could be a good partner to gain more insights from the segment manufacturers perspective and bolster the case for smart segments.

### **7.2.2 X-ray computerised tomography**

The calculated strains using the FEM assumed that VWSGs did not change vertical positions after their placement. Further investigations using NDTs could clarify this assumption

and capture more accurately sensors positions variations after being submitted to vigorous vibration during the casting.

The use of a scanning technique such as the X-ray computerised tomography able to capture more accurately the position of the sensors after casting is recommended. Ideally the scan should be done on the entire beam focusing on the area where the sensors are embedded. However, this could be challenging as the size and the weight of the beam could pose problem inserting it into the scanner. A sampling of a core of the beam containing sensors could render better results.

### **7.2.3 Characterisation of sensors behaviour for instrumented ring**

An improved three-point bending testing of smart segment could yield more realistic strains values. Fixed end support at the extremities of the beam and distributed loads, achieved in a testing rig similar to the one used in <sup>195</sup>, would be preferred to the simple supported beam configuration.

This testing setup would allow an understanding of the segment behaviour when interacting in a ring as the compression efforts are transmitted from segment to segment under loads ground loadings.

### **7.2.4 Deployment of additional sensors**

Other sensors could be added to the smart segment to fully capture its structural behaviour during its lifetime. In addition to strains, the tunnels convergence and loads on the segment's ends are the most essential parameters to be considered for monitoring.

The capability to operate with wireless sensors makes MEMs sensor a choice worthy of further investigation to capture tunnels deformations such as tunnels ovalisation caused by convergence. Wireless sensors nodes could be equipped with inertial measurement unit programmed to calculate the relative convergence of smart segment in the same ring.

Experimental load cell using piezo-resistive composite materials could be explored. They not only offer a cost-effective alternative but also can be deployed using a spray-coating end-tool <sup>167</sup> that can be fit to a robotic arm. Piezoelectric load mounted on the ends of the beam during the test would allow the measurement of segment-to-segment compression resulting from the ground loadings.

### **7.2.5 Cost Benefit Analysis using a probabilistic approach.**

While the economic justification presented in this study offers insights for comparing the smart segment to existing wired and wireless solutions, it lacks a comprehensive CBA that considers both the costs associated with pre-construction operations on the segments and the benefits of using smart segments.

A more preferable approach would involve a probabilistic analysis. While several studies have addressed CBA of SHM, one study<sup>196</sup>, in particular, could be adapted for this purpose. Key steps would entail detailed identification of costs (such as damage to segments during pre-construction operations) and the benefits of using smart segments to mitigate these costs. This would include building a Finite Element (FE) model simulating the evolution of strains over time and establishing tolerances along with their probability of occurrence.

Furthermore, implementing a long-term probabilistic approach to the cost-benefit analysis would involve utilizing a real-world road tunnel as a case study to demonstrate the comparative advantages of smart segments over on-site instrumentation solutions.

# A. Appendix

## A. 1 Sensors datasheet



## Concrete Embedment Gages

### Special Use Sensors – Concrete Embedment Strain Gages


The EGP-Series Embedment Strain Gage is specially designed for measuring mechanical strains inside concrete structures. The sensing grid, constructed of a nickel-chromium alloy (similar to Karma), has an active gage length of 4 in (100 mm) for averaging strains in aggregate materials. A rugged 5 in (130 mm) outer body of proprietary polymer concrete resists mechanical damage during pouring, minimizes reinforcement of the structure, and provides protection from moisture and corrosive attack. The grid, cast within the polymer concrete to ensure maximum strain sensitivity, is self-temperature-compensated to minimize thermal output when installed in concrete structures. Each gage incorporates a heavy-duty 10 ft (3 m) cable with 22-AWG (0.643 mm dia.) leadwires; a three-wire construction to the sensing grid helps minimize temperature effects in the instrumentation leads. Special lengths of preattached cable will be quoted upon request. Micro-Measurements M-LINE accessory cable 322-DJV is available for adding cable length in the field.



Rugged and reliable, EGP-Series Strain Gages are available in both 120-ohm (EGP-5-120) and 350-ohm (EGP-5-350) resistances.

#### SPECIFICATIONS

- **Construction:** Strain sensing grid cast in a sturdy, water-resistant material.
- **Sensing Grid:** Nickel-chromium alloy on polyimide backing. Active gage length of 4 in (100 mm) nominal. Grid resistance of 120 or 350 ohms,  $\pm 0.8\%$ .
- **Outer Body:** Proprietary polymer concrete. 5 x 0.7 x 0.4 in (130 x 17 x 10 mm) nominal.
- **Cable:** Three 10 ft (3 m) leads of 22-AWG (0.643 mm dia.) stranded tinned copper in 0.015 in (0.4 mm) thick PVC insulation. Nominal cable diameter of 0.2 in (5 mm). (Other lengths quoted upon request.)
- **Temperature Range:** The normal usage range is  $+25^{\circ}$  to  $+125^{\circ}\text{F}$  ( $-5^{\circ}$  to  $+50^{\circ}\text{C}$ ). Extended range is  $-25^{\circ}$  to  $+150^{\circ}\text{F}$  ( $-30^{\circ}$  to  $+60^{\circ}\text{C}$ ).
- **Strain Range:**  $\pm 0.5\%$  (5000  $\mu\epsilon$ ).

GAGE DESIGNATION	 <b>RoHS COMPLIANT</b>	RES. IN OHMS	DIMENSIONS			
			Legend: ES = Each Section			
			ACTIVE GAGE LENGTH	OUTER BODY WIDTH	OUTER BODY LENGTH	OUTER BODY THICKNESS
EGP-5-120		120 $\pm$ 0.8%	4	0.7	5	0.4
			100	17	130	10
EGP-5-350		350 $\pm$ 0.8%	4	0.7	5	0.4
			100	17	130	10

# Internal strain of concrete, synthetic resin

## KM Strain Transducers

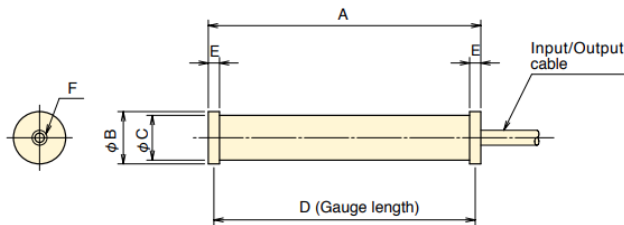
Civil engineering design



The KM series strain transducers are designed to measure strain in materials such as concrete, synthetic resin which undergo a transition from a compliant state to a hardened state. Their extremely low modulus (40N/mm<sup>2</sup> approx. except for KM-A) and waterproof construction are ideally suited for internal strain measurement during the very early stages of curing. They are totally impervious to moisture absorption, producing excellent stability for long-term strain measurement. Relative temperature measurement is also possible with the KM-A and KM-B. The built-in thermocouple sensor of the KM-AT/KM-BT enable actual temperature measurement in addition to strain measurement. Adding to the above embedment use, surface strain measurement onto concrete, H-beam steel is also available with various optional fittings.

The KM series is compliant to CE marking except for KM-30 and KM-50F.

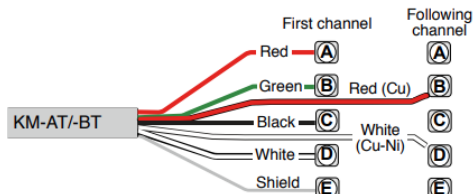
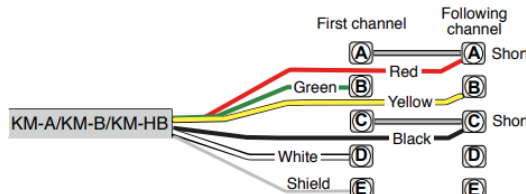
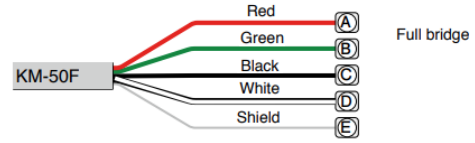
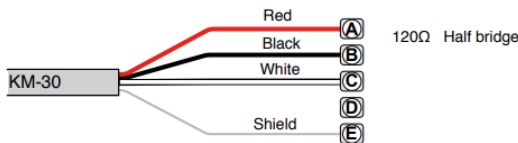
Protection ratings: IP67 equivalent for KM-30  
IP68 equivalent for KM-50F ~ KM-200AT



### ■ DIMENSION

TYPE	Dimension					
	A	φ B	φ C	D	E	F
KM-30	34	12	10	31	3	M3 DP4
KM-50F	54	20	17	50	4	M3 DP6
KM-100A	104	20	17	100	4	M3 DP6
KM-100B	104	20	17	100	4	M3 DP6
KM-100HB	104	20	17	100	4	M3 DP6
KM-200A	205	28	23	200	5	M5 DP8
KM-100AT	104	20	17	100	4	M3 DP6
KM-100BT	104	20	17	100	4	M3 DP6
KM-200AT	205	28	23	200	5	M5 DP8

### ■ CONNECTION TO DATA LOGGER



Consecutive 2 channels should be required for simultaneous measurement of strain and temperature.

Stranded cables of Green, White and shield are connected to the first channel. Remaining cables of Red, Yellow and Black should be connected directly to the following channel for temperature measurement, making short-circuit between A-A and C-C with copper wire for strain measurement.

Consecutive 2 channels should be required for simultaneous measurement of strain and temperature.

Stranded cables of Red, Green, Black, White and shield to the first channel for strain measurement. Thermocouple of single core Red and White should be connected directly to the following channel for temperature measurement.

### ■ SPECIFICATIONS

TYPE	KM-30	KM-50F	KM-100A	KM-100B	KM-100HB	KM-200A	KM-100AT	KM-100BT	KM-200AT	
Capacity	±5000x10 <sup>-6</sup> strain									
Gauge length	31mm	50mm	100mm			200mm	100mm	200mm		
Rated output (Approximately)	2.5mV/V 5000με	4mV/V 8000με	2.5mV/V 5000με			5mV/V 10000με	2.5mV/V 5000με	5mV/V 10000με		
Non-linearity	1%RO									
Apparent elastic modulus	40N/mm <sup>2</sup>		1000N/mm <sup>2</sup>	40N/mm <sup>2</sup>		1000N/mm <sup>2</sup>	40N/mm <sup>2</sup>	1000N/mm <sup>2</sup>		
Strain measurement	120Ω Half bridge	350Ω Full bridge								
Temperature measurement	-		Strain gauge 350Ω Quarter 3-wire (50x10 <sup>-6</sup> strain/°C)				Thermocouple T			
Allowable temperature range	-20 ~ +60°C		-20 ~ +80°C		-20 ~ +180°C		-20 ~ +80°C			
Input/Output resistance	120Ω (Half bridge)	350Ω Full bridge								
Weight	12 g	45 g	75 g		80 g	220 g	75 g		220 g	

#### Input/Output cable :

KM-30 φ 2.4mm 0.04mm<sup>2</sup> 3-core shielded vinyl cable 2m  
 KM-50F φ 6mm 0.35mm<sup>2</sup> 4-core shielded chloroprene cable 2m  
 KM-100A/-100B φ 9mm 0.3mm<sup>2</sup> 5-core shielded fluoroplastic cable 2m  
 KM-200A φ 11.5mm 0.5mm<sup>2</sup> 5-core shielded chloroprene cable 2m

#### KM-100AT/-100BT :

φ 9mm 0.3mm<sup>2</sup> 4-core shielded T-thermocouple compound cable 2m

#### KM-200A :

φ 11.5mm 0.5mm<sup>2</sup> 4-core shielded T-thermocouple compound cable 2m

## MODEL 4200 SERIES



Model 4202 (front), Model 4200 (center) and Model 4210 (rear) Concrete Embedment Strain Gauges.

### APPLICATIONS

The Model 4200, 4202 and 4210 are designed to measure strains in or on:

- Foundations
- Piles
- Bridges
- Dams
- Containment vessels
- Tunnel liners
- Mass concrete with coarse aggregates
- Laboratories and/or where space limitations exist (Model 4202)

### OPERATING PRINCIPLE

The Model 4200 Series Vibrating Wire Embedment Strain Gauges are designed for direct embedment in concrete. The Model 4200 (standard model) has a 153 mm gauge length and is commonly used for strain measurements in foundations, piles, bridges, dams, containment vessels, tunnel liners, etc. The Model 4210 has a 250 mm gauge length and is designed for use in mass concrete

with coarse aggregates. It is extra rugged to resist bending and has large flanges to provide greater engagement area. The 4202 and 4204 (51 mm and 102 mm gauge lengths, respectively) are designed for laboratory use and/or where there are space limitations.

Strains are measured using the vibrating wire principle: a length of

steel wire is tensioned between two end blocks that are embedded directly in concrete. Deformations (i.e. strain changes) of the concrete mass, will cause the two end blocks to move relative to one another, thus altering the tension in the steel wire. The tension is measured by plucking the wire and measuring its resonant frequency of vibration using an electromagnetic coil.

### ADVANTAGES AND LIMITATIONS

The Model 4200 Series Strain Gauges enjoy all the advantages of vibrating wire sensors, which includes excellent long term stability, maximum resistance to the effects of water, and a frequency output suitable for transmission over very long cables.

All components are made from stainless steel for corrosion protection and the gauges are fully waterproof. The Model 4210 is very rugged and

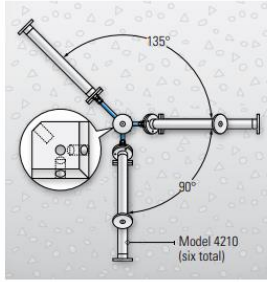
designed to withstand the rigors of concrete placement.

Each gauge incorporates a thermistor so that the temperature can be read and displayed by the readout.

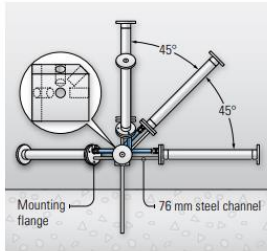
Extended range, low modulus and high temperature versions are also available. The Model 4200-6 and 4200-7 are designed for measuring large strains, 5,000 and 10,000

microstrain respectively. The Model 4200L (low modulus version) is particularly suitable for measuring curing strains in concrete. The Model 4200HT is designed for short-term use at temperatures up to 200 °C while the Model 4200HT-T is designed for long-term use at temperatures up to 220 °C, making it particularly suitable for installation in steam-cured spun concrete piles.

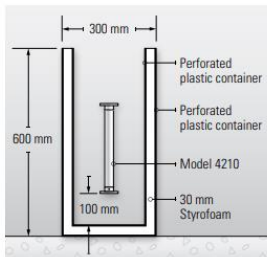




Top view of a Model 4210 Strain Gauge rosette configuration. Inset shows rosette fixture (enlarged for detail).



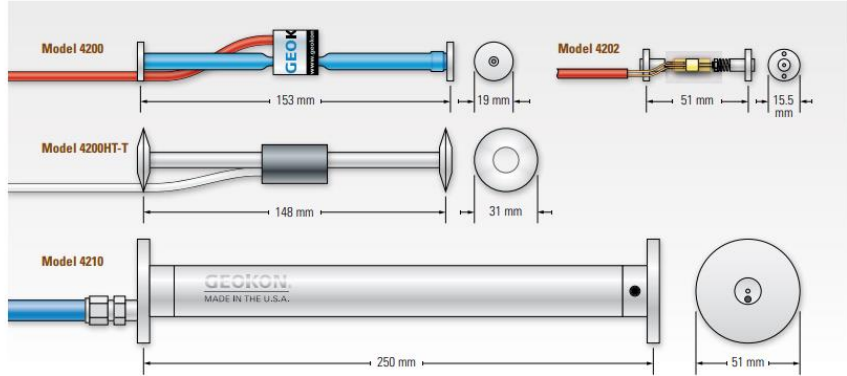
Front view of a Model 4210 Strain Gauge rosette configuration. Inset shows rosette fixture (enlarged for detail).



"No stress-strain" enclosure using the Model 4210.



Model 4200 Strain Gauge mounted to reinforcing bar using Model 4200-SPACER brackets.



Dimensions of the 4200 Series Strain Gauges.

#### SYSTEM COMPONENTS

The strain gauges are shipped ready for installation with the correct amount of cable attached. Installation is accomplished by attaching the strain gauge onto, or suspending it between, reinforcing bar. In mass concrete, rosette fixtures are used to hold multiple strain gauges in different orientations, allowing the measurement of strain in multiple directions.

Also available are no stress-strain enclosures (double-wall plastic containers lined with Styrofoam) designed for use in concrete dams. These enclosures isolate one strain gauge from the stress field in the concrete, thereby allowing the effects of moisture, temperature, autogenous growth, etc., to be estimated and corrected.

All models are equipped with integral thermistors for the simultaneous measurement of temperature.

Model GK-404 and GK-406 Readouts can display the strain measured by Model 4200 Strain Gauges in microstrain. Other compatible readouts and dataloggers are shown in the ordering information below.

#### TECHNICAL SPECIFICATIONS

	4200	4200-6/4200-7	4200L	4200HT	4200HT-T	4202	4204	4210
Range <sup>1</sup>	3000 $\mu\epsilon$	4200-6: 5000 $\mu\epsilon$ 4200-7: 10000 $\mu\epsilon$	3000 $\mu\epsilon$	3000 $\mu\epsilon$	3000 $\mu\epsilon$	3000 $\mu\epsilon$	3000 $\mu\epsilon$	3000 $\mu\epsilon$
Resolution	1.0 $\mu\epsilon$	2.0 to 5.0 $\mu\epsilon$	1.0 $\mu\epsilon$	1.0 $\mu\epsilon$	1.0 $\mu\epsilon$	0.4 $\mu\epsilon$	1.0 $\mu\epsilon$	0.4 $\mu\epsilon$
Accuracy <sup>2</sup>	$\pm 0.5\%$ F.S. <sup>3</sup>	$\pm 0.5\%$ F.S.	$\pm 0.5\%$ F.S. <sup>3</sup>	$\pm 0.5\%$ F.S. <sup>3</sup>	$\pm 0.5\%$ F.S.	$\pm 0.5\%$ F.S. <sup>3</sup>	$\pm 0.5\%$ F.S. <sup>3</sup>	$\pm 0.5\%$ F.S. <sup>3</sup>
Nonlinearity	< 0.5% F.S.	$\pm 2.5$ -4.0% F.S.	< 0.5% F.S.	< 0.5% F.S.	< 0.5% F.S.	< 0.5% F.S.	< 0.5% F.S.	< 0.5% F.S.
Coil Resistance	180 $\Omega$	180 $\Omega$	180 $\Omega$	120 $\Omega$	50 $\Omega$	180 $\Omega$	180 $\Omega$	180 $\Omega$
Frequency Datum <sup>4</sup>	800 Hz	800 Hz	800 Hz	800 Hz	800 Hz	2600 Hz	1250 Hz	2600 Hz
Thermal Coefficient of Expansion	12.2 ppm/ $^{\circ}$ C	variable	12.2 ppm/ $^{\circ}$ C	12.2 ppm/ $^{\circ}$ C	12.2 ppm/ $^{\circ}$ C	12.2 ppm/ $^{\circ}$ C	12.2 ppm/ $^{\circ}$ C	12.2 ppm/ $^{\circ}$ C
Temperature Range	-20 $^{\circ}$ C to +80 $^{\circ}$ C <sup>1</sup>	-20 $^{\circ}$ C to +80 $^{\circ}$ C <sup>1</sup>	-20 $^{\circ}$ C to +80 $^{\circ}$ C <sup>1</sup>	-20 $^{\circ}$ C to +200 $^{\circ}$ C	-20 $^{\circ}$ C to +220 $^{\circ}$ C	-20 $^{\circ}$ C to +80 $^{\circ}$ C <sup>1</sup>	-20 $^{\circ}$ C to +80 $^{\circ}$ C <sup>1</sup>	-20 $^{\circ}$ C to +80 $^{\circ}$ C <sup>1</sup>
Cable Type	4-conductor, 2 twisted pairs, 22 AWG (for all models)							
Cable Jacket	Red PVC, 4.75 mm $\varnothing$	Red PVC, 4.75 mm $\varnothing$	Red PVC, 4.75 mm $\varnothing$	White Teflon <sup>®</sup> , 5.20 mm $\varnothing$	White Teflon, 5.20 mm $\varnothing$	Red PVC, 4.75 mm $\varnothing$	Red PVC, 4.75 mm $\varnothing$	Blue PVC, 6.35 mm $\varnothing$
Active Gauge Length	153 mm (6.025")	153 mm (6.025")	153 mm (6.025")	153 mm (6.025")in.)	148 mm (1.9")	51 mm (2")	102 mm (4.016")	254 mm (10")

<sup>1</sup>Other ranges available on request. | <sup>2</sup>Transducer accuracy established under laboratory conditions:  $\pm 0.5\%$  F.S. with standard batch calibration. <sup>3</sup> $\pm 0.1\%$  F.S. with individual calibration. | <sup>4</sup>Typical. | <sup>5</sup>Other lengths available on request.



Model 4200-6 Extended Range (5,000 µε) Strain Gauge.



Model 4200-7 Extended Range (10,000 µε) Strain Gauge.



Model 4200L Low Modulus Strain Gauge.



Model 4200HT-T High Temp (220° C) Strain Gauge.



4200HT High Temp (200° C) Strain Gauge

#### ORDERING INFORMATION<sup>1</sup>

**4200:** Vibrating Wire Strain Gauge, concrete embedment type, 153 mm gauge length. (Strain gauge only.)

**4200A-1:** Model 4200 Strain Gauge, complete with plucking coil, thermistor, hose clamp, and 3 m cable.

**4200A-2:** Model 4200 Strain Gauge, complete with plucking coil, thermistor and hose clamp. Cable sold separately.

**4200L:** Model 4200 Strain Gauge, low modulus version for measuring concrete curing strains, complete with plucking coil, thermistor, and hose clamp. Cable sold separately.

**4200-6:** Model 4200 Strain Gauge, 5,000 microstrain range, complete with plucking coil, thermistor and hose clamp. Includes individual calibration. Cable sold separately.

**4200-7:** Model 4200 Strain Gauge, 10,000 microstrain range, complete with plucking coil, thermistor and hose clamp. Includes individual calibration. Cable sold separately.

**4000-1:** Plucking coil, thermistor and hose clamp. Cable sold separately.

**4000-3:** Plucking coil, thermistor and hose clamp. Includes 3 m cable.

**4200-SPACER:** Pair of mounting brackets for attaching strain gauges to #4 through #11 reinforcing bar. Includes two 254 mm cable ties.

**4200ROS:** Model 4200 Strain Gauge for rosette mount, complete with plucking coil, thermistor and hose clamp. Cable sold separately.

**4200-3:** Rosette Mount for Model 4200ROS. Specify method of attachment to rosette.

**4200-4:** No-stress strain enclosure. Double-wall plastic container lined with Styrofoam. Allows a strain gauge to be isolated from the stress field in the concrete.

**4202:** Vibrating Wire Strain Gauge, concrete embedment type, 51 mm gauge length, complete with integral plucking coil and thermistor. Cable sold separately.

**4204A-1:** Vibrating Wire Strain Gauge, concrete embedment type, 102 mm gauge length, complete with plucking coil, thermistor, hose clamp, and 3 m cable.

**4204A-2:** Vibrating Wire Strain Gauge, concrete embedment type, 102 mm gauge length, complete with plucking coil, thermistor and hose clamp. Cable sold separately.

**4204L:** Vibrating Wire Strain Gauge, low modulus version for measuring concrete curing strains, 102 mm gauge length, complete with plucking coil, thermistor and hose clamp. Cable sold separately.

**02-187V3:** Red PVC Cable, 4.75 mm (±0.25 mm) [0.187"] Ø, 2 twisted pairs, for the above.

**4210:** Vibrating Wire Strain Gauge, concrete embedment type, 250 mm gauge length, complete with integral plucking coil and thermistor. Cable sold separately.

**4210-1:** Rosette Mount for Model 4210. Specify method of attachment to rosette.

**4210-2:** No-stress strain enclosure for 250 mm gauge. Double-wall plastic container lined with Styrofoam. Allows a strain gauge to be isolated from the stress field in the concrete.

**2-250V6-E:** Blue PVC Cable, 6.35 mm (±0.25 mm) [0.250"] Ø, 2 twisted pairs, for the above.

**4200HT:** Vibrating Wire Strain Gauge, High Temperature (200°C), concrete embedment type, 6" gauge length, complete with integral plucking coil, high temperature thermistor. For short-term use.

**4200HT-T:** Vibrating Wire Strain Gauge, High Temperature (220°C), concrete embedment type, 6" gauge length, complete with integral plucking coil, high temperature thermistor. For long-term use.

**02-250T:** White Teflon Cable, 5.20 mm (±0.25 mm) [0.156"] Ø, 2 twisted pairs, for the above.

<sup>1</sup>Unless otherwise specified, strain gauges are batch calibrated. Individual calibrations are available upon request for an additional fee.

#### COMPATIBLE READOUTS AND DATALOGGERS

**GK-404:** Handheld Readout

**GK-406:** Vibrating Wire Analyzer

**8600 Series:** Multi-Channel Dataloggers

**8800 and 8900 Series:** GeoNet Wireless Data Acquisition System

**8920 and 8930 Series:** GeoNet Cellular and Wi-Fi Network Loggers

**8940 Series:** GeoNet Dataloggers

## A. 2 Arduino Code

```
#include <ModbusMaster.h> // For Modbus communication
#include <Wire.h>
#include "wiring_private.h"
ModbusMaster node; // Initialise a modbusmaster node object

// == 1 GLOBAL VARS ==
// DE and RE are both hooked up to pin 2 of arduino (PWM)
const int enablePin = 6; // pin is held high for transmit, low for receive
byte sensorAddress = 0x01; // the address of the sensor, default = 1
bool smallSensor = false; // set this to true if using geokon 4202 (small vw sensor), otherwise false for 4200 (large sensor)
int readDelay = 1000; // milliseconds between strain readings. Ensure this is not lower than 370 ms.

// == 1 END GLOBAL VARS ==

// == 2 SUPPORT FUNCTIONS ==
// function 1 required to make MAX485 work
void preTransmission() {
    digitalWrite(enablePin, HIGH); // transmit delay(10);
}
// function 2 required to make MAX485 work
void postTransmission() {
    delay(1); // must set delay(1). delay(2) = E0 error, delay(1) = 0 (no error).
    digitalWrite(enablePin, LOW); // receive
}
// function to convert two 16-bit hex values into a float (as per geokon manual) // and
https://gregstoll.com/~gregstoll/floattohex/
float hexToFloat(uint16_t A, uint16_t B)
{
    // This will work for IEEE-754 floating point responses in two parts
    unsigned int data[2] = {A, B};
```

```

float floatingNumber;
memcpy(&floatingNumber, data, 4);
return floatingNumber;
}
// function to read temperature of geokon sensor
float getTemperature()
{
uint16_t resultMain; // read the onboard thermistor resistance (2 registers at 0x0102)
resultMain = node.readHoldingRegisters(0x0102, 2);
if (resultMain == node.ku8MBSuccess)
{
// if error code returned = 0 (no error)
// Uncomment below to output extra info if we're debugging
// Serial.print("T Hexcode = ");
// Serial.print(node.getResponseBuffer(0x00),HEX); // Serial.print(" "); // Serial.println(node.getResponseBuffer(0x01),HEX);
// convert the data (hex) into float
float TempC = hexToFloat(node.getResponseBuffer(0x00), node.getResponseBuffer(0x01));

// This function is the fit between resistance and temperature between 0 and 30 degC (see excel sheet)
float T = 197.14 - 21.5 * log(TempC);
// to do: calibrate, can't rely on factory data.
return T;
} else
{ return -1000;
}
// function returns an unphysical value if read fails
}
}
// function to ping and read frequency of geokon sensor's vibrating wire
float getFrequency()
{

```

```

uint16_t resultMain; //ping the VW strain gauge by writing 1 to 0x0118
resultMain = node.writeSingleRegister(0x0118, 1); // wait at least 370 ms delay(readDelay);
//read two holding registers at 0x0100 to retrieve frequency
resultMain = node.readHoldingRegisters(0x0100, 2);
if (resultMain == node.ku8MBSuccess) { // if error code returned = 0 (no error)
// Uncomment below to output extra info if we're debugging
// Serial.print("F Hexcode = ");
// Serial.print(node.getResponseBuffer(0x00),HEX);
// Serial.print(" ");
// Serial.println(node.getResponseBuffer(0x01), HEX);
// convert the data (hex) into float
float Frq = hexToFloat(node.getResponseBuffer(0x00), node.getResponseBuffer(0x01));
return Frq;
} else
{
return -1; // function returns an unphysical value if read fails
}
}

// function to convert VW frequency to strain according to geokon manual //
https://www.geokon.com/content/manuals/4200-4202-4204-4210\_Strain\_Gages.pdf
float freqToStrain(float Frequency, bool smallSensor) {
float gaugeFactor;
float datumFreq;

if (smallSensor == false) { // if we're using the larger form factor (4200 gauge)
gaugeFactor = 3.304; // gauge factor is 3.304
datumFreq = 842.32; // Frequency at 0 strain is about 842.32 Hz. This value changes
with the nut adjustment, the sensor positions and the room environment. The number
given is for illustration purpose only.
}
}

```

```

else { // otherwise we're using the 4204 strain gauge (the small one)
    gaugeFactor = 0.3910; // gauge factor is 0. 3910
    datumFreq = 2310; // Freq at 0 strain is about 2310 Hz, but this freq is tunable using
the nut on the sensor
}
// Apply following equation to convert freq to strain
float strain = gaugeFactor * (pow(Frequency, 2) - pow(datumFreq, 2)) * 0.001; // to do:
this is not temperature corrected
return strain;

}
// == 2 END SUPPORT FUNCTIONS ==

// == 3 MAIN SETUP, LOOP ==
void setup() {
    pinMode(enablePin, OUTPUT); // switch on enablePin
    digitalWrite(enablePin, LOW); // initialise in receive mode
    // Default serial port must be used for serial monitor - this connected internally to usb
    // initialize serial communication at 9600 bits per second:

    Uart mySerial (&sercom3, 0, 1, SERCOM_RX_PAD_1, UART_TX_PAD_0);
    Serial.begin(115200);
    mySerial.begin(115200);
    pinPeripheral(0, PIO_SERCOM); //Assign RX function to pin 0
    pinPeripheral(1, PIO_SERCOM); //Assign TX function to pin 1
    // Serial.begin(115200); // ensure baud rate on your serial monitor is set to 115200
    while (!Serial) {}; // wait for serial monitor to be opened by user

    // This part of the code is for Arduino mega. Mega has more serial ports. The first of
these is "Serial1" on pins 19 (RX) and 18 (TX)

    mySerial.begin(115200); // Modbus communication for VW gauge runs at 115200 baud

```

```

node.begin(sensorAddress, mySerial); // Initialise modbus sensor to communicate over
serial port 1

// callbacks allow us to configure RS485 correctly
node.preTransmission(preTransmission);
node.postTransmission(postTransmission);
Serial.println("Setup complete");

}
void loop () {
// get freq and temperature readings
float Freq = getFrequency();
float Temperature = getTemperature();

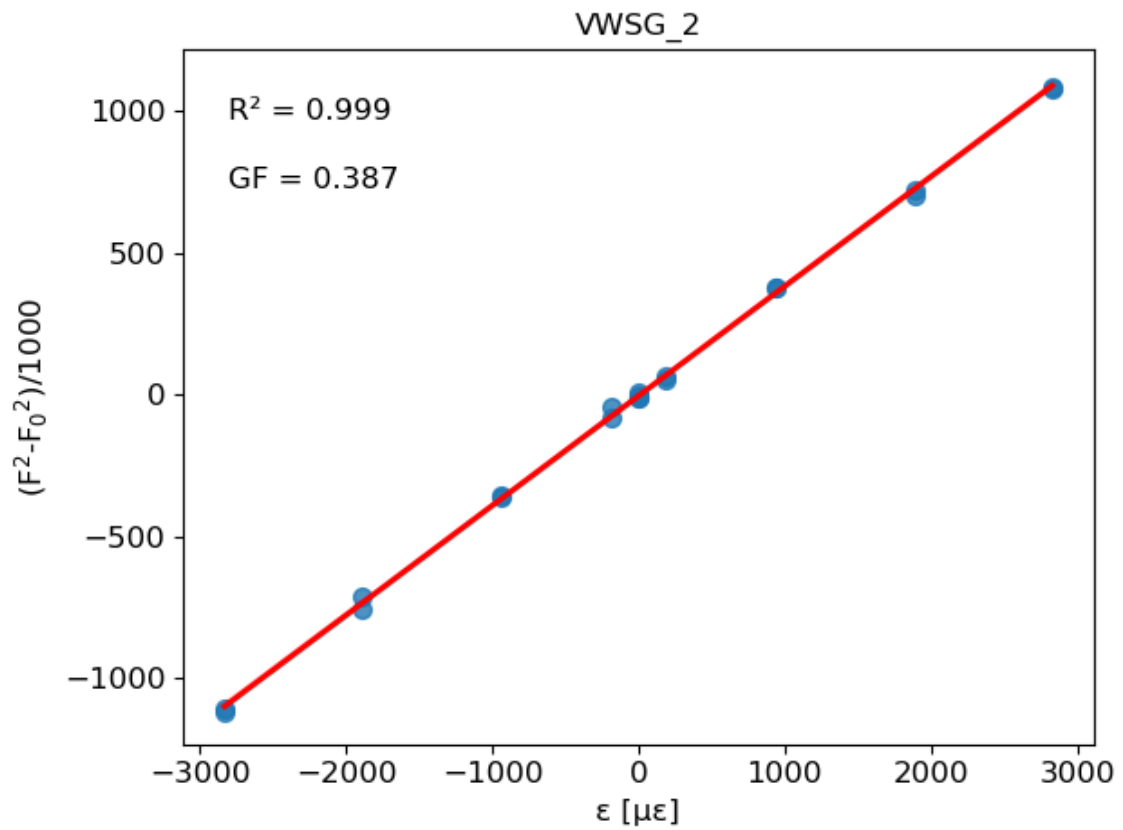
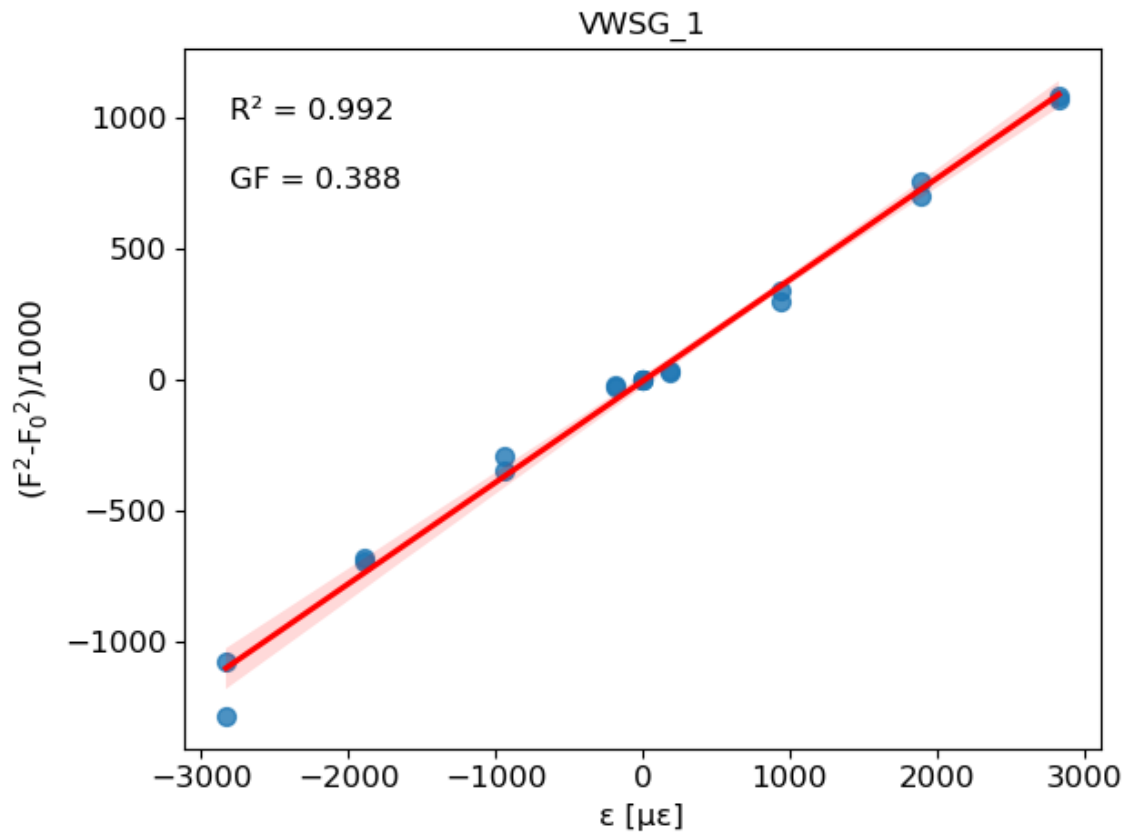
// convert frequency to strain

float strain = freqToStrain(Freq, smallSensor);

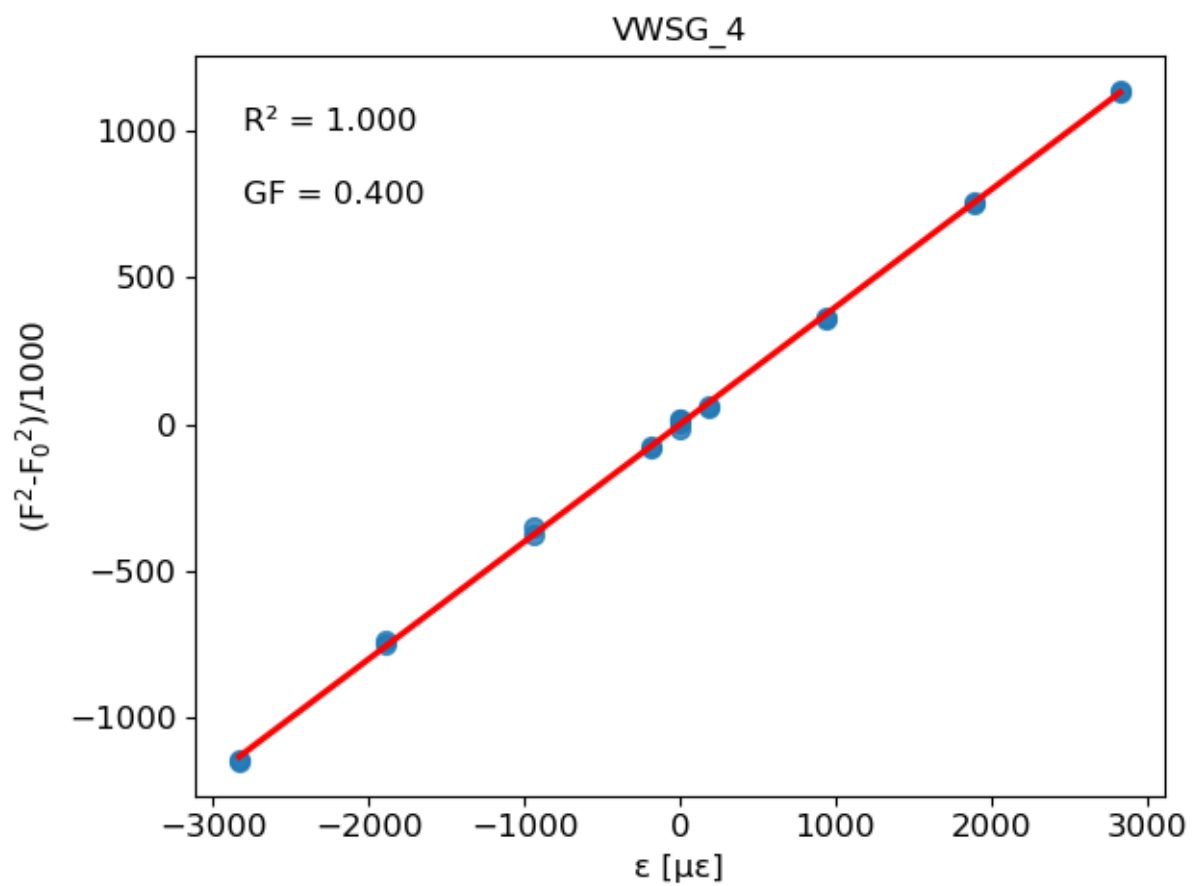
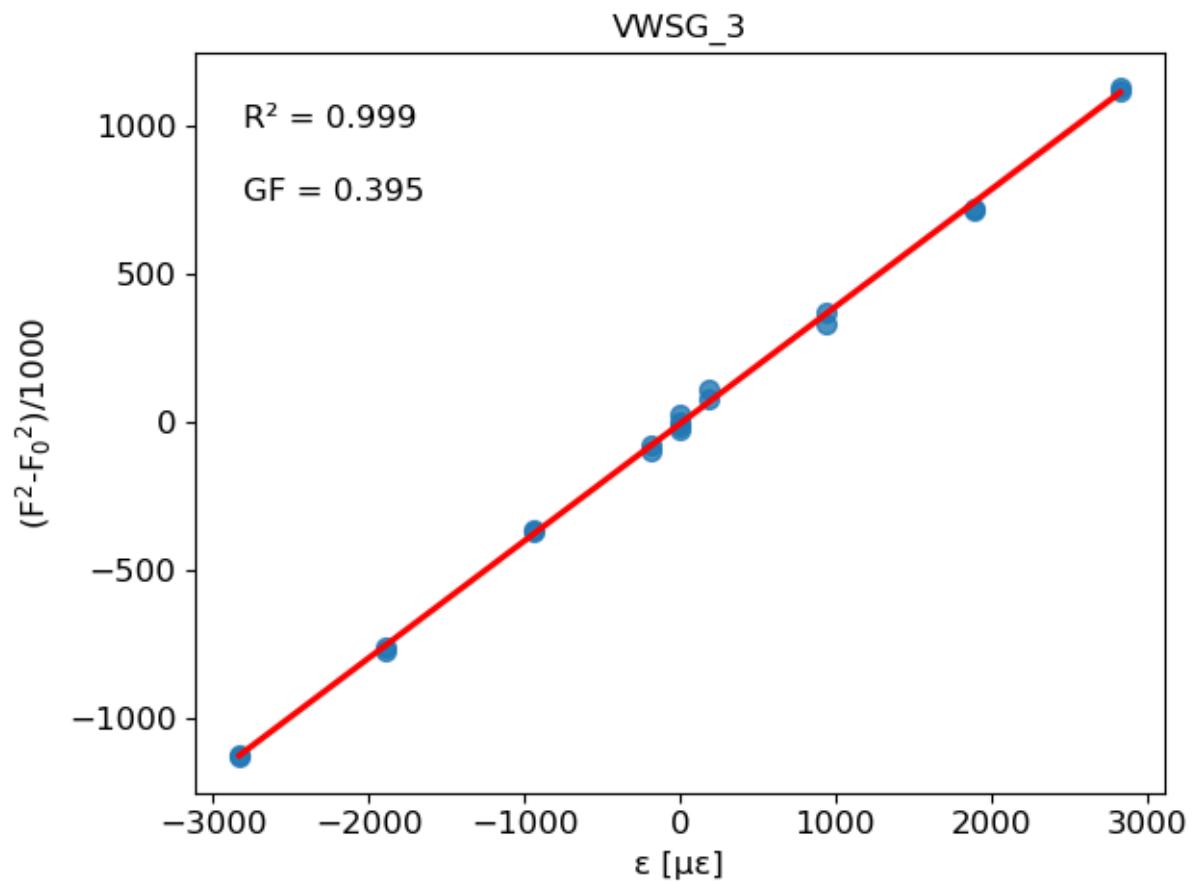
// print to Serial monitor
Serial.print("Frequency: ");
Serial.print(Freq);
Serial.print(" Hz ");
Serial.print("Strain: ");
Serial.print(strain);
Serial.print(" microstrain ");
Serial.print("Temperature = ");
Serial.print(Temperature);
Serial.println(" degC");
void SERCOM3_Handler()
{mySerial.IrqHandler();
}
}
// == 3 END MAIN SETUP, LOOP ==

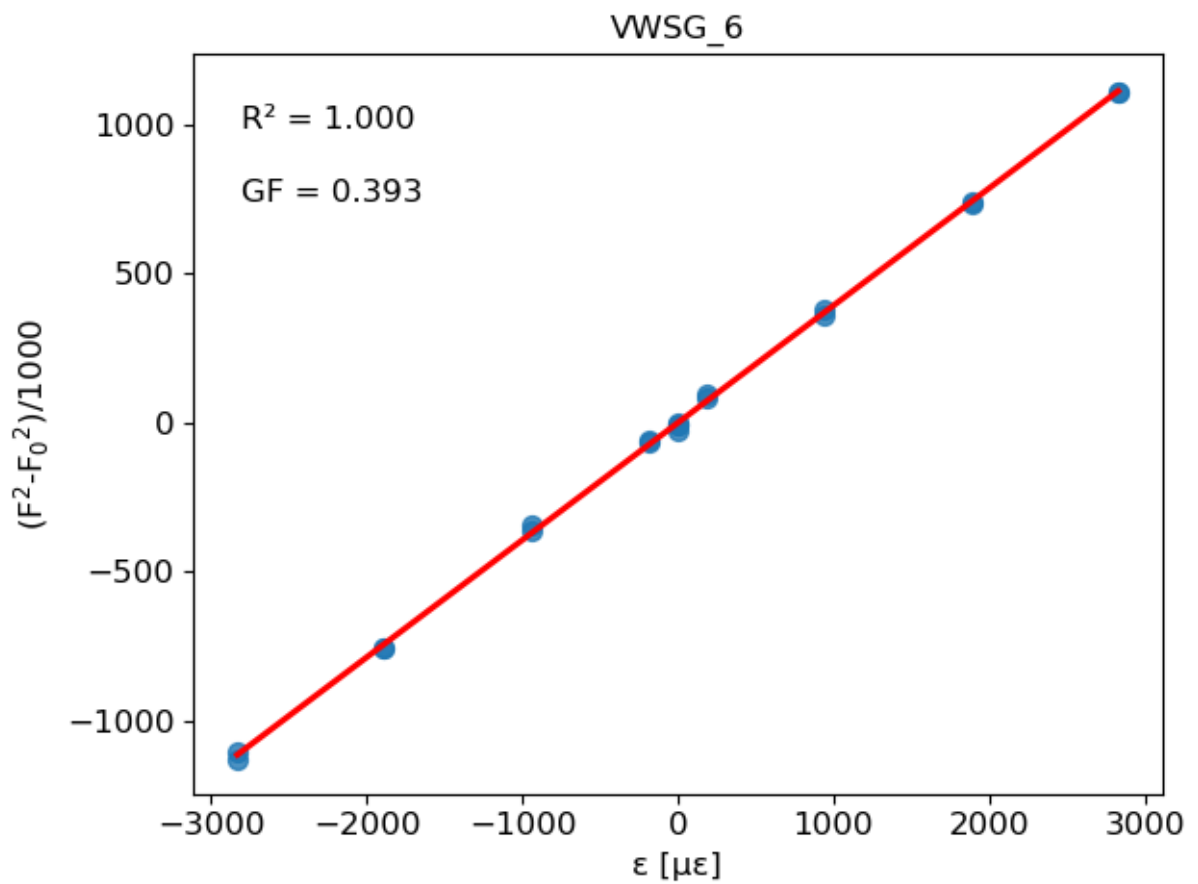
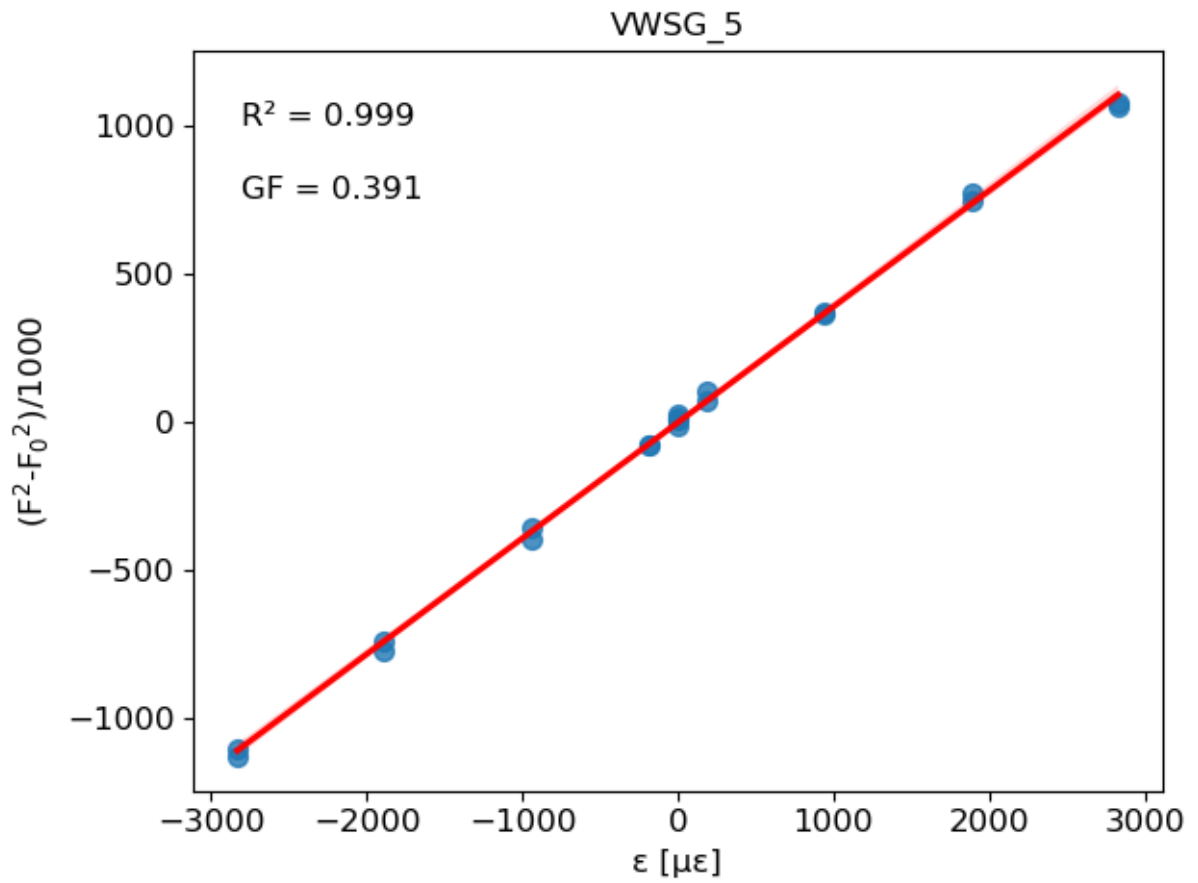
```

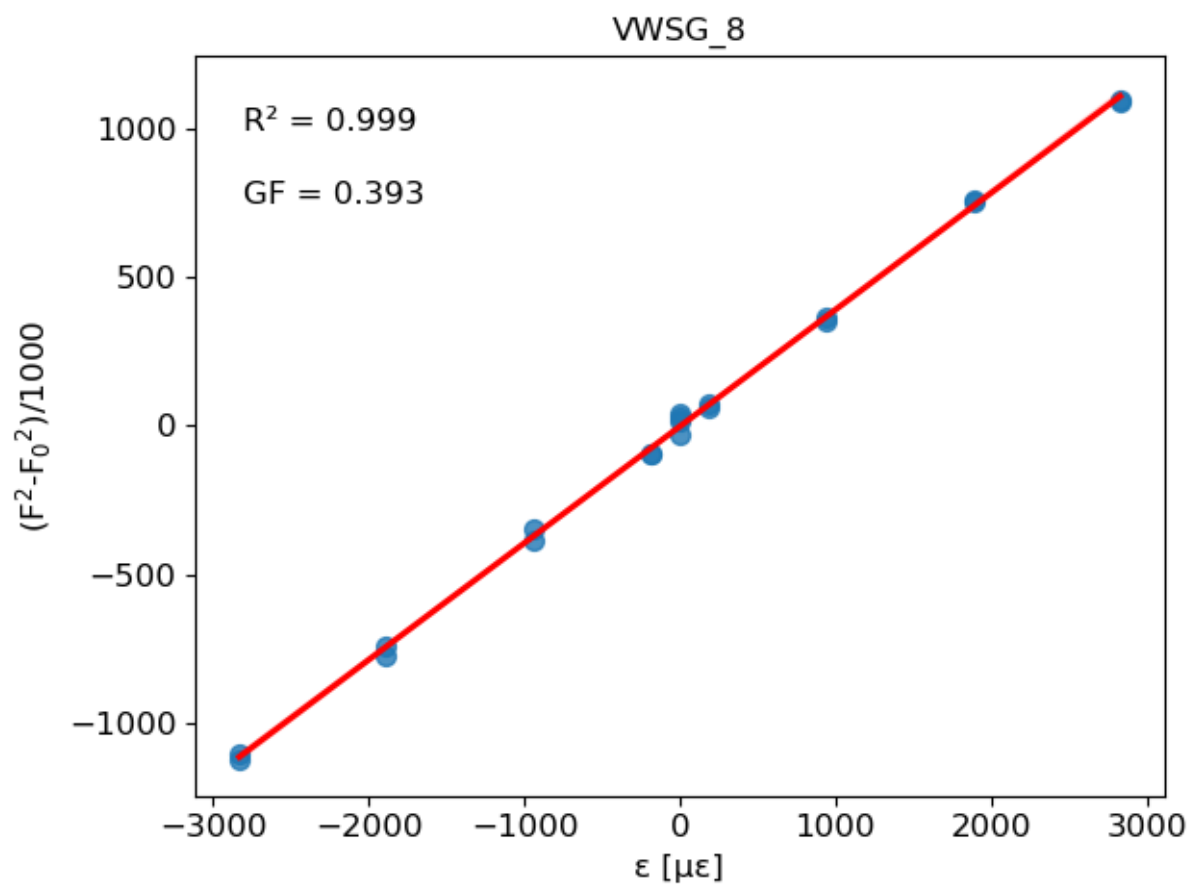
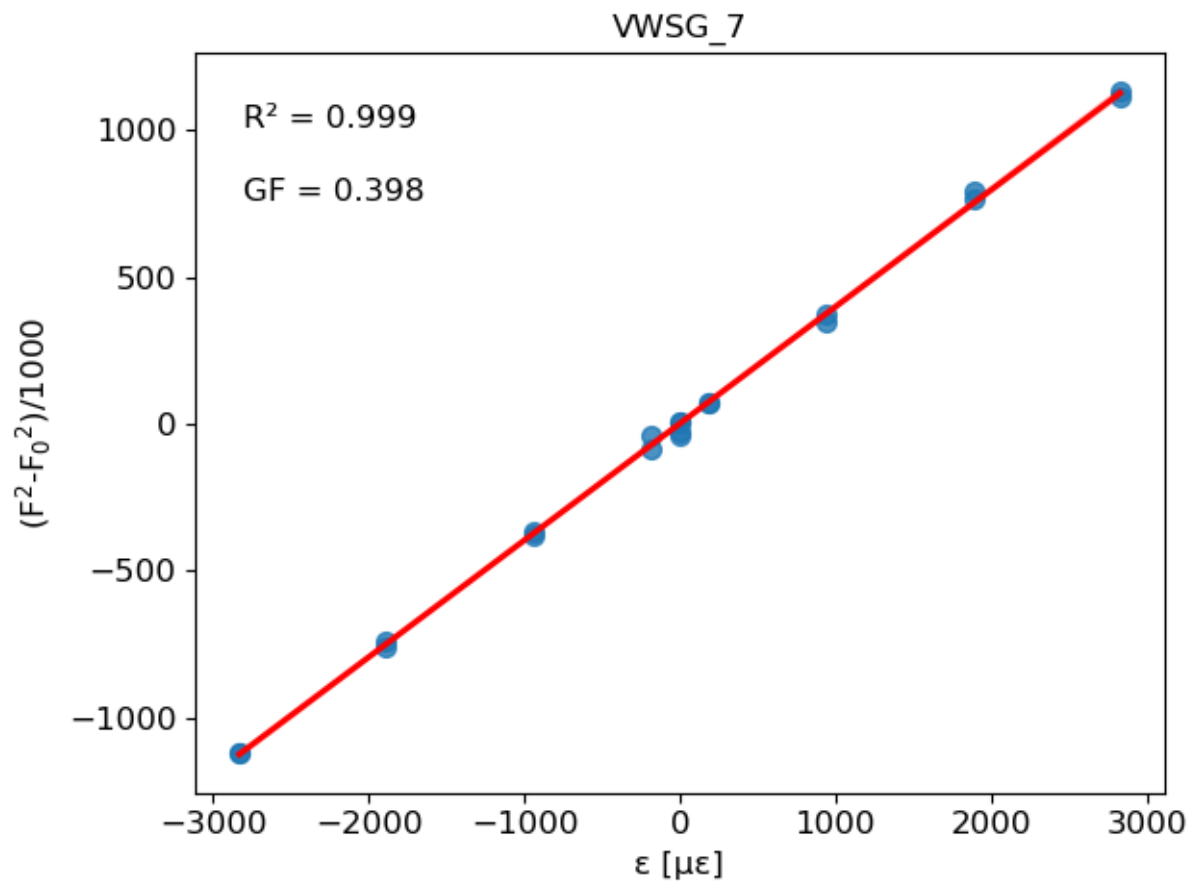
### A. 3 VWSG initial calibration results

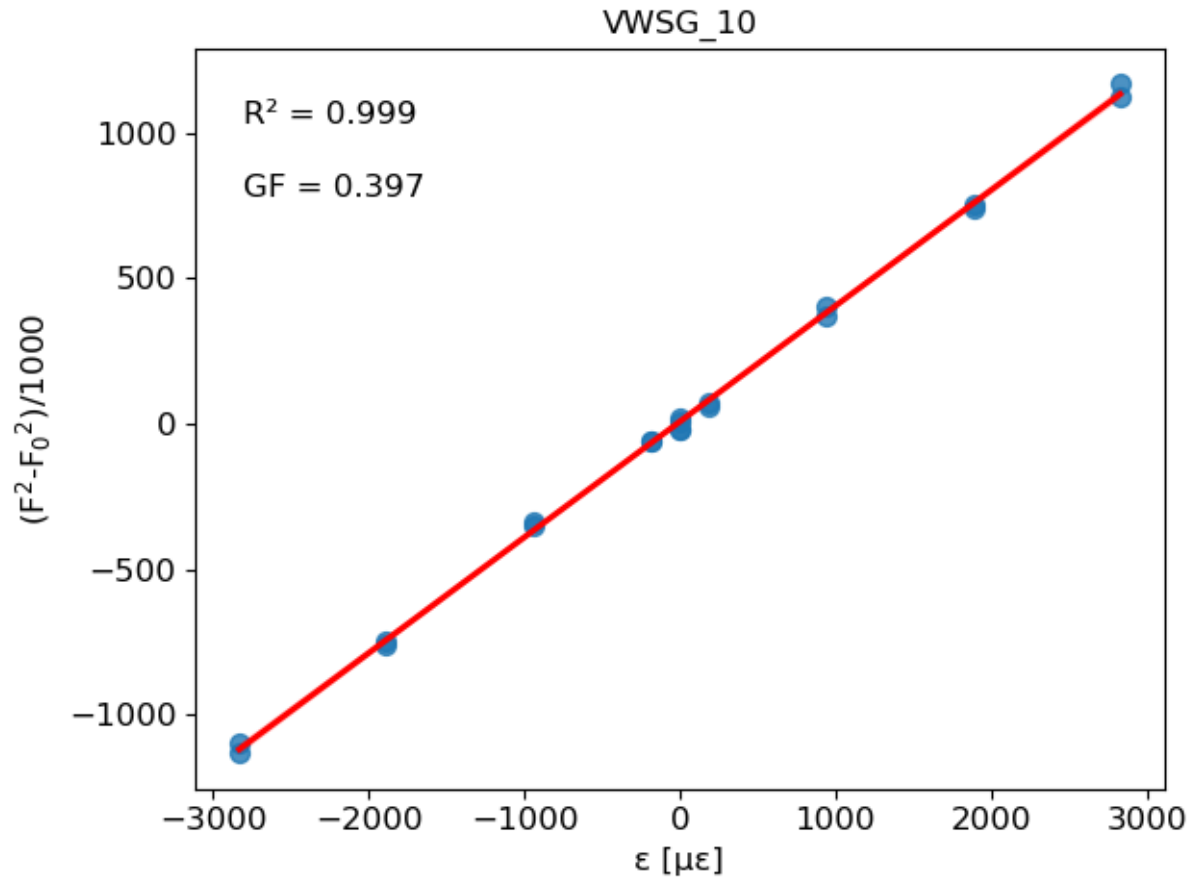
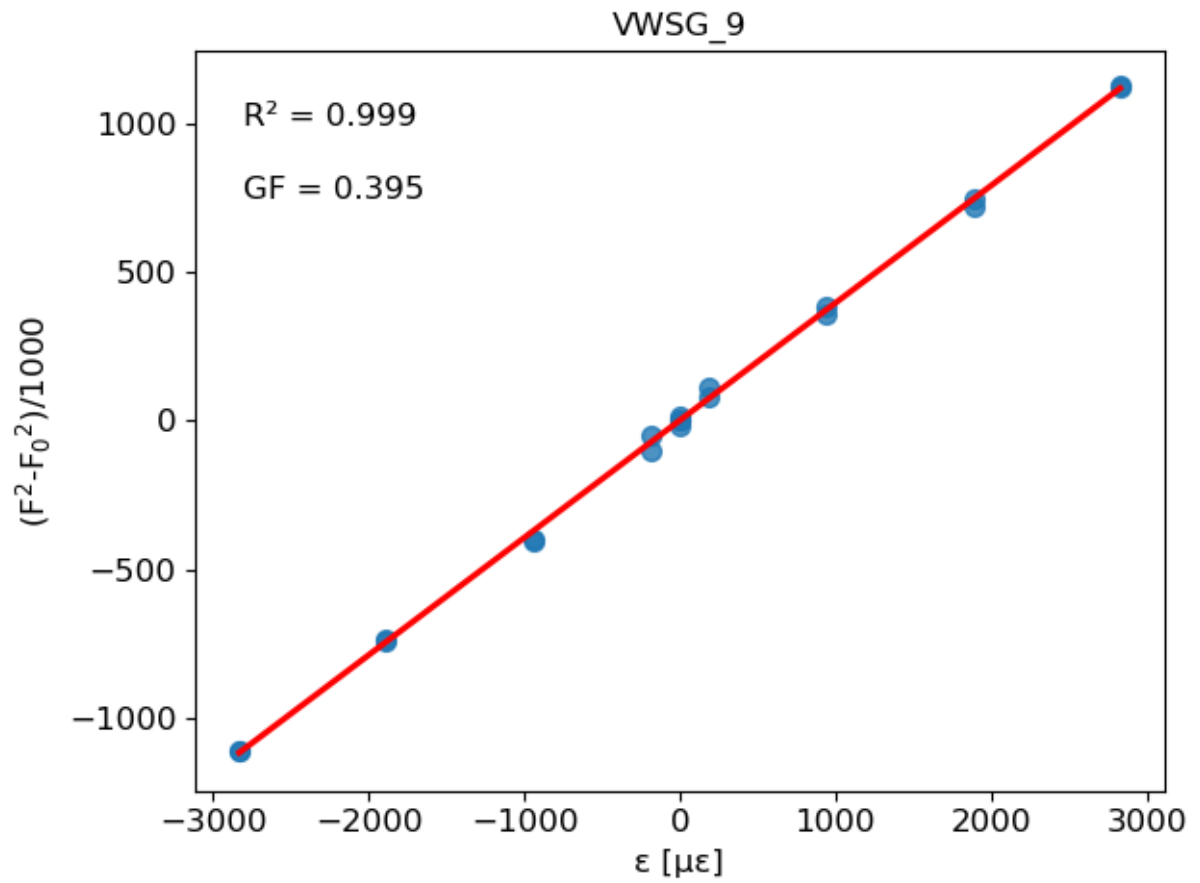




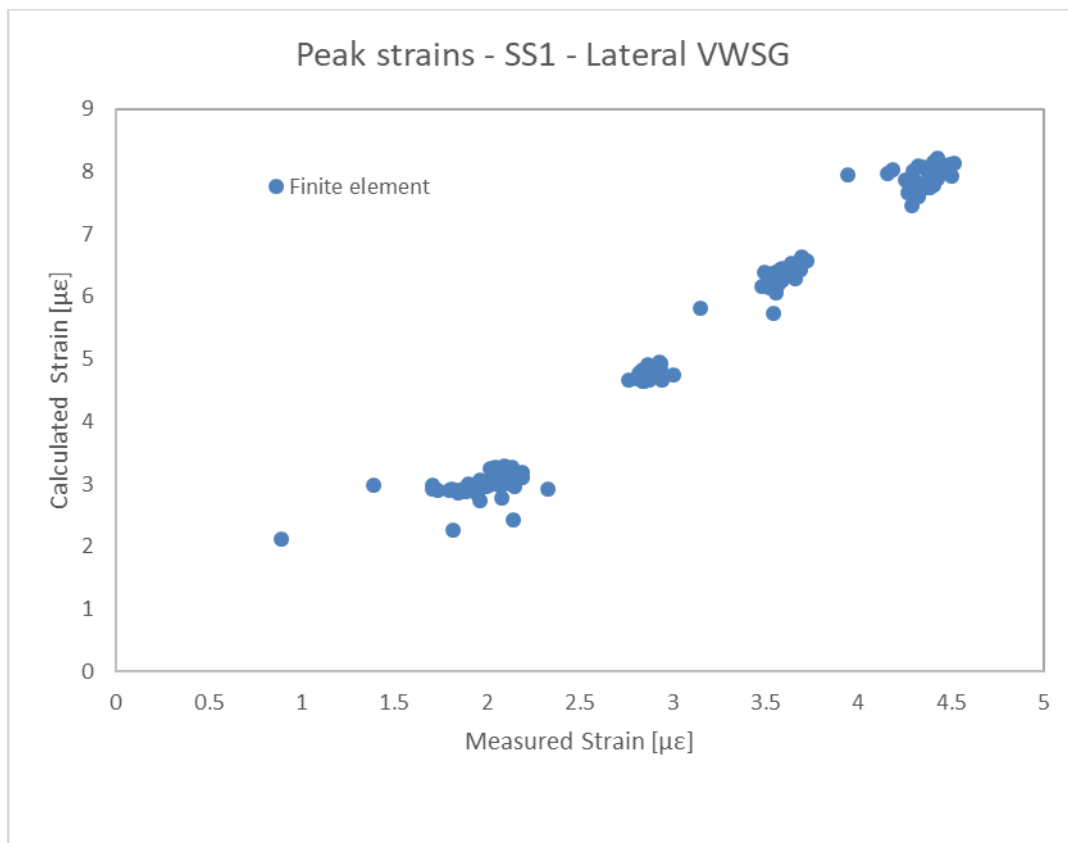
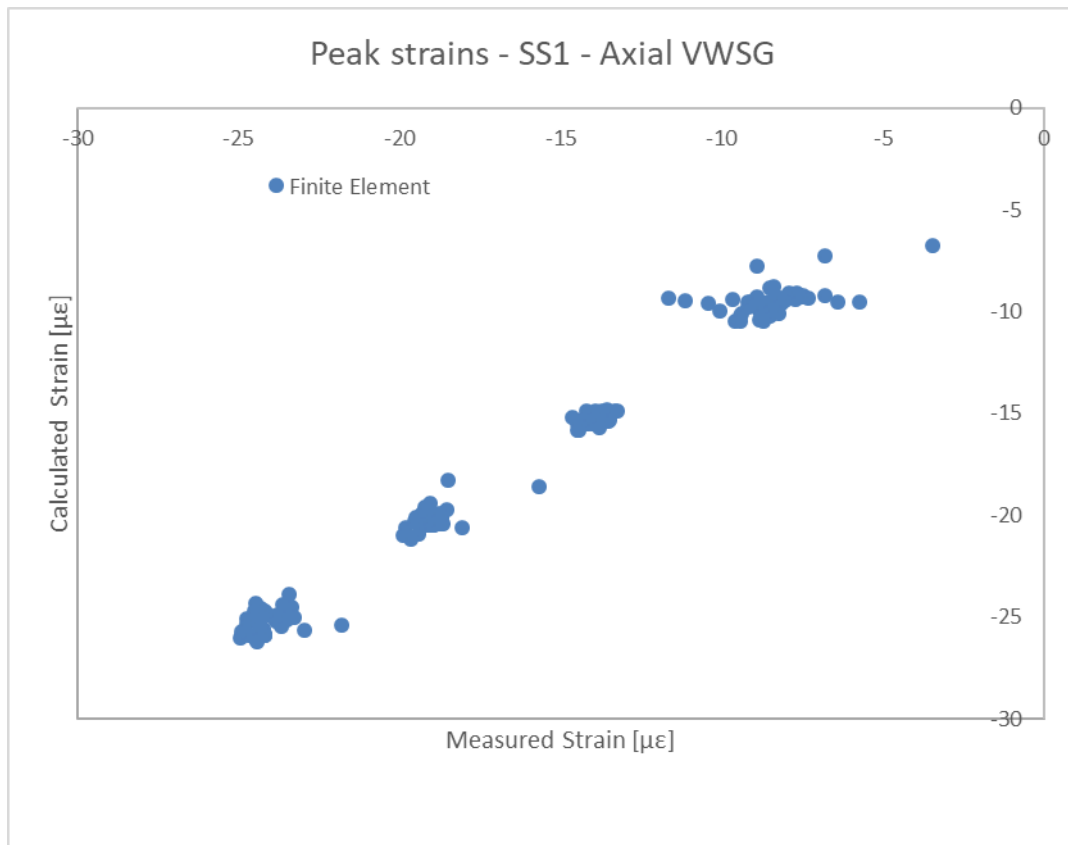


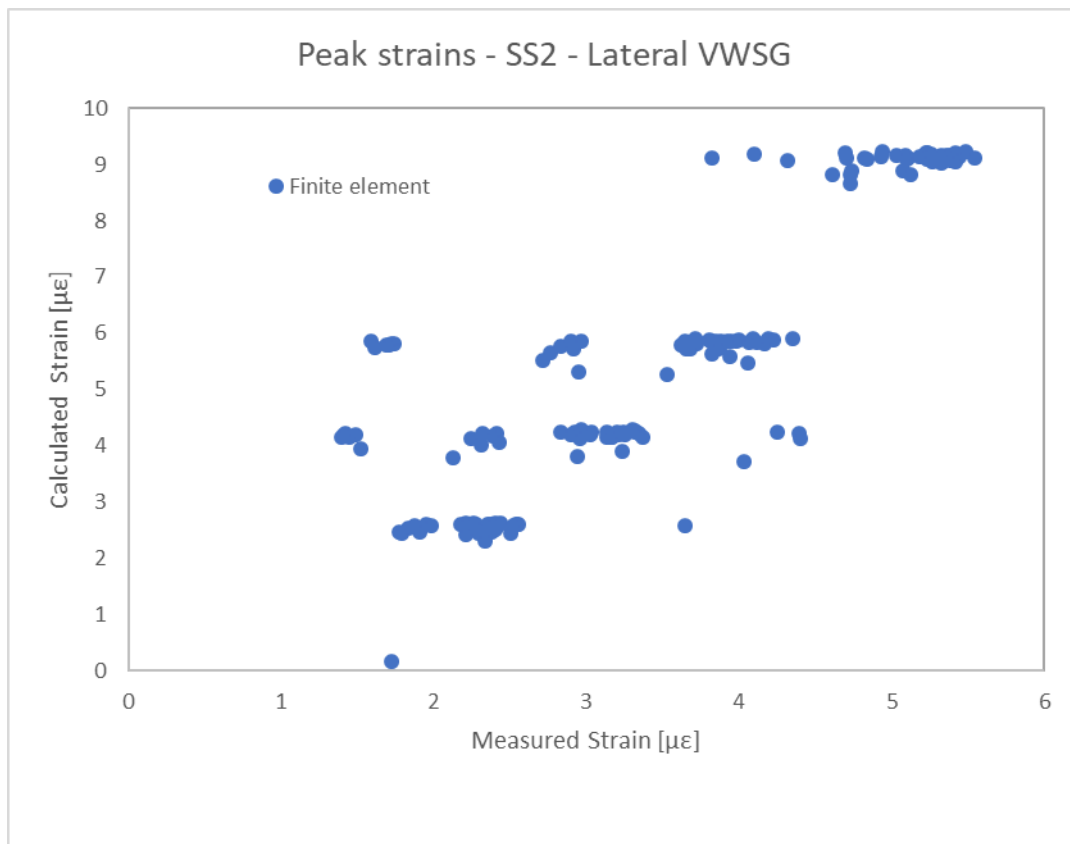
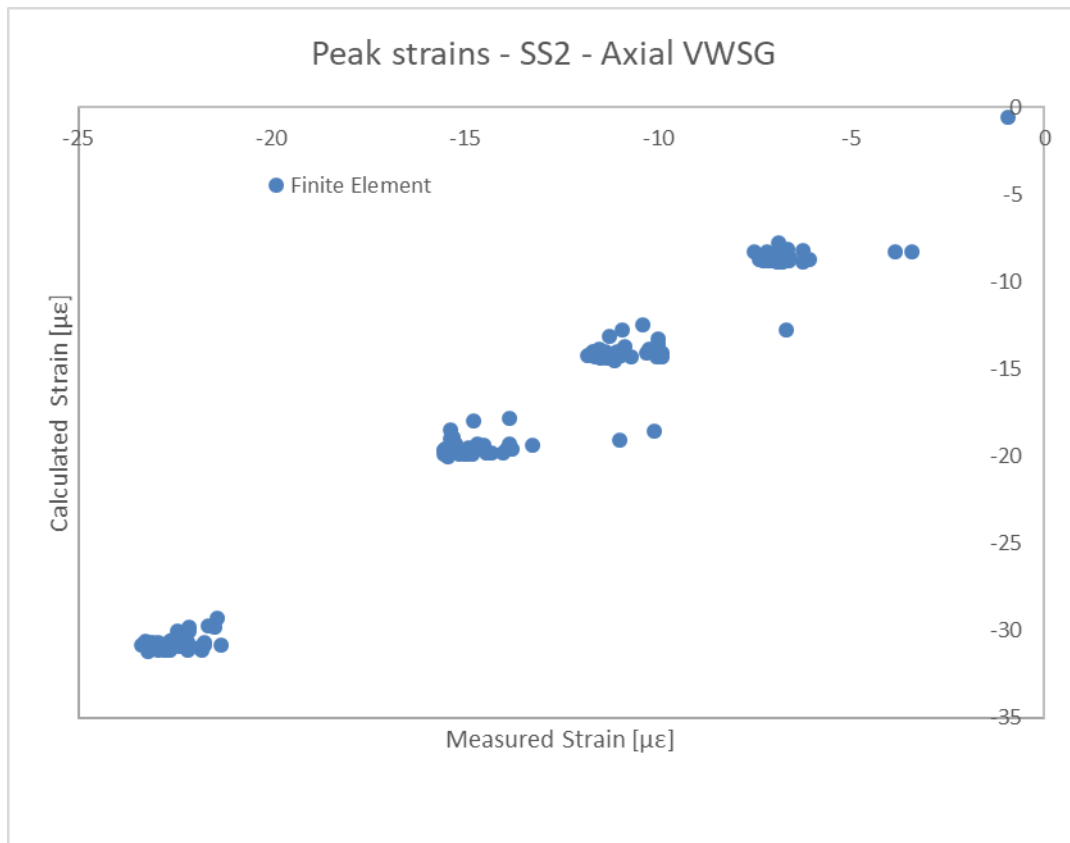


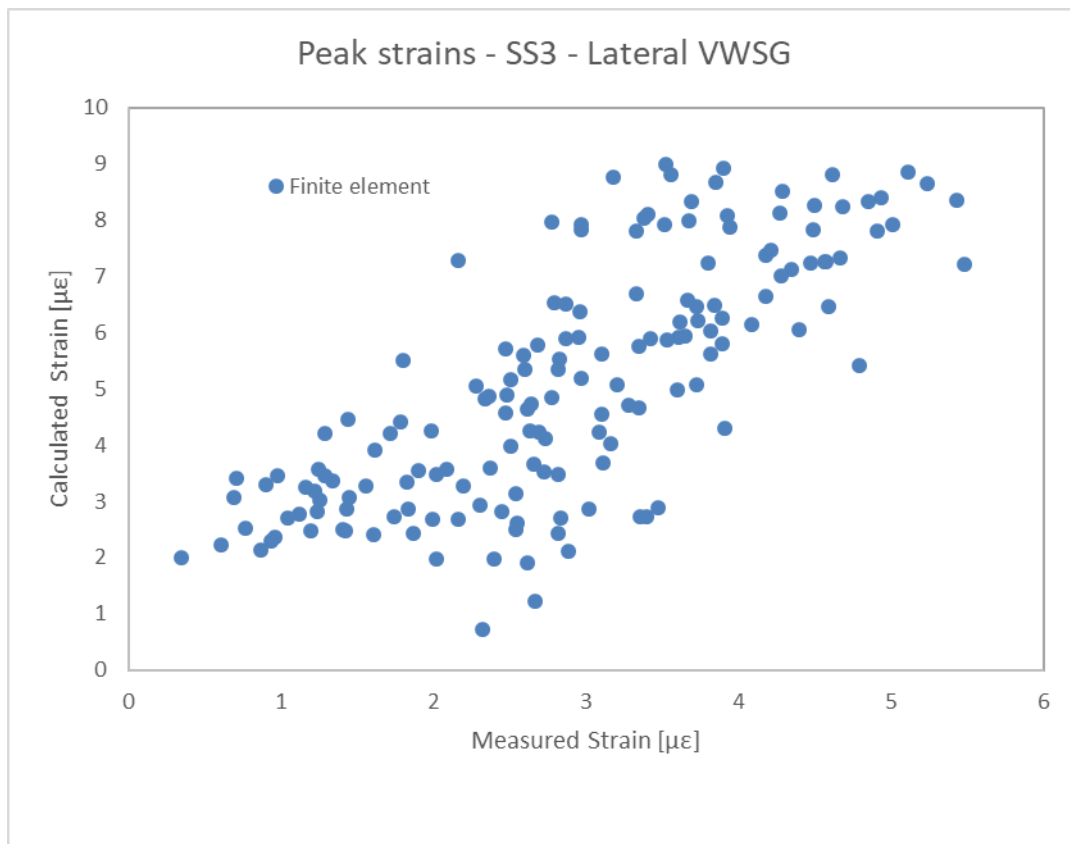
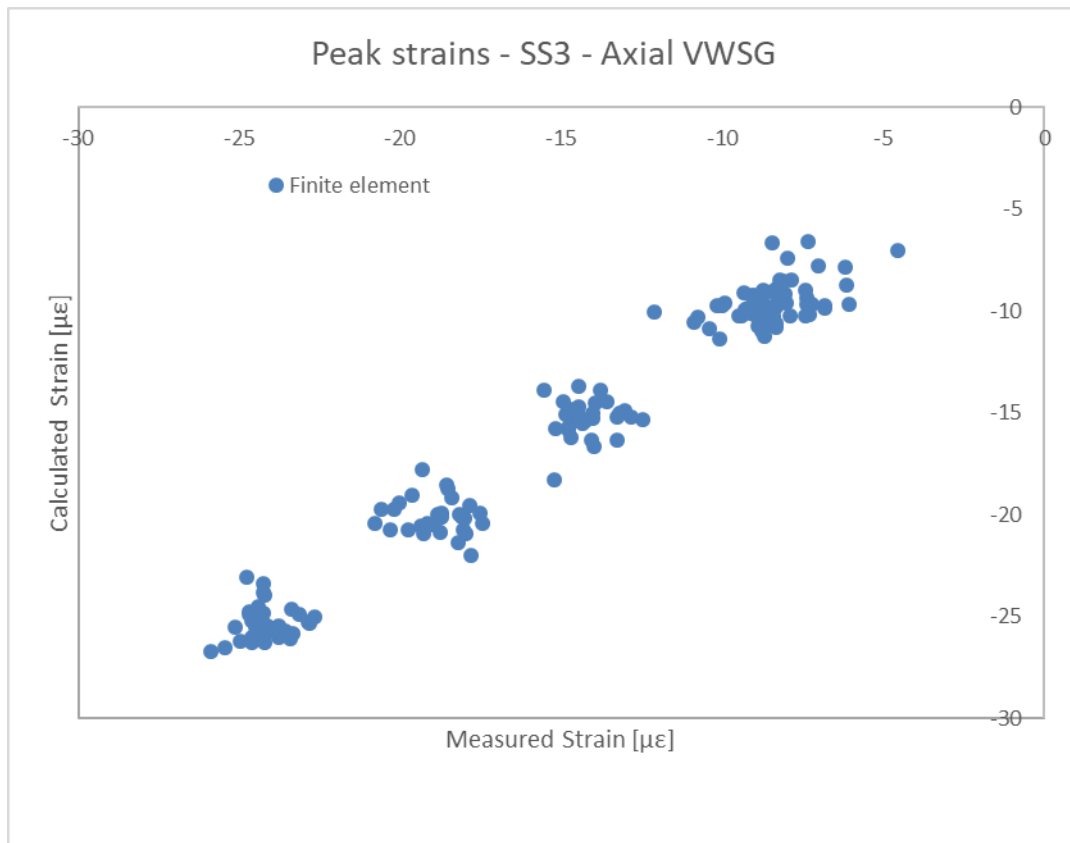


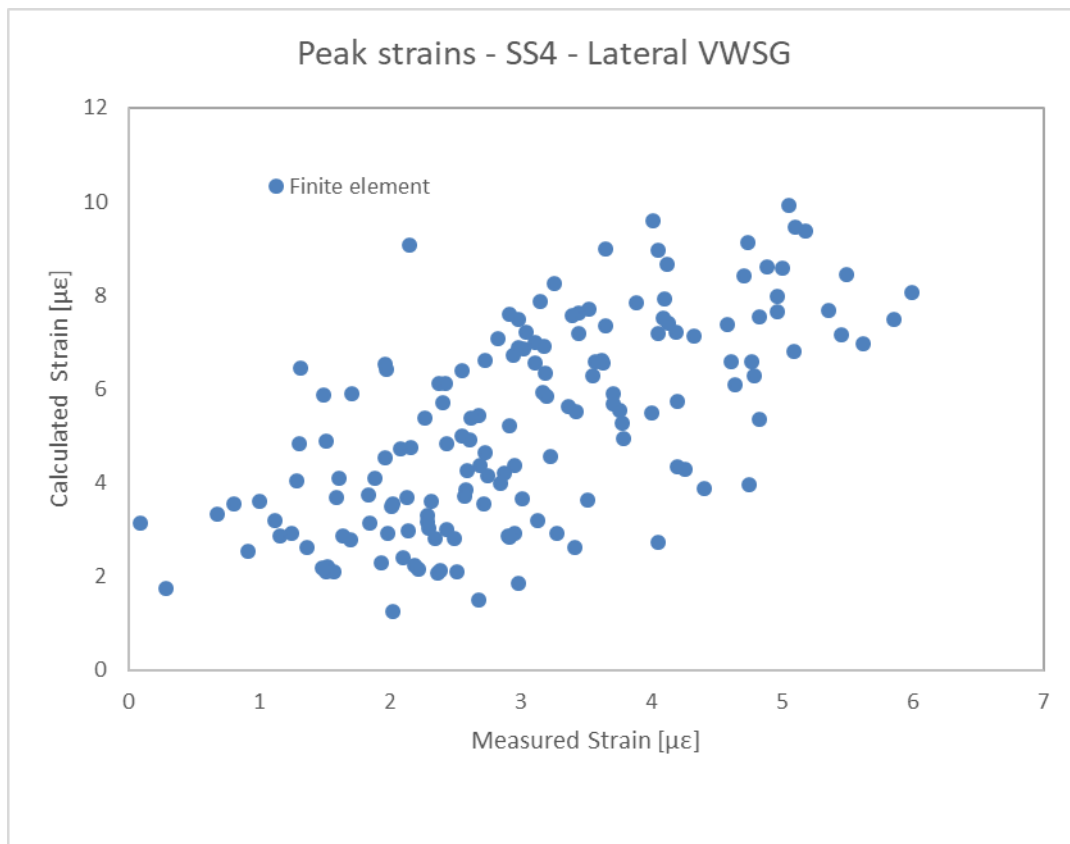
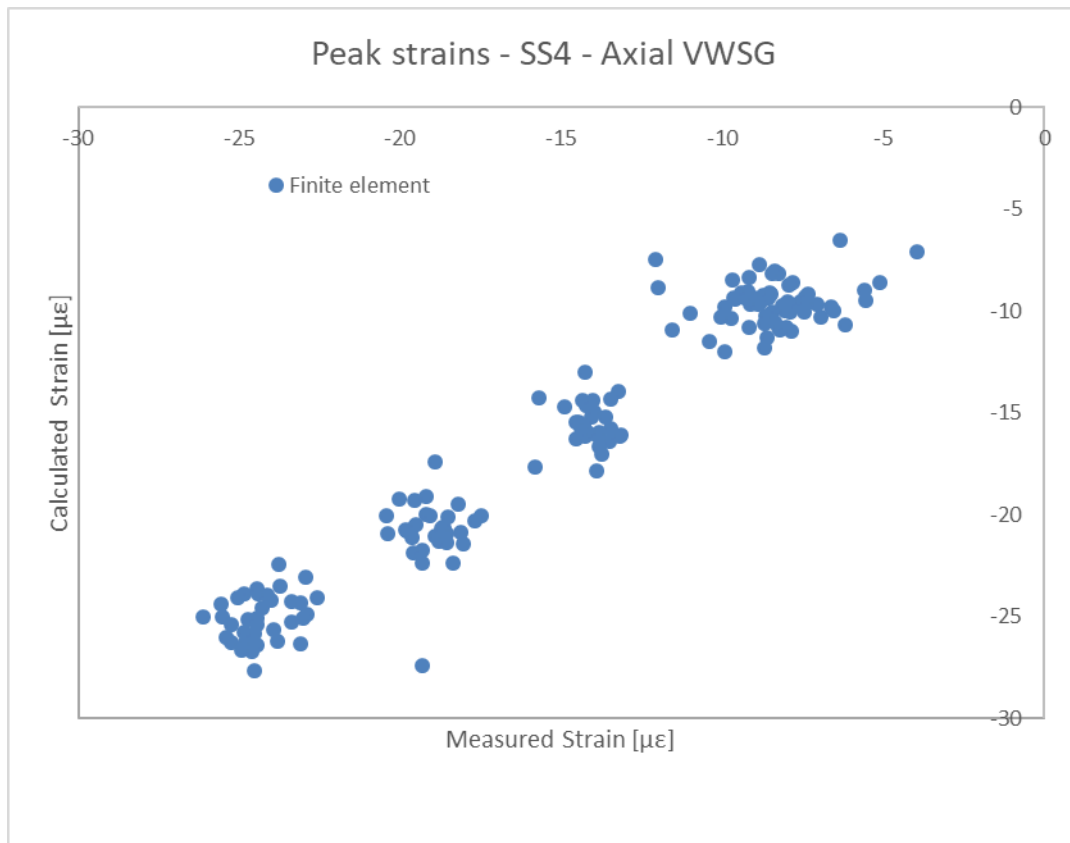


### A. 4 Smart segment Peak strains – Finite Element Model

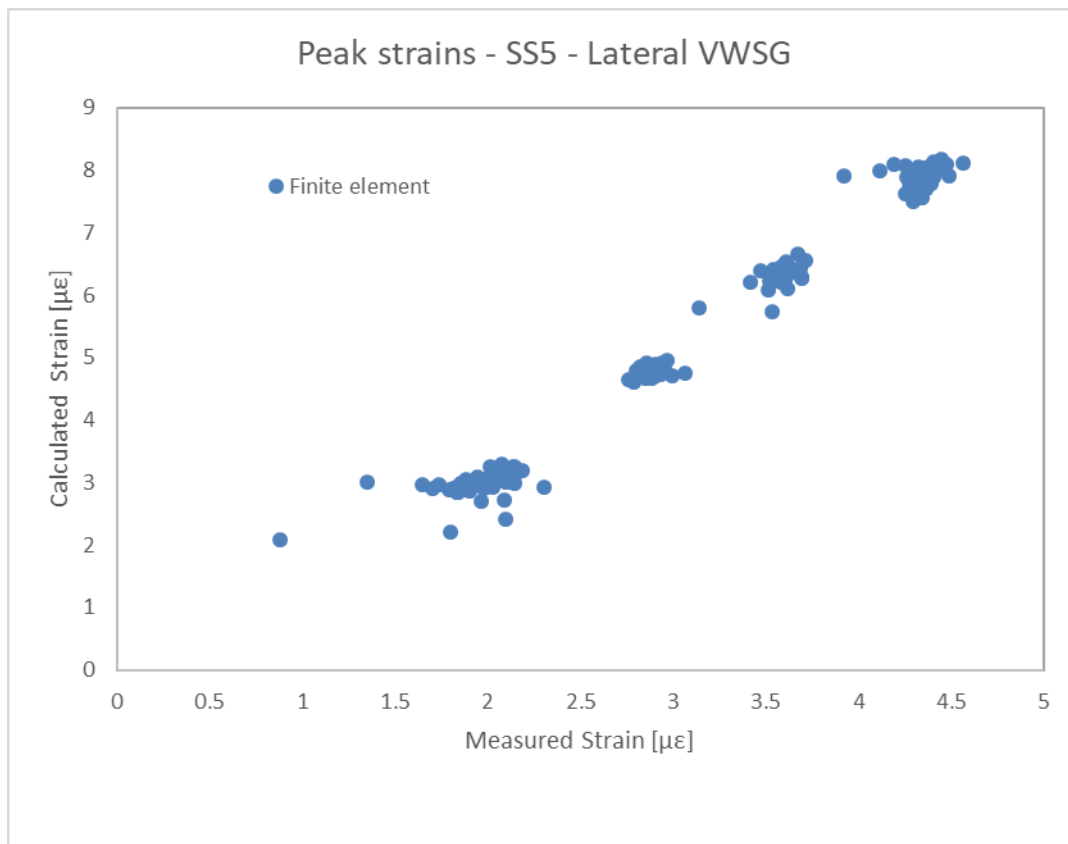
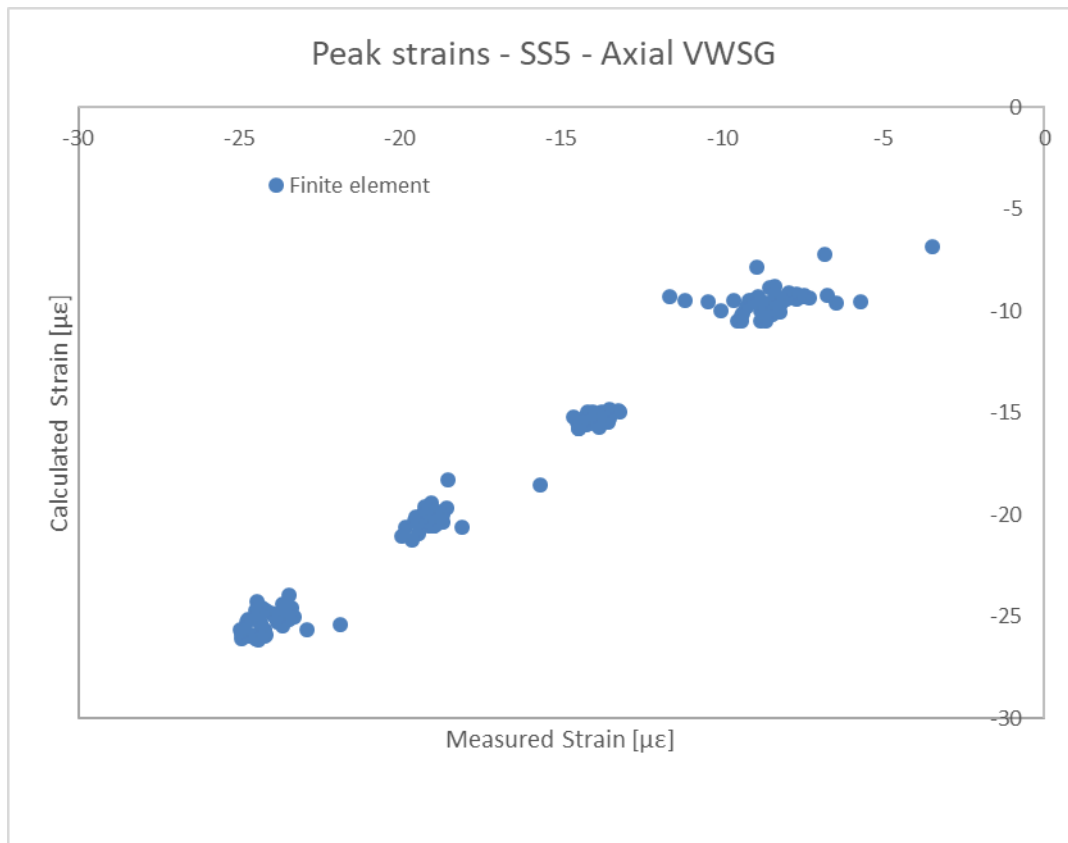


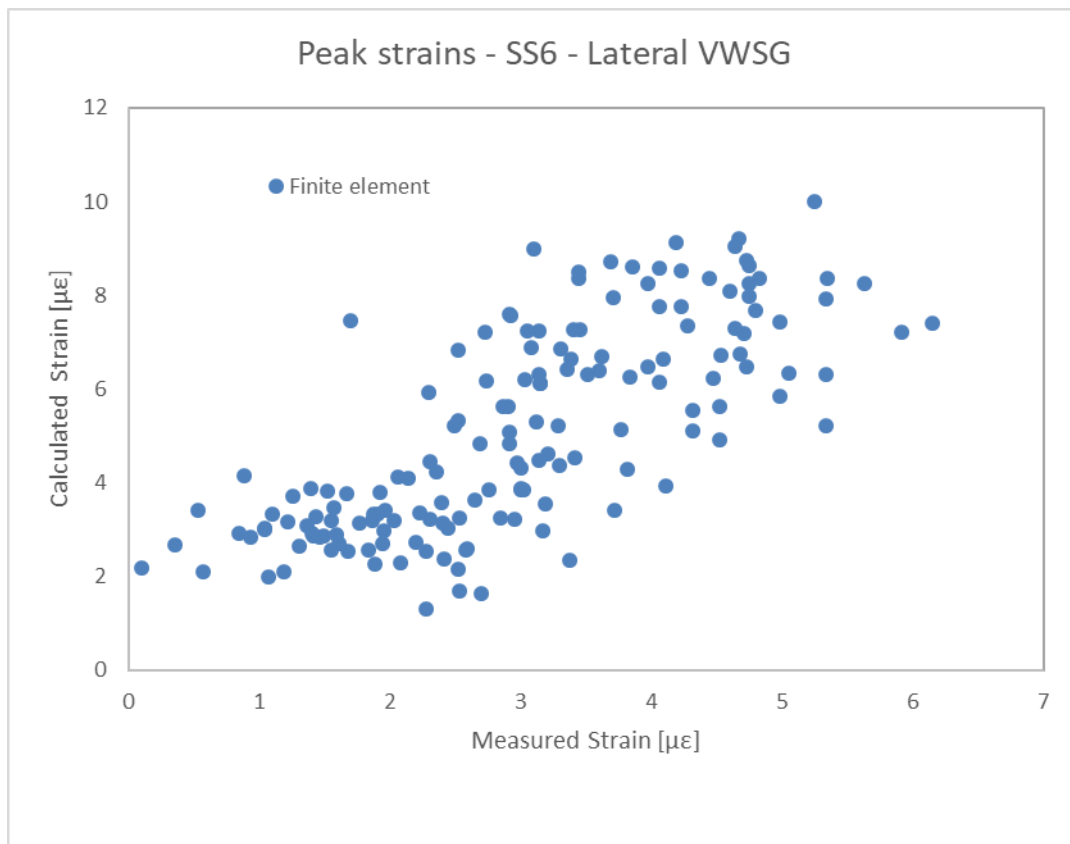
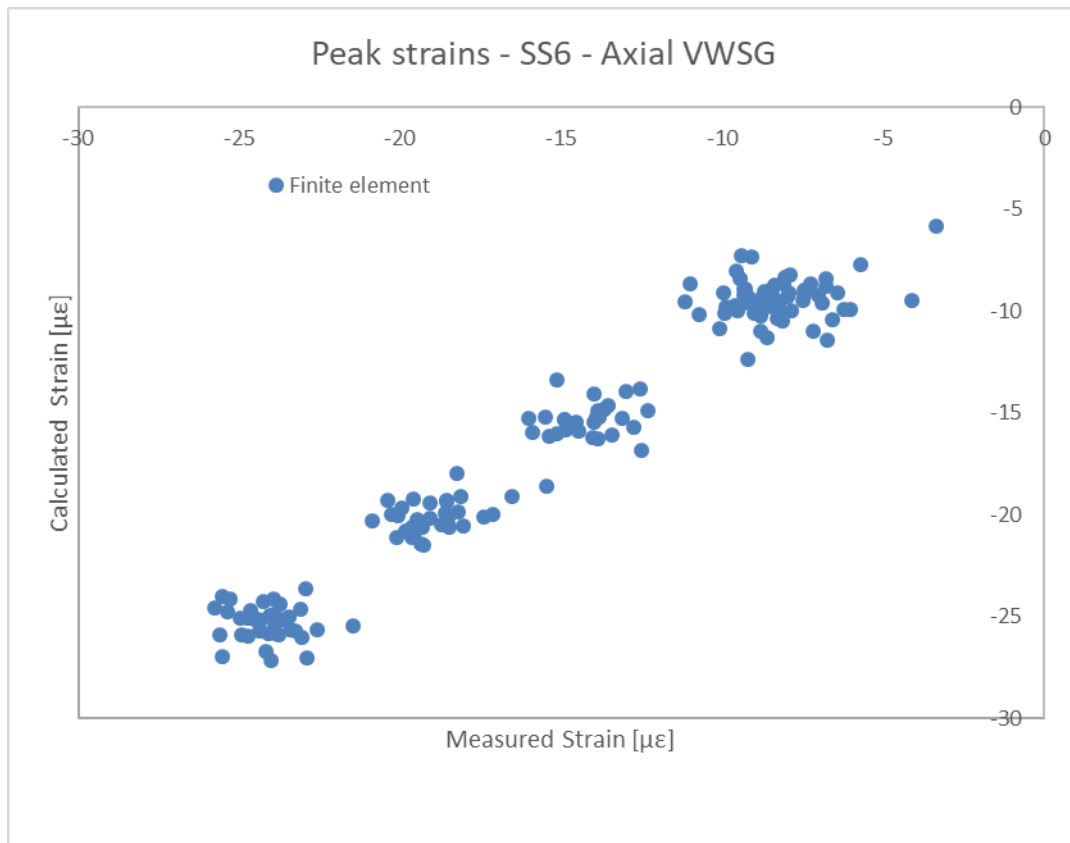


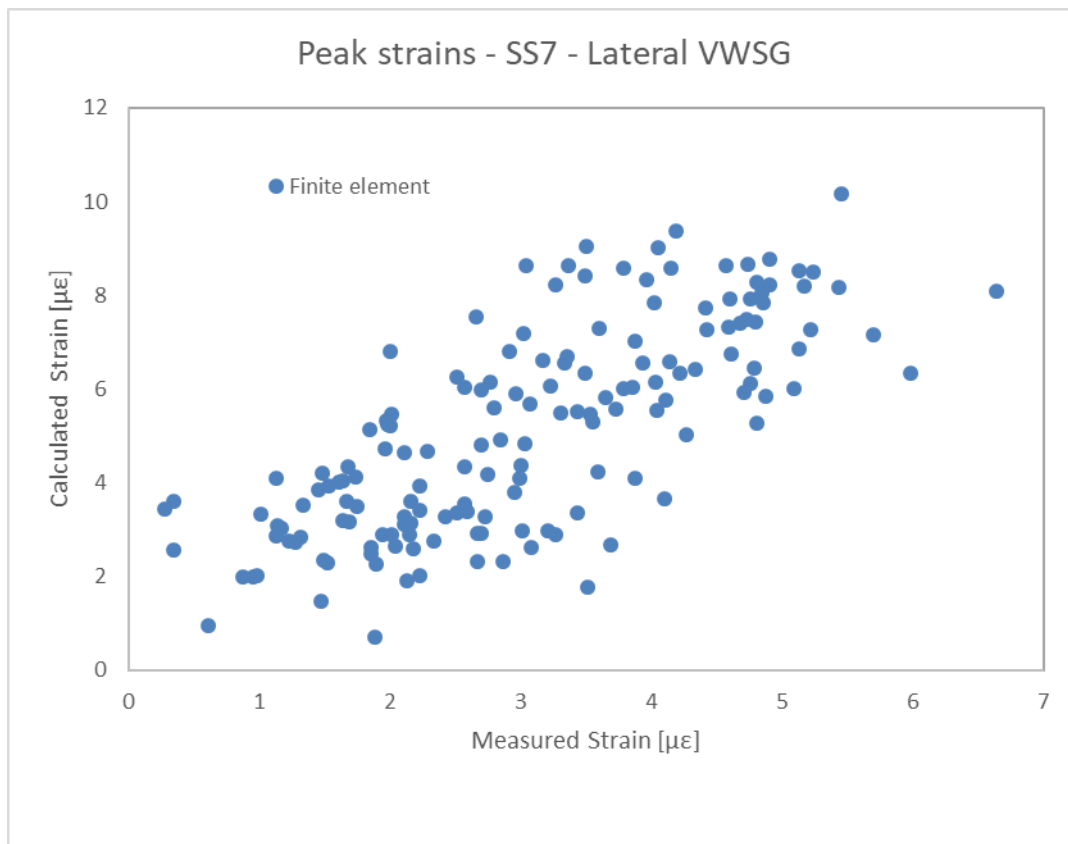
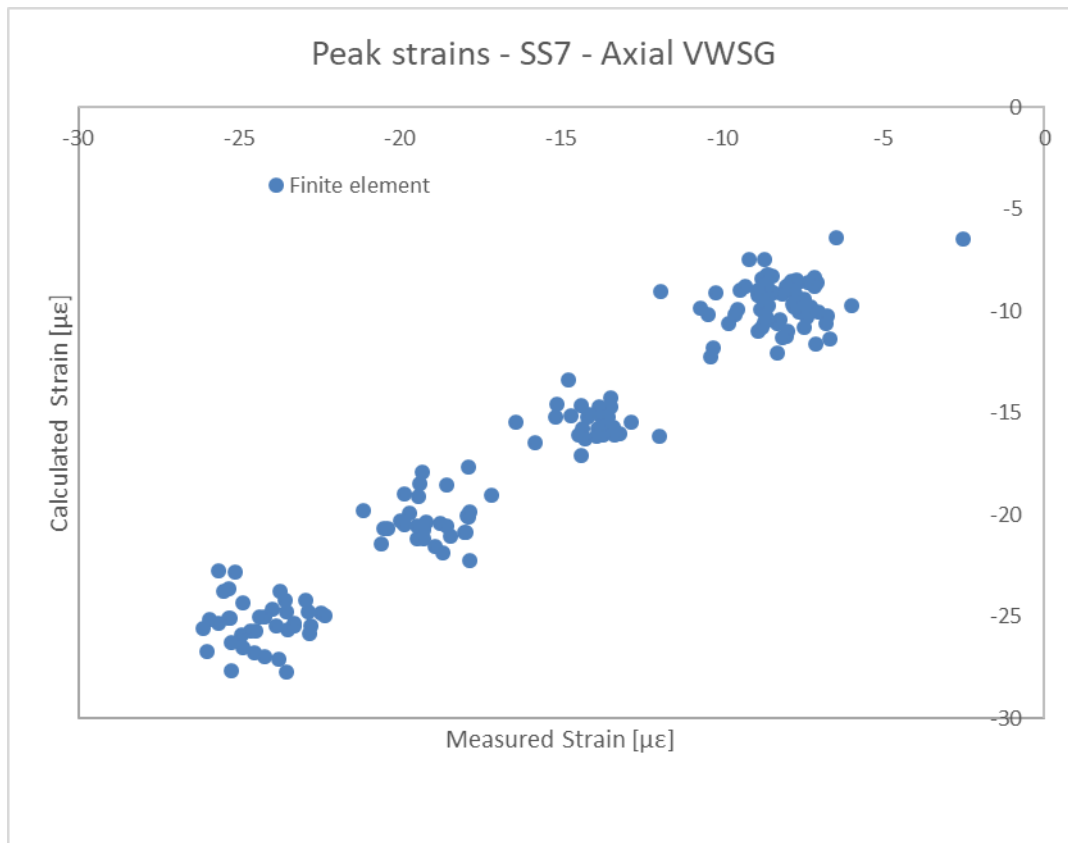


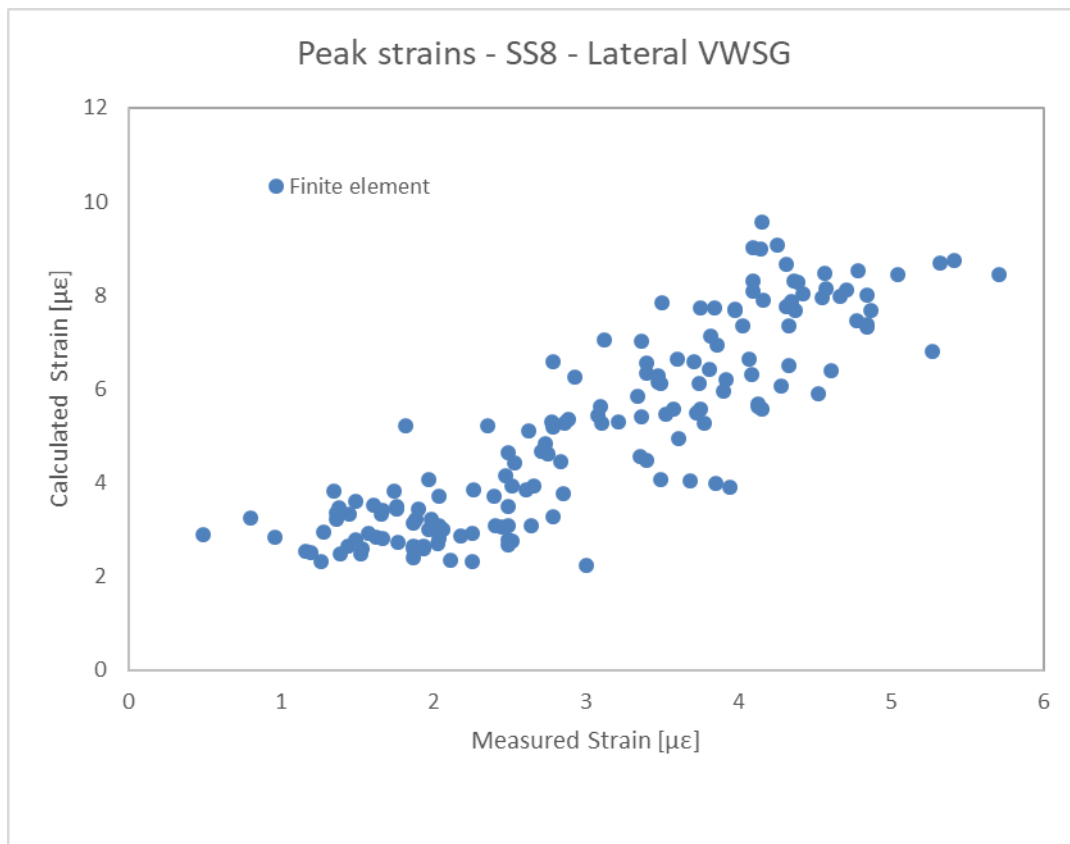
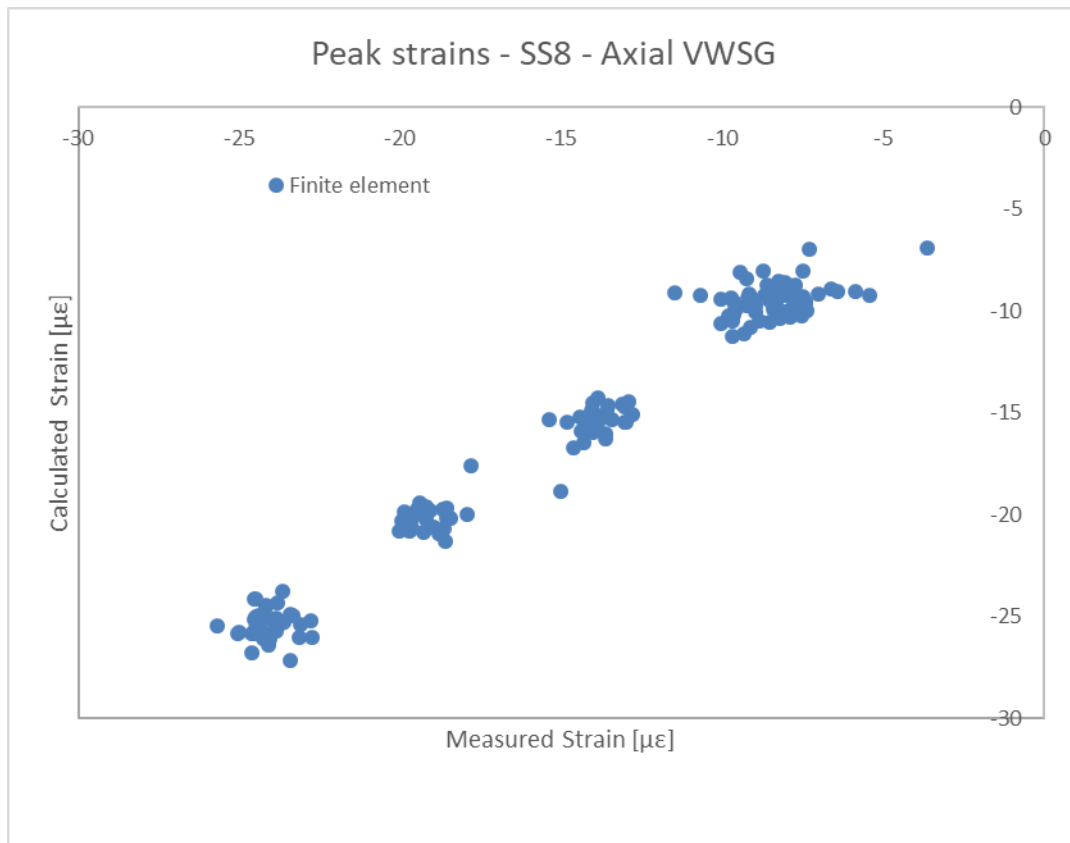


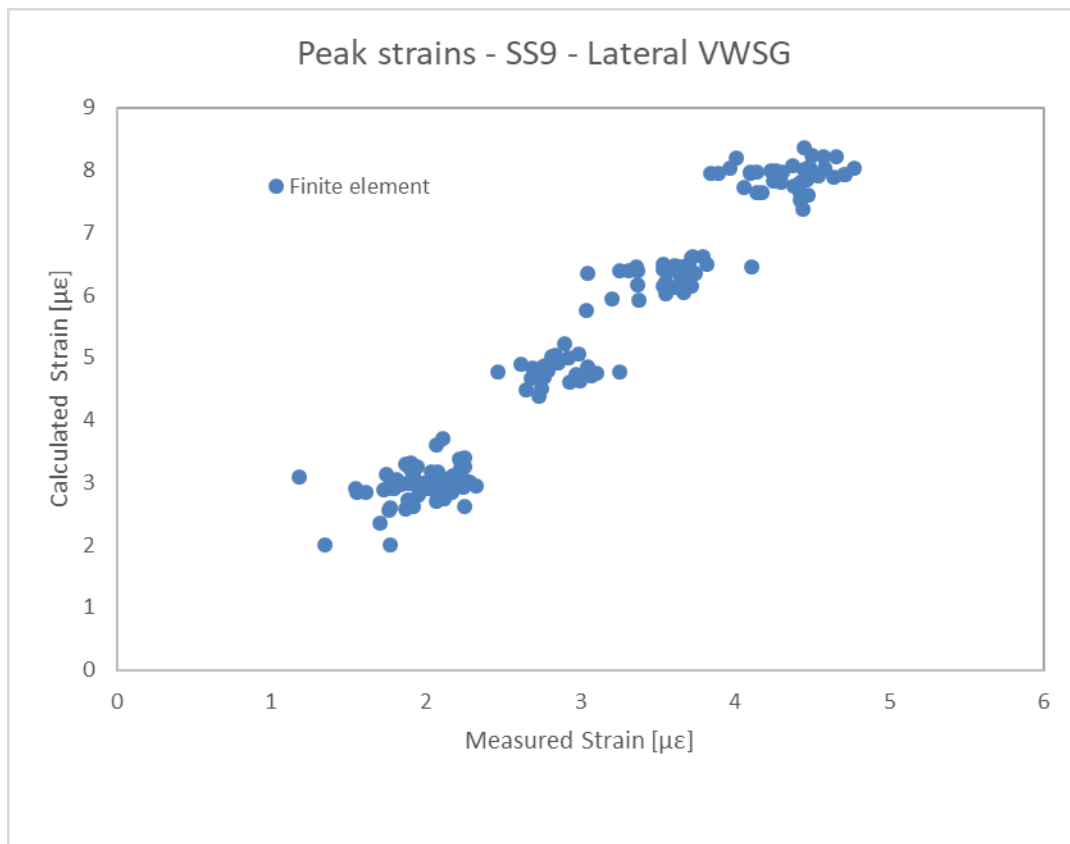
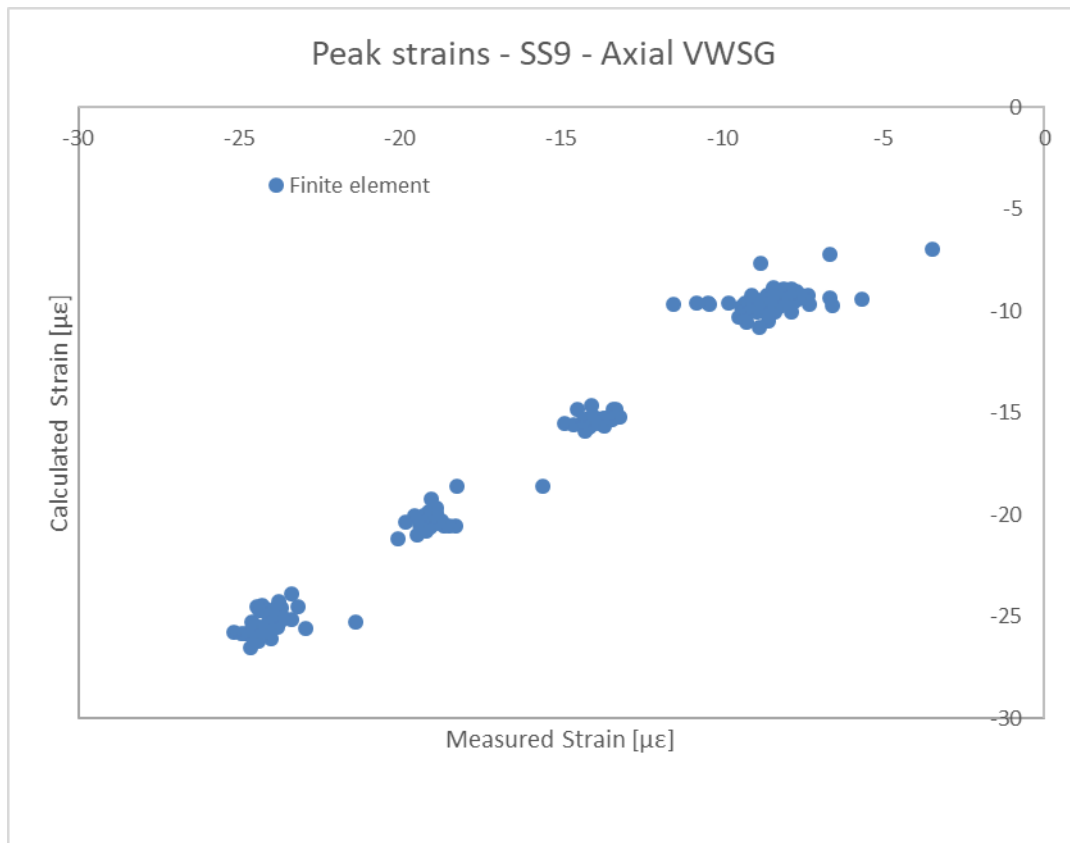


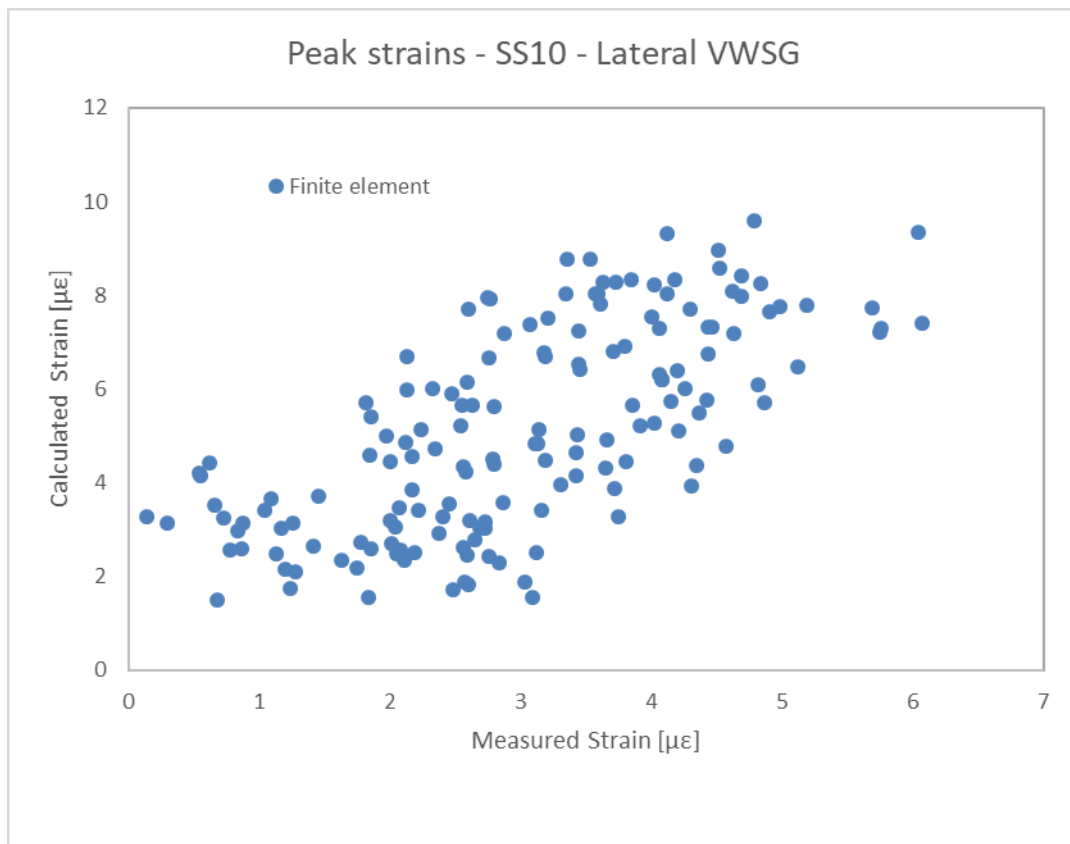
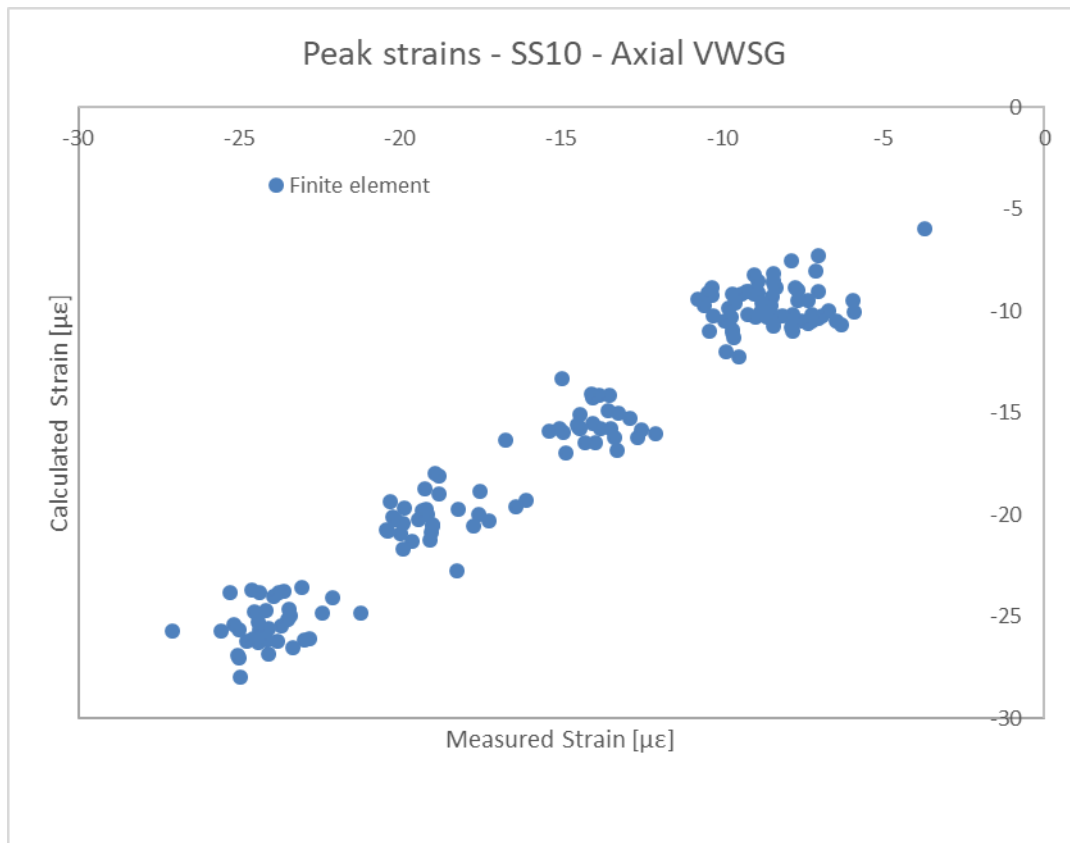




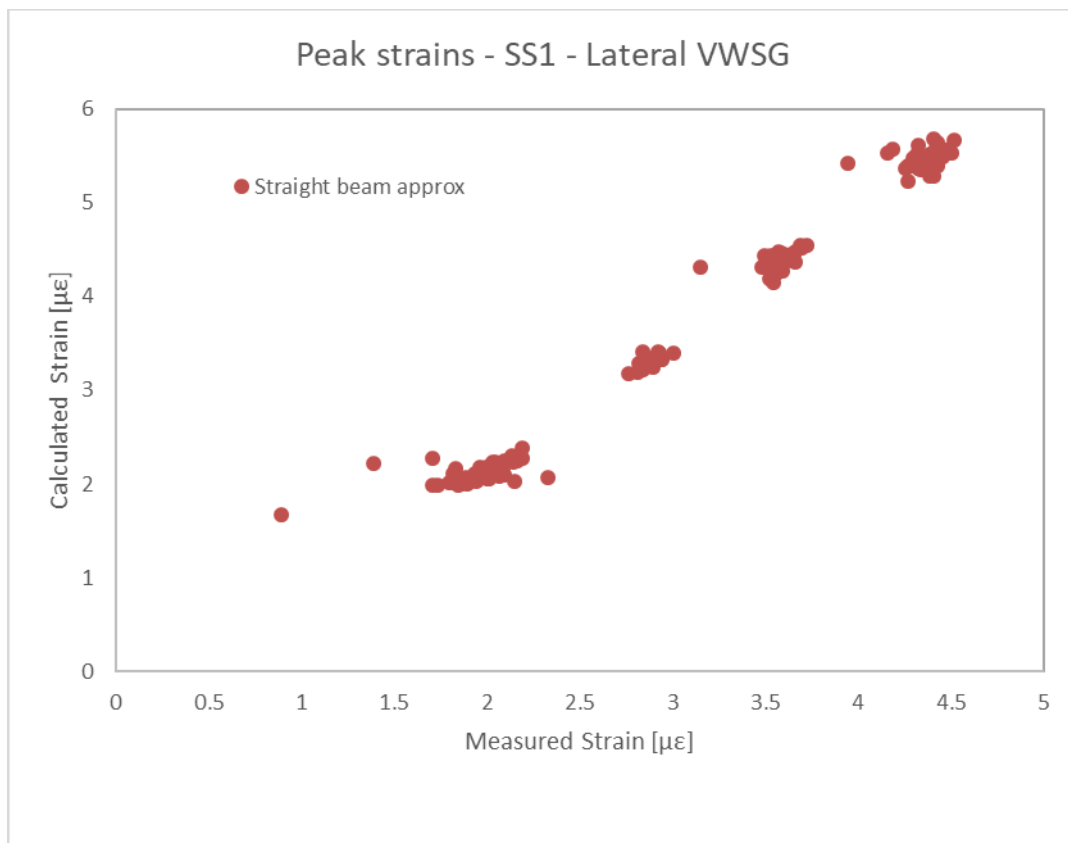
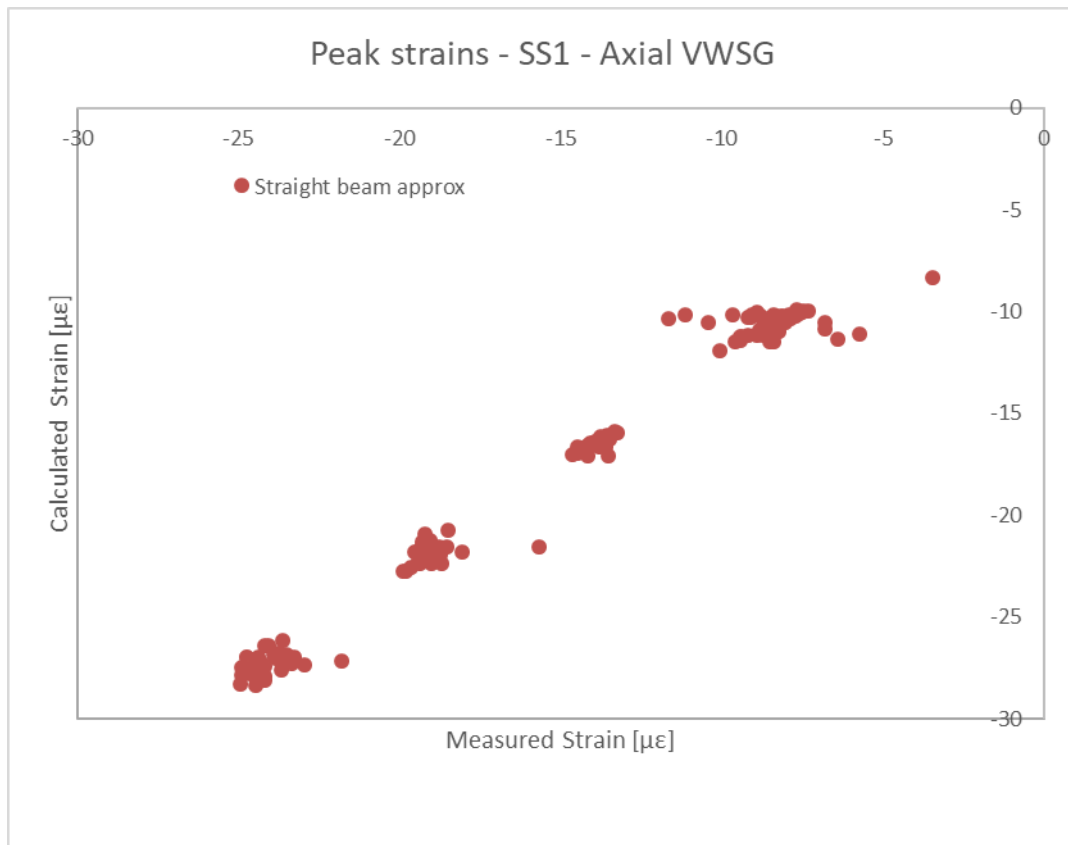


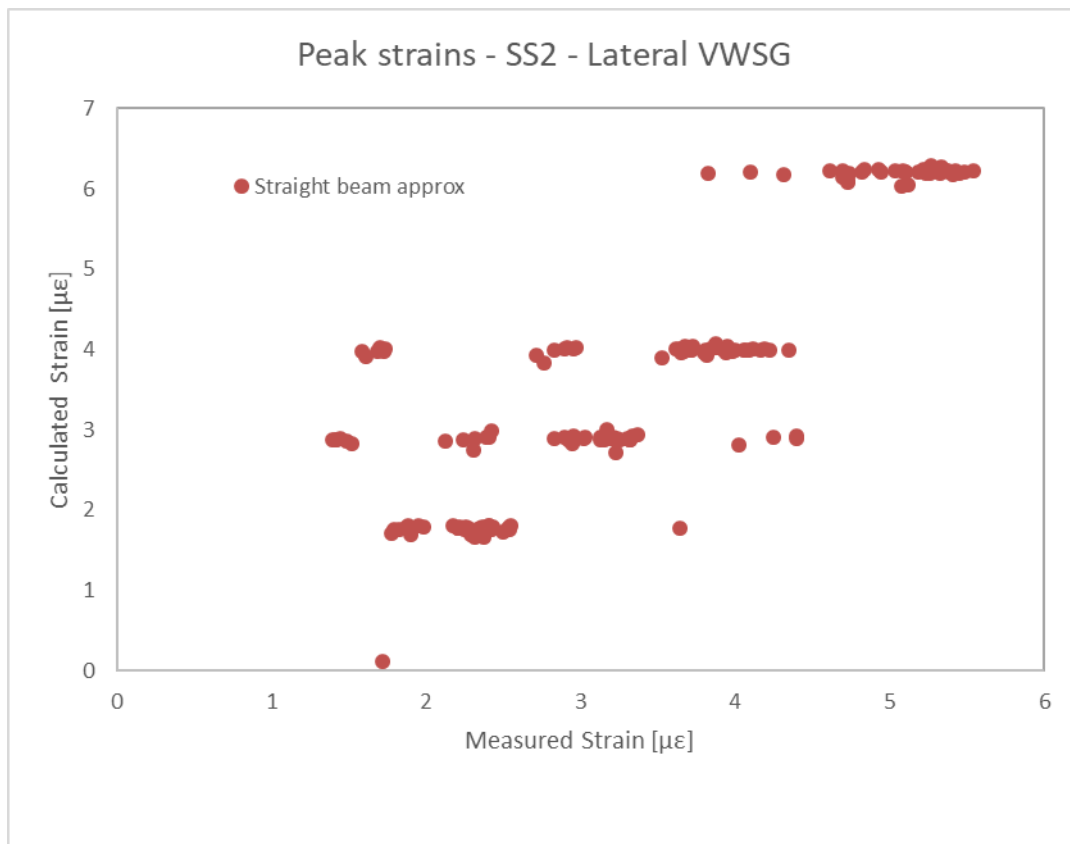
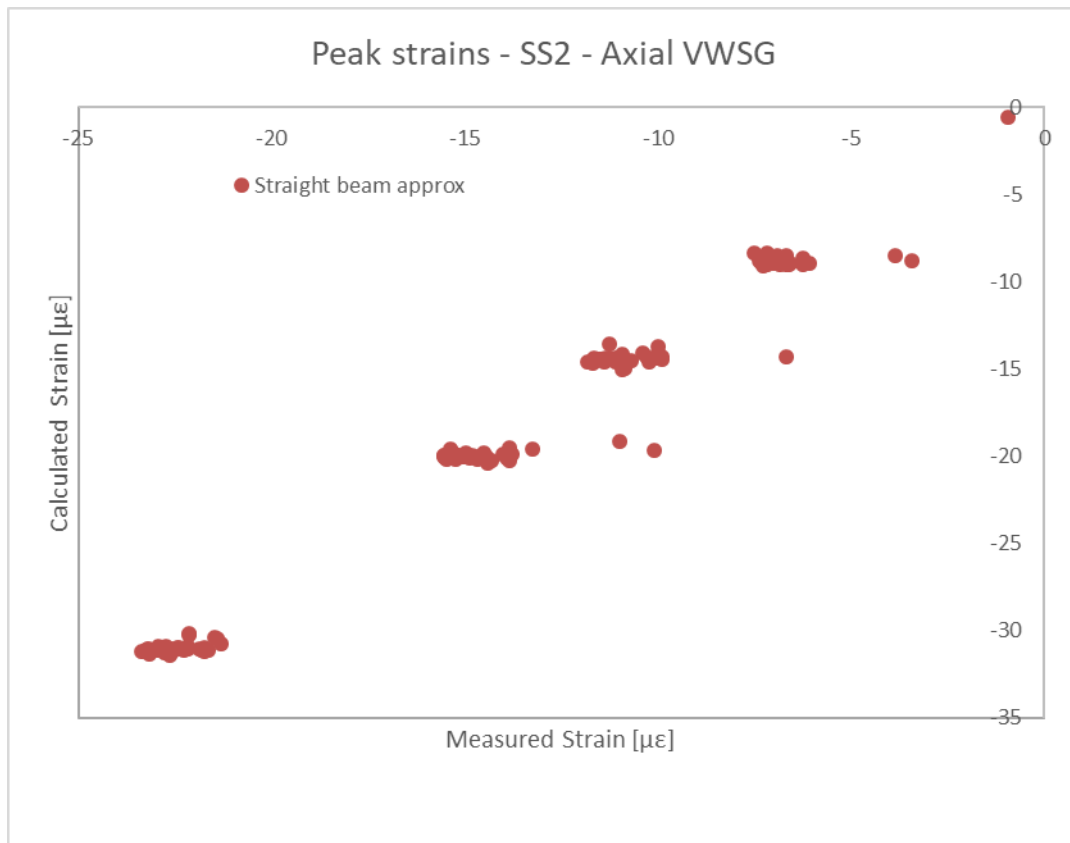




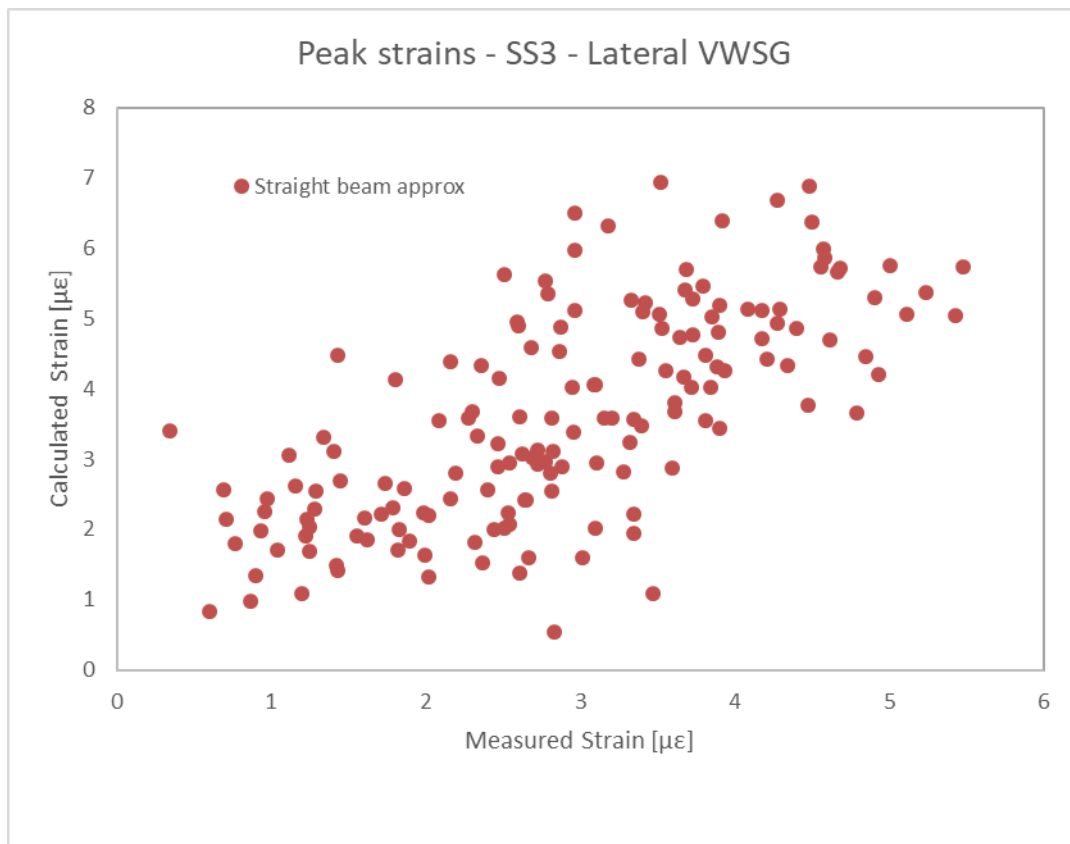
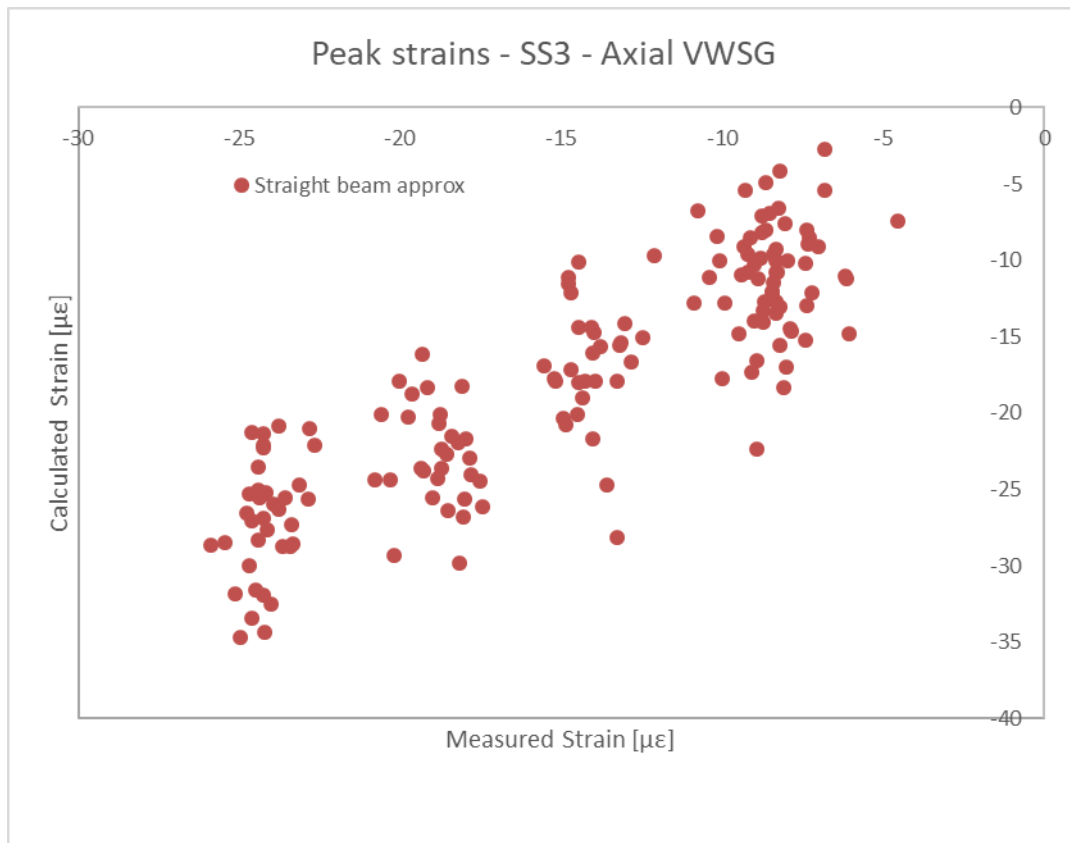


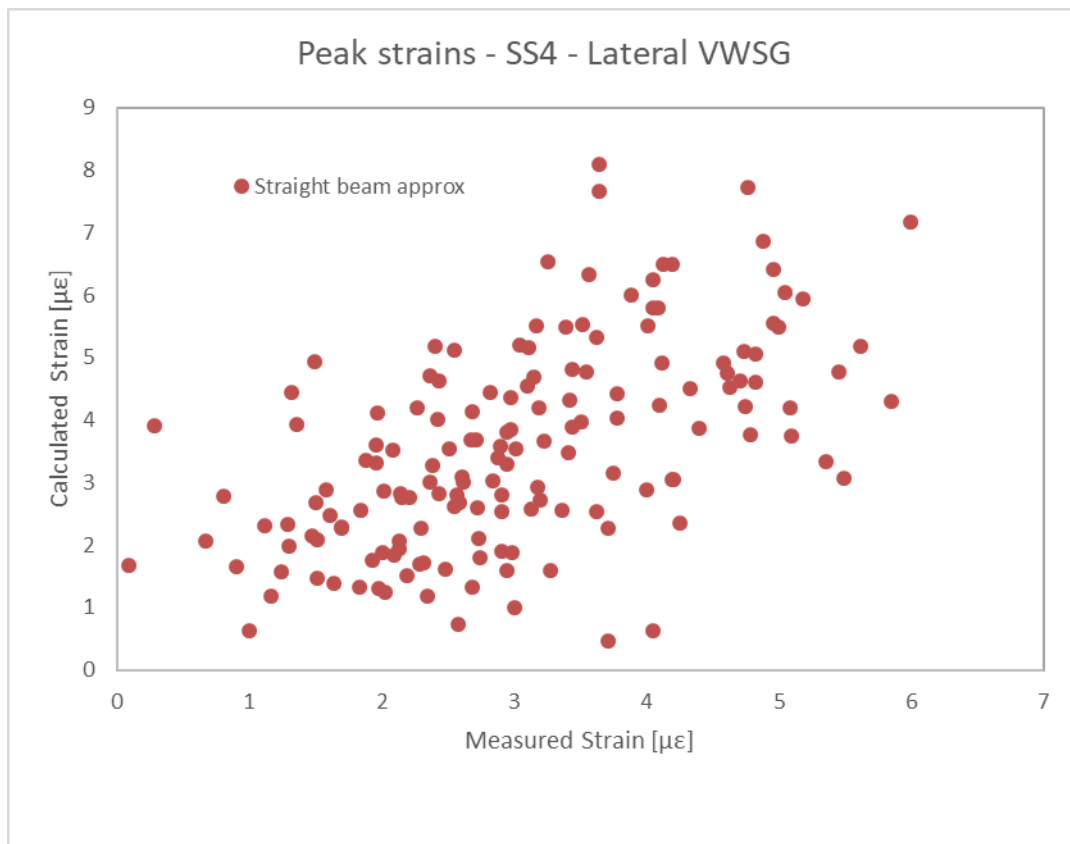
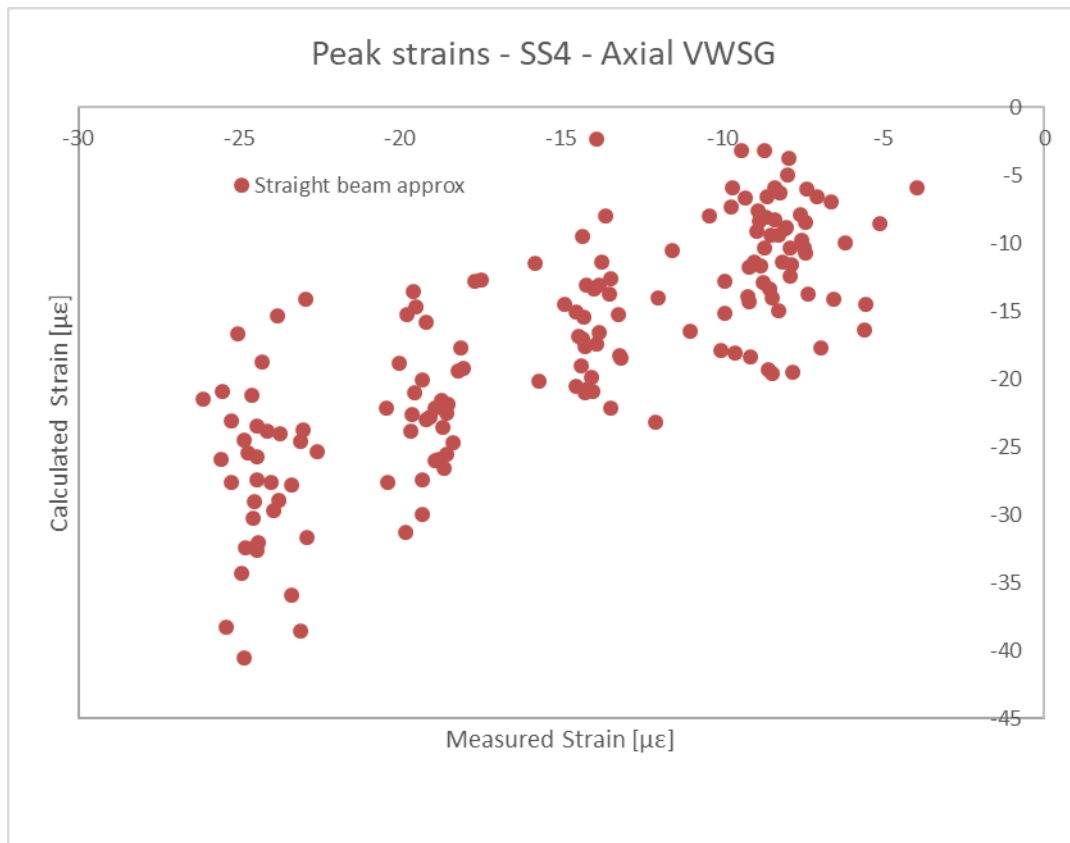
### A. 5 Smart segment Peak strains – Straight beam approximation

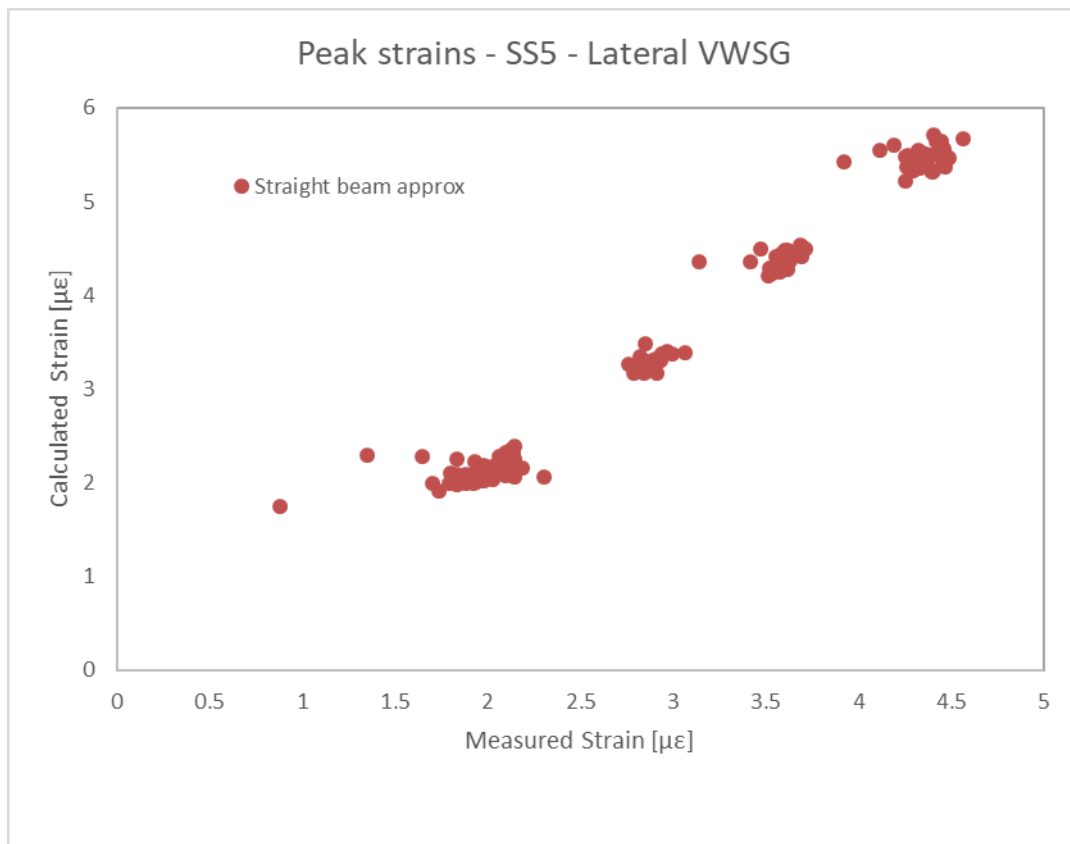
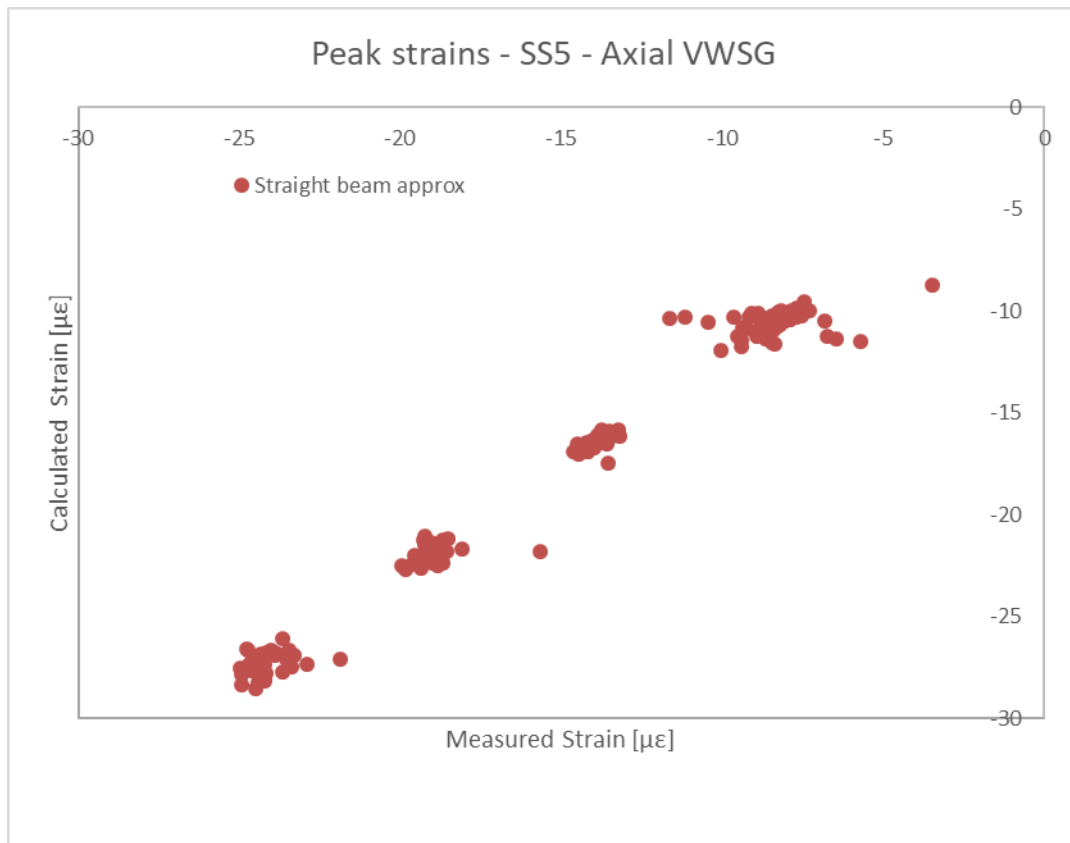


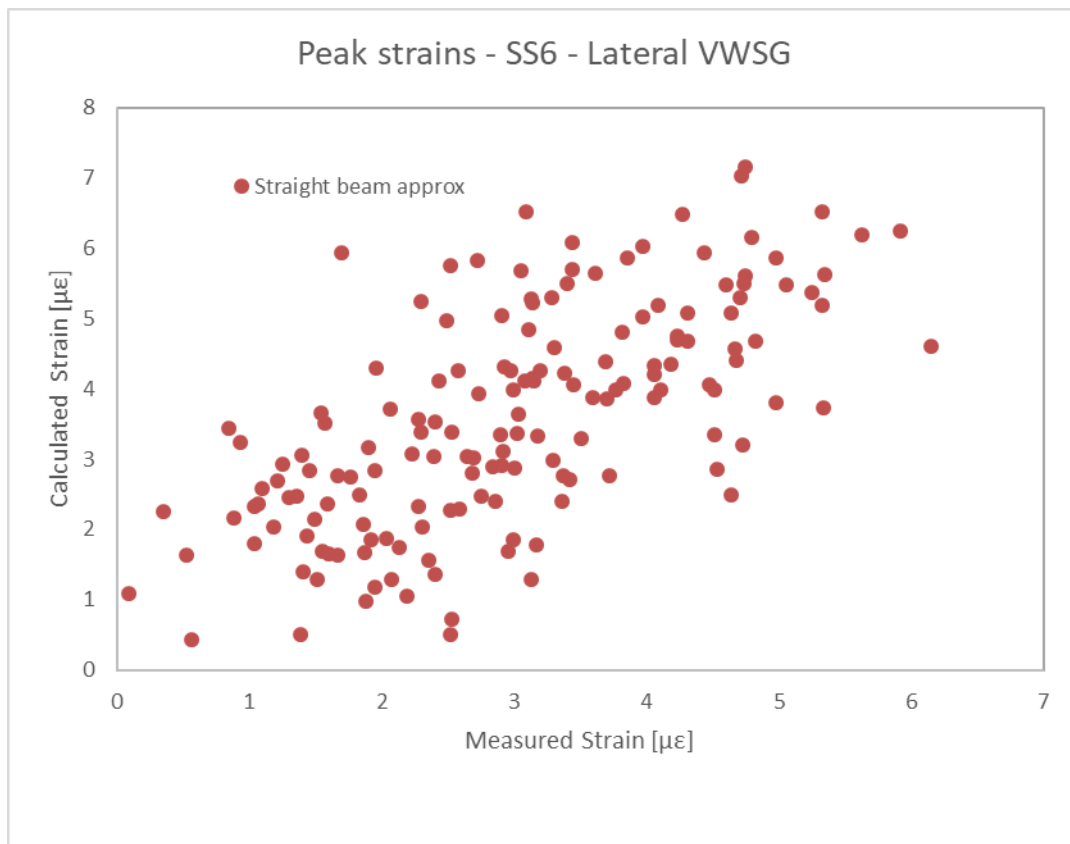
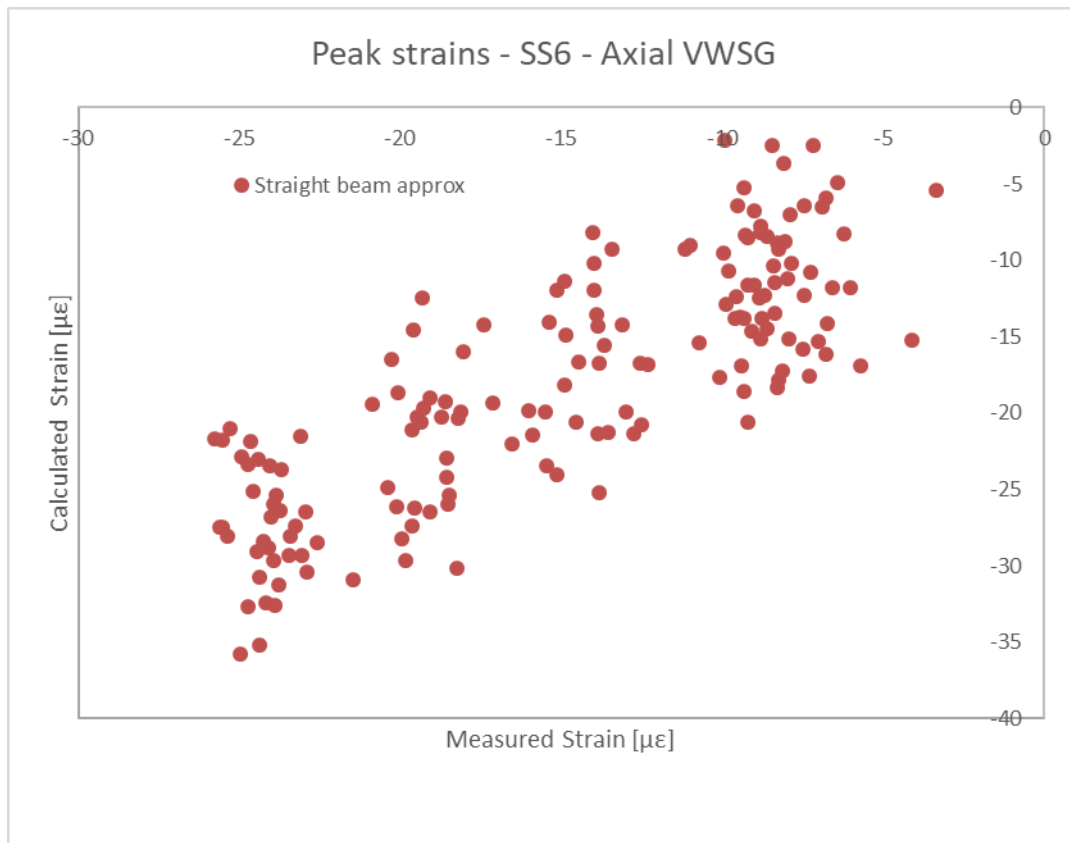


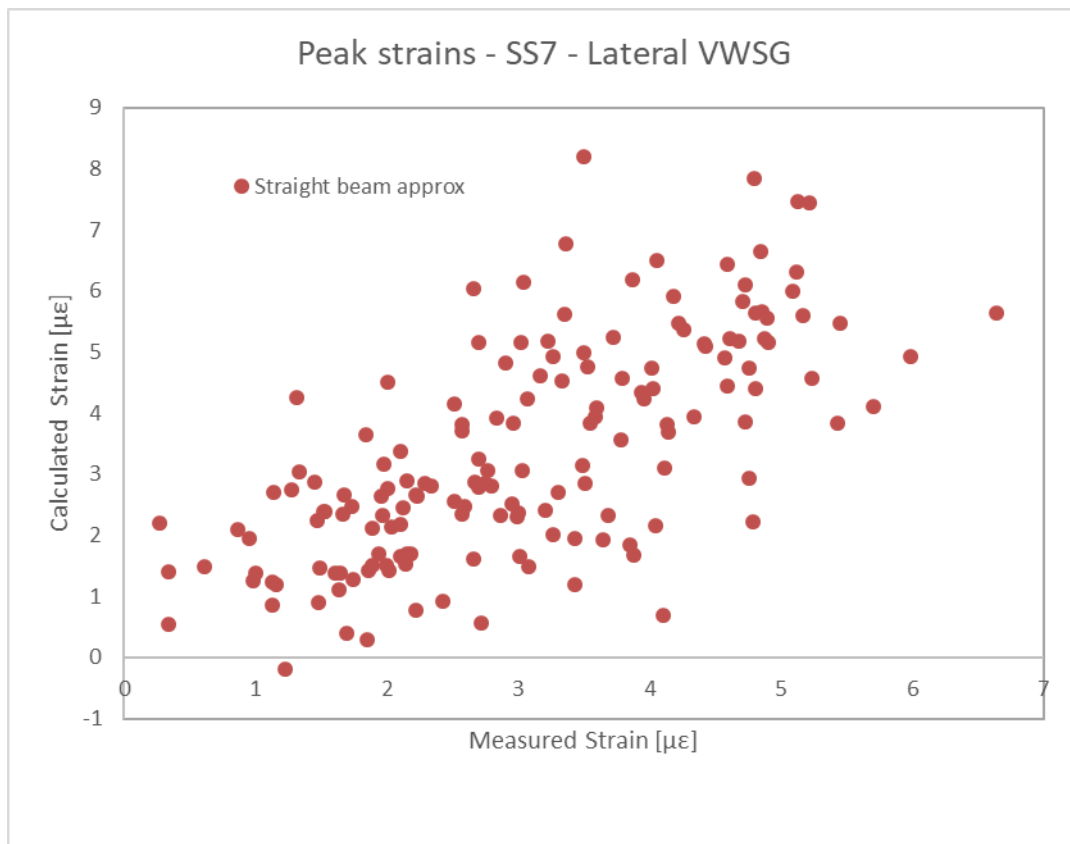
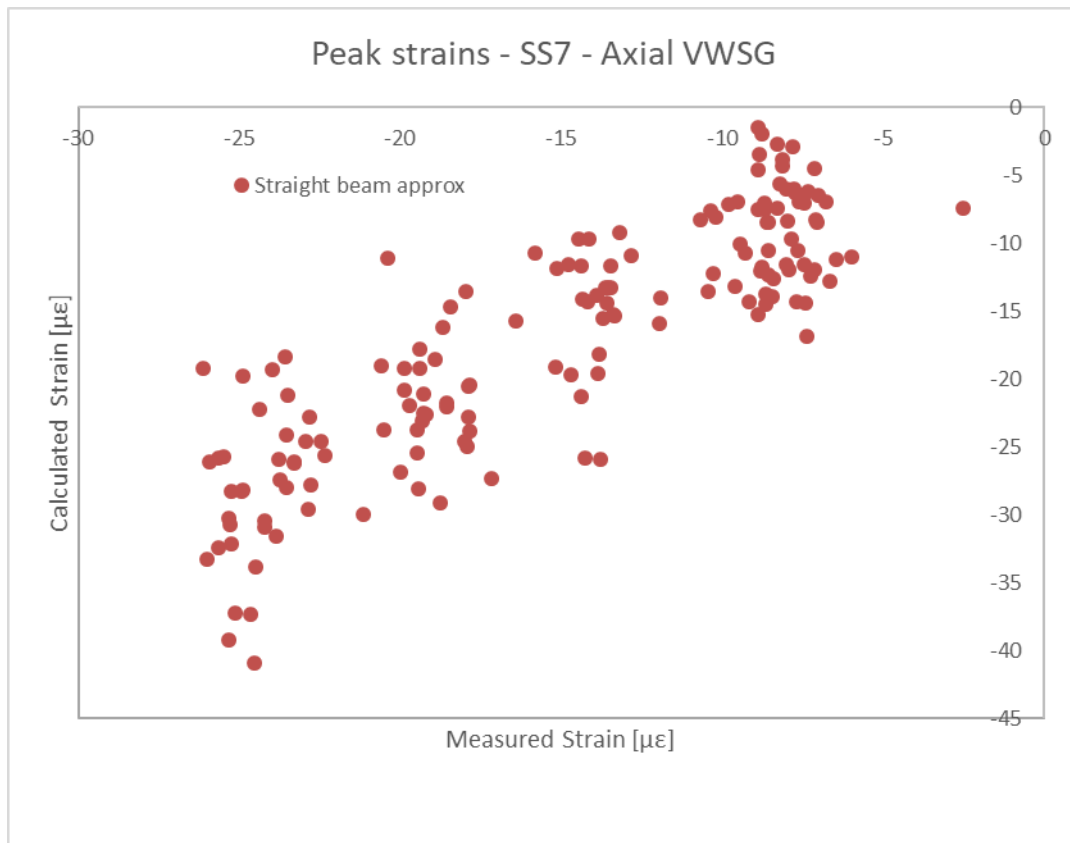


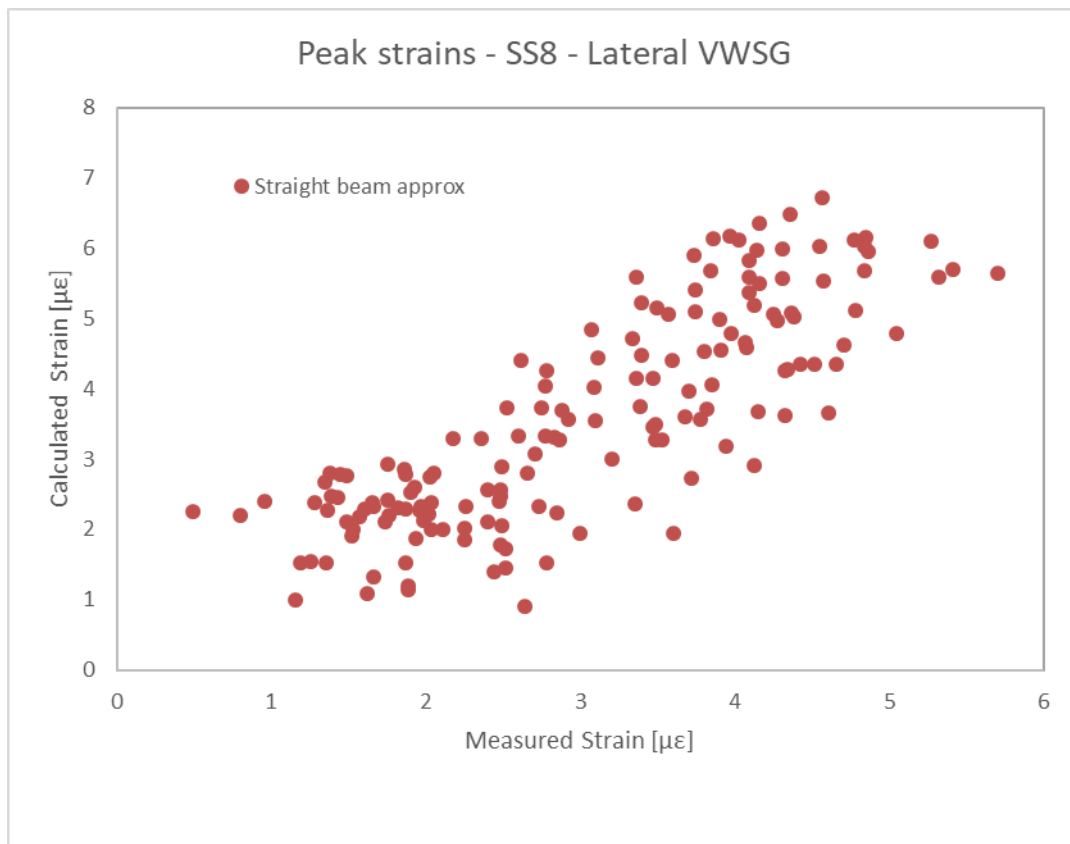
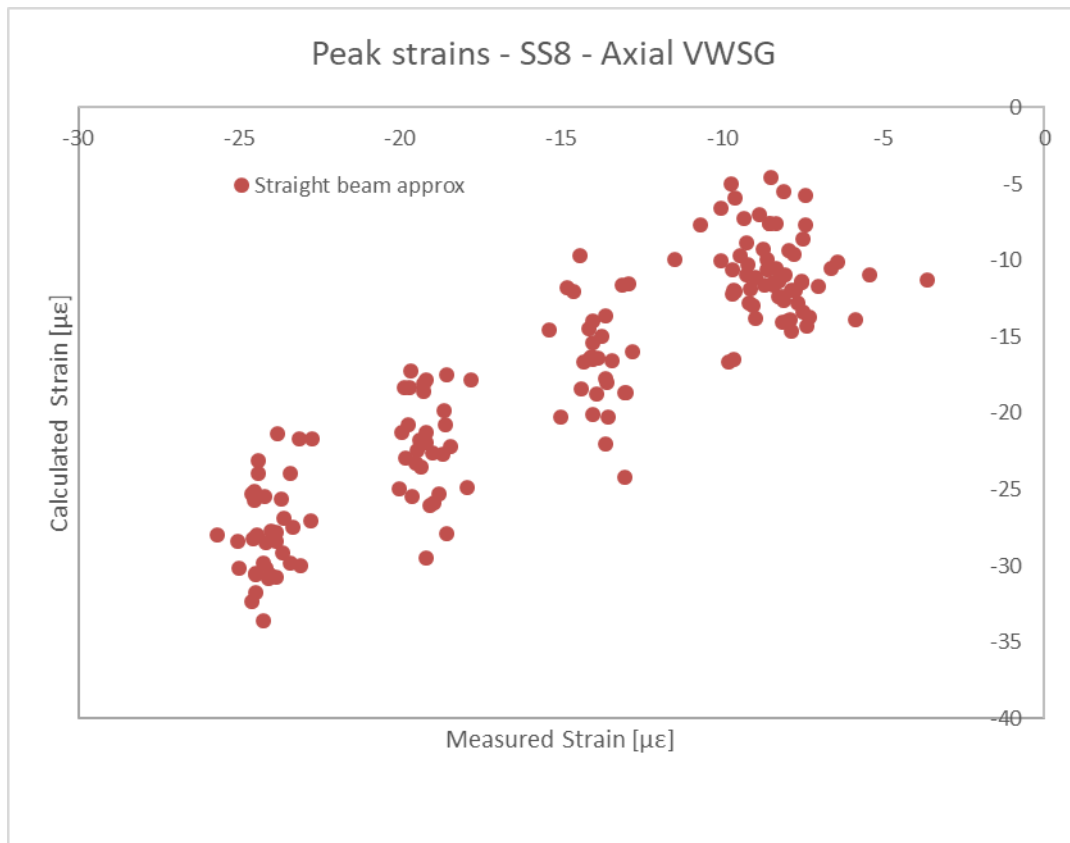


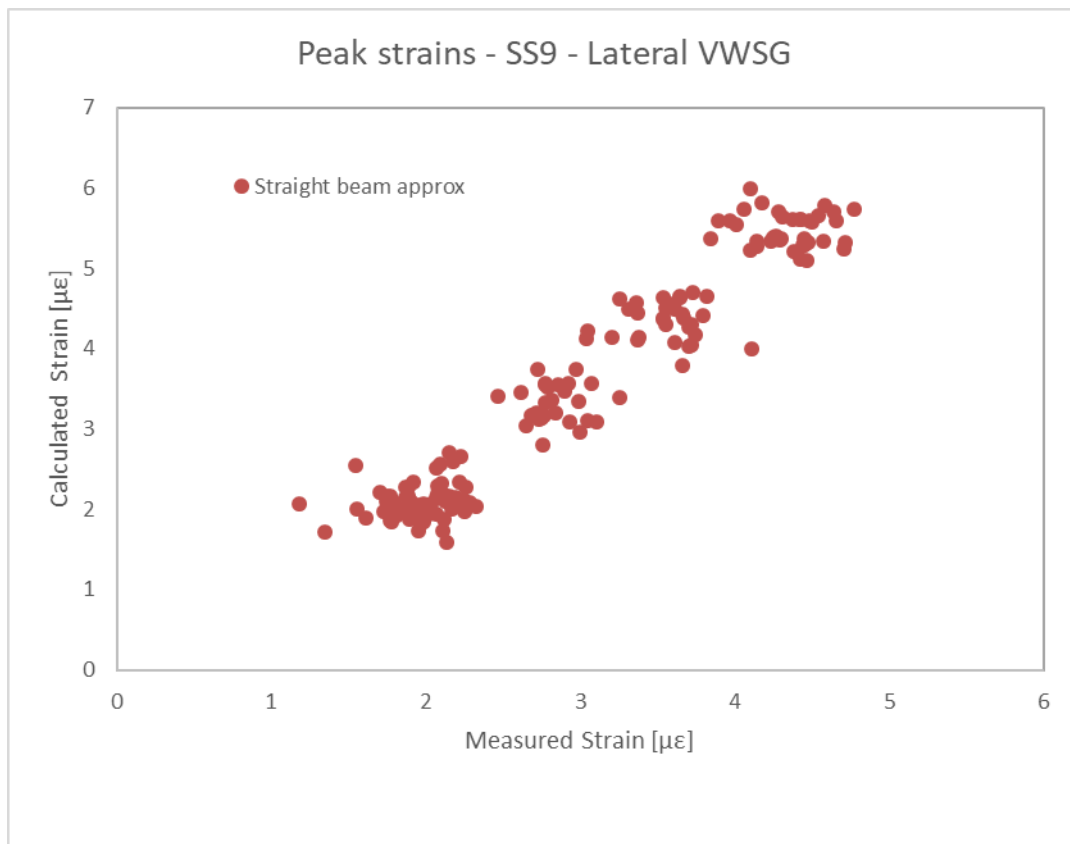
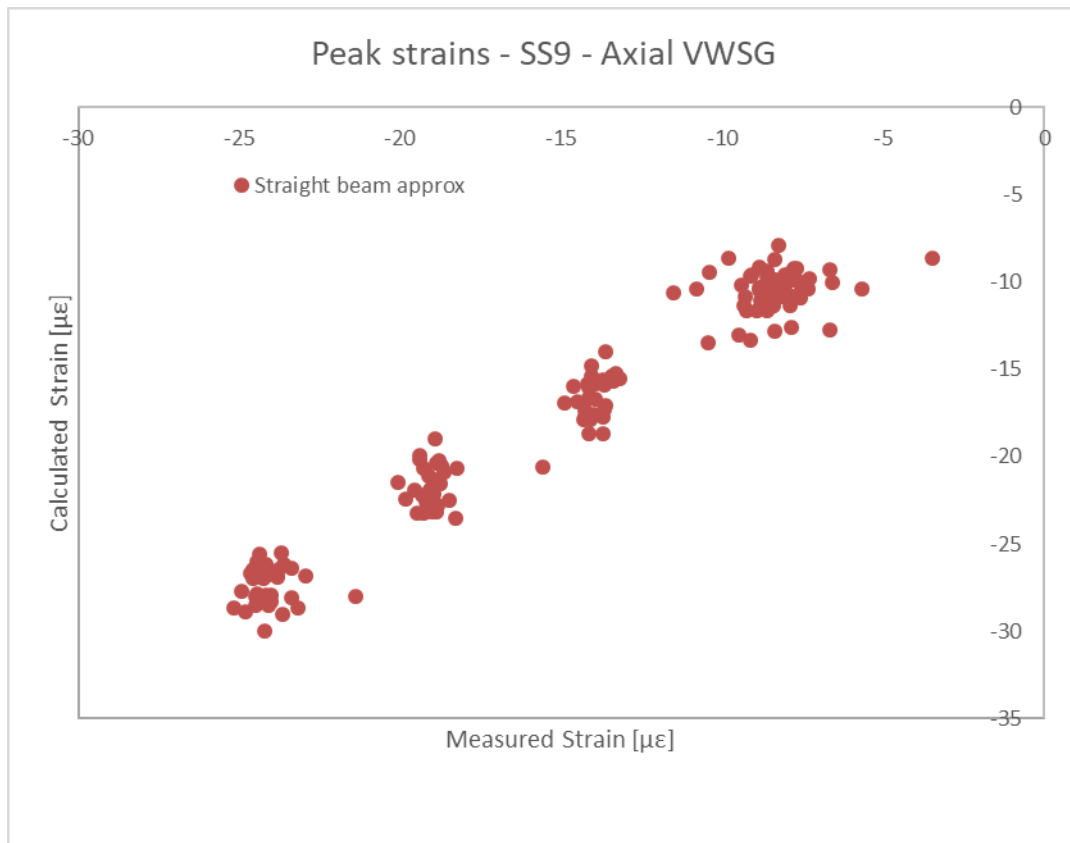


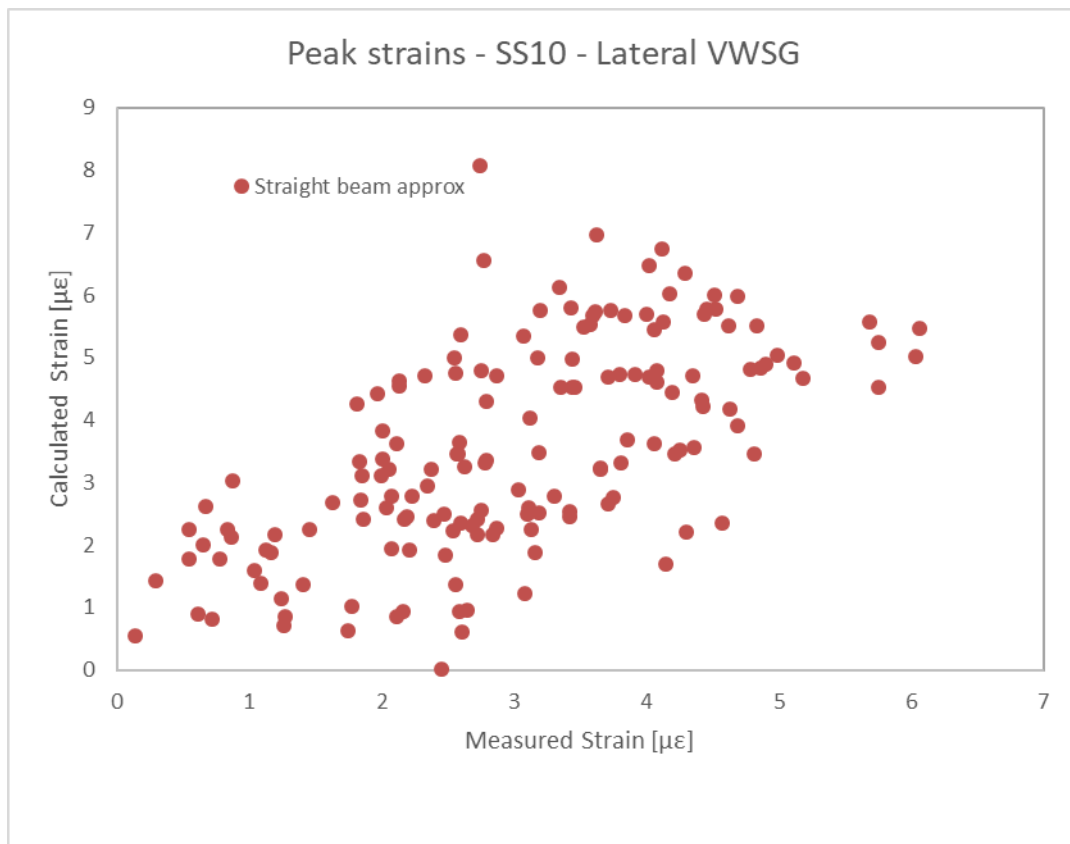
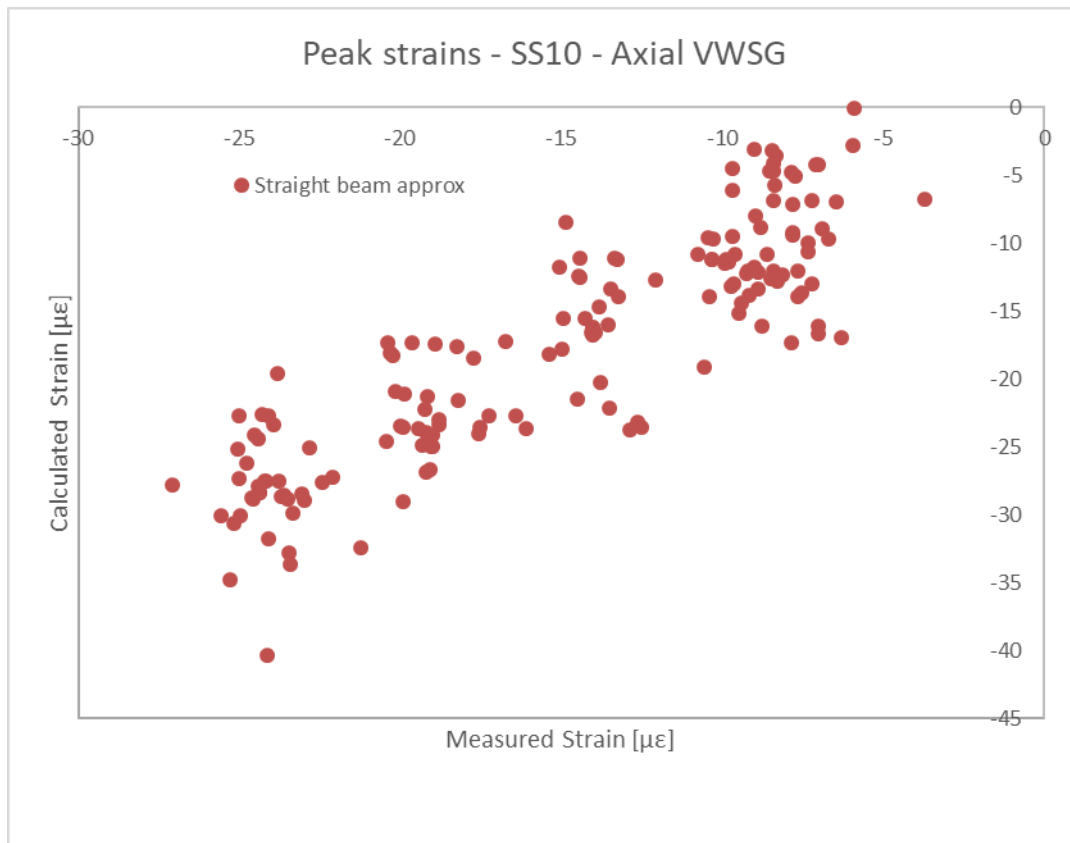














## A. 6 Tunnel Monitored Reviewed From COWI

In the following lines, three tunnel projects where monitoring systems were used are introduced. These tunnels primarily serve as water tunnels, handling sewage or raw water. In the first tunnel, the monitoring system was integrated throughout the construction process. Meanwhile, in the other two tunnels, the monitoring systems were strategically placed within sections of existing tunnels to assess the effects of excavating new tunnels above them. Details of the monitoring system densities can be found in Table A-1.

Table A -1. Monitoring density

Project name	Density of sensors
DTSS2 – T09	3 optical fibres running along 7.9km tunnel
LRWT	18 sensors over 65m
TWRMTS	32 sensors over 120 meters

This approximately represents a density of 0.3 sensors/meters for the last two tunnels.

### A. 6. 1. DTSS2 – T09

*Description (type, geometry, country, year)*

Built in Singapore in 2017, the DTSS2 – T09 is a 7900 m sewage tunnel. A typical ring section consists of two layers as shown in Figure A-1. A segmental layer with 5+1 type of section and a concrete protective layer made of SFRC with respective thicknesses of 300mm and 225mm.

For detailed structural analysis and detailing ten sections have been selected. The distance between consecutive sections varies between 190-2290m.

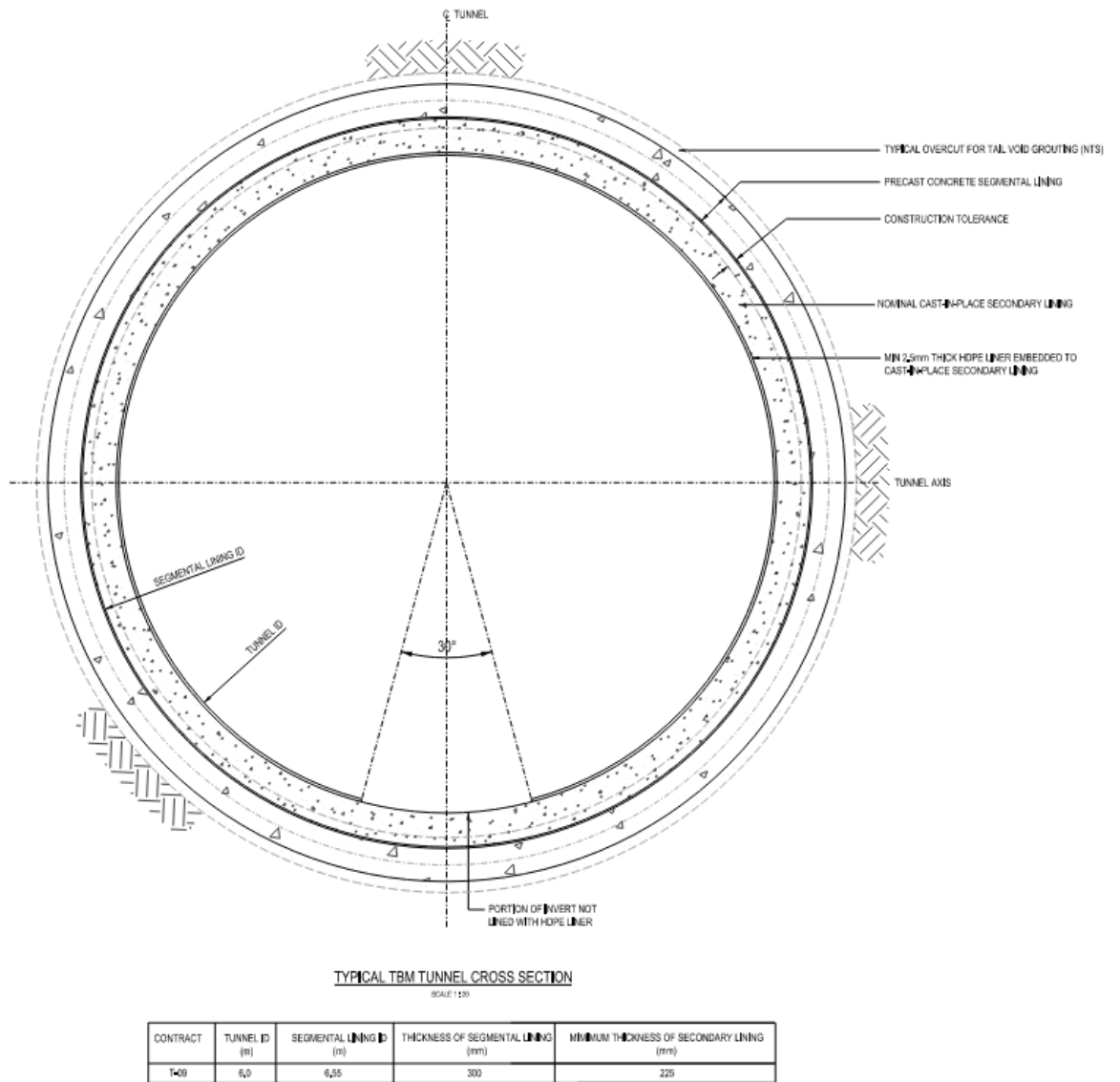


Figure A-1. Typical tunnel segment

*Monitoring system (type of monitoring and density)*

This system comprises three fibre optic cables (Figure 2) running along the tunnel's length. Its primary purpose is to offer insights into the overall bending and settlement of the tunnel. Additionally, there's potential for extrapolating further data from the fibre optic cables to evaluate strains.

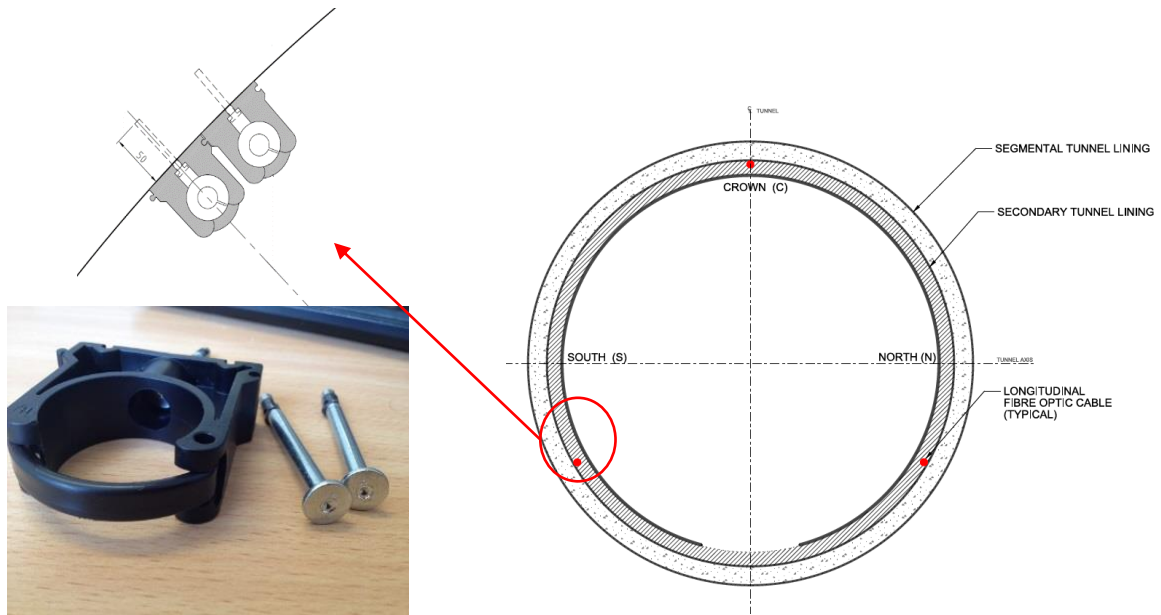


Figure A-2. FO monitoring system on the DTSS - T09

## A.6.2. LEE RAW WATER TUNNEL LRWT

*Description (type, geometry, country, year)*

The Lee Raw Water Tunnel, which was originally constructed in the 1960s, is of particular interest in this report. Specifically, a 60-meter section of the tunnel, located approximately 3.4 meters below the new Thames Tideway Tunnel and at an approximate angle of 65 degrees was examined. In November 2013, this particular section of the LRWT tunnel was strengthened and made waterproof with a 220mm layer of reinforced concrete lining. It's worth noting that the LRWT tunnel was originally designed in a "Don-Seg" segmental format, consisting of 12 trapezoidal segments of equal size.

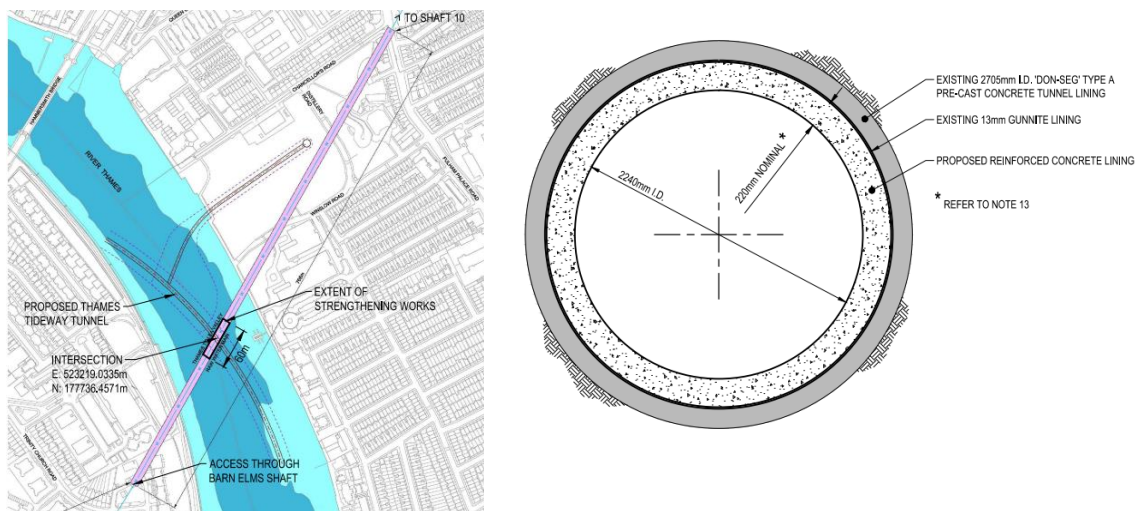


Figure A-3. LRWT tunnel

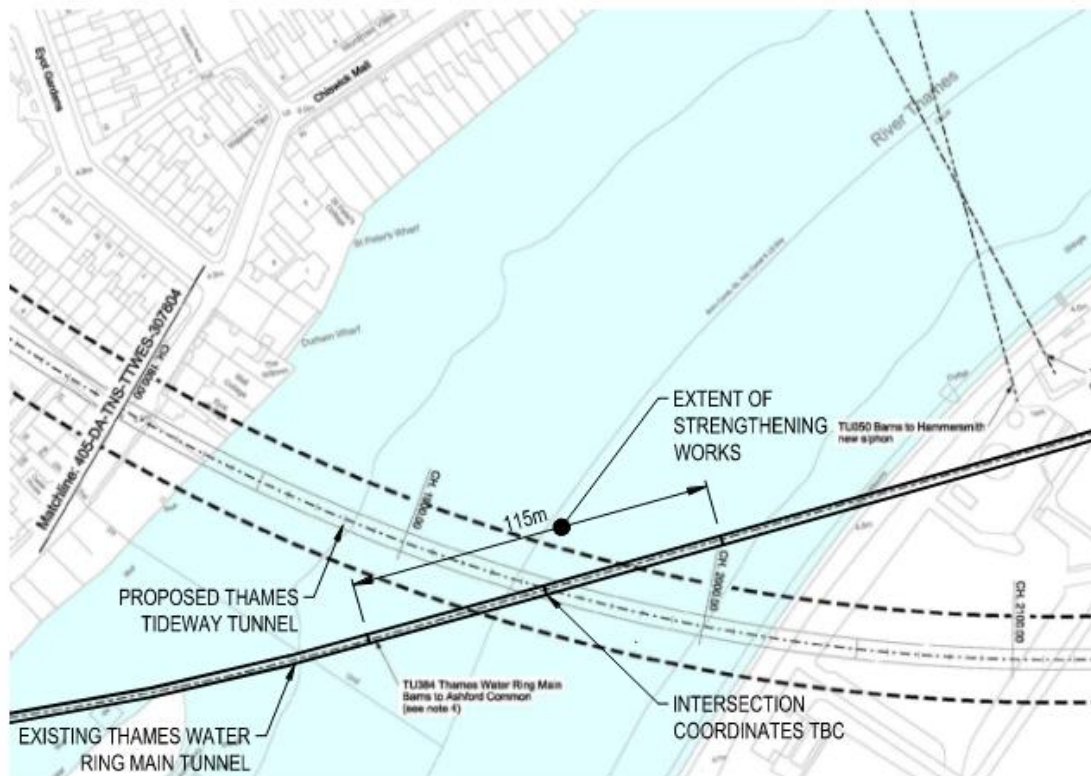
*Monitoring system (type of monitoring and density)*

During the reinforcement of the studied section of the LRWT a structural monitoring system consisting of a series of 14 embedded vibrating wire strain gauges in the new lining (6 longitudinal and 8 circumferential) and 4 circumferential surfaces mounted VWSG on the existing lining.

### **A. 6. 3 THAMES WATER RING MAIN TUNNEL STRENGTHNING (TWRMTS)**

*Description (type, geometry, country, year)*

The Thames water ring main tunnel was built in the 1960s. The part concerned in this report is a 115m long section 3.3 m under the new Thames Tideway Tunnel at an angle of approximately 32 degrees. This section of the LRWT tunnel has been strengthened and waterproofed with 250mm of reinforced concrete lining in November 2013. The existing TWRMTS is "Wedge-lock" segmental tunnel (12 trapezoidal segments of equal size).



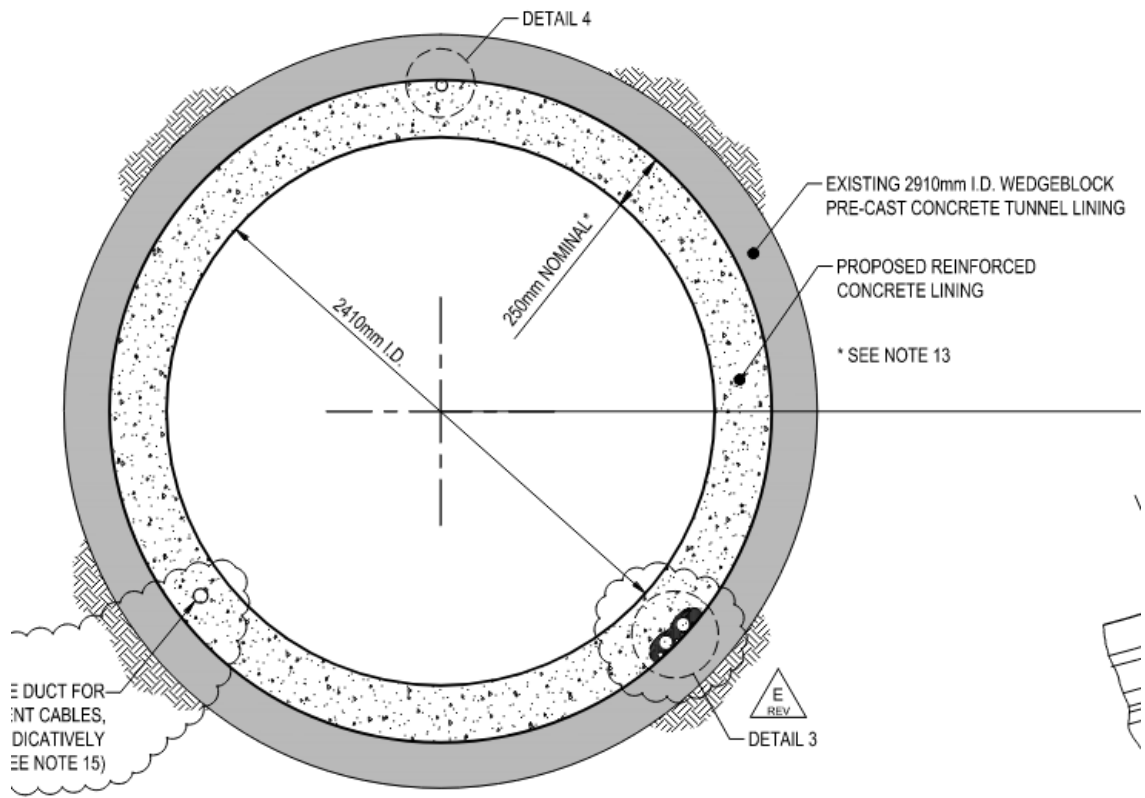
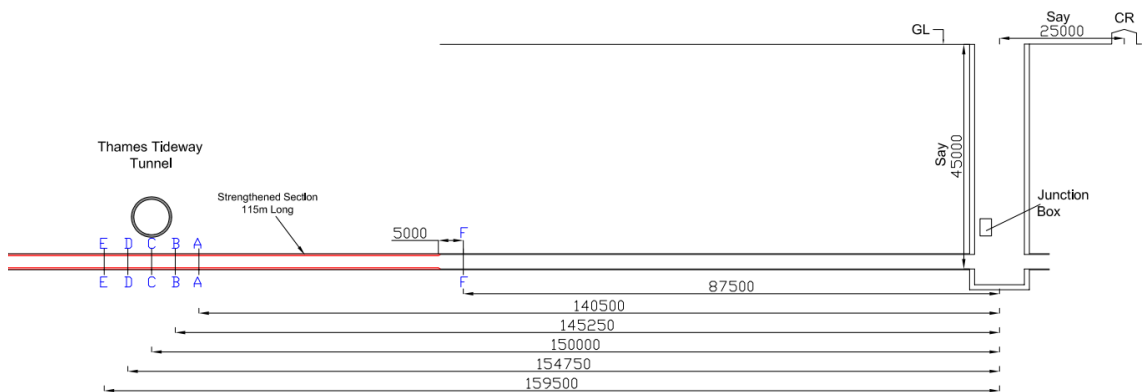


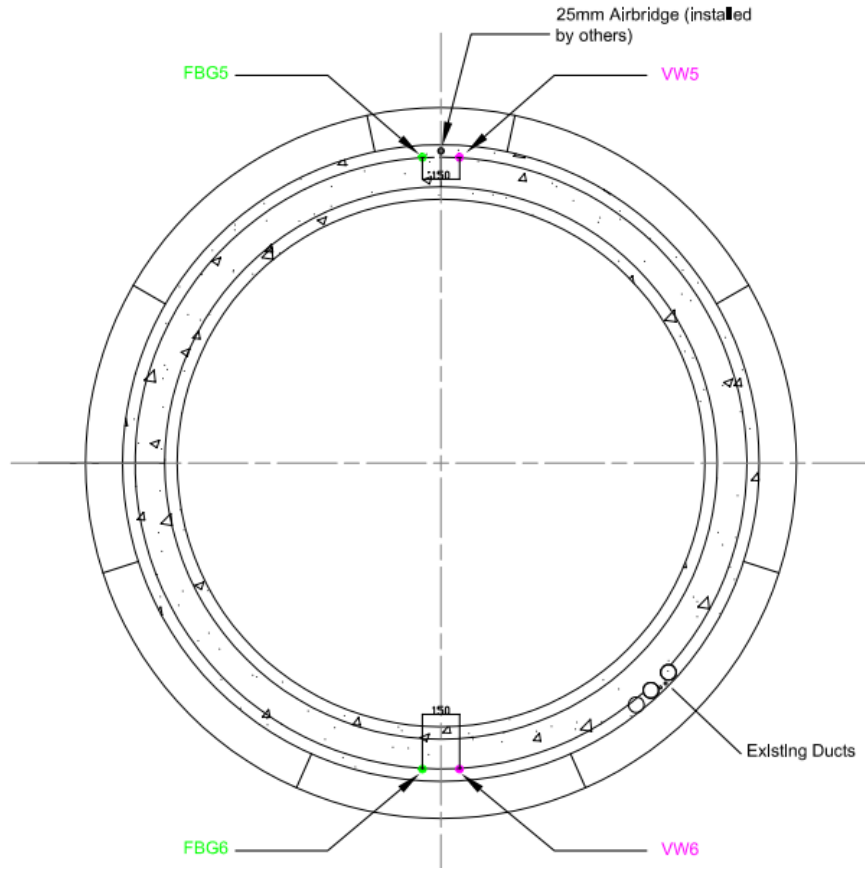
Figure A-4. TWRTTS tunnel

*Monitoring system (type of monitoring and density)*

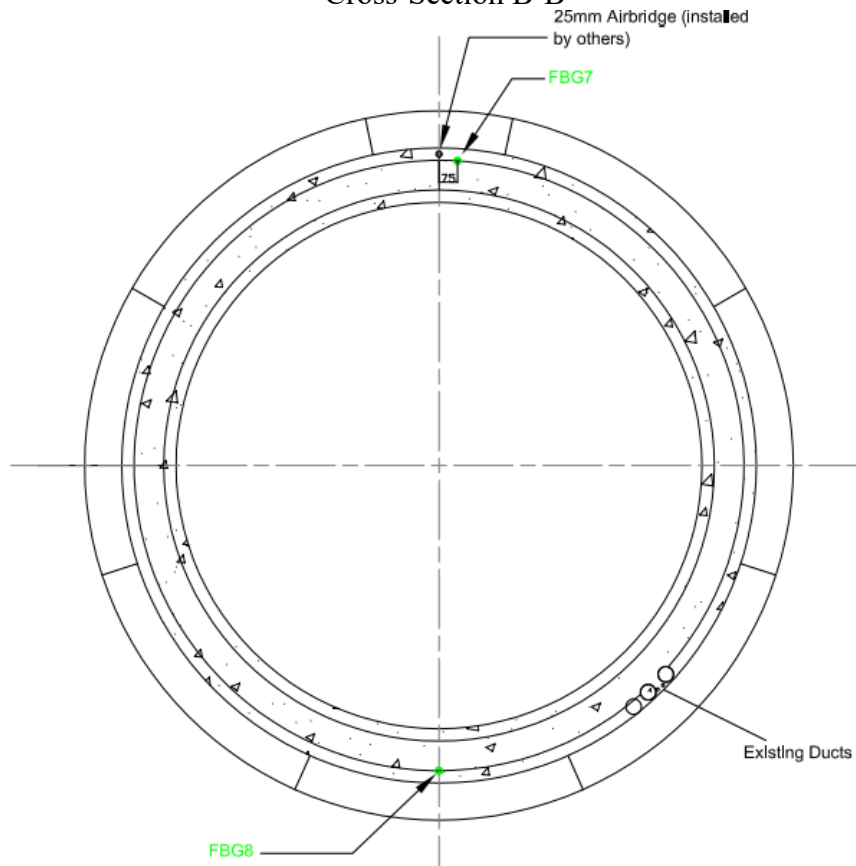
During the reinforcement of the studied section of the TWRTS a structural monitoring system consisting of a series of 14 embedded vibrating wire strain gauges in the new lining (6 longitudinal and 8 circumferential) and 4 circumferential surfaces mounted VWSG on the existing lining. At the same time, 14 FBGs sensors were installed. 10 of those are embedded into the new lining and 4 surface mounted on the existing lining.



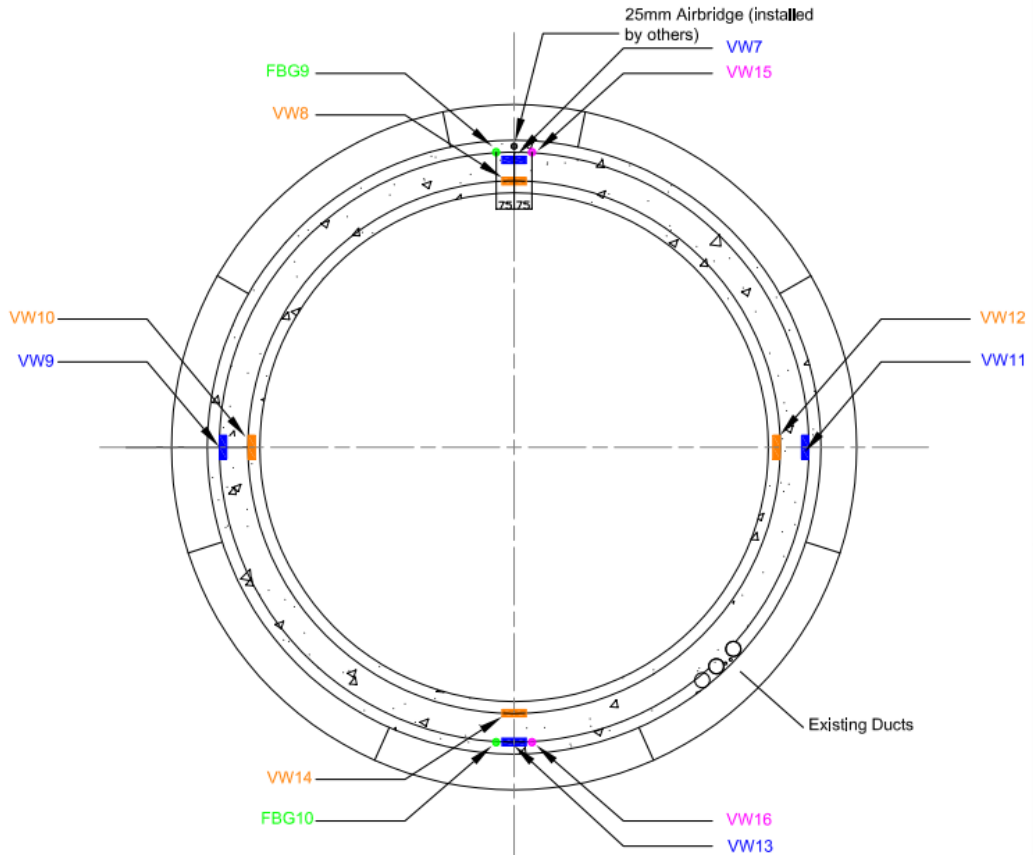
### Cross section A-A



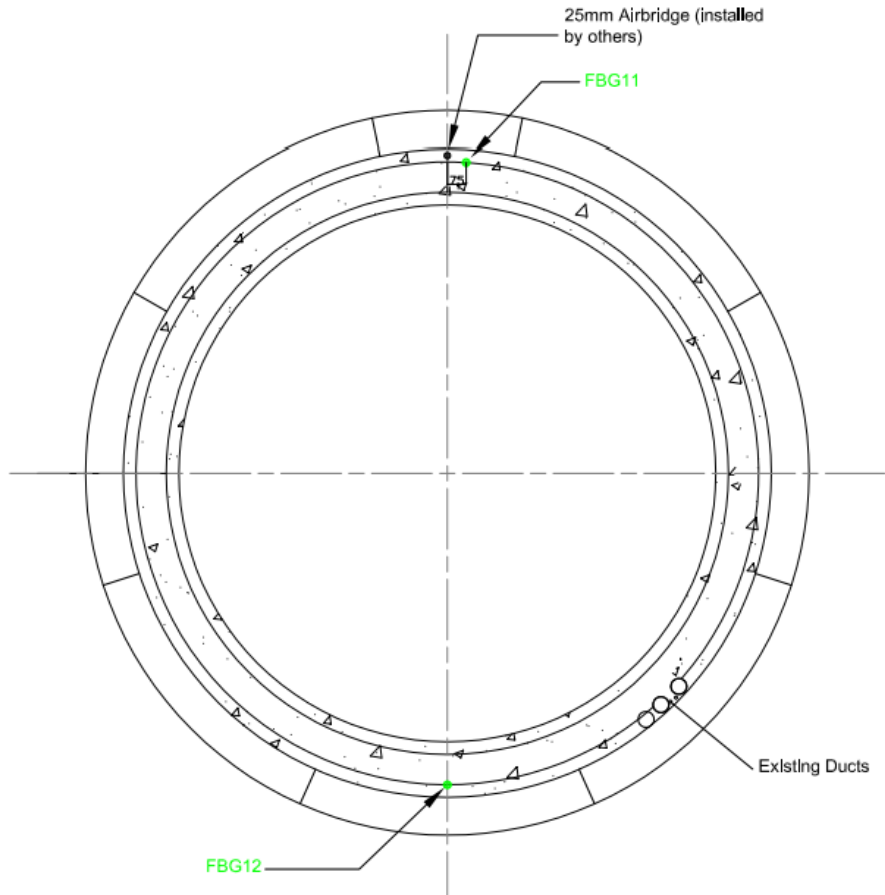
### Cross-Section B-B



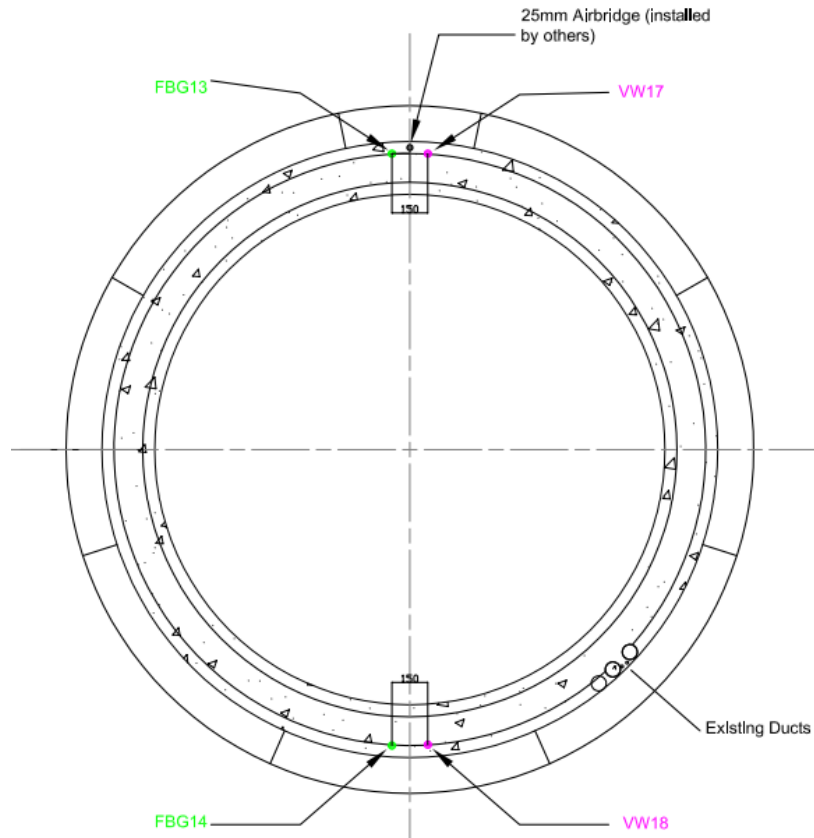
### Cross section C-C



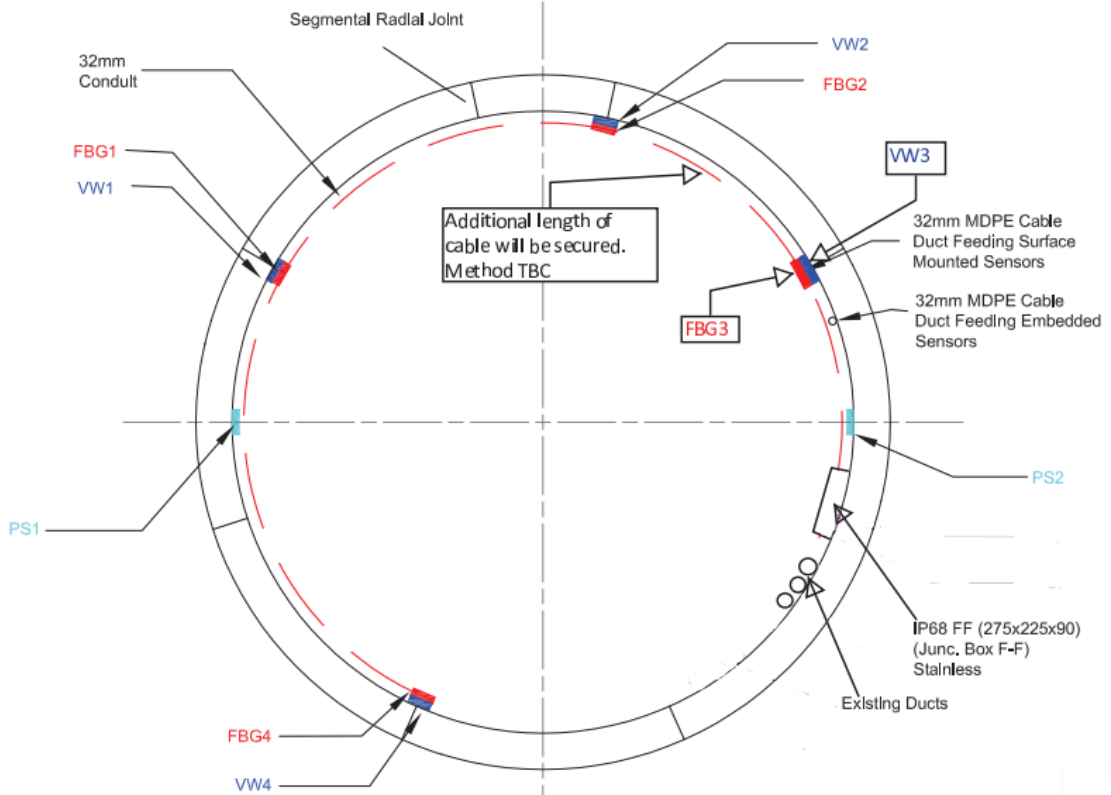
### Cross section D-D



### Cross-Section E-E



### Cross section F-F



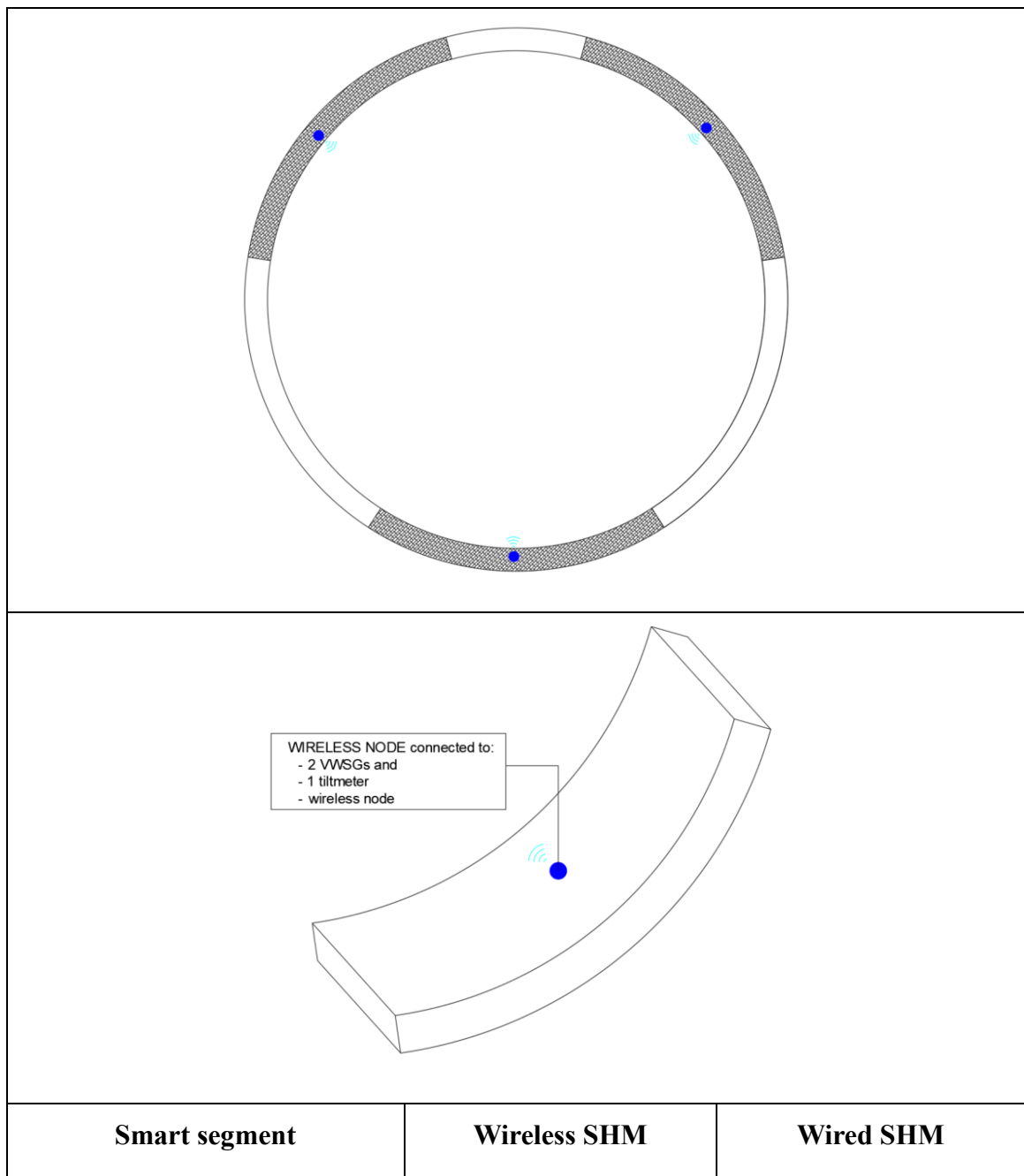



## A. 7 Instrumentation Cost


### A7.1. Sensors

In the current configuration, the tunnel ring is equipped with three smart segment and three consecutive smart rings form a monitoring ring. This configuration is meant to provide enough redundancy to measure different monitoring parameters across the smart segments, rings and the whole tunnel.

Table A-2. Detailing of the composition and cost a smart tunnel ring



<b>Strain sensors</b>		
<p>Embedded Geokon</p>  <p>Unit Cost: £140.</p>	<p>Surface mounted Geokon</p>  <p>Unit Cost: £140.</p>	<p>Surface mounted Geokon</p>  <p>Unit Cost: £140.</p>
<b>Tilt sensor</b>		
 <p>Unit Cost: £600</p>	 <p>Unit Cost: £600</p>	 <p>Unit Cost: £600.</p>
<b>Wireless node</b>		
 <p>The lab-made wireless node is made of:</p> <ul style="list-style-type: none"> <li>- 1 arduino Nano board</li> <li>- 1 VWSG addressable interface board</li> <li>- 2 RS-485 board</li> </ul>		

- 2x3.7V Lithium battery - 1 metallic enclosure Cost: £300-400		
<b>Wireless Gateway</b>		
A standard WSN gateway can be reasonably estimated at £400.  1 gateway per monitoring sections would be enough	A standard WSN gateway can be reasonably estimated at £400	NA
<b>Data Acquisition module</b>		
		 <p>Unit Cost: £5,000</p> <p>Each unit can read up to 16 VWSG sensors.</p>

### A. 7.2. Cost of instrumentation and installation

The total number of sensors and other elements essential to the SHM system and the corresponding cost of the hardware are presented in the Table A-3 and Table A-4. This cost is for the configuration of 10 monitoring containing 1 smart tunnel ring each. The values for 2 or 3 smart rings are proportionate to this configuration.

Table A-3. Detailed composition of the hardware of a tunnel ring

Hardware	Quantity of elements per smart ring		
	Smart segment	Wireless	Wired
Embedded VWSG	120 u	0 u	0 u
Surface-mounted VWSG	0 u	120 u	120 u
Tiltmeter	30 u	30 u	30 u
Wireless node	30 u	30 u	0 u
WSN Gateway	10 u	10 u	0 u
Cables -wired SHM	0 m	0 m	1090 m
Cables	30 m	30 m	30 m
Data acquisition mod.	0 u	0 u	9 u

Table A-4. Cost of hardware per tunnel ring

Hardware	Cost of hardware per smart ring (£)		
	Smart segment	Wireless	Wired
Total cost Hardware (£)	50,890	50,890	83,160

The installation cost of the monitoring systems, presented in Table A-5, can be estimated as being 30% of the total hardware cost for both the wired solution and the on-site wireless solution. For the smart segment, the fitout cost will be assumed zero as the sensors have been already embedded in the factory.

Table A-5. Fitout cost of monitoring system

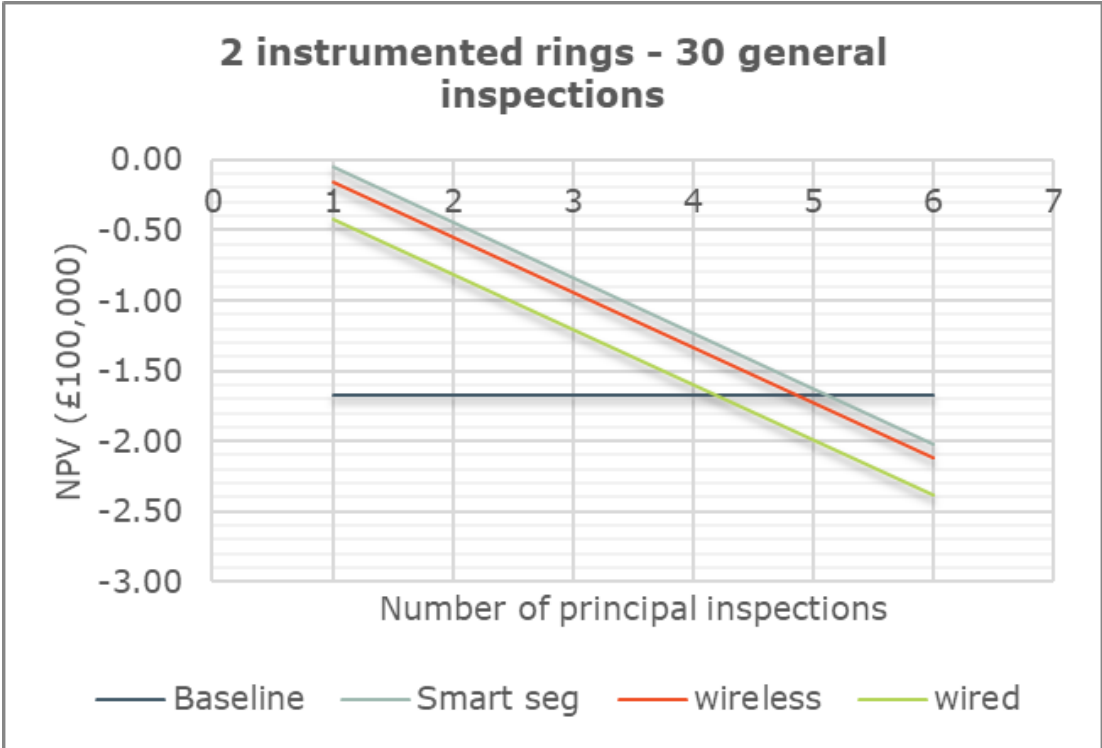
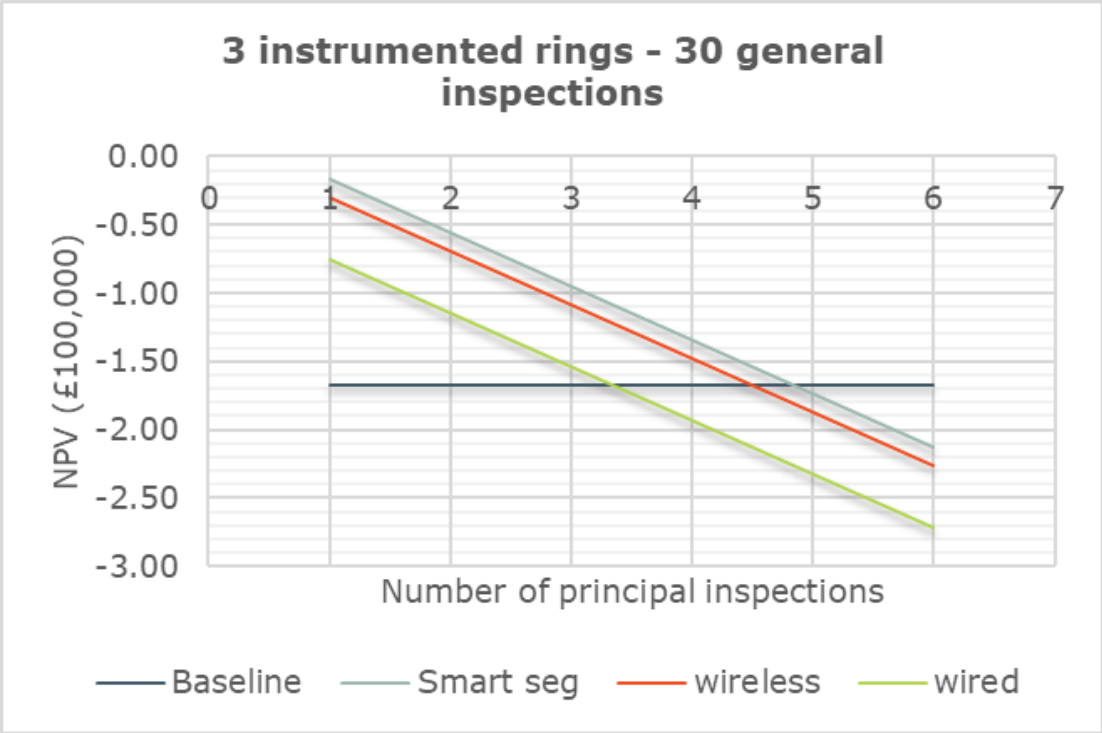
	Smart segment		Wireless		Wired
Fitout Cost					
SHM Fitout cost 3 rings	0% x £50,890 <b>£0.00</b>	=	30% x 50,890 <b>£15,267</b>	=	30% x £88,070 = <b>£26,421</b>
SHM Fitout cost 2 rings	0% x £35,290 <b>£0.00</b>	=	30% x £35,290 <b>£10,587</b>	=	30% x £35,290 = <b>£18,768</b>
SHM Fitout cost 1 ring	0% x £19,690 <b>£0.00</b>	=	30% x £19,690 <b>£5,907</b>	=	30% x £19,690 = <b>£12,588</b>

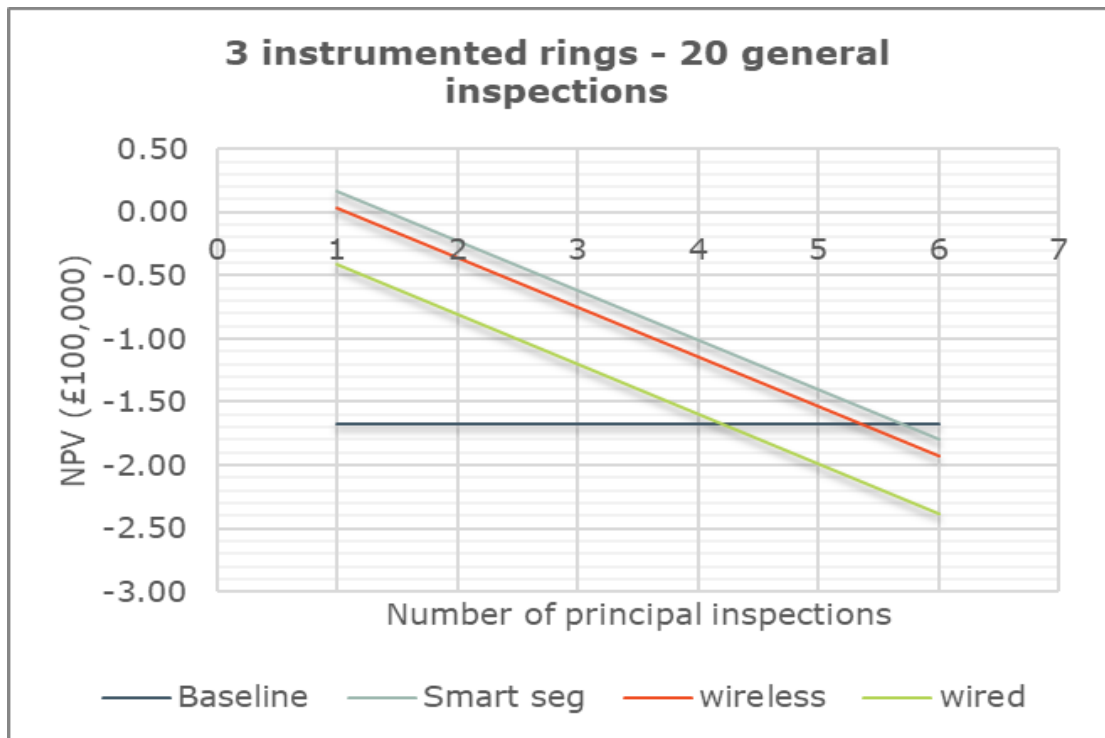
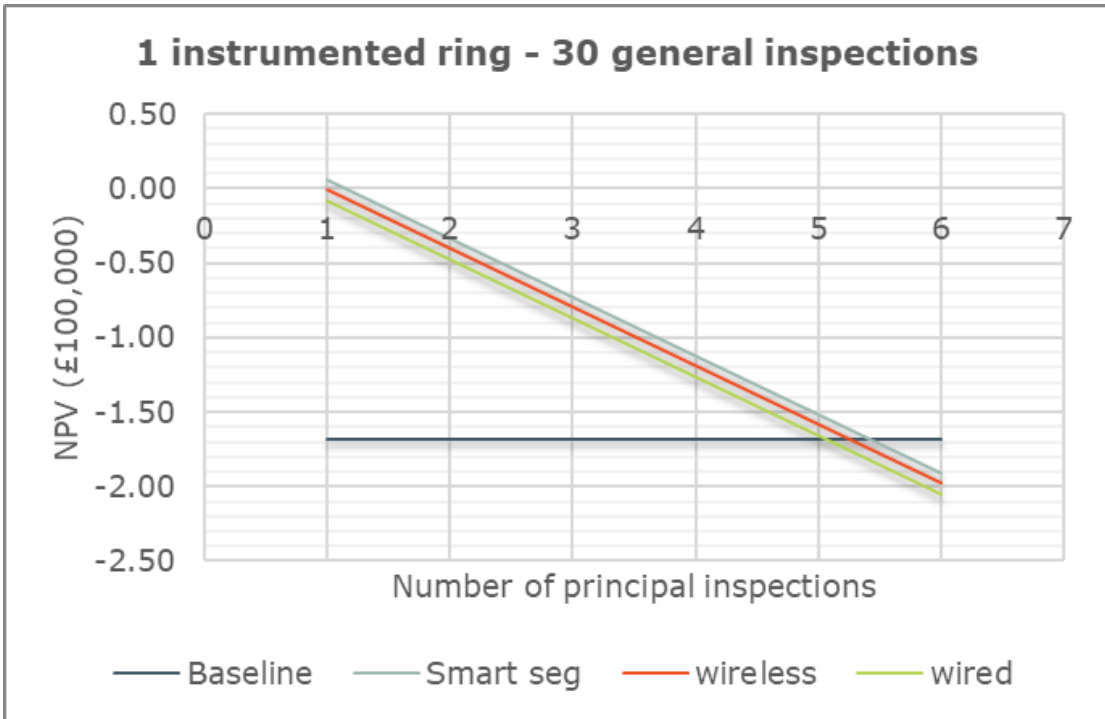
## **A. 8 NPV Detailed Results**

Table A-6 contains results of NPV expressed as x £100,000. The coloured cells are negative NPV. The plots in the next pages provide an visualisation of the information contained in the table.

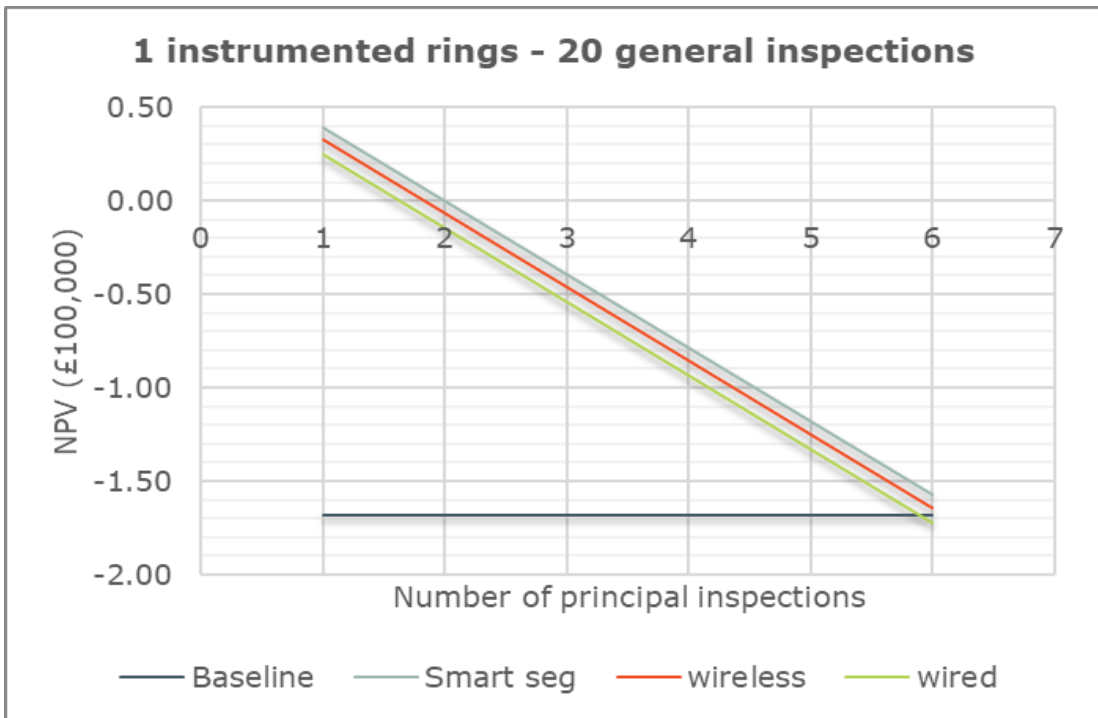
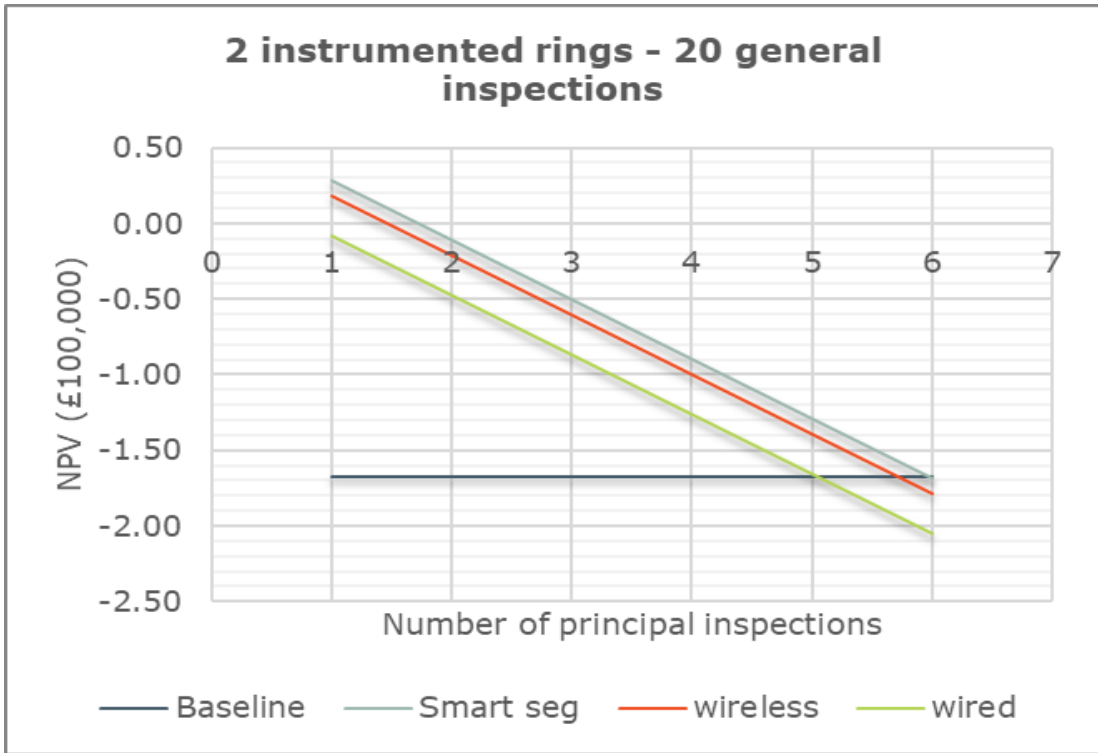
Table A-6. Results of NPV for differred scenarios and configuration

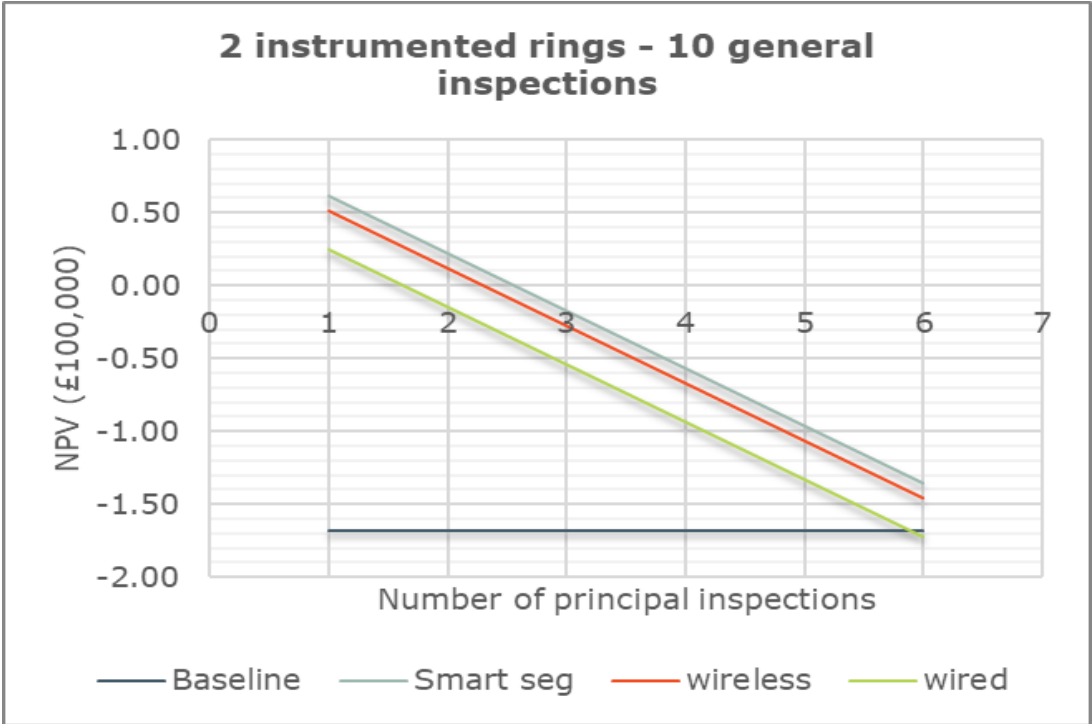
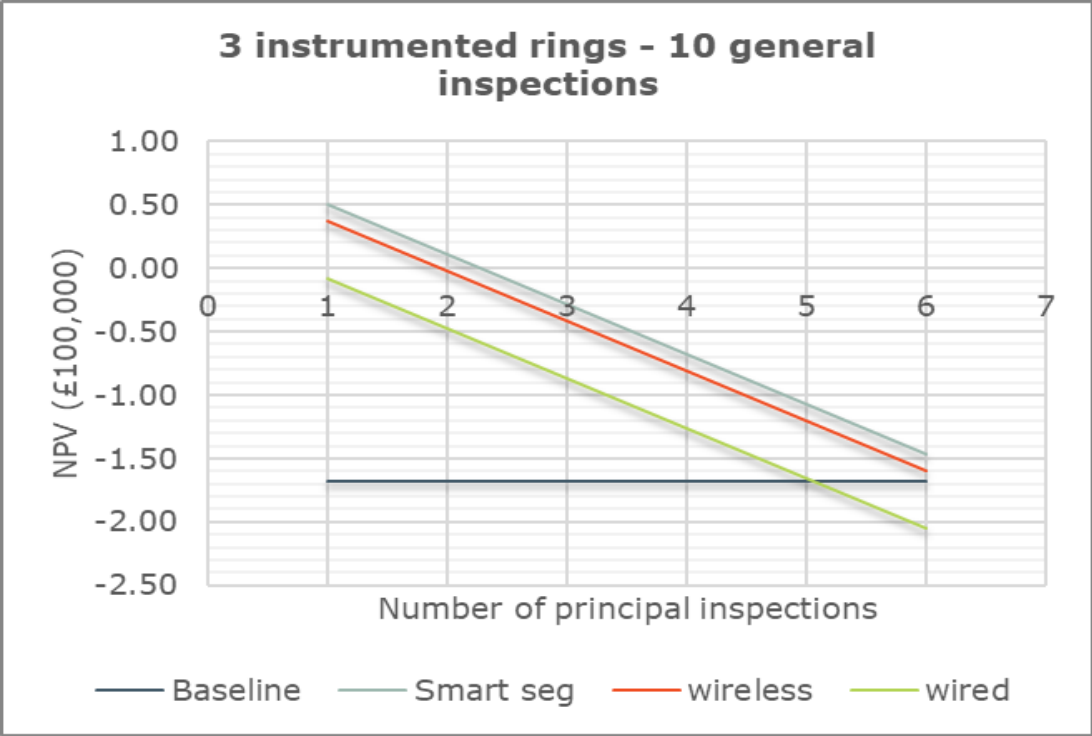
3 INSTRUMENTED RINGS/SECTION					2 INSTRUMENTED RINGS/SECTION					1 INSTRUMENTED RING/SECTION				
30 Gen_insp														
Nr princip inspection	Baseline	Smart seg	wireless	wired	Nr princip inspection	Baseline	Smart seg	wireless	wired	Nr princip inspection	Baseline	Smart seg	wireless	wired
6	-1.679	-2.13	-2.265	-2.718	6	-1.679	-2.019	-2.12	-2.385	6	-1.679	-1.907	-1.975	-2.053
5	-1.286	-1.737	-1.872	-2.324	5	-1.286	-1.625	-1.727	-1.992	5	-1.286	-1.514	-1.582	-1.659
4	-0.892	-1.343	-1.478	-1.931	4	-0.892	-1.232	-1.333	-1.598	4	-0.892	-1.12	-1.188	-1.266
3	-0.499	-0.95	-1.085	-1.537	3	-0.499	-0.838	-0.94	-1.205	3	-0.499	-0.727	-0.795	-0.872
2	-0.105	-0.556	-0.691	-1.144	2	-0.105	-0.445	-0.546	-0.811	2	-0.105	-0.333	-0.401	-0.479
1	0.288	-0.163	-0.298	-0.75	1	0.288	-0.051	-0.153	-0.418	1	0.288	0.06	-0.008	-0.085
20 Gen_insp														
Nr princip inspection	Baseline	Smart seg	wireless	wired	Nr princip inspection	Baseline	Smart seg	wireless	wired	Nr princip inspection	Baseline	Smart seg	wireless	wired
6	-1.347	-1.798	-1.933	-2.385	6	-1.347	-1.686	-1.788	-2.053	6	-1.347	-1.575	-1.643	-1.72
5	-0.953	-1.404	-1.539	-1.992	5	-0.953	-1.293	-1.394	-1.659	5	-0.953	-1.181	-1.249	-1.327
4	-0.56	-1.011	-1.146	-1.598	4	-0.56	-0.899	-1.001	-1.266	4	-0.56	-0.788	-0.856	-0.933
3	-0.166	-0.617	-0.752	-1.205	3	-0.166	-0.506	-0.607	-0.872	3	-0.166	-0.394	-0.462	-0.54
2	0.227	-0.224	-0.359	-0.811	2	0.227	-0.112	-0.214	-0.479	2	0.227	-0.001	-0.069	-0.146
1	0.621	0.17	0.035	-0.418	1	0.621	0.281	0.18	-0.085	1	0.621	0.393	0.325	0.247
10 Gen_insp														
Nr princip inspection	Baseline	Smart seg	wireless	wired	Nr princip inspection	Baseline	Smart seg	wireless	wired	Nr princip inspection	Baseline	Smart seg	wireless	wired
6	-1.014	-1.465	-1.6	-2.053	6	-1.014	-1.354	-1.455	-1.72	6	-1.014	-1.242	-1.31	-1.388
5	-0.621	-1.072	-1.207	-1.659	5	-0.621	-0.96	-1.062	-1.327	5	-0.621	-0.849	-0.917	-0.994
4	-0.227	-0.678	-0.813	-1.266	4	-0.227	-0.567	-0.668	-0.933	4	-0.227	-0.455	-0.523	-0.601
3	0.166	-0.285	-0.42	-0.872	3	0.166	-0.173	-0.275	-0.54	3	0.166	-0.062	-0.13	-0.207
2	0.56	0.109	-0.026	-0.479	2	0.56	0.22	0.119	-0.146	2	0.56	0.332	0.264	0.186
1	0.953	0.502	0.367	-0.085	1	0.953	0.614	0.512	0.247	1	0.953	0.725	0.657	0.58

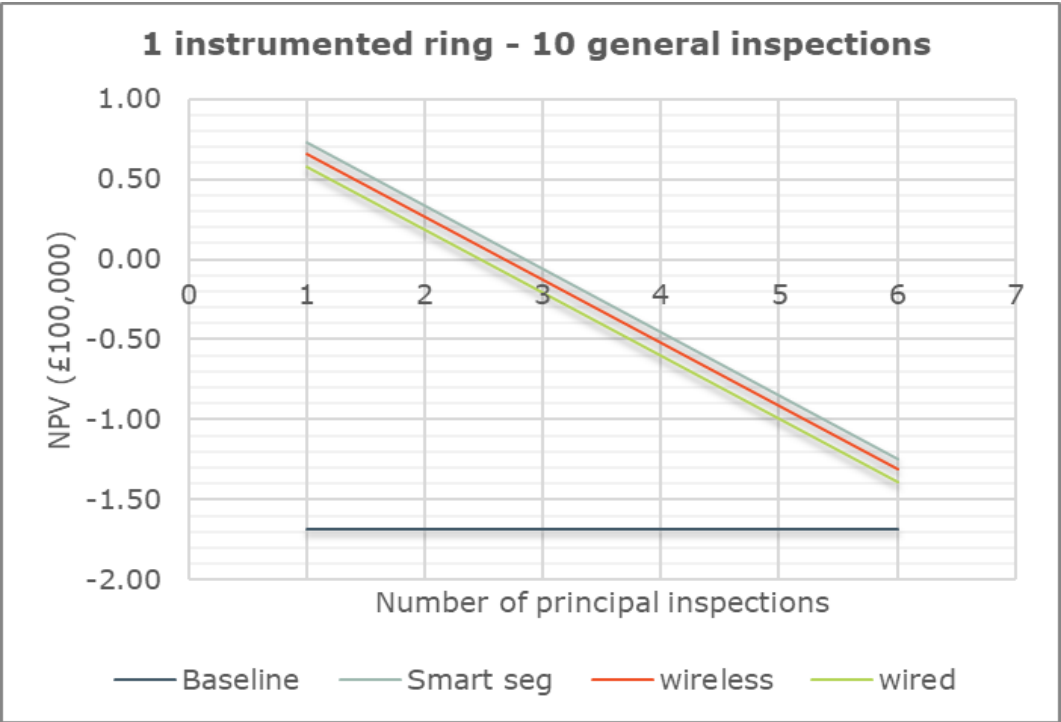












# Bibliography

1. Road Tunnel Association - UK and Eire Directory. <http://roadtunnelassociation.org.uk/Directory.html#top>.
2. National Highways. *Connecting the Country*. [https://nationalhighways.co.uk/media/ob11qvqr/cre22\\_0150-masterplan-national-highways-ris3\\_final-1.pdf](https://nationalhighways.co.uk/media/ob11qvqr/cre22_0150-masterplan-national-highways-ris3_final-1.pdf) (2023).
3. Hoefft, M., Pieper, M., Eriksson, K. & Bargstädt, H. J. Toward Life Cycle Sustainability in Infrastructure: The Role of Automation and Robotics in PPP Projects. *Sustainability* 2021, Vol. 13, Page 3779 **13**, 3779 (2021).
4. Yang, D. Y. & Frangopol, D. M. Bridging the gap between sustainability and resilience of civil infrastructure using lifetime resilience. *Routledge Handbook of Sustainable and Resilient Infrastructure* 419–442 (2018) doi:10.4324/9781315142074-23/BRIDGING-GAP-SUSTAINABILITY-RESILIENCE-CIVIL-INFRASTRUCTURE-USING-LIFETIME-RESILIENCE-DAVID-YANG-DAN-FRANGOPOL.
5. Chea, C. P., Bai, Y., Pan, X., Arashpour, M. & Xie, Y. An integrated review of automation and robotic technologies for structural prefabrication and construction. *Transportation Safety and Environment* **2**, 81–96 (2020).
6. Li, C. Z. ; *et al.* The Application of Advanced Information Technologies in Civil Infrastructure Construction and Maintenance. *Sustainability* 2022, Vol. 14, Page 7761 **14**, 7761 (2022).
7. Zhang, W.-H., Lu, D.-G., Qin, J., Thöns, S. & Faber, M. H. Value of information analysis in civil and infrastructure engineering: a review. *Journal of Infrastructure Preservation and Resilience* 2021 2:1 **2**, 1–21 (2021).
8. The British Tunnelling Society and The Institution of Civil Engineers. 2 Project definition. in *Tunnel lining design guide* 8–19 (Thomas Telford Publishing, 2004). doi:10.1680/TLDG.29866.0002.
9. The British Tunnelling Society and The Institution of Civil Engineers. 4 Design life and durability. in *Tunnel lining design guide* 40–58 (Thomas Telford Publishing, 2004). doi:10.1680/TLDG.29866.0004.

10. International Tunneling and underground space Association. *ITA Report N°22-Guidelines for the Design of Segmental Tunnel Linings*. (2019).
11. Triantafyllou, T. and S. M. Fibre-reinforced Polymer Reinforcement Enters Fib Model Code 2010. *Structural Concrete : Journal of the FIB* 14.4 335–41 (2013).
12. Report, I. *Concrete Segments - Vol. 1 : Design Aspects ITAtech Activity Group Support*. (2016).
13. Benedetto, A. & Pajewski, L. Innovative Inspection Procedures for Effective GPR Surveying of Critical Transport Infrastructures (Pavements, Bridges and Tunnels). in *Civil Engineering Applications of Ground Penetrating Radar* 71–95 (2015).
14. Konishi, S., Kawakami, K. & Taguchi, M. Inspection Method with Infrared Thermometry for Detect Void in Subway Tunnel Lining. in *Procedia Engineering* vol. 165 474–483 (Elsevier Ltd, 2016).
15. Cao, R., Ma, M., Liang, R. & Niu, C. Detecting the void behind the tunnel lining by impact-echo methods with different signal analysis approaches. *Applied Sciences (Switzerland)* **9**, (2019).
16. Loupos, K. *et al.* Autonomous robotic system for tunnel structural inspection and assessment. *Int J Intell Robot Appl* **2**, 43–66 (2018).
17. Menendez, E., Victores, J. G., Montero, R., Martínez, S. & Balaguer, C. Tunnel structural inspection and assessment using an autonomous robotic system. *Autom Constr* **87**, 117–126 (2018).
18. Huang, Z., Chen, Z., Shao-Kun, M. A. & Fan, X.-D. (. *Machine Inspection Equipment for Tunnels: A Review*. *Journal of Highway and Transportation Research and Development* vol. 15 (2021).
19. Sjölander, A., Belloni, V., Ansell, A. & Nordström, E. Towards Automated Inspections of Tunnels: A Review of Optical Inspections and Autonomous Assessment of Concrete Tunnel Linings. *Sensors* vol. 23 Preprint at <https://doi.org/10.3390/s23063189> (2023).
20. Alsayed, A., Yunusa-Kaltungo, A., Quinn, M. K., Arvin, F. & Nabawy, M. R. A. Drone-assisted confined space inspection and stockpile volume estimation. *Remote Sens (Basel)* **13**, (2021).

21. Yang, D. Y. & Frangopol, D. M. Life-cycle management of deteriorating civil infrastructure considering resilience to lifetime hazards: A general approach based on renewal-reward processes. *Reliab Eng Syst Saf* **183**, 197–212 (2019).
22. Herráiz, D., KenichiSoga, AFidler, P. R. & Battista, N. Monitoring project requirements. in *Wireless Sensor Networks for Civil Infrastructure Monitoring* 7–22 doi:10.1680/wsncim.61514.007.
23. The British Tunnelling Society and The Institution of Civil Engineers. 8 Instrumentation and monitoring. *Tunnel lining design guide* 122–136 (2004) doi:10.1680/TLDG.29866.0008.
24. Cuelho, E., Stephens, J., Smolenski, P. & Johnson, J. *EVALUATING CONCRETE BRIDGE DECK PERFORMANCE*. (2006).
25. Chen, H.-P. & Ni, Y.-Q. *Structural Health Monitoring of Large Civil Engineering Structures*.
26. Glisic, B. One Hundred Years of Strain Sensing in Civil Structural Health Monitoring. in *Structural Health Monitoring 2019 Enabling Intelligent Life-cycle Health Management for Industry Internet of Things (IIOT)* (ed. Fu-Kuo Chang, Alfredo Guemes, F. K.) 1704–1714 (DEStech Publications Inc., Stanford, USA, 2019).
27. Geokon Inc. Model 4200 Series Vibrating Wire Strain Gages Instruction Manual. (2018).
28. You, Lin Xu; Yong, X. *Structural Health Monitoring of Long-Span Suspension Bridges*. (CRC Press, London, 2011). doi:https://doi.org/10.1201/b13182.
29. Ge, Y., Elshafie, M. Z. E. B., Dirar, S. & Middleton, C. R. The response of embedded strain sensors in concrete beams subjected to thermal loading. *Constr Build Mater* **70**, 279–290 (2014).
30. Neild, S. A., Williams, M. S. & McFadden, P. D. Development of a vibrating wire strain gauge for measuring small strains in concrete beams. *Strain* **41**, 3–9 (2005).
31. Sreeshylam, P., Ravisankar, K., Parivallal, S., Kesavan, K. & Sridhar, S. Condition monitoring of prestressed concrete structures using vibrating wire sensors. *International Journal of COMADEM* **11**, 46–54 (2008).

32. Simon, A., Courtois, A., Clauzon, T., Coustabeau, E. & Vinit, S. Long-term measurement of strain in concrete : durability and accuracy of embedded vibrating wire strain gauges. *SMAR 2015: Third Conference on Smart Monitoring, Assessment and Rehabilitation of Civil Structures* (2015).
33. Glišić, B. & Inaudi, Daniele. *Fibre Optic Methods for Structural Health Monitoring*. (John Wiley & Sons, 2007).
34. Mohamad, H., Bennett, P. J., Soga, K., Mair, R. J. & Bowers, K. Behaviour of an old masonry tunnel due to tunnelling-induced ground settlement. *Geotechnique* **60**, 927–938 (2010).
35. Gue, C. Y. *et al.* The monitoring of an existing cast iron tunnel with distributed fibre optic sensing (DFOS). *J Civ Struct Health Monit* **5**, 573–586 (2015).
36. Di Murro, V. *et al.* Distributed fibre optic long-term monitoring of concrete-lined tunnel section TT10 at CERN. (2016) doi:10.1680/tfitsi.61279.027.
37. Domaneschi, M. *et al.* *Structural Health Monitoring of In-Service Tunnels. Int. J. Sustainable Materials and Structural Systems* vol. 4 (2020).
38. Gómez, J., Casas, J. R. & Villalba, S. Structural Health Monitoring with Distributed Optical Fiber Sensors of tunnel lining affected by nearby construction activity. *Autom Constr* **117**, 103261 (2020).
39. Grunicke, U. H., Lienhart, W. & Vorwagner, A. Long-term monitoring of visually not inspectable tunnel linings using fibre optic sensing. *Geomechanics and Tunneling* **14**, 19–32 (2021).
40. Mohamad, H. *et al.* Monitoring Twin Tunnel Interaction Using Distributed Optical Fiber Strain Measurements. (2012) doi:10.1061/(ASCE)GT.1943-5606.0000656.
41. Fajkus, M. *et al.* Analysis of the highway tunnels monitoring using an optical fiber implemented into primary lining. *Journal of Electrical Engineering* **68**, 364–370 (2017).
42. Glisic, B., Badoux, M., Jaccoud, J.-P. & Inaudi, D. *Monitoring A Subterranean Structure with the SOFO System*. (2000).

43. Buchmayer, F., Monsberger, C. M. & Lienhart, W. *Benefits of Strain and Temperature Monitoring of Conventional Tunnel Cross Sections Using Distributed Fibre Optic Sensors*. (2019).
44. Monsberger, C. M. & Lienhart, W. Distributed fiber optic shape sensing along shotcrete tunnel linings: Methodology, field applications, and monitoring results. *J Civ Struct Health Monit* **11**, 337–350 (2021).
45. Wagner, L. *et al.* Direct and Distributed Strain Measurements Inside a Shotcrete Lining: Concept and Realisation. *Rock Mech Rock Eng* **53**, 641–652 (2020).
46. De Battista, N. *et al.* *Strain Monitoring Using Embedded Distributed Fibre Optic Sensors in a Sprayed Concrete Tunnel Lining during the Excavation of Cross-Passages Smart Infrastructure View Project ITN-FINESSE Innovative Training Network on Optical Fiber Sensors View Project St.* (2015).
47. Gómez, J., Casas, J. R. & Villalba, S. Structural Health Monitoring with Distributed Optical Fiber Sensors of tunnel lining affected by nearby construction activity. *Autom Constr* **117**, 103261 (2020).
48. Monsberger, C. M., Lienhart, W. & Moritz, B. In-situ assessment of strain behaviour inside tunnel linings using distributed fibre optic sensors: Beurteilung des In-situ-Dehnungsverhaltens der Tunnelschale mittels verteilter faseroptischer Messsysteme. *Geomechanik und Tunnelbau* **11**, 701–709 (2018).
49. Gehwolf, P. *et al.* Deformation measurements of tunnel segments at a newly developed test rig / Deformationsmessungen an Tübbinggen mit einem neu entwickelten Prüfstand. *Geomechanik und Tunnelbau* **9**, 180–187 (2016).
50. Lienhart, W., Buchmayer, F., Klug, F. & Monsberger, C. M. Distributed Fiber Optic Sensing Applications at the Semmering Base Tunnel. *Proceedings of the Institution of Civil Engineers - Smart Infrastructure and Construction* 1–13 (2020) doi:10.1680/jsmic.20.00006.
51. Abdulkarem, M., Samsudin, K., Zaman Rokhani, F. & Fadlee Rasid, M. A. Wireless sensor network for structural health monitoring: A contemporary review of technologies, challenges, and future direction. *Struct Health Monit* **19**, 693–735 (2020).



52. Tunnel Business Magazine. How IoT Is Shaping the Future of Risk Management in Tunneling. [https://tunnelingonline.com/how-iot-technology-is-shaping-the-future-of-risk-management-in-the-tunneling-industry/?oly\\_enc\\_id=9463B3029134D5T](https://tunnelingonline.com/how-iot-technology-is-shaping-the-future-of-risk-management-in-the-tunneling-industry/?oly_enc_id=9463B3029134D5T) (2019).
53. Huston, D. *Structural Sensing, Health Monitoring and Performance Evaluation. Journal of Petrology* vol. 369 (Taylor & Francis, Burlington, Vermont, USA, 2011).
54. Wireless Connectivity Options for IoT Applications - Technology Comparison | Bluetooth® Technology Website. <https://www.bluetooth.com/blog/wireless-connectivity-options-for-iot-applications-technology-comparison/>.
55. Safaei, M., Sodano, H. A. & Anton, S. R. A review of energy harvesting using piezoelectric materials: State-of-the-art a decade later (2008-2018). *Smart Mater Struct* **28**, (2019).
56. Anton, S. R. & Sodano, H. A. A review of power harvesting using piezoelectric materials (2003–2006). *Smart Mater Struct* **16**, R1 (2007).
57. Kim, H., Tadesse, Y. & Priya, S. Piezoelectric energy harvesting. in *Energy Harvesting Technologies* 3–39 (Springer US, 2009). doi:10.1007/978-0-387-76464-1\_1.
58. Penella, M. T. & Gasulla, M. *Instrumentation and Measurement Technology Conference-IMTC*. (2007).
59. Revibe Energy. Implementing vibration energy harvesting within the railway industry. <https://revibeenergy.com/railway-customer-reference/> (2020).
60. Perpetuum. Rail Applications | THE WORLD LEADER IN VIBRATION HARVESTER POWERED WIRELESS SENSING SYSTEMS. <https://perpetuum.com/rail-applications/>.
61. Revibe Energy. Implementing vibration energy harvesting within aviation. <https://revibeenergy.com/aviation-customer-reference/> (2020).
62. Mide. *PIEZOELECTRIC ENERGY HARVESTERS|Manual*. (2013).
63. Perpetuum. Industrial Applications | THE WORLD LEADER IN VIBRATION HARVESTER POWERED WIRELESS SENSING SYSTEMS. <https://perpetuum.com/industrial-applications/>.

64. Fierce electronics (Sensor Staff). Perpetuum Launches Vibration Energy–Harvesting Microgenerator | FierceElectronics. <https://www.fierceelectronics.com/components/perpetuum-launches-vibration-energy-harvesting-microgenerator> (2006).
65. Cedrat Technologies. *Data Sheet Vibration Energy Harvesting\_with\_APA400M-MD*.
66. Jiang, X., Li, Y., Li, J., Wang, J. & Yao, J. Piezoelectric energy harvesting from traffic-induced pavement vibrations. *Journal of Renewable and Sustainable Energy* **6**, 043110 (2014).
67. Ding, G., Zhao, X., Wang, J. & Xu, C. Vibration energy harvesting from roads under traffic loads. *Road Materials and Pavement Design* **21**, 780–799 (2020).
68. Zhang, Y., Zhang, H., Lü, C., Chen, Y. & Wang, J. Piezoelectric energy harvesting from roadway deformation under various traffic flow conditions. *J Intell Mater Syst Struct* **31**, 1751–1762 (2020).
69. Wang, H., Jasim, A. & Chen, X. Energy harvesting technologies in roadway and bridge for different applications – A comprehensive review. *Applied Energy* vol. 212 1083–1094 Preprint at <https://doi.org/10.1016/j.apenergy.2017.12.125> (2018).
70. Leica Geosystems. Leica Geosystems announces new most accurate total station | Leica Geosystems. [https://leica-geosystems.com/en-gb/about-us/news-room/news-overview/2020/02/2020\\_02\\_19\\_ts60](https://leica-geosystems.com/en-gb/about-us/news-room/news-overview/2020/02/2020_02_19_ts60).
71. Kechavarzi, C. *et al.* Tunnel monitoring. in *Distributed Fibre Optic Strain Sensing Monitoring Civil Infrastructure* 133–168 (ICE Publishing, Online, 2016). doi:10.1680/dfossmci.60555.133.
72. Alhaddad, M., Meng, M. D., Soga, K. & Devriendt, M. A new photogrammetric system for high-precision monitoring of tunnel deformations. (2019) doi:10.1680/jtran.18.00001.
73. Middleton, C. R., Fidler, P. R. A. & Vardanega, P. J. Technologies for bridge monitoring. in *Bridge Monitoring* 29–56 (ICE Publishing, 2016). doi:doi:10.1680/mobs.60593.029.
74. Cambridge Centre for Smart Infrastructures and Construction. CSattAR shortlisted for three New Civil Engineer Tunnelling Awards | Cambridge Centre for Smart

- Infrastructure and Construction. <https://www-smartinfrastucture.eng.cam.ac.uk/news/csattar-shortlisted-for-three-new-civil-engineer-tunneling-awards>.
75. Alhaddad, M. *et al.* Cast-iron tunnels' tolerance to imposed longitudinal settlement curvature. *Geotechnique* **71**, 1044–1055 (2021).
  76. Mair, R. J. Briefing: Advanced sensing technologies for structural health monitoring. *Proceedings of the Institution of Civil Engineers: Forensic Engineering* **169**, 46–49 (2016).
  77. Utterberry – Main site. <https://utterberry.com/>.
  78. Bennett, P. J., Kobayashi, Y., Soga, K. & Wright, P. Wireless sensor network for monitoring transport tunnels. *Proceedings of the Institution of Civil Engineers: Geotechnical Engineering* **163**, 147–156 (2010).
  79. Alhaddad, M. *et al.* Multi-Suite Monitoring of an Existing Cast Iron Tunnel Subjected to Tunnelling-induced Ground Movements. 293–307 (2014) doi:10.1061/9780784413449.030.
  80. Xu, X. *et al.* Performance monitoring of timber structures in underground construction using wireless SmartPlank. *Smart Struct Syst* **15**, 769–785 (2015).
  81. Rodenas Herráiz, D., Soga, K., Fidler, P. R. A. & de Battista, N. London Underground tunnel lining replacement monitoring (UK). *Wireless Sensor Networks for Civil Infrastructure Monitoring* 1–6 (2016) doi:10.1680/WSNCIM.61514.173.
  82. Moritz, B., Heissenberger, R., Schachinger, T. & Lienhart, W. Long-term monitoring of railway tunnels. *Geomechanik und Tunnelbau* **14**, 35–46 (2021).
  83. Lienhart Beng, W., Buchmayer Bsc, F., Klug Bsc, F. & Monsberger, C. M. Distributed fibre-optic sensing applications at the Semmering Base Tunnel, Austria. (2019) doi:10.1680/jsmic.20.00006.
  84. Michelin, F., Nahli, A., Lamour, V. & Le, T. D. Holistic approach for the construction monitoring of the Grand Paris Express metro network. *Lecture Notes in Civil Engineering* **62**, 265–272 (2020).

85. Gómez, J., Casas, J. R. & Villalba, S. Structural Health Monitoring with Distributed Optical Fiber Sensors of tunnel lining affected by nearby construction activity. *Autom Constr* **117**, 103261 (2020).
86. Barrias, A., Rodriguez, G., Casas, J. R. & Villalba, S. Application of distributed optical fiber sensors for the health monitoring of two real structures in Barcelona. <https://doi.org/10.1080/15732479.2018.1438479> **14**, 967–985 (2018).
87. Sakiyama, F. I. H., Lehmann, F. & Garrecht, H. Structural health monitoring of concrete structures using fibre-optic-based sensors: A review. *Magazine of Concrete Research* **73**, 174–194 (2021).
88. Gue, C. Y. *et al.* Monitoring the Behaviour of an Existing Royal Mail Tunnel: London Underground Bond Street Station Upgrade Works. in 525–535 (American Society of Civil Engineers (ASCE), 2017). doi:10.1061/9780784480441.055.
89. Kechavarzi, C. *et al.* Tunnel monitoring. in *Distributed Fibre Optic Strain Sensing for Monitoring Civil Infrastructure* 133–168 (ICE Publishing, 2016). doi:doi:10.1680/dfossmci.60555.133.
90. Gehwolf, P. *et al.* Deformation measurements of tunnel segments at a newly developed test rig / Deformationsmessungen an Tübingen mit einem neu entwickelten Prüfstand. *Geomechanik und Tunnelbau* **9**, 180–187 (2016).
91. Radončić, N., Kern, M., Weissnar, M. & Moritz, B. Dehnmessgeber in Tübbingsegmenten - Funktionsweise, Auswertung und Interpretation. *Geomechanik und Tunnelbau* **8**, 265–272 (2015).
92. Qi, T., Liang, X., Jin, Z. & Qian, W. An experimental approach to evaluating the long-term performance of segmental linings. *International Journal of Physical Modelling in Geotechnics* **21**, 150–167 (2021).
93. Kesavan, K., Ravisankar, K., Parivallal, S., Sreeshylam, P. & Sridhar, S. Experimental studies on fiber optic sensors embedded in concrete. *Measurement (Lond)* **43**, 157–163 (2010).
94. Cheng, W. C., Ni, J. C. & Shen, S. L. Experimental and analytical modeling of shield segment under cyclic loading. *International Journal of Geomechanics* **17**, 1–18 (2017).

95. Meda, A., Rinaldi, Z., Caratelli, A. & Cignitti, F. Experimental investigation on precast tunnel segments under TBM thrust action. *Eng Struct* **119**, 174–185 (2016).
96. Trabucchi, I. *et al.* A hybrid solution proposal for precast tunnel segments. *Structural Concrete* **22**, 1534–1548 (2021).
97. Warsi, Z. H. *et al.* Sensors for structural health monitoring: A review. *2019 2nd International Conference on Latest Trends in Electrical Engineering and Computing Technologies, INTELLECT 2019* (2019) doi:10.1109/INTELLECT47034.2019.8955453.
98. Vijayan, D. S. *et al.* Development of Intelligent Technologies in SHM on the Innovative Diagnosis in Civil Engineering—A Comprehensive Review. *Buildings* **2023**, Vol. 13, Page 1903 **13**, 1903 (2023).
99. Micro Measurements. EGP Concrete Embedment Strain Gage. <https://docs.micro-measurements.com/?id=2647>.
100. Tokyo Sokki Kenkyujo Co., L. TML Strain gauges 2017. *Tech Note 98* (2017).
101. Lab, T. M. I. *Internal Strain of Concrete, Synthetic Resin Civil Engineering Design KM Strain Transducers A B C D E Red KM-30 KM-50F*.
102. Neild, S. A., Williams, M. S. & McFadden, P. D. Development of a vibrating wire strain gauge for measuring small strains in concrete beams. *Strain* **41**, 3–9 (2005).
103. Calder, P. A. & Glisic, B. Influence of mechanical and geometrical properties of embedded long-gauge strain sensors on the accuracy of strain measurement. (2012) doi:10.1088/0957-0233/23/6/065604.
104. Smith, L. M., Brodt, G. L. & Stafford, B. Performance assessment and reinstatement of vibrating wire strain gauges in nuclear power plant structures. *Transactions of Structural Mechanics in Reactor Technology (SMiRT 16)* 1–8 (2001).
105. Cuelho, E., Stephens, J. & Akin, M. *SEVEN - YEAR EVALUATION OF THREE INSTRUMENTED BRIDGE DECKS IN SACO, MONTANA*. (2010).
106. Grainger, B. N. *The Strain Behaviour of Prestressed Concrete Reactor Pressure Vessels Over 20 Years*. (1989).

107. Bhalla, S., Yang, Y. W., Zhao, J. & Soh, C. K. Structural health monitoring of underground facilities - Technological issues and challenges. *Tunnelling and Underground Space Technology* **20**, 487–500 (2005).
108. Azenha, M., Faria, R. & Ferreira, D. Identification of early-age concrete temperatures and strains: Monitoring and numerical simulation. *Cem Concr Compos* **31**, 369–378 (2009).
109. Rite, E. *Vibrating Wire Strain Gauges Users' Manual*. (2019).
110. Simmonds, A. J. LONG TERM MONITORING USING VIBRATING WIRE SENSORS. in *The 6 th International Conference on Structural Health Monitoring of Intelligent Infrastructure* (2013).
111. Taheri, S. A review on five key sensors for monitoring of concrete structures. *Constr Build Mater* **204**, 492–509 (2019).
112. Bennett, P. J., Kobayashi, Y., Soga, K. & Wright, P. Wireless sensor network for monitoring transport tunnels. *Proceedings of the Institution of Civil Engineers - Geotechnical Engineering* **163**, 147–156 (2010).
113. Middleton, C. R. Technologies for bridge monitoring. in *Bridge Monitoring* (ICE Publishing, London, 2016). doi:10.1680/mobs.60593.29.
114. Jiang, S. & Georgakopoulos, S. V. Optimum wireless powering of sensors embedded in concrete. *IEEE Trans Antennas Propag* **60**, 1106–1113 (2012).
115. Gharbia, M., Chang-Richards, A. Y. & Zhong, R. Y. Robotic technologies in concrete building construction: A systematic review. in *Proceedings of the 36th International Symposium on Automation and Robotics in Construction, ISARC 2019* 10–19 (International Association for Automation and Robotics in Construction I.A.A.R.C), 2019). doi:10.22260/isarc2019/0002.
116. Cheng, J. C. P., Lu, Q. & Deng, Y. Analytical review and evaluation of civil information modeling. *Autom Constr* **67**, 31–47 (2016).
117. Atkin, B. L. & Gill, E. M. CAD and Management of Construction Projects. *J Constr Eng Manag* **112**, 557–565 (1986).

118. Toriumi, F. Y., Bittencourt, T. N. & Futai, M. M. UAV-based inspection of bridge and tunnel structures: an application review. *Revista IBRACON de Estruturas e Materiais* **16**, e16103 (2022).
119. Zhang, R., Hao, G., Zhang, K. & Li, Z. Unmanned aerial vehicle navigation in underground structure inspection: A review. *Geological Journal* **58**, 2454–2472 (2023).
120. Hennage, D. H., Nopola, J. R. & Haugen, B. D. Fully Autonomous Drone for Underground Use. Preprint at <https://dx.doi.org/> (2019).
121. Cook, Z., Kazemeini, M., Barzilov, A. & Yim, W. Low-altitude contour mapping of radiation fields using UAS swarm. *Intell Serv Robot* **12**, 219–230 (2019).
122. Ajay Kumar, G., Patil, A. K., Patil, R., Park, S. S. & Chai, Y. H. A LiDAR and IMU Integrated Indoor Navigation System for UAVs and Its Application in Real-Time Pipeline Classification. *Sensors 2017, Vol. 17, Page 1268* **17**, 1268 (2017).
123. Papachristos, C., Khattak, S., Mascarich, F., Dang, T. & Alexis, K. Autonomous aerial robotic exploration of subterranean environments relying on morphology-aware path planning. *2019 International Conference on Unmanned Aircraft Systems, ICUAS 2019* 299–305 (2019) doi:10.1109/ICUAS.2019.8797885.
124. Castaño, A. R., Romero, H., Capitán, J., Andrade, J. L. & Ollero, A. Development of a Semi-autonomous Aerial Vehicle for Sewerage Inspection. *Advances in Intelligent Systems and Computing* **1092 AISC**, 75–86 (2020).
125. Turner, R. M., MacLaughlin, M. M. & Iverson, S. R. Identifying and mapping potentially adverse discontinuities in underground excavations using thermal and multispectral UAV imagery. *Eng Geol* **266**, 105470 (2020).
126. Bendris, B. & Becerra, J. C. Design and Experimental Evaluation of an Aerial Solution for Visual Inspection of Tunnel-like Infrastructures. *Remote Sensing 2022, Vol. 14, Page 195* **14**, 195 (2022).
127. Li, Y., Ma, J., Zhao, Z. & Shi, G. A Novel Approach for UAV Image Crack Detection. *Sensors 2022, Vol. 22, Page 3305* **22**, 3305 (2022).
128. Doychinov, V. *et al.* Infrastructure Robotics Research at the University of Leeds.

129. Sadeghi Esfahlani, S. Mixed reality and remote sensing application of unmanned aerial vehicle in fire and smoke detection. (2019) doi:10.1016/j.jii.2019.04.006.
130. Anderson, M. J. *et al.* The ‘Smellicopter,’ a bio-hybrid odor localizing nano air vehicle. *IEEE International Conference on Intelligent Robots and Systems* 6077–6082 (2019) doi:10.1109/IROS40897.2019.8968589.
131. Burgués, J., Hernández, V., Lilienthal, A. J. & Marco, S. Smelling nano aerial vehicle for gas source localization and mapping. *Sensors (Switzerland)* **19**, (2019).
132. Victores, J. G., Martínez, S., Jardón, A. & Balaguer, C. Robot-aided tunnel inspection and maintenance system by vision and proximity sensor integration. *Autom Constr* **20**, 629–636 (2011).
133. Zhuang, F., Zupan, C., Chao, Z. & Yanzheng, Z. A cable-tunnel inspecting robot for dangerous environment. <https://doi.org/10.5772/5610> **5**, 32 (2008).
134. Tang, S., Chen, S., Liu, Q., Wang, B. & Guo, X. A small tracked robot for cable tunnel inspection. *Lecture Notes in Electrical Engineering* **122 LNEE**, 591–598 (2011).
135. Cai, J. L., Xie, X. Y., Zhou, B., Zhou, Y. X. & Zeng, W. C. Rapid automatic inspection system for tunnel lining based on a mobile vehicle. *Tunnels and Underground Cities: Engineering and Innovation meet Archaeology, Architecture and Art- Proceedings of the WTC 2019 ITA-AITES World Tunnel Congress* 1852–1859 (2019) doi:10.1201/9780429424441-195/RAPID-AUTOMATIC-INSPECTION-SYSTEM-TUNNEL-LINING-BASED-MOBILE-VEHICLE-CAI-XIE-ZHOU-ZHOU-ZENG.
136. Menendez, E., Victores, J. G., Montero, R., Martínez, S. & Balaguer, C. Tunnel structural inspection and assessment using an autonomous robotic system. *Autom Constr* **87**, 117–126 (2018).
137. Peel, H., Luo, S., Cohn, A. G. & Fuentes, R. Localisation of a mobile robot for bridge bearing inspection. *Autom Constr* **94**, 244–256 (2018).
138. Peel, H., Morgan, G., Peel, C., Cohn, A. & Fuentes, R. Inspection Robot with Low Cost Perception Sensing.



139. Bock, T. The future of construction automation: Technological disruption and the upcoming ubiquity of robotics. *Autom Constr* **59**, 113–121 (2015).
140. Liang, C. J., Kamat, V. R. & Menassa, C. C. Teaching robots to perform quasi-repetitive construction tasks through human demonstration. *Autom Constr* **120**, 103370 (2020).
141. Feng, C., Xiao, Y., Willette, A., McGee, W. & Kamat, V. R. Vision guided autonomous robotic assembly and as-built scanning on unstructured construction sites. *Autom Constr* **59**, 128–138 (2015).
142. Bock, T. L. T. *Construction Robots*. (Cambridge University Press, 2017).
143. Bock, T. L. T. *Site Automation*. (Cambridge University Press, 2016).
144. Bock, T. & Linner, T. *Robot-Oriented Design*. (Cambridge University Press, New York, 2015). doi:10.1017/CBO9781139924146.
145. Bock, T. & Linner, T. *Robotic Industrialization : Automation and Robotic Technologies for Customized Component, Module, and Building Prefabrication*. (Cambridge University Press, Cambridge, 2015).
146. Bock, T. & Linner, T. *Robot-Oriented Design : Design and Management Tools for the Deployment of Automation and Robotics in Construction*.
147. Bock, T. & Linner, T. *Robotic Industrialization : Automation and Robotic Technologies for Customized Component, Module, and Building Prefabrication*. (Cambridge University Press, Cambridge, 2015).
148. Nematollahi, B., Xia, M. & Sanjayan, J. Current progress of 3D concrete printing technologies. in *ISARC 2017 - Proceedings of the 34th International Symposium on Automation and Robotics in Construction* 260–267 (International Association for Automation and Robotics in Construction I.A.A.R.C), 2017). doi:10.22260/isarc2017/0035.
149. Weckenmann. All products. <https://weckenmann.com/en/products/all-products> (2019).
150. Progress-M. Shuttering and deshuttering robots. <https://www.progress-m.com/en/products/shuttering-robots> (2019).

151. Tuna, G., Mumcu, T. V., Gulez, K., Gungor, V. C. & Erturk, H. Unmanned aerial vehicle-aided wireless sensor network deployment system for post-disaster monitoring. *Communications in Computer and Information Science* **304** CCIS, 298–305 (2012).
152. Iyer, V., Kim, M., Xue, S., Wang, A. & Gollakota, S. Airdropping Sensor Networks from Drones and Insects. 14 (2020) doi:10.1145/3372224.3419981.
153. Corke, P. *et al.* Autonomous deployment and repair of a sensor network using an unmanned aerial vehicle. *Proc IEEE Int Conf Robot Autom* **2004**, 3602–3608 (2004).
154. Sørensen, L. Y., Jacobsen, L. T. & Hansen, J. P. Low Cost and Flexible UAV Deployment of Sensors. *Sensors 2017, Vol. 17, Page 154* **17**, 154 (2017).
155. Drone deploys sensors by shooting them as darts. <https://newatlas.com/drones/sensor-dart-shooting-drone/>.
156. Zhou, H., Lynch, J. & Zekkos, D. Autonomous wireless sensor deployment with unmanned aerial vehicles for structural health monitoring applications. *Struct Control Health Monit* **29**, (2022).
157. Erdelj, M. & Miranda, K. Mobile Robot Deployment in the Context of WSN. Nathalie Mitton and David Simplot-Ryl. *Wireless Sensor and Robot Networks From Topology Control to Communication Aspects*, Worldscientific. 978 (2014) doi:10.1142/9789814551342\_0004i.
158. Valecce, G. *et al.* Robotic-aided IoT: automated deployment of a 6TiSCH network using an UGV. *IET Wireless Sensor Systems* **9**, 438–446 (2019).
159. Gruebele, A. M., Zerbe, A. C., Coad, M. M., Okamura, A. M. & Cutkosky, M. R. Distributed Sensor Networks Deployed Using Soft Growing Robots. doi:10.1109/RoboSoft51838.2021.9479345.
160. Ajeil, F. H., Ibraheem, I. K., Azar, A. T. & Humaidi, A. J. Autonomous navigation and obstacle avoidance of an omnidirectional mobile robot using swarm optimization and sensors deployment. *Int J Adv Robot Syst* **17**, (2020).
161. Popa, D. O., Stephanou, H. E., Helm, C. & Sanderson, A. C. Robotic deployment of sensor networks using potential fields. *Proc IEEE Int Conf Robot Autom* **2004**, 642–647 (2004).

162. Soua, R., Saidane, L. & Minet, P. Sensors deployment enhancement by a mobile robot in wireless sensor networks. *9th International Conference on Networks, ICN 2010* 121–126 (2010) doi:10.1109/ICN.2010.29.
163. Farinha, A., Zufferey, R., Zheng, P., Armanini, S. F. & Kovac, M. Unmanned Aerial Sensor Placement for Cluttered Environments. *IEEE Robot Autom Lett* **5**, 6623–6630 (2020).
164. Triantafyllou, P. *et al.* A benchmarking framework for systematic evaluation of robotic pick-and-place systems in an industrial grocery setting. *Proc IEEE Int Conf Robot Autom* **2019-May**, 6692–6698 (2019).
165. Mnyusiwalla, H. *et al.* A Bin-Picking Benchmark for Systematic Evaluation of Robotic Pick-and-Place Systems. *IEEE Robot Autom Lett* **5**, 1389–1396 (2020).
166. Highways, N. Lower Thames Crossing - The Lower Thames Crossing route - National Highways. [/our-roads/lower-thames-crossing/what-is-the-lower-thames-crossing/the-lower-thames-crossing-route/](#) (2020).
167. McAlorum, J., Perry, M., Vlachakis, C., Biondi, L. & Lavoie, B. Robotic spray coating of self-sensing metakaolin geopolymers for concrete monitoring. *Autom Constr* **121**, 103415 (2021).
168. CONSOLIS. Monitoring the structural health of grandstands - Connect Consolis. <https://connect.consolis.com/references/hungarian-stadium/> (2018).
169. Lirola, J. M., Castañeda, E., Lauret, B. & Khayet, M. A review on experimental research using scale models for buildings: Application and methodologies. *Energy and Buildings* vol. 142 72–110 Preprint at <https://doi.org/10.1016/j.enbuild.2017.02.060> (2017).
170. Noor, F. A. *Small Scale Modelling of Concrete Structures*. *Small Scale Modelling of Concrete Structures* (CRC Press, 1992). doi:10.1201/9781482286700.
171. Tuset, J., Pera, J. & Cubaud, J.-C. Etude de modèles réduits de structures en micro-béton armé. *Bulletin technique de la Suisse romande* (1973).
172. Kamperharez. Fibres product Overview. Preprint at (2021).

173. Almansa, E. M. & Cánovas, M. F. Dosificación de hormigón reforzado con fibras de acero. *Materiales de Construcción* **1997**, 11–26 (1997).
174. GCP Applied Technologies. ADVA® XR 3009 | Resource | GCP Applied Technologies. <https://gcpat.uk/en-gb/solutions/products/adva-high-range-water-reducers/adva-xr-3009>.
175. Adfill Construction Fibres. Datasheet Adfil SF 86. 749.
176. Bekaert. *Datasheet Steel Fibre Dramix 3D 6535BG*.
177. Krampeharex. *Datasheet Wire Fibre DE 25-0-40*. vol. 49 (2021).
178. British Standard. *Test Methods for Fibres in Concrete - Part 1: Reference Concretes*. vol. 3 (2006).
179. Arockiasamy, M., Ball, H. P. & Galer, R. E. Guide for Specifying, Proportioning, Mixing, Placing, and Finishing Steel Fiber Reinforced Concrete. *ACI Mater J* **90**, 1–10 (1993).
180. British Standard. *BS EN 12350-3-2019-Testing Fresh Concrete. Vebe Test*.
181. ITAtech. *Guideline for Good Practice of Fibre Reinforced Precast Segment - Vol.2: Production*. vol. 2 (2018).
182. British Standards. BS EN 12390-3:2019: Testing hardened concrete: Compressive strength of test specimens. Preprint at (2019).
183. British Standards. BS EN 14651:2005 +A1:200: Test method for metallic fibre concrete — Measuring the flexural tensile strength ( limit of proportionality ( LOP ), residual ). **3**, 1–17 (2007).
184. Meda, A. & Rinaldi, Z. *Tests on Precast Tunnel Segment in Concrete Newly High Tensile Strength Steel Fibers Dramix 4D 80/60BG*. (2015).
185. Cheng, W.-C., Ni, J. C. & Shen, S.-L. Experimental and Analytical Modeling of Shield Segment under Cyclic Loading. *International Journal of Geomechanics* **17**, 04016146 (2017).
186. Boresi, A. P. (Arthur P. *Advanced Mechanics of Materials*. (Wiley, New York, 1993).

187. Du, J., Sugumaran, V. & Gao, B. RFID and multi-agent based architecture for information sharing in prefabricated component supply chain. *IEEE Access* **5**, 4132–4139 (2017).
188. Sparkes, P. W. J. A. *Structural Health Monitoring in Civil Engineering*. (CIRIA, London, 2020).
189. William Bergeson, PE and Steve Ernst, P. (FHWA). *Tunnel Operations, Maintenance, Inspection, and Evaluation (TOMIE) Manual*. (2015).
190. Centre d'Etudes des Tunnels. Road tunnel civil engineering inspection guide Book 1: from disorder to analysis, from analysis to rating Guides. (2013).
191. National Highways. Design Manual for Roads and Bridges Highway Structures & Bridges Inspection & Assessment CS 452 Inspection and records for road tunnel systems (formerly BD 53/95) Revision 0. (2020).
192. National Highways. Design Manual for Roads and Bridges Highway Structures & Bridges Maintenance & Operation CM 430 Maintenance of road tunnels (formerly BA 72/03) Revision 0. (2020).
193. Chris Hoy. Highway tunnel inspection costs. *private communication* Preprint at (2023).
194. KPMG Australia. *ARE WE INVESTING FOR THE FUTURE OR DISCOUNTING IT?* <https://assets.kpmg.com/content/dam/kpmg/au/pdf/2021/infrastructure-project-investment-discount-rate.pdf> (2021).
195. Petraroia, D. N. & Mark, P. Variable, full-scale tester for tunnel linings. *Structural Concrete* **22**, 3353–3367 (2021).
196. Torti, M., Venanzi, I., Laflamme, S. & Ubertini, F. *Life-Cycle Management Cost Analysis of Transportation Bridges Equipped with Seismic Structural Health Monitoring Systems*. [https://faculty.sites.iastate.edu/laflamme/files/inline-files/Laflamme\\_J89\\_2021\\_0.pdf](https://faculty.sites.iastate.edu/laflamme/files/inline-files/Laflamme_J89_2021_0.pdf) (2021).